

Engineering theranostic liposomes for image guided drug delivery as a novel nanomedicine for cancer therapy

A thesis submitted to the University of Manchester for

the degree of Doctor of Philosophy

in the Faculty of Biology, Medicine and Health

2016

James D. B. Gubbins B.Sc. M.Res.

School of Health Sciences

COPYRIGHT STATEMENT

- i. The author of this thesis (including any appendices and/or schedules to this thesis) owns certain copyright or related rights in it (the “Copyright”) and s/he has given The University of Manchester certain rights to use such Copyright, including for administrative purposes.
- ii. Copies of this thesis, either in full or in extracts and whether in hard or electronic copy, may be made only in accordance with the Copyright, Designs and Patents Act 1988 (as amended) and regulations issued under it or, where appropriate, in accordance with licensing agreements which the University has from time to time. This page must form part of any such copies made.
- iii. The ownership of certain Copyright, patents, designs, trade marks and other intellectual property (the “Intellectual Property”) and any reproductions of copyright works in the thesis, for example graphs and tables (“Reproductions”), which may be described in this thesis, may not be owned by the author and may be owned by third parties. Such Intellectual Property and Reproductions cannot and must not be made available for use without the prior written permission of the owner(s) of the relevant Intellectual Property and/or Reproductions.
- iv. Further information on the conditions under which disclosure, publication and commercialisation of this thesis, the Copyright and any Intellectual Property University IP Policy (see <http://documents.manchester.ac.uk/display.aspx?DocID=24420>), in any relevant Thesis restriction declarations deposited in the University Library, The University Library’s regulations (see <http://www.library.manchester.ac.uk/about/regulations/>) and in The University’s policy on Presentation of Theses

Acknowledgements

Firstly I thank my parents, Julie and Mark, who have always shown a quizzical intrigue towards my professional endeavours. They have shown me unconditional support throughout a challenging period of my professional life, and for that I am truly grateful.

To my friends from UoM, UCL and from further afield, thank you for being there, and thank you for all the support you have given me. I wouldn't have got this far if it wasn't for you.

The last few years have been tough but eminently satisfying. As with most projects in this industry of academic research, the work is never truly over, a study will never truly be out of exploratory options and someone else will inevitably continue working towards improving and adding to your work. However, there is always a time when one must finish and move on, and most importantly appreciate such enlightening opportunities such as working through a PhD in theranostic liposome design. I walk away from this work feeling truly lucky to have played a part in the development of such an important and exciting field, and wish the best of luck to the next person who will further develop this work.

In light of this sentiment I want to thank all those professors, staff scientists and students who have come before me in this field of research, and contributed such ground-breaking developments from which I have learned and been so inspired. Really I wouldn't be here today if the old school didn't pave the way.

Following on from this I thank my supervisor Prof. Kostas Kostarelos for granting me this opportunity and so kindly hosting me in his lab. I cannot have hoped for more input and dedication to my PhD than he has personally invested. For someone so dedicated to his work and lab management, the time he invested in my liposome development, my fascination with lasers and basketball and squash games, has been astounding.

My co-supervisor Dr. Neus Lozano Valdes has been a true saviour and a great friend. Through the midst of seemingly inescapable ICG related ruts I found myself in, she was always there to advise and encourage me. I owe her so much, for her persistent help, the amount she has stood up for me and how she helped me calm my mind when the project appeared to go awry. I shall never forget the hours of last minute presentation review, endless formatting and ICG discussions that you endured for me. Nor shall I forget all the basketball, squash, croquetas and catching glimmers of sun outside the AV Hill whilst recovering from certain meetings! Really thank you so much.

I thank AstraZeneca and specifically Marianne Ashford and Paul Gellert for funding my project, and giving me such useful feedback, encouragement and insight. I very much appreciate the meetings we have had and the opportunities to speak at the sites in Macclesfield and Alderley Park. I've found it so interesting having the opportunity to meet AZ staff members and gain such valuable insights into drug development and working within the pharmaceutical industry.

I thank Dr. Zahraa Al-Ahmady for all her training, assistance and advice towards the development of my project. I am truly grateful.

I thank Dr. Alisdair Macpherson from the Photonics Institute for his tireless efforts to explain lasers to me in words of one syllable and for working tirelessly to provide me with the opportunity to carry out the pilot experiments which provided the proof of concept I needed to take my work to another level. He was the only one in the Lancashire area who would help me and could give me the opportunity to surpass this final hurdle, and for that I am extremely grateful.

Last but not least, I thank all those from the nanomedicine lab both past and present. Especially Melissa, Giulia, Debora, Davide, Leon, Kirsty, Amalia, Yein, Leon, Irene and Chris. You really made it pleasure to come to the lab on those long days of repetitive formulations and endless centrifugation cycles and DOX incubations. Thanks so much for the amusement, support and friendship.

I finally add that the greatest satisfaction I could possibly have from this project is if what I have developed in the following pages can one day aid in the development of a clinical nanomedicine. This is the reason why I came into this field of research, and what has driven me up to this point.

Abstract

Cancer mortality is progression-dependent thus its treatment relies on effective therapy and monitoring of responses. Nanoparticles have long been used to improve the therapeutic index of drugs by facilitating their transit to the target site at higher concentrations than free drugs, whilst protecting healthy tissues from an often potent and cytotoxic payload. Through the EPR (enhanced permeability and retention) effect, injected, PEGylated nanoparticles preferentially accumulate in tumour tissue deeming them eminently suitable for cancer intervention for delivery of both therapeutic and contrast agents. The development of theranostic liposomal systems comprising both imaging and therapeutic capabilities exploits the facets of liposomes, and forms an elegant strategy to address major problems which hinder effective cancer therapy. Liposomes can be tailored to be thermosensitive in a low hyperthermic range of $\sim 42^{\circ}\text{C}$, above physiological temperature but below that which can induce tissue damage. This allows the use of heating as an external triggering modality to induce targeted drug release. Throughout the course of this work, the photoacoustic contrast agent ICG was successfully incorporated into PEGylated doxorubicin-encapsulating liposomes, marrying two FDA approved entities.

The project commenced with the development of the basic liposomal-DOX. Differing lipid compositions of varying fluidities were tested against those which have been previously established. These compositions carried a range of phase transition temperatures, above which the liposomes release the encapsulated DOX. This study concluded with the generation of a library of liposomes with differing release kinetics at 42°C in simulated physiological conditions.

The second section of the project investigated the methodology behind the incorporation of ICG into the liposomal bilayers. The lipid composition used for the study was based on the DOXIL[®] formulation, due to its robust structure and establishment in the field of cancer therapy. The protocols used varied on the basis of chronology in regards to the liposome preparation protocol. The *film insertion* method incorporated the ICG in initial lipid film generation. The *freeze fracture* protocol introduced the ICG during lipid film hydration. The *post insertion* protocol introduced ICG in the final stages of DOX loading. The downsizing protocol was also varied between extrusion and sonication. Through varying of the protocols and downsizing methodology, it was possible to incorporate differing ICG concentrations and attain differing levels of structural stability. The most successful liposome was then tested for its imaging potential *in vivo* through a photoacoustic imaging modality namely multispectral optoacoustic tomography. This validated accumulation of the liposomes at the tumour site along with co-localisation of both drug and dye.

The project culminated in the combination of the two studies, producing a thermosensitive theranostic ICG labelled liposomal doxorubicin system. The system showed improved blood stability than the current clinical systems, and demonstrated imaging potential through IVIS based fluorescence imaging. Through exploitation of the photothermal effects of ICG within a thermosensitive lipid vesicle, it was also possible to induce drug release through irradiation with a non-thermal near-infrared laser. This shows promise for future therapy, allowing simultaneous imaging, optimum release induction and monitoring response to therapy, in a cheap, effective and time-efficient manner.

Table of Contents

Acknowledgements	III
Abstract	V
List of Tables	IX
List of Figures	X
List of Abbreviations	XII
1 Introduction	1
1.1 Cancer	2
1.1.1 Molecular basis for cancer	3
1.1.2 Tumour structure and nanoparticle extravasation	5
1.1.3 Metastasis	8
1.2 Overview of clinical nanomedicine	9
1.3 Liposomes	9
1.3.1 Constitution and physical chemistry	10
1.3.2 Lipid Phase Transition	13
1.4 Liposomes for cancer intervention	13
1.4.1 Early History	13
1.4.2 The reticuloendothelial system pitfall	14
1.4.3 Boosting Delivery	14
1.4.4 Stealth® Liposomes	15
1.4.5 Liposomes for imaging	15
1.4.5.1 Liposome based MSOT imaging	17
1.5 Liposomes for therapy	20
1.6 Controlled release liposome systems	255
1.6.1 Thermosensitive Liposomes	27
1.6.2 Theranostic liposomes	29
2 Project aims and hypotheses	33
2.1 Thermosensitivity	33
2.2 Theranostics	34
2.3 Thermosensitive theranostics and the photothermal trigger	36
3 Materials and Methods	38
3.1 Chemicals	38

3.2	Liposome Preparation.....	38
3.2.1	Film insertion protocol:	39
3.2.2	Freeze fracture protocol:.....	39
3.2.3	Post insertion protocol:	39
3.2.4	Reheat insertion protocol:.....	40
3.3	Phospholipid quantification	40
3.4	ICG incorporation Efficiency.....	40
3.5	Encapsulation Efficiency.....	40
3.6	Dynamic Light Scattering and Laser Doppler Micro-electrophoresis.....	41
3.7	Doxorubicin Release and Retention.....	41
3.8	Transmission Electron microscopy.....	41
3.9	Fluorescence Anisotropy Measurements.	42
3.10	4T1 Murine Tumour Xenograft	43
3.11	IVIS biodistribution imaging	44
3.12	Blood stability of [¹⁴ C]-DOX liposomes in vivo	44
3.13	Blood radioactivity measurements	44
3.14	Photothermal release experiments	45
3.15	MSOT.....	45
4	Optimisation of the Composition of Thermosensitive Liposomes	47
4.1	Introduction	47
4.2	Results.....	51
4.2.1	Probing Membrane Rigidity Through Modulation of DPPC:DSPC ratio	51
4.2.2	Utilisation of sonication rather than extrusion for liposome preparation	58
4.2.3	Addition of Indocyanine Green (ICG) as a bilayer stabilising and imaging agent .	60
4.2.3.1	Incorporation of ICG into the DPPC:DSPC:DSPE-PEG ₂₀₀₀ (60:40:5) Liposome	60
4.2.3.2	Incorporation of Low Concentration ICG into differing lipid ratios of the DPPC:DSPC:DSPE-PEG ₂₀₀₀ Liposome.....	66
4.2.3.3	Pushing the boundaries of ICG incorporation into the more fluid lipid ratios of the DPPC:DSPC:DSPE-PEG ₂₀₀₀ Liposome.....	69
4.3	Discussion	77
4.3.1	Probing Membrane Rigidity Through Modulation of DPPC:DSPC ratio	77
4.3.2	Utilisation of sonication rather than extrusion for liposome preparation	79
4.3.3	Addition of Indocyanine Green (ICG) as a bilayer stabilising and imaging agent .	79

4.4	Conclusion	85
5	Optimisation of liposomal ICG Incorporation into NTS-Liposomes	87
5.1	Introduction.....	87
5.2	Results	90
5.2.1	Protocols for the incorporation of ICG into liposomal DOX	90
5.2.2	Physicochemical characterisation of liposomes	92
5.2.3	DOX retention at 4°C and release at 37°C in 50% serum.....	96
5.2.4	DPH/ANS anisotropy	98
5.2.5	Optical density and stability of liposomes.....	100
5.2.6	<i>In vivo</i> MSOT Imaging of liposome-ICG-DOX	102
5.3	Discussion	104
5.4	Conclusion	112
6	Design and optimisation of theranostic thermosensitive Liposomes	113
6.1	Introduction.....	113
6.2	Results	116
6.2.1	Physicochemical liposome characterisation.....	116
6.2.2	Optical liposome properties	118
6.2.3	Physical Liposome Properties	121
6.2.4	IVIS based murine xenograft biodistribution.....	123
6.2.5	Water-bath heated DOX release	127
6.2.6	ICG as a trigger for the photothermoinductive release of DOX.....	131
6.2.7	[¹⁴ C]-DOX liposome circulation profile of film insertion sonicated system	135
6.3	Discussion	137
6.4	Conclusion	143
7	Conclusions and perspectives for future work.....	145
7.1	Stabilising the ThermoDox® composition at 37°C.....	147
7.2	Gain tuneable control over the doxorubicin release rate at 42°C	147
7.3	Optimising ICG incorporation into the DOXIL® formulation liposome	149
7.4	Demonstrating the imaging potential of the NTS liposome-ICG-DOX via MSOT	150
7.5	Optimising the incorporation of ICG into thermosensitive liposomes	151
7.6	Demonstrating liposome efficacy as a theranostic through imaging and stability.	152
7.7	Achieving laser induced ICG-based photothermia to induce DOX release	153
7.8	Limitations and future work.....	154
7.9	Final thoughts.....	156
8	Bibliography	158

List of Tables

Table 1.1 Clinically progressing liposomes designed for cancer therapy.	21
Table 1.2. Triggerable liposomes designed for controlled payload release.	26
Table 1.3 Theranostic liposomes designed for cancer application.....	31
Table 4.1. Characterisation of non-thermosensitive and thermosensitive liposomes.....	52
Table 4.2. Characterisation of sonicated thermosensitive liposomes.....	58
Table 4.3. Characterisation of DPPC:DSPC:DSPE-PEG2000 (60:40:5) incorporating ICG.....	62
Table 4.4. Characterisation of DPPC:DSPC:DSPE-PEG2000:ICG 5µM at differing lipid ratios.....	66
Table 4.5. Characterisation of Thermosensitive and non-thermosensitive liposomes incorporating higher ICG concentration.....	70
Table 5.1. Tabulated physicochemical characterisation of each of the liposome systems constructed.	95
Table 6.1. Physicochemical characterisation of sonicated liposomes comprising various proportions of DPPC:DSPC along with DOX and ICG.	118
Table 6.2. Physicochemical characterisation of sonicated post inserted liposomes comprising DOX, ICG and a combination of the two.....	124

List of Figures

Figure 1.1 : Cancer 5-year survival by stage, Data obtained from ²⁵⁶	3
Figure 1.2 TP53 interactome Consisting of 209 proteins and 274 interactions from Pathway Commons PCViz ⁴	4
Figure 1.3 Oxygen and pH gradient based upon distance from the tumour vasculature ²⁵⁷	6
Figure 1.4 Chemical structures of constituent lipids. ³³	12
Figure 1.5 The bases of MSOT imaging.....	17
Figure 1.6 The NIR optical window for <i>in vivo</i> imaging. This is represented in the form of tissue light absorption of a number of endogenous chromophores across the visible spectrum. (Adapted from ²⁵⁹ .).....	19
Figure 1.7 The mechanism of liposomal DOX loading via the remote active loading protocol ¹⁰¹	23
Figure 1.8 Probability of progression free survival of CAELYX TM /DOXIL [®] (PLD) vs DOX alone in its use as a first line treatment for metastatic breast cancer. Figure adapted from ¹⁰⁶	24
Figure 1.9 The mechanism of enhanced grain boundary permeability through the use of pore-stabilising MSPC in the ThermoDox [®] formulation liposome. (Adapted from ¹²³).....	29
Figure 4.1 Mechanism of MSPC mediate pore formation at grain boundaries between gel and liquid phase lipid populations. Figure adapted from ²⁸	48
Figure 4.2 Combination of Liposomal DOX with ICG upgrading therapeutic liposomes to theranostic systems with which it would be possible to both image and treat cancer patients.....	50
Figure 4.3. The variance in phase transition temperature of DPPC:DSPC:DSPE-PEG ₂₀₀₀ based liposomes as the DPPC:DSPC ratio is modified.....	54
Figure 4.4 Doxorubicin release profiles at 37°C and 42°C for a) DPPC:MSPC:DSPE-PEG ₂₀₀₀ in HBS and b) in 50% mouse serum, c) HSPC:Chol:DSPE-PEG ₂₀₀₀ in HBS and d) in 50% mouse serum.	55
Figure 4.5 Doxorubicin release profiles of extruded DPPC:DSPC:DSPE-PEG ₂₀₀₀ at differing DPPC:DSPC ratios at a) 37°C and b) 42°C in 50% mouse serum.	56
Figure 4.6 Doxorubicin release profiles of sonicated DPPC:DSPC:DSPE-PEG ₂₀₀₀ at differing DPPC:DSPC ratios at a) 37°C and b) 42°C in 50% mouse serum.	59
Figure 4.7 Optical spectra of 7.5µM ICG in differing solvents.....	61
Figure 4.8 Variance in phase transition temperatures of the 60:40 liposome system when the ICG content is altered.....	63
Figure 4.9 Stability of ICG absorbance spectra over a week in DPPC:DSPC:DSPE-PEG ₂₀₀₀ (60:40:5) liposomes incorporating ICG in comparison to free 2.5µM ICG in HBS.....	65
Figure 4.10 Absorbance spectra of liposomal ICG of two differing lipid compositions based on DPPC:DSPC;DSPE-PEG ₂₀₀₀ at an [ICG] of 5µM.....	68
Figure 4.11 Absorbance spectra of liposomal ICG of the 90:10 system at an [ICG] of 7.5µM. Spectra were read at different points of the liposome production protocol, before and after gel filtration, and after DOX loading.....	71

Figure 4.12 TEM micrographs of DPPC:DSPC:DSPE-PEG ₂₀₀₀ (80:20:5) Liposomes in a) without ICG and in b) with 5µM ICG.	73
Figure 4.13 DOX release profiles of DPPC:DSPC based liposome-ICG-DOX systems at a) 37°C and b) 42°C in the presence of 50% mouse serum.	75
Figure 4.14 DOX release profiles of DPPC:DSPC based liposome-ICG-DOX systems at 42°C at differing [ICG] for a) 90:10 and b) 80:20 in the presence of 50% mouse serum.	76
Figure 4.15 Mathematically modelled structures of ICG and DOPE (dioleoylphosphoethanolamine) annotated with relative polar regions in blue, and hydrophobic regions in yellow. Adapted from ⁵⁹ . 80	80
Figure 4.16 , AFM micrographs showing increased lateral mobility of DMPC lipids from a bilayer to monolayer, following gel to liquid phase transition. Adapted from ⁶²	83
Figure 5.1. Schematic representation of the three liposome-ICG-DOX construction methodologies and relative differences in chronology of ICG incorporation.	91
Figure 5.2. Testing ICG integration during the post insertion protocol by varying the initial ICG concentration between 0 and 800µM.	94
Figure 5.3. DOX retention and release of liposome-ICG-DOX systems prepared via each of the three protocols.	97
Figure 5.4. DPH/ANS fluorescence anisotropy of each of the liposome-ICG-DOX formulations.	99
Figure 5.5. Characterisation of optical properties of the liposome constituents prepared via the three aforementioned protocols.	101
Figure 5.6. <i>In-vivo</i> validation of tumour accumulation of liposome-ICG-DOX prepared via the <i>post-insertion</i> protocol.	103
Figure 5.7. Characterisation of the reheat insertion protocol of ICG and DOX incorporation into HSPC:cholesterol:DSPE-PEG ₂₀₀₀ liposome.	109
Figure 5.8. Fluorescence cryosection image for validation of the MSOT signal derived from the ICG at 800nm.	111
Figure 6.1. Liposomes were prepared via sonication. ICG incorporation was achieved through either the film insertion (top) or post insertion (bottom) protocol.	115
Figure 6.2. Relationships between initial ICG concentration and final DOX EE or OD at varying lipid ratios.	120
Figure 6.3. Relationships between initial ICG concentration and final size or surface charge at varying lipid ratios.	122
Figure 6.4. 4T1 tumour growth profiles.	123
Figure 6.5. IVIS mediated murine 4T1 tumour xenograft 50:50 liposome biodistribution assay displaying ICG and DOX fluorescence as well as DOX fluorescence intensity.	126
Figure 6.6. DOX release profiles at 37°C and 42°C in 50% mouse serum of 50:50 and 60:40 formulations comprising DOX and ICG.	130
Figure 6.7. Laser based photothermia of liposomal DOX in NTSL and thermosensitive constructs with and without incorporated ICG.	133

Figure 6.8. TEM micrographs of 50:50 formulation liposomes before and after laser irradiation....	134
Figure 6.9. [14C]-DOX standard curve equating radioactivity with DPM following serial dilution....	135
Figure 6.10. Blood stability profile of the film inserted, sonicated 50:50-ICG-DOX system vs free DOX.	136
Figure 6.11. TEM micrograph of an air filled phosphatidylcholine based 5 μ m microparticle displaying grain boundary structure.	138

List of abbreviations

ANS	8-anilino-1-naphthalenesulphonic acid
AS	Ammonium sulphate
AuNR	Gold nanorod
BSA	Bovine serum albumin
Chol	Cholesterol
CMC	Critical micelle concentration
CT	Computational tomography
ddH ₂ O	Double distilled/deionised Water
DLS	Dynamic light scatterer
DMSO	Dimethylsulphoxide
DOPE	1,2-dioleoyl-sn-glycero-3-phosphoethanolamine
DOX	Doxorubicin
DOTAP	N-[1-(2,3-dioleoyloxy)propyl]-N,N,N-trimethylammonium methylsulphate
DPH	1,6-diphenyl-1,3,5-hexatriene
DPPC	1,2-dipalmitoyl-sn-glycero-3-phosphocholine
DSC	Differential scanning calorimetry
DSPC	1,2-distearoyl-sn-glycero-3-phosphocholine
DSPE-PEG ₂₀₀₀	1,2-distearoyl-sn-glycero-3-phosphoethanolamine-N-[methoxy(polyethyleylene glycol)-2000] ammonium salt)
ECM	Extracellular matrix
EPR	Enhanced permeability and retention
Gm1	Ganglioside
HBS	HEPES buffered saline
HCl	Hydrochloride/hydrochloric acid

HEPES	4-(2-Hydroxyethyl)piperazine-1-ethanesulphonic acid
HIFU	High intensity focused ultrasound
HIF-1	Hypoxia inducible factor-1
HSPC	Hydrogenated soy L- α -phosphatidylcholine
ICG	Indocyanine green
ID	Injected dose
IVIS	<i>In vivo</i> imaging system
LTS(L)	Low-temperature sensitive (liposome)
MLV	Multilammellar vesicle
MMP	Matrix metalloprotease
MRI	Magnetic resonance imaging
MSOT	Multispectral optoacoustic tomography
MSPC	1-stearoyl-2-hydroxy-sn-glycero-3-phosphocholine
mV	Millivolt
NIR	Near-infrared
NTS(L)	Non-low temperature sensitive (Liposome)
OD	Optical density
PC	Phosphocholine
PDI	Polydispersity index
PDT	Photodynamic therapy
PE	Phosphoethanolamine
PEG	Polyethylene glycol
PET	Positron emission tomography
PS	Phosphoserine
PTT	Photothermal therapy
RES	Reticuloendothelial system
RFA	Radiofrequency ablation

SPION	Superparamagnetic iron oxide nanoparticle
Stewart Reagent	ammonium ferrocyanide
SUV	Single unilamellar vesicle
T_m	Phase transition temperature/melting temperature
TEM	Transmission electron microscopy
US	Ultrasound
VEGF	Vascular endothelial growth factor
W	Watt

Chapter 1

1 Introduction

Cancer is a highly complex family of diseases best characterised by uncontrolled proliferation of neoplastic cells emanating from a plethora of different cell types. These neoplasia continue to amass into lesions comprising numerous differing cellular phenotypes, obstructing the function of the organs in which they are located. Over time, subpopulations of cells break free from the encapsulating tumour margins and through way of the lymphatic system and vasculature, spread to both proximal and distant sites in the body, into which they extravasate and seed secondary lesions. If left untreated, this condition is often fatal. Cancer treatment relies on a combination of imaging and cytotoxic therapy designed to eradicate cancerous cells. Chemotherapy utilises cytotoxic agents targeted to dividing cells, often interacting with the uncondensed DNA, or obstructing cellular organelles involved in mitosis. One of the crucial drawbacks with chemotherapeutics is their high toxicity and lack of targeting. Following systemic administration, these cytotoxic agents are effective in treating chemo-sensitive cancerous cell populations within the tumour mass, however they also kill healthy proliferative tissue. These proliferative tissues comprise hair follicles, much of the gastrointestinal lining, proliferating immune cells amongst others. The resultant side effects are highly debilitating, to the extent that many patients are either too weak to cope with the toxicity and die from the therapy, or opt for palliative care, forgoing treatment altogether. Systemic administration of unpackaged chemotherapeutics results in poor circulation half-lives and a lack of targeting, resulting in a low tumour uptake.

The invention of nanoscopic drug delivery systems revolutionised the application of chemotherapy. Through the combination of vehicles and chemotherapeutics, it was possible to stabilise circulation half-lives, significantly improve drug safety and increase the therapeutic index through increased uptake in the tumour site. Although limited systems are presently available for clinical use, there are numerous systems in ongoing clinical trials¹. Nanoparticles are defined as systems with a diameter roughly between 1 and 100 nm. They may be comprised of a wide variety of different constituents such as lipids, peptides and metals. They are often readily functionalised, and provide an exceedingly high surface area for drug encapsulation or surface modifications. Due to their small size, they can readily penetrate through fenestrations in the vasculature and disseminate through the tumour tissue. Not only can these vehicles be designed to carry chemotherapeutics, but they can be functionalised with a number of additional attributes. One of the most important modifications are coatings

designed to evade the immune system They can be decorated with imaging agents allowing their use as contrast agents in a number of radiological and optical diagnostic applications. Combination of both imaging and therapeutic agents is an exciting development in nanomedicine design. This would allow both tracking of drug delivery to the tumour site, therapy, and monitoring of disease progression. This combination of therapeutic and diagnostic agents is known as theranostics. Furthermore, additional functions of these nanoparticles are to release their payloads upon reaching the tumour site. This can be achieved in a number of ways through nanoparticle constituent design allowing the particles to be responsive to intrinsic and extrinsic cues. Triggering agents can be incorporated within these particles to induce release in response to a number of external stimuli, and allow release induction at the point of peak tumour accumulation.

The rest of this chapter will delve deeper into the intrinsic characteristics of this disease, along with the reality of the field of nanomedicines designed for its intervention.

1.1 Cancer

Cancer is one of the leading causes of death in the developed world. It is a disease characterised by uncontrolled cellular proliferation resulting in the obstruction of the functionality of the specific tissue type resulting in organ failure and eventual death when left untreated by effective means. There are around 200 different families of cancer with no tumour exactly the same as another. With variation between molecular characteristics and tissue types, some cancers show a higher lethality rate and faster progression than others. But what is certain is that the further a cancer is allowed to progress, the lower the chance of survival, as depicted in **Figure 1.1**. There are a plethora of sources which cause this often fatal illness, ranging from UV light, to carcinogenic chemicals and ionizing radiation. What is common to all of these stimuli is that they all induce DNA damage, which when undetected or poorly repaired result in disruption and alteration of the genetic code within the genome of the affected cell. This is known as a mutation. The location of a mutation is crucial to fate of this cell. If it occurs within non-coding intronic DNA, a microsatellite sequence of repetition of the code for example, the resultant effect can be unnoticeable. If it however falls within a gene coding for proteins involved in regulation of the cell cycle or DNA damage response, then this can induce uncontrolled proliferation of this mutated cell.

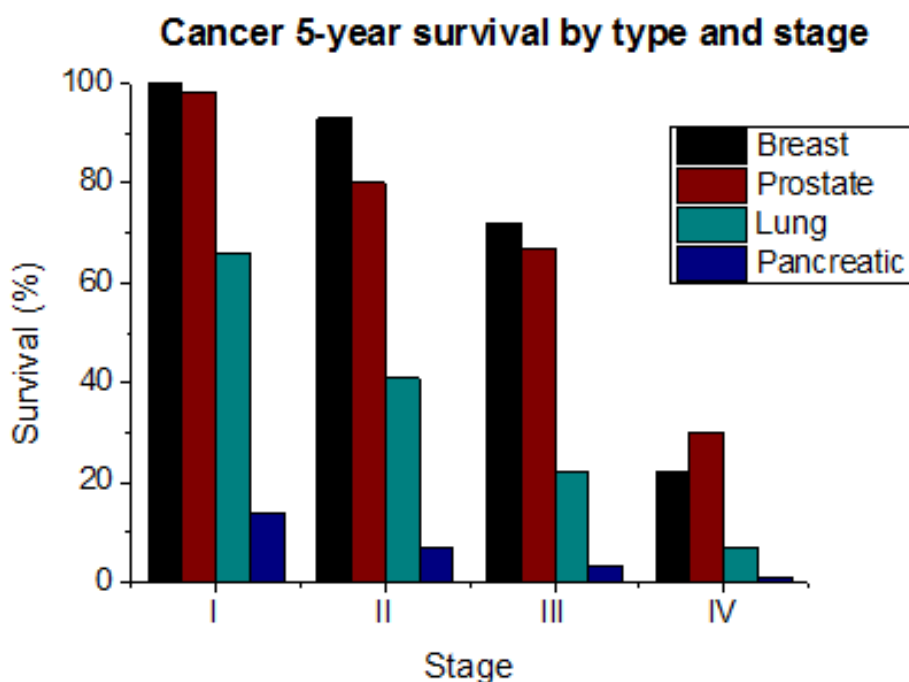


Figure 1.1 Cancer 5-year survival by stage. Data obtained from²⁸⁵.

1.1.1.1 Molecular basis for cancer

The basis for the development of cancer lies in the specific mutation of regions within certain genes. These genes are characterised as tumour suppressor genes and oncogenes. Tumour suppressor genes such as TP53², inhibit the cell cycle in response to DNA damage, stimulate DNA repair and/or induce cellular apoptosis if the damage is beyond repair. TP53 does all three of these functions amongst others. According to the International cancer genome consortium, TP53 is the most commonly mutated gene across cancers found in >50% of cases. What makes this protein known as the guardian of the genome so problematic once mutated, is that as it functions a tetramer³, it only takes one mutation in one copy of this gene to disrupt its overall activity, in the regions crucial for the formation of this quaternary protein structure, as well as mutations in the DNA binding domain which disrupt its ability to function as a transcription factor rendering it obsolete. As visualised in **Figure 1.2** TP53 interacts with 209 distinct proteins via 274 unique interactions discovered so far, exemplifying the complexity of the cellular functions of this tumour suppressor⁴.

Oncogenes such as the small g-protein H-RAS⁵ stimulate cellular proliferation in response to the activation of g-protein coupled receptors which are involved in signal transduction between growth factor bound receptors and downstream signalling proteins.

Mutations in H-RAS, a protein which forms a pivotal role in the signal transduction chain, can leave this protein constitutively active. The mutation G12V⁶ for example which substitutes the 12th amino acid in the protein chain with valine in place of glycine has this effect. This means that the protein no longer requires GTP binding for activation of downstream signalling to MEK and will do so continuously resulting in stimulation of cell cycle progression, and thus relentless growth of this cell population.

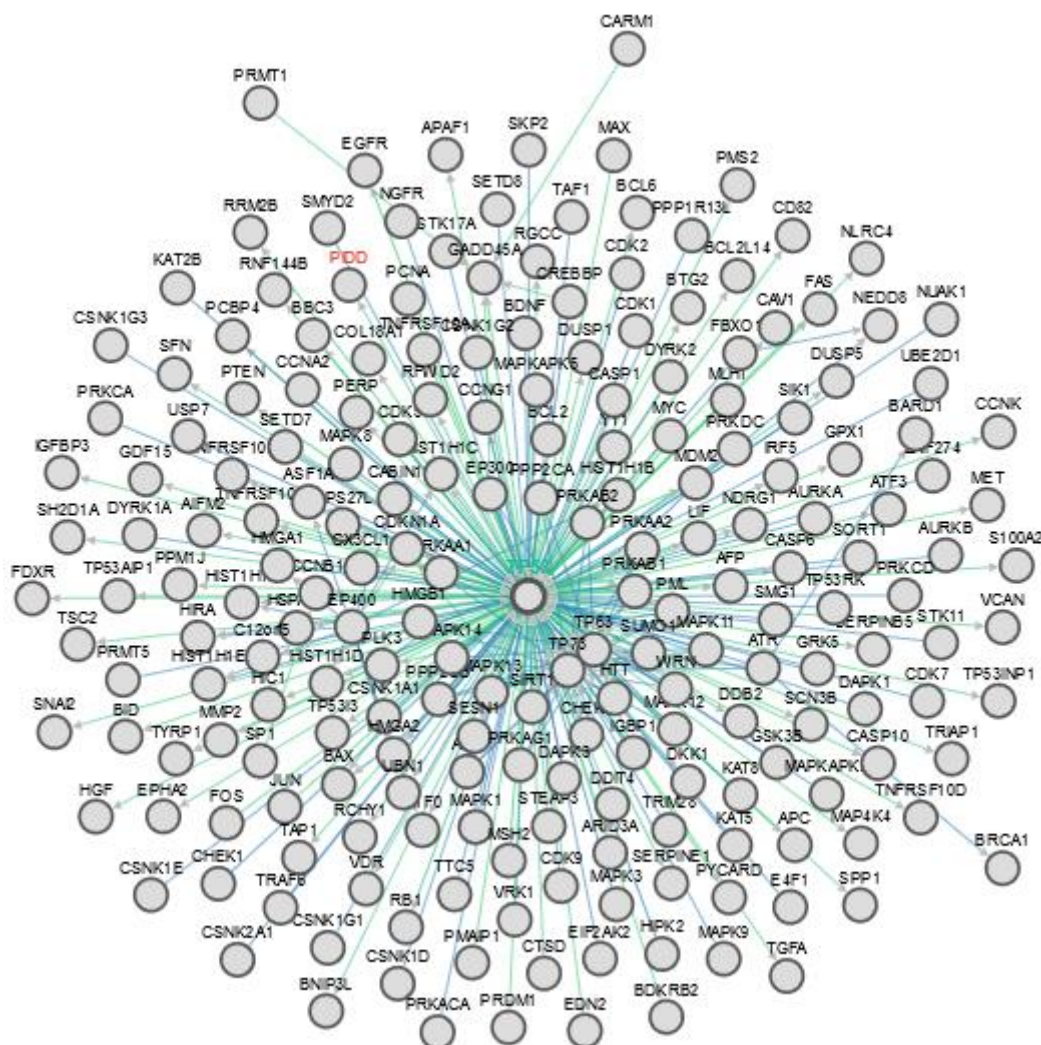


Figure 1.2 TP53 interactome Consisting of 209 proteins and 274 interactions from Pathway Commons PCViz⁴.

The accumulation of mutations to generate fast proliferating cancers often follow what is known as the Knudson Hypothesis⁷, also known as the two hit hypothesis which draws in genetic pre-dispositions for cancer development. Knudson discovered differences in the age at which someone may develop retinoblastoma, a cancer of the retina, discovering certain families showed a higher propensity to develop this pathology at a younger age than those

with no family history of the disease. He differentiated the two as inherited and sporadic disease types. The protein commonly associated with the development of this cancer is known as RB1 and is a tumour suppressor gene. As there are two sets of chromosomes, there are also 2 alleles of this gene active in any one cell. It was discovered that for formation of this tumour type to occur, both genes had to be inactivated through mutation. Those people predisposed to this tumour type were found to have an inherited mutation in one allele of these genes, and those who developed it sporadically did not. Knudson thus postulated that those who sporadically developed retinoblastoma did so at a later age because it took longer to accumulate a mutation in each allele of this gene within the appropriate cells than those predisposed who required a mutation in just the one active allele. This thus accounted for the age difference in disease development.

With mutations in genes responsible for halting uncontrolled neoplasia following mutation (tumour suppressor genes) and genes which drive cellular proliferation (oncogenes), neoplastic lesions can soon develop into tumours. However these tumours will not comprise a single cell type solely on the basis of the negligence of genomic proofreading as well as the rapid DNA replication rate. This results in the rapid accumulation of additional mutations due to errors in DNA synthesis generating a spread of genomically unstable, karyotypically diverse cells in this error accumulation analogous to the game Chinese whispers. The resultant tumour tissue will thus no longer be strictly a clonal expansion of a karyotypically distinct cell type, adding additional hurdles to its intervention. This is but one of the many factors involved in the patterning of tumour tissue.

1.1.2 Tumour structure and nanoparticle extravasation

Despite the large range of differing tumour majority karyotypes and resultant structure, the way that tumours develop from an early neoplasia to a fully-fledged, vascularised tumour show many similarities. In the early stages of tumour development cells undergo initial expansion and molecular based patterning as previously described reaching a size of about 1-2 mm³. Size is dependent on the relative growth and metabolic rate of cells within the neoplasia, which up to that point rely on oxygen diffusion from the surrounding niche. At this point, cells within the core of the lesion suffer from nutrient starvation and hypoxia due to the limitations of oxygen diffusion throughout the lesion⁸. The metabolic stress shifts the cells to rely on more glycolysis based anaerobic respiration which is significantly less efficient in the production of ATP, than the complete aerobic pathway involving oxygen

dependent oxidative phosphorylation. Resultant acidification in the form of lactate production subsequently decreases the pH of the tissue as displayed in **Figure 1.3**. The overall process is known as the Warburg effect and is postulated to be a strategy to increase cellular biomass more efficiently rather than economising glucose for ATP production⁹.

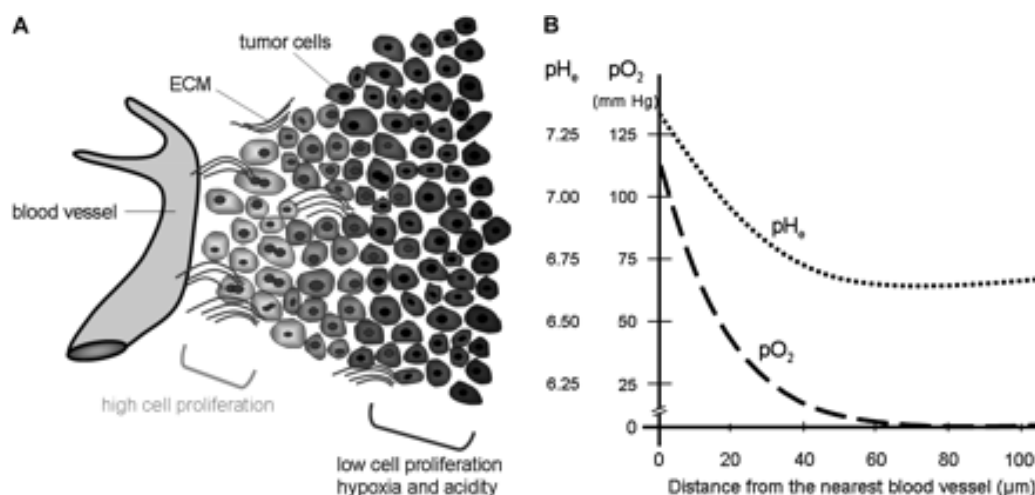


Figure 1.3 Oxygen and pH gradient based upon distance from the tumour vasculature²⁸⁶. **A)** demonstrates the effects on cellular proliferation, and **B)** the quantification of the oxygenation and pH of the tissue, in relation to distance from the vasculature.

The distance a tumour cell is from the vasculature can have profound effects on its characteristics due to the established oxygen and nutrient gradient. As the distance increases between the cells and the blood vessels, the nutrient and oxygen concentration decreases. The effect is stabilised by the relative interstitial pressure, and thus those cells reduce their rate of proliferation, adopting a more quiescent phenotype. The effect occurs up to a certain distance where the cells become so starved, they undergo necrosis, leaking their contents into the tumour stroma and developing into a necrotic core. This develops a patterning of cellular phenotypes within the tumour structure ranging from highly proliferative and gluttonous cells to more quiescent ones such as ‘cancer stem cells’¹⁰. When challenged with traditional chemotherapeutics, such heterogeneity proves quite an obstacle. These chemicals require incorporation into the DNA during mitosis, and are thus only effective against proliferating cells. With the combination of the reduction in proliferation rate and higher distances from the blood vessels and high interstitial pressure, chemotherapeutics will struggle to reach and show little efficacy against these cells.

The subsequent situation results in several changes in the transcriptome of these cancer cells with the overexpression of TP53 which in normal cells may induce caspase dependent apoptosis as well as the expression of hypoxia inducible factor 1 (HIF-1)¹¹. HIF-1 is an important response element which in hypoxic conditions is uninhibited to act as a transcription factor resulting in the production of vascular endothelial growth factor (VEGF)¹² as well as its receptor VEGFR1. VEGF is the most potent and versatile growth factor for the growth of blood vessels allowing tumour angiogenesis, and thus increasing the blood supply and with it oxygen and nutrient supply throughout the tumour tissue, allowing it to grow in size. Tumour angiogenesis requires the breakdown of the tumour's basal lamina (tumour boundary), a signal of the lesion turning from a benign neoplasm to a malignant tumour as it invades healthy peripheral tissues. This process allows the invasion of neovasculature which sprouts from existing blood vessels in response to proangiogenic signalling factors. Specifically the recruitment of endothelial progenitor cells to the site of neovascularisation which differentiate to form the neovascular endothelium and penetrate the tumour site following VEGF's pro mitogenic effect on endothelial cells and its induction of increased vascular permeability.

As a result of the rapid growth rate of tumour cells with their accompanied overproduction of growth factors and their receptors, vascular endothelial cells rapidly increase their turnover rate from 1000 days in normal tissue to just 50-60 hours¹³. The resultant effect is a chaotic, highly disorganised tumour vasculature riddled with defects and tortuous vessels. In some cases, tumour cells are even integrated into the walls forming "mosaic" blood vessels¹⁴.

The implications of the vascular architecture favours uptake of nanoparticles into the tumour stroma as a result of the EPR (enhanced permeation and retention) effect^{15,16}. This manifests itself from the extensive blood supply combined with the highly fenestrated vessels and secretion of vascular permeability factors which enhance the uptake of oxygen and nutrients to the rapidly dividing tumour cells. This results in a significantly higher level of extravasation of nanoparticles into the tumour stroma than other bodily tissues with 10-200 fold upregulation in uptake over normal tissues in the case of most polymeric macromolecular drugs¹⁷. Varying degrees of nanoparticle uptake depend on a number of factors relating to the tumour microenvironment in addition to the level and permeability of the tissue vascularisation^{18,19}. High interstitial pressures within the tumour tissue due to high levels of fluid leakage into the tumour stroma coupled with poor lymphatic drainage. This can disrupt the exchange of molecules between the vasculature and the tumour tissue. The tumour

stroma itself, comprises collagen bundles along with other extracellular matrix components, stromal fibroblasts and stromal modulating growth factors. This provides a reactive scaffold which not only supports the growth and angiogenesis of the tumour itself, but through paracrine signalling modulates tissue patterning, interaction with the surrounding extra-tumoural tissue and maintenance of local inflammation. Each tumour comprises differing densities of tissue stroma, which at high densities can limit perfusion and uptake on nanoparticles and therapeutics through modulation of trans-capillary drug transport through receptor mediated interstitial fluid pressure regulation, thus high stroma density levels can be a predictive factor of poor disease outcome²⁰. Stromal fibroblasts also mediate the pro-inflammatory nature of the tumour and thus infiltration of tumour associated macrophages which dictate another crucial element of the tumour microenvironment²¹. High macrophage infiltration is also a predictive factor in poor disease outcome across numerous cancers²². As part of the RES (reticuloendothelial system), phagocytic macrophages are primarily involved in clearance of therapeutics, especially injected nanoparticles from the circulation to the spleen²³. They are also involved in maintenance of tumour progression and resistance to therapy through chronic low-level TNF- α mediated expression of anti-apoptotic proteins via NF- κ B²⁴.

1.1.3 Metastasis

Metastasis is a process responsible for the vast majority of fatalities from cancer, crucial to the progression from stages 1 through 4, it is defined as the spread of cancer cells from the primary tumour to proximal tissues and further to distant sites, establishing secondary neoplastic lesions. Under metabolic stress as a result of a lack of nutrients and hypoxia, some cancer cells, much like bacteria, become cytotactic²⁵. Although many cancer cells are not adhesion dependent or contact inhibited, to become cytotactic, they must significantly change their phenotype. The initial process requires the cells to break free of their intracellular adhesions, disassemble from their tissue and migrate away, a process physically and molecularly similar to that observed during epithelial to mesenchymal cell transition, a form of redifferentiation observed during embryonic neural tube development²⁶. These cells undergo rapid cytoskeletal reorganisation coupled with the expression of certain matrix metalloproteases (MMPs) which facilitate the degradation of the extracellular matrix (ECM)²⁷. This allows the cells to penetrate through the tumour stroma, breaking through the basal lamina and invading regional lymph vessels, thus being transported to proximal lymph nodes representing the progress from stage I to II.

As metastatic cells continue to penetrate through the tissue, and local lymph and blood vessels, the cells breach the confines of the organ of origin and spread to regional tissues. For example in the case of prostate cancer, the bladder, colon and pelvis, signifying progression to stage III. Fewer than 1 in 1000 cells actually survive circulation in the blood stream to form metastases^{28,29}, so establishment of secondary lesions requires a significant number of motile cells breaking through the tumour and local vasculature. Upon reaching the appropriate area, often regions with high capillary beds due to the narrow vessels and lower flow rate, metastatic cancer cells adhere to the wall of the vasculature and extravasate into the local tissue. These regions are generally the liver, the lungs, the bones and brain³⁰. Upon engraftment, the metastases continue to grow as a primary tumour does, arising from a few especially malignant cells to fully fledged tumours.

1.2 Overview of clinical nanomedicine

The field of clinical research into nanomedicine is an extensive one, with 789 ongoing clinical trials involving nanomedical products and applications. 485 of these trials involve liposomes demonstrating the importance of these systems in the clinical field¹. Apart from liposomes, the rest of the nanoparticles in clinical development are based on a number of differing constituents. These include protein based systems such as FDA approved Abraxane^{®31}, iron oxide based Nanotherm^{®32} and the polymer based BIND-014³³. In terms of size, 76% of the constructs are 100-200 nm diameter and 63% are for therapeutic use rather than for use in medical devices. 73% were designed for intravenous administration, 78% of which depend on passive targeting and in terms of therapeutic applications 55% were formulated for use in cancer therapy¹. In summary, the clinical nanomedical field is dominated by passively targeted liposomes for use in cancer therapy in the range of 100-200 nm.

1.3 Liposomes

Liposomes are one of the most versatile delivery platforms in pharmaceutical development. Discovered by Alec D. Bangham in the early 60's³⁴, liposomes are artificially formulated spherulites of concentric lamellae. A region of aqueous solvent separates these liquid crystal lattices from each other. These bilayers can be disrupted to form vesicles comprised of a single phospholipid bilayer and an aqueous core. The name results from an amalgamation of the greek words: "lipo" (fat) + "soma" (body) = liposome (fatbody). Since

Bangham's discovery, many developments have been made in the liposome field to tailor liposome composition in order to address a plethora of biomedical requirements.

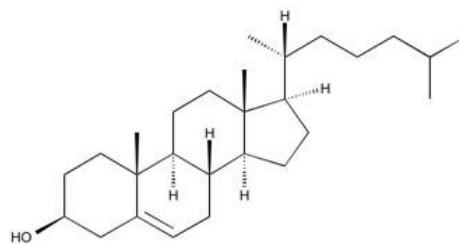
1.3.1 Constitution and physical chemistry

Liposomes are lyotropic and thermotropic liquid crystals, comprising amphiphilic phospholipids, which express different liquid crystalline properties depending on their environment. Lyotropism relates to the relative concentrations of two or more entities required for the expression of liquid-crystalline properties. In the case of liposomes, these two components refer to the amphiphilic properties of the constituent phospholipids; the hydrophilic head and hydrophobic tail. The basics of the phospholipid arrangements can be explained through the preference to adopt the thermodynamically least enthalpically demanding orientation³⁵. At low concentrations of lipids in aqueous solutions, there is no evidence of higher order packing. This is because the Gibbs free energy required to assemble with other phospholipids will not reduce the overall enthalpy required for the ordering of water molecules around the hydrophobic tail groups. When this concentration is increased above the critical micelle concentration (CMC) of the lipid, the phospholipids will arrange into micelles to reduce the enthalpic requirements of the system. This manifests itself through the orientation of the phospholipids into spherical monolayers, with the hydrophilic head group immersed in the polar solvent and the hydrophobic tail amongst the tails of the other lipids. The size of these micelles depends on the salt content of the aqueous buffer, the chain length of the constituent lipid, the electrostatic repulsion between the head groups and rigidity of the tails contributing to packing and curvature of the structure^{36,37,38}. Increasing the concentration results in interactions between distant micelles, coalescence into hexagonal rod formations and further networks of these rods, until formation of the phospholipid bilayer in the lamellar phase. Past this concentration the structures become inverted as the lipid becomes the majority fraction, resulting in the formation of inverse hexagonal rods and micelles³⁹.

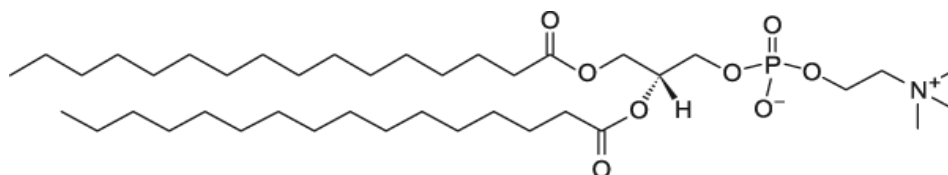
Thermotropism of a lipid bilayer is defined by the ability of the bilayer to undergo a change in the ordering of the bilayer in response to a temperature specific to the constituent lipids⁴⁰. This temperature, known as the phase transition (melting) temperature (T_m), varies between the populations of phospholipids. Understanding of the T_m is crucial for liposome production for the purposes of vesicle formation, downsizing and drug encapsulation. The T_m depends on the length and saturation of the phospholipid acyl chains. The longer the acyl chain, the higher the transition temperature, due to the increased number of Van der Waals

interactions attained between the saturated hydrocarbon chains. The higher the number of unsaturation bonds, the lower the transition temperature. This is explained by the difference in physical structure resulting from the C=C double bond, which induces a kink in the chain, disrupting the ordered structure of the bilayer providing extra space for the constituent lipids in which to move⁴¹.

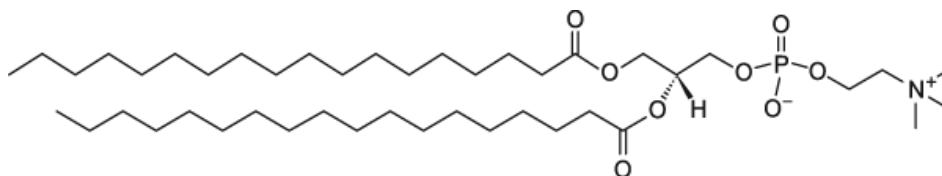
Liposomes design relies very much on the qualities required from the nanocarrier, and thus the selection of lipids for their formulation must be meticulously chosen. Many liposomes including all that are detailed in this thesis are comprised of a mixture of different lipids at differing ratios. This allows specific designation of their rigidity, circulation half-life and thermosensitivity. The major lipid components used in this work are as follows: DPPC (16:0) is a saturated phospholipid with a chain length of 16 carbons and a T_m of 41.3°C to 41.8°C⁴². DSPC (18:0 PC) a saturated phospholipid has a chain length of 18 carbons and a T_m of 54.9°C⁴³. DSPE-PEG₂₀₀₀ comprises polyethylene glycol (PEG) ligated to DSPE, and was developed as a way to incorporate PEG onto the surfaces of liposomes⁴⁴. The function of this bulky molecule is to enhance evasion of the immune system through mimicking of cellular glycolipids thus stabilising circulation half-lives. Cholesterol acts to rigidify membranes, and is a primary component in cellular lipid rafts⁴⁵. Cholesterol stabilises the bilayer by filling gaps between the phospholipids and associating predominantly in the hydrophobic domain. This increases the lipid packing density within the bilayer, and thus decreases the mobility of the lipids and permeability of the bilayer. This lipid greatly stabilises liposomes reducing their propensity to leak their payloads, become penetrated by circulating lipoproteins and succumb to shear stresses during circulation⁴⁶. The structures of these lipids utilised in liposome production are represented in **Figure 1.4**⁴⁷.



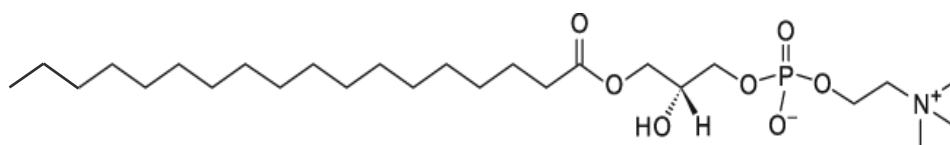
Cholesterol (Chol)



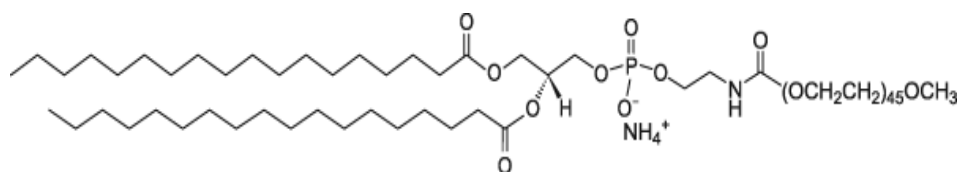
Dipalmitoylphosphatidylcholine (DPPC)



Distearoylphosphatidylcholine (DSPC)



Monostearoylphosphatidylcholine (MSPC)

Distearoylphosphoethanolamine-polyethylene glycol₂₀₀₀ (DSPE-PEG₂₀₀₀)**Figure 1.4** Chemical structures of constituent lipids.⁴⁷

1.3.2 Lipid Phase Transition

In terms of liposome bilayers, the thermotropic phase transition from the solid gel-phase to the fluid liquid crystalline phase have important implications. In the gel phase, the acyl chains of the constituent lipids are nearly fully extended, allowing tighter molecular packing and more Van der Waals interactions. This results in a rigid bilayer with limited lateral mobility⁴⁸. Following the phase transition the added energy to the system results in higher lateral mobility of the lipid population resulting in a fluid bilayer. In liposomes comprising lipids of different transition temperatures, when one population becomes fluid, grain boundaries appear between the liquid and gel state populations where the two grains interact at differing states. The acyl tails interact at different levels of mobile and immobile conformational states resulting in defects between the resultant packing of the molecules⁴⁹. This results in permeability of the bilayer through the formation of defects along these boundaries allowing access to the aqueous core of the liposome. The discovery of the generation of this permeability following phase transition⁵⁰, has been essential for the development of drug encapsulating and especially thermosensitive liposomes. Through the generation and disruption of gradients across the liposomal bilayer, it is possible to use this as a trigger to direct the trans-membrane flux of agents in and out of the vesicle.

1.4 Liposomes for cancer intervention

1.4.1 Early History

Until the early 1970s, liposomes had mainly been used to study the behaviour and structure of model biological membranes as well as their response towards antibiotics and proteins of the complement immune response⁵¹⁻⁵³. Liposomes first started to be used for the interests of therapy in the early 70's with the incorporation of anti-Cosackie A-21 antibodies for to inhibit infection of the cosackie A-21 *in vitro*⁵⁴. The first time liposomes were used in humans was in 1976 to deliver amyloglucosidase using a lecithin:cholesterol:phosphatidic acid (7:2:1) liposome to a child suffering from type II glycogenosis⁵⁵. This did appear to work better than the non-liposomal enzyme, to reduce liver glycogen levels. Further uses of liposomes were reported toward the end on the 70's, which addressed tumour radiolabelling, development of novel vaccines and improved delivery of insulin for diabetics, each with relative success⁵⁶. In addition to this, liposomes were also being postulated and tested in

humans as novel drug vehicles for the potential treatment of cancer⁵⁷.

1.4.2 The reticuloendothelial system pitfall

In the mid to late 70's, drugs and radioactive tracers were routinely incorporated into liposomes for the purposes of therapy or biodistribution studies. It was found that the presence of serum plasma proteins could have a significant effect on the rate of release of liposomes at 37°C⁵⁸. The presence of plasma proteins also inhibited the liposomes from endocytosis by hepatocytes⁵⁹.

In vivo it was also found that liposomes were being cleared from the bloodstream by the reticuloendothelial system (RES) with high levels of liposome tissue distribution in the liver, spleen and lungs. The resultant biodistribution is as a result of opsonisation and phagocytosis by the Kupffer cells of the liver and macrophages of the spleen. The level of uptake and distribution within the system varied depending on the charge of the liposome, in this case using multilamellar vesicles (MLVs)⁶⁰, the size⁶¹ and the structure and composition⁵⁰. Uptake into the RES of drug or radioactive tracer carrying liposomes was leading to immunosuppression through the depletion of macrophages as well as toxicity, while the rapid release in the bloodstream of protein sensitive formulations defeated the point of the encapsulation in the first place. It did not bode well for the therapeutic efficacy of liposomes *in vivo*, leading researchers to consider how to adapt their liposomes to avoid these pitfalls. It eventually led to the incorporation of non-lipid constituents to the liposome bilayer.

1.4.3 Boosting Delivery

In the late 80's, a number of groups addressed the issue of liposomal affinity towards the RES. In their appreciation of the shortfalls of liposomes as *in vivo* drug delivery vectors, they considered the differences in surface architecture of the liposome's bilayer and that of a cell. One of the main differences was the level of glycosylation of glycolipids and glycoproteins on the cell surface. Treatment of various blood cells with neuraminidase to remove sialic acid, (an N/O- linked glycan), had been shown to significantly affect the cell fate. Specifically, in the case of transfused lymphocytes, relocating them from their lymph node residence to the liver⁶² as well as platelets from the bloodstream to the liver⁶³.

In light of this research, attempts were made to emulate the effect of glycosylation by incorporating low ratios of gangliosides, which are glycosphingolipids carrying one or more sialic acid groups, into liposomes of different phospholipid compositions⁶⁴. In line with the postulations made, the concomitant incorporation of the glycolipids and phospholipids resulted in an increase in blood to RES ratio, thereby evading the RES and increasing the

circulation of the liposomes over the glycolipid free formulations. Further investigations focused on the liposome properties which promote the evasion of the RES. It was concluded that the G_{m1} ($II^3\text{NeuAc-GgOse4Cer}$) gangliosides provided the most effective evasion and stabilising effect in comparison to the others tested⁶⁵.

The other properties increasing circulation time were more rigid bilayers, negatively charged surfaces, G_{m1} of at least 7 mol % and a planar orientation of G_{m1} hydroxyl groups. In terms of size, the smaller the liposome, the higher the tissue penetration and retention^{66,67}. The exact size did vary between compositions however extrusion through a 0.1 μM pore size membrane generally resulted in the best results⁶⁵. These discoveries greatly improved the therapeutic potential of liposomes, paving the way for a wave of novel formulations and designation of the term “Stealth®” Liposome.

1.4.4 Stealth® Liposomes

Stealth® refers to the aforementioned steric stabilisation of liposomes through incorporation of glycosylated lipids allowing evasion of the RES and general stabilisation of the vehicle. Observations into the developments in extending circulation times of liposomes through glycosylation led to achievement of similar effects with proteins through conjugation with polyethylene glycolation⁶⁸. Merging the two concepts grafting polyethylene glycol₅₀₀₀ (PEG₅₀₀₀) onto phosphoethanolamine (PE) slightly improved on the effects of the G_{m1} in terms of stability and showing about a 20% increase in concentration in circulation and blood:RES ratio up to 5 hours⁶⁹. PEG chain length was then optimized to 1900 and grafted onto DSPE⁴⁴. This allowed easy introduction of PEG into the liposome, whilst doubling liposome blood circulation at 2h and by increasing by 100 times at 24h over the unmodified control. This provided an exciting new platform for therapy.

1.4.5 Liposomes for imaging

Cancer imaging is indispensable for the development of a cogent treatment strategy. It is essential for the staging of the disease as well as monitoring response to therapy. A number of differing imaging modalities are currently used in imaging such as X-ray based computational tomography (CT), magnetic resonance imaging (MRI), positron emission tomography (PET), ultrasound (US) and optical based imaging modalities such as *in vivo* imaging system (IVIS) and photoacoustic imaging reliant on both optical and ultrasound modalities. To accompany this, a number of liposome based contrast agents have been developed to facilitate tumour imaging. PEGylated liposomes passively target solid tumours through the enhanced permeability and retention (EPR) effect¹⁵ as previously described.

Some of the contrast agents used have been shown to cause tissue damage for example the MRI contrast agent Magnevist^{®70}, thus liposomal delivery of contrast agents can not only improve tumour imaging due to their preferential accumulation in the tumour site, but also reduce the relative toxicity associated with the uptake of these agents into healthy tissue. One of the most commonly used contrast agents are superparamagnetic iron oxide nanoparticles (SPIONs). These have been successfully coated for direct *in vivo* applications along with liposomal incorporation to improve circulation half-lives and thus tumour accumulation in addition to the facilitation of clearance^{71,72}. In addition to SPIONs, other isotopes such as manganese based liposomes have also been developed⁷³ along with gadolinium based systems⁷⁴. Mannitol based systems have also been used for ultrasound mediated imaging⁷⁵ in addition to conventional microbubbles⁷⁶. Liposomal Iodine is used for CT contrast due to its increased electron density successfully allowing tissue contrast⁷⁷. Radiolabelled liposomes are frequently used in preclinical research for analysis of nanoparticle tissue distribution. This allows scintigraphic imaging along with conventional β -counter based tissue liquid scintigraphy allowing accurate quantification of tissue accumulation⁷⁸. The incorporation of PET tracers allows detailed molecular imaging of the nanoparticles, and can also provide functional information such as tumour apoptosis⁷⁹. Liposomes incorporating the [¹⁸F] fluorine isotope as used in the conventional [¹⁸F]-fluorodeoxyglucose successfully allows PET based brain imaging⁸⁰.

1.4.5.1 Liposome based MSOT imaging

Photoacoustic imaging for biomedical purposes is a powerful imaging modality combining both optical and ultrasonic elements. Multispectral optoacoustic tomography is a recent iteration of this technology, and its performance far surpasses existing optical and ultrasound mediated imaging modalities as well as a number of non-optical techniques. It combines picomolar sensitivity⁸¹, $\sim 50 \mu\text{M}$ resolution and tissue penetration with a low cost of manufacture, ease of use and excellent safety specifications⁸². The technique is excellent for the detection of photoacoustic contrast agents as well as carrying the ability to provide morphological contrast of the tissue structure based on the innate photoacoustic signature generated at specific wavelengths from certain tissues and endogenous chromophores. This allows superimposition of contrast agent generated signal over the tissue structure without

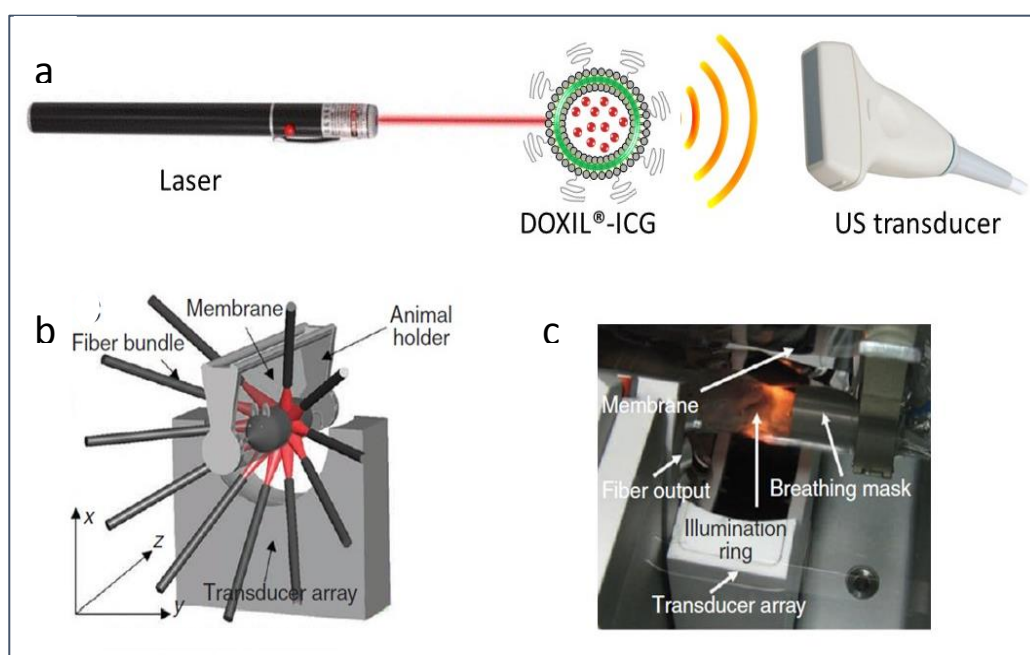


Figure 1.5 The basis of MSOT imaging for monitoring of nanoparticle biodistribution. **a)** the basic constituents of MSOT imaging comprising pulsed laser irradiation, a contrast agent combined with a nanoparticle such as the DOXIL[®] formulation liposome combined with ICG. **b)** schematic representation of the MSOT system in use with the animal immobilised in the centre of the device, cradled in a membrane and submerged in a water bath. The laser light is delivered in a radial array surrounding the animal. This is then surrounded by an additional transducer array for ultrasound detection. **c)** is a photograph of the MSOT in action as depicted in b. (b and c adapted from²⁸⁷)

the use of CT or MRI coupling.

The operation of the system for the imaging of nanoparticle bound contrast agents can be described in greater depth as it is depicted in **Figure 1.5a**. This application of MSOT comprises 3 basic constituents: pulsed light irradiation, a photoacoustic contrast agent such as

ICG, and transducers for ultrasound detection. For operation of the imaging system, the subject is anaesthetised, inserted into a membrane sleeve in the centre of the machine and submerged into the central water bath. At specific time-points following administration of the appropriate contrast agent/hybrid construct, laser light at a number of wavelengths is used to irradiate the subject. This is delivered in the form of 10ns light pulses at a repetition rate of 10Hz via a 10 arm radial fibre-optic array to provide illumination over a 2 dimensional plane at tuneable wavelengths from 680 nm to 900 nm⁸³.

This allows improved resolution of the contrast agent throughout the tissue as well as providing a spatial description of its location. As a result of the photothermal (PTT) attributes of the contrast agent ICG, upon irradiation the local heating surrounding this molecule induces local pressure changes which when pulsed at the correct frequency, generates ultrasound waves. These ultrasound waves are detected via a radial transducer array split into 64 elements, or further multiples of this in more recent iterations. This array surrounds the central water tank, which exists to facilitate the ultrasound conductance to the transducers.

The incorporation of multiple wavelengths of illumination improves the signal to noise ratio and allows compensation for movements during acquisition. Apart from compensation for movement, the multispectral approach allows better subtraction of background signal emanating from the tissue in terms of both tissue absorbance and variations in light propagation. It both facilitates signal unmixing and allows the detection of contrast agents or tissues which absorb light at differing wavelengths.⁸⁴ MSOT therefore requires the contrast agent to absorb light in a narrow spectral bandwidth. The utilisation of a number of wavelength also allows the use of a number of contrast agents simultaneously which can potentially allow the detection of systems comprising components labelled with multiple contrast agents such as gold nanorods, ICG and additional dyes. This has been demonstrated with the simultaneous imaging of IRdye800 conjugated to an integrin targeting peptide, alongside imaging of haemoglobin's intrinsic signatures at differing oxidation states⁸⁵. ICG's extremely low toxicity with a LD₅₀ of 50-80mg/kg in animals sets it apart from alternative contrast agents utilised in differing imaging modalities⁸⁶. The picomolar sensitivity of MSOT surpasses many alternative imaging modalities such as μ M X-Ray based imaging and nanomolar MRI and ultrasound. PET and SPECT have slightly higher sensitivities in the range of 1-10 femtomoles. However MSOT does make up for this in its safety profile, much cheaper manufacturing and operating costs and resolution in the range of 50 μ m in comparison to 1-2 mm for PET/SPECT⁸². MSOT allows non-invasive, live imaging of the probe with multiple irradiations possible at different time-points. Due to ICG's absorbance maxima falling in the

near infrared (NIR) region, this allows greater tissue penetration of the light used for irradiation thus improving photoacoustic signal generation facilitating detection through several centimetres of tissue. The high tissue penetration is due to the optical window of tissue transmittance in this region of the visible spectrum as displayed in **Figure 1.6**. The low absorbance of NIR light by endogenous tissue chromophores such as melanin and haemoglobin is the major contributing factor to the enhanced light transmittance. ICG's fluorescent properties also allows for IVIS based imaging⁸⁷.

A number of liposomes have been used for successful photoacoustic imaging based on multispectral optoacoustic tomographic imaging (MSOT). These systems have previously incorporated gold nanorods for their photoplasmonic and optoacoustic properties⁸⁸, and most importantly indocyanine green (ICG) which is the optimum contrast agent for this imaging modality. When incorporated into liposomes, the signal is 1.3 times higher than that of the free dye, and 3.2 times more than the previous benchmark contrast agent, gold nanorods^{89,90}. This makes liposomal ICG the optimum contrast agent for this imaging modality.

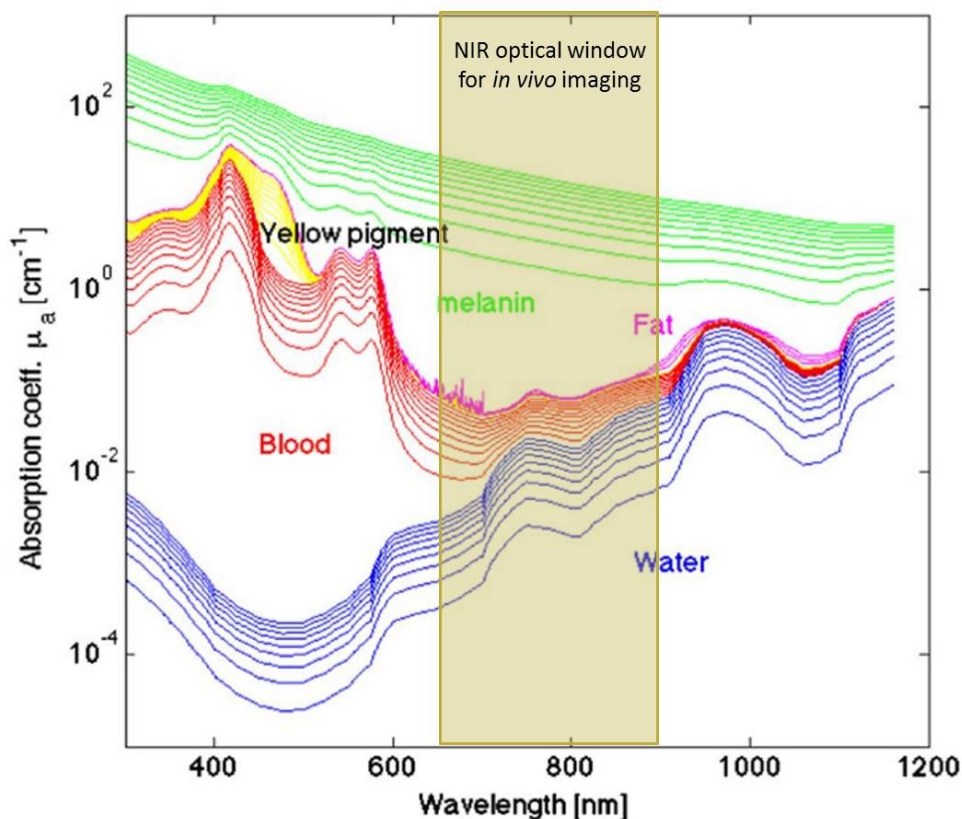


Figure 1.6 The NIR optical window for *in vivo* imaging. This is represented in the form of tissue light absorption of a number of endogenous chromophores across the visible spectrum. (Adapted from²⁸⁸.)

1.5 Liposomes for therapy

Traditional chemotherapy is fraught with side effects due to the lack of targeting of the compounds to the tumour site. The damage to the body can negatively affect the patient's prognosis through acute side effects, as well as reduce the willingness of the patient to continue treatment⁹¹. The combination of liposomes with chemotherapeutics is a logical step to increase the concentration of the drug at the tumour site and reduce the side effects. This has been shown to significantly reduce doxorubicin induced cardiotoxicity in early studies⁹². Success in tumour treatment requires a long circulation time to allow accumulation into the tumour tissue, and liposomes to be small enough to permeate deep into the tumour tissue⁹³.

Table 1.1 displays a number of liposomal therapeutics for cancer therapy at differing stages of clinical progression. What is striking is the large variation in devised strategies for cancer intervention based on the therapeutic ingredients of these varied systems. These range from traditional chemotherapeutics such as DOX⁹⁴, docetaxel⁹⁵ and cisplatin⁹⁶, to a number of differing strategies such as the delivery of cancer vaccines (JVRS-100⁹⁷), PDT photosensitisers⁹⁸ and siRNA based therapy⁹⁹. This demonstrates the innovation surrounding liposome based therapeutics and their utilisation to deliver therapeutic agents, the efficacy of which wholly depend on a suitable delivery vector.

The most commonly used drugs for liposome incorporation in current clinical research are paclitaxel and doxorubicin. Paclitaxel is a bulky, hydrophobic molecule first isolated from pacific yew bark in 1971¹⁰⁰. It is part of the taxane family of chemotherapeutics, specifically targeting dividing cells hence its selection for cancer therapy. Its mechanism of action is the interference in cellular division through interaction with microtubule networks during spindle formation. By stabilising the networks it prevents microtubule detachment from centrosomes resulting in incomplete mitosis and eventual cellular apoptosis¹⁰¹. Paclitaxel liposomes have not shown much increased efficacy in clinical trials with a 73% partial response elicited in patients with advanced gastric cancer in comparison to a 71% response from the drug alone¹⁰². However the same argument stands with this system as with DOXIL[®], that it greatly reduced the related side effects, allowing a higher overall dose to be given¹⁰³.

Table 1.1 Clinically progressing liposomes designed for cancer therapy

Name	Drug	Targeting	Application	Stage	Ref
DOXIL	DOX	passive	Kaposi Sarcoma	Approved	94
DaunoXome	Daunorubicin	passive	Kaposi Sarcoma	Approved	104
Visudyne	Verteporfin	passive	PDT	Approved	98
DepoCyte	Cytarabine	passive	Neoplastic Meningitis	Approved	105
Marqibo	Vincristine	Passive	Ph-ve ALL	Approved	106
Onivyde	Irinotecan	passive	Pancreatic cancer	Approved	107
Alocrest	Vinorelbine	passive	Solid tumours	I	108
ATI-1123	Docetaxel	passive	Solid tumours	I	95
Atu027	siPKN3	passive	Solid tumours	I	109
Brakiva	Topotecan	passive	Solid tumours	I	110
IHL-305	Irinotecan	passive	Solid tumours	I	111
JVRS-100	DNA vaccine	NA	Leukaemia	I	97
LEM	Mitoxantrone	passive	Solid tumours	I	112
Lipotecan	Camptothecin	Passive	Solid tumours	I	113
Endotag-1	Paclitaxel	passive	Solid tumours	II	114
NanoVNB	Vinorelbine	passive	Colorectal Carcinoma	II	115
SPI-77	Cisplatin	passive	Solid tumours	II/III	96
EGFR antisense DNA DC-Chol	EGFR Antisense DNA	passive	Head and neck	I	99
Atragen	Tretinoin	passive	Kaposi Sarcoma	II	116
MBP-Y003	Methotrexate	transferrin	Lymphoma	Pre-clinical	117
MBP-Y005	Gemcitabine	transferrin	Solid tumours	Pre-clinical	118

Doxorubicin is an a DNA intercalating anthracycline¹¹⁹, closely related to the antibiotic daunorubicin first isolated from *Streptomyces peucetius*. Its DNA intercalation acts as a mitotic inhibitor and was proven short after its discovery to be an effective antineoplastic agent in rodents¹²⁰. Upon trialling the drug in children suffering from a plethora of cancers, mostly leukaemia, a high success rate of complete and good remissions in 83% of previously untreated patients¹²¹. However this was at the expense of severe toxicity induced side effects such as leukopenia and cardiotoxicity. One of the Phosphotidycholine (PC), Phosphotidylserine (PS) and cholesterol (chol) at a molar ratio of 0.6:0.2:0.3 per mole of doxorubicin which was encapsulated through film hydration. The study aimed to monitor cardiotoxicity and response of murine leukaemia to the liposomal vs the free doxorubicin. The results showed an exceptional increase in overall survival following treatment, the most noteworthy being 128% vs 18% in the free doxorubicin. The cardiotoxicity was much reduced following administration of the liposomal doxorubicin over the free⁹².

Through the development of a remote active loading protocol as displayed in **Figure 1.7**, is based on the establishment of a pH/salt gradient, it is possible to load liposomes with 100% of the DOX HCl necessary for therapeutic doses¹²². The mechanism by which this is possible, relies on the initial hydration of the lipid film with ammonium sulphate pH 8.5/5.4, and subsequent external buffer exchange to one of a differing pH and salt content such as hydroxyethylpiperazineethanesulfonic acid (HEPES) buffer pH 7.4, following liposome formation. After buffer exchange, doxorubicin is added to the lipid suspension, and the liposomes are heated to a point close to their overall T_m . At this point the predominant lipid population undergoes a gel-liquid phase transition, opening grain boundaries between populations. With the lipid bilayer becoming permeable, the doxorubicin which is weakly basic and uncharged in the HEPES buffer (HBS) environment as DOX-NH₂, can freely permeate the bilayer upon which it binds SO_4^{2-} and subsequently precipitates as (DOX-NH₃)₂SO₄. Although the incubation temperature and time varied depending on the liposome bilayer composition, the weight ratio of lipid to doxorubicin remained at 20:1 for the generation of systems carrying a therapeutic payload. Later developments in liposomal doxorubicin resulted in the FDA approval of the first nanodrug: DOXIL[®], a rigid doxorubicin encapsulating stealth[®] liposome comprised of HSPC:Chol:DSPE-PEG₂₀₀₀ (56.3:38.2:5.5). It was first trialled in humans in 1994¹²³ for the basis of *in vivo* pharmacokinetic characterization. It maintained a half-life of 45 hours, induced reduced side effects over free doxorubicin as well as a significantly higher accumulation in tumour tissue.

It gained fast-track FDA approval in 1995¹²⁴ for AIDS related Kaposi sarcoma and subsequently recurrent ovarian cancer based on a significantly improved safety profile over DOX alone. In a study monitoring its efficacy against Kaposi sarcoma, patients experienced 40% complete response and 38% partial response¹²⁵. When combined with carboplatin, 63% of ovarian cancer sufferers experienced overall response with 38% experiencing complete response¹²⁶

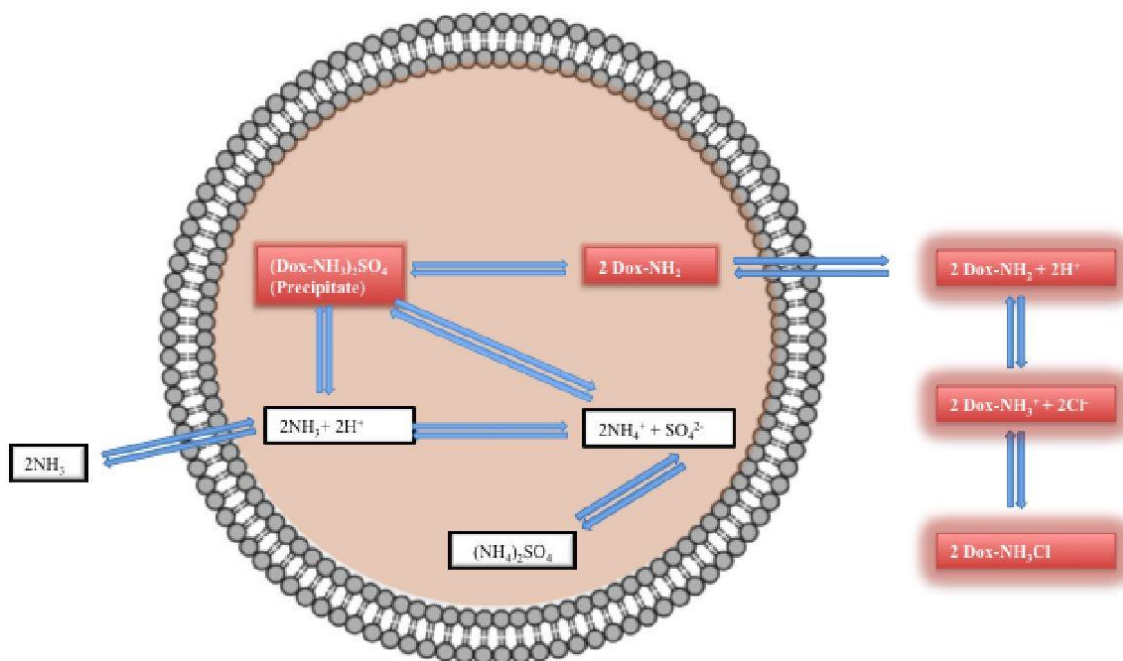


Figure 1.7 The mechanism of liposomal DOX loading via the remote active loading protocol¹²².

An improved safety profile is highly important when treating patients with drugs as toxic as DOX, as most often with free chemotherapeutics, the therapeutic dose may surpass the maximum tolerated dose for the individual patient. This allows the prescription of chemotherapy when otherwise a palliative option would be pursued based on the relative quality of life years that would be gained from the free agent. Despite the improvements in terms of reduced side-effects, DOXIL[®] did not elicit a particularly improved therapeutic response. For the treatment of metastatic breast cancer, it generated an overall survival following treatment of 21 months in comparison to 22 months in the cohort treated with DOX alone. DOXIL[®] treatment showed less progression free survival of 6.9 months in comparison to 7.8 months when treated with free DOX as represented in **Figure 1.8**¹²⁷ ..

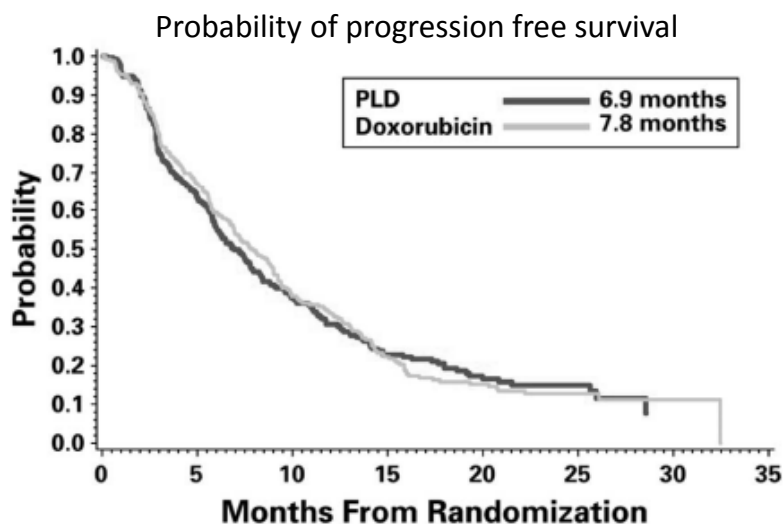


Figure 1.8 Probability of progression free survival of CAELYX®/DOXIL® (PLD) vs DOX alone in its use as a first line treatment for metastatic breast cancer. Figure adapted from¹²⁷.

The postulations behind the inconsistency between increased tumour accumulation of DOX, and the lack of improved therapeutic outcome was based on the same properties which provided increased circulation half-lives and resilience during circulation. The fundamental composition of the system is too rigid to allow DOX release, necessary for the intercalation of the DOX into the DNA of the target cancer cells. The problem is that it is not sufficient to only get the nanocarriers to the site of prospective action, the payload must be released at the site. This has also been demonstrated as a major set-back in the case of liposomal cisplatin, based on the same lipid composition^{128,129}. Until recently, the fundamental action of DOXIL® was unknown, however recent experiments have shed light on the release mechanism. The basis of this relates back to the active loading protocol, and is basically a reversal of this process. It is actually the build-up of ammonia in the tumour site, a metabolite of glutaminolysis, which reverses the DOX precipitation. Due to the low pH within the liposome¹³⁰, the surrounding uncharged ammonia passes into the core of the liposome and becomes protonated by the DOX sulphate. This relinquishes the charged state of the DOX compound as it reverts back to the initial DOX-NH₂, which facilitates its passage across the liposomal bilayer as an uncharged molecule¹³¹. With this in mind, it is important to consider payload release rather than simply drug delivery when designing a therapeutic nanodrug.

1.6 Controlled release liposome systems

One of the most important concepts behind liposomal drug delivery is to improve the delivery of the payload to the specific site of action. In terms of chemotherapeutics systems, it is important maintain the drug intra-liposomally during delivery, to reduce side effects relating to toxicity of the free drug. It is also important to reach high concentrations of the drug in the tumour site, which requires release of the drug from the liposome. This called researchers to not only focus on inhibiting release of the payload during circulation by monitoring stability of the bilayer through release studies, but to also induce release at the target site. This forces researches to forge a fine balance between stability and triggerability. Through the design of lipid compositions which would respond to triggering stimuli this was made possible, issuing in a new generation of liposomes. **Table 1.2** highlights mechanisms which have been exploited for this purpose. There is a wide range of mechanisms that have been developed to facilitate the availability of the payload to the target cells. These triggering mechanisms can be split into two main groups: a) triggering in response to conditions of the tumour microenvironment, and b) response to conditions generated through external induction. Endogenous triggering mechanisms can involve a number of different stimuli. pH sensitive PEG linkers enhance uptake of liposomes as a result of PEG unsheathing in the low pH of the tumour stroma^{132,133}. Acidification of endosomes following vesicle pinocytosis/endocytosis induces endosome lysis through a number of differing mechanisms^{134,135}. The use of enzyme sensitive liposomal compositions have also been used to trigger release both extracellularly¹³⁶ and cytosolically¹³⁷. External triggering mechanisms have successfully been used to induce release via a number of different mechanisms. The use of UV responsive lipid constituents can induce rupture of liposomal bilayers resulting in release¹³⁸. Gas filled liposomes allow targeted release under ultrasound applications as a result of an internal cavitation of the liposomes¹³⁹. Otherwise the majority of liposomes have been designed to release in response to heating of the system which is possible through a number of mechanisms. Thermosensitive liposomes comprised of low T_m lipids had been shown to be effective, externally triggerable, drug delivery vehicles since the late 1970's¹⁴⁰. The use of SPIONs based on iron oxide have been used in combination with an external magnetic field which rapidly alternates in the range of 360kHz inducing vibrations and subsequent heating. Coupled with thermosensitive liposomes this allows molecularly targeted heating to induce payload release¹⁴¹. External water-bath mediated heating, radiofrequency ablation (RFA) or high intensity ultrasound (HIFU) can be used to induce membrane destabilisation mediated by a number of constituent elements including peptides^{142,143}, polymers¹⁴⁴ or intrinsic lipidic components¹⁴⁵.

Table 1.2 Triggerable liposomes designed for controlled payload release

Responsive element	Trigger	Payload	Mechanism	Outcome	Ref
pH sensitive PEG linkage	Low pH of 5.5 in the tumour microenvironment	DOX/ Plasmid DNA	Unsheathes PEG enhancing cellular internalisation	Improved B-Lymphoma cytotoxicity	¹³² ¹³³
pH sensitive peptide modification	Endosome acidification	Mastoparan	peptide fusion with endosomal bilayer releases payload into cytoplasm	Increased cytosolic cyt C	¹³⁴
pH sensitive Gal modified lipoplexes	Proton sponge effect from endosome acidification	Plasmid DNA	Surface galactose acts as proton sponge inducing endosome rupture	Improved hepatocyte gene delivery	¹³⁵
Redox sensitive S-S-DNA lipoplexes	Cytosolic enzyme reduction	Plasmid DNA	Enzymes reduce lipids inducing reorganisation and releasing DNA	Improved transgene expression	¹³⁷
MMP9 sensitive lipopeptide	MMP9 cleavage of bilayer associated lipopeptide	Carboxyfluoroscein	MMP9 cleaves lipopeptide head destabilising bilayer	CF release in presence of MMP9 only	¹³⁶
SPION modified magneto-sensitive	Alternating magnetic field causing SPION based heating	Pyranine dye	Heating induces polymer dehydration based membrane destabilisation	Dye release under alternating magnetic field	¹⁴¹
UV-sensitive diacetylene-lipid	UV induces lipid polymerisation	DOX	Photopolymerisation of lipids compromised bilayer structure inducing release	DOX released under UV irradiation	¹³⁸
Ultrasound sensitive lipobubbles	Ultrasound induces bubble cavitation	DOX	US facilitates cell uptake via sonoporation, and cavitation causes collapse and release	Increased survival and tumour DOX uptake	¹³⁹
ELP thermosensitive peptide modification	External heating causes ELP precipitation	DOX	ELP aggregation destabilises bilayer under heating	ELP dependent DOX release	¹⁴³
L-Zipper thermosensitive peptide modification	External heating causes L-Zipper conformational change	DOX	L-Zipper stabilises membrane but opens central pore under heating facilitating DOX release	Stabilisation at 37°C and facilitation of release at 42°C	¹⁴²
Thermosensitive PNIPAM polymer modification	Heating causes polymer shrinkage and deprotection of bilayer	Calcein	PNIPAM shrinkage exposes membrane, inducing destabilisation	Stabilisation at 30°C and rapid release at 40°C	¹⁴⁴
Lysolipid enhanced thermosensitivity	Heating to T _m induces lysolipid mediated pore stabilisation	DOX	At T _m , lysolipid stabilises grain boundaries facilitating DOX release	Rapid DOX release at 42°C in presence of Lysolipid	¹⁴⁵

1.6.1 Thermosensitive Liposomes

Considering the aforementioned studies using unPEGylated liposomes, and the issuing in of the era of Stealth® liposomes, the amalgamation of the two was an exciting prospect for cancer therapy. DPPC had been well characterised as the low temperature thermosensitive lipid of choice with a T_m close of 41.3°C to 41.9°C. DSPE-PEG₂₀₀₀ became the PEGylated lipid of choice following the developments in the field⁴⁴. The attraction of this temperature of phase transition is the ability to be above physiological temperatures, but below temperatures which may risk damage to tissue through protein denaturation, to reduce healthy tissue damage, and increased tumour tissue necrosis. Tumour thermal ablation also risks pneumothorax, tissue infection and potential haemorrhage¹⁴⁶. At 42°C, the tissue will not be damaged, and increased bloodflow coupled with vasodilation allows enhanced permeation of the liposomes into the tumour tissue.

The next question was which chemotherapeutic to encapsulate for this mechanism. Through the discovery of the ammonium sulphate gradient doxorubicin loading protocol¹²², it was possible to load close to 100% doxorubicin at therapeutic concentrations. At temperatures above the DPPC T_m , the bilayer once again becomes permeable, disrupting the gradient which favoured loading allowing release of the drug. Pushing forward with the doxorubicin encapsulating stealth liposome approach, groups focused on a composition with rapid release dynamics at the desired temperature of 42°C to target the tumour vasculature. They did this by incorporating the lipid MSPC, known as a phospholipid comprises a single acyl chain which results in a conical rather than cylindrical shape as seen in the aforementioned diacyl phospholipids. As a result of this shape, the lysolipid associates at grain boundaries between lipid populations, stabilising pore formation at the T_m , accelerating doxorubicin release¹⁴⁷, as depicted in **Figure 1.9**. The low temperature sensitive (LTSL) formulation was tested *in vitro*¹⁴⁸ against a more rigid DPPC:HSPC:Chol:DSPE-PEG₂₀₀₀ tradition thermosensitive liposome (TTSL) with a more gradual release profile as previously characterized *in-vitro*¹⁴⁹. The *in vivo* results for the LTSL liposome showed a substantially improved effect in terms of complete response over the TTSL when heated to 42°C with no effect observed when heated to 34°C. None of the treatment

groups showed morbidity, with most mice gaining weight post treatment. The LTSL was coined as ThermoDox[®] and showed efficacy in human trials for breast cancer recurrence at the chest wall with a total target lesion response rate of 45%¹⁵⁰. Limited side effects were observed, the most common being grade 3, leukopenia and grade 2 neutropenia reversible through g-CSF treatment. Myelosuppression is an indication of either the liposome's transit into the RES and bone marrow, which has been addressed with PEGylation, or poor stability resulting in release of free doxorubicin into the circulation. The ThermoDox[®] formulation has poor stability in 50% mouse serum at 37°C and at 42°C in HBS as is tested later in this thesis. This therefore called for the development of a new thermosensitive liposome, with better serum stability at physiological temperatures, but also with release triggerable at 42°C. By increasing the serum stability of the system, it is less likely to produce doxorubicin related side-effects such as myelosuppression and cardiotoxicity. However this may be at the

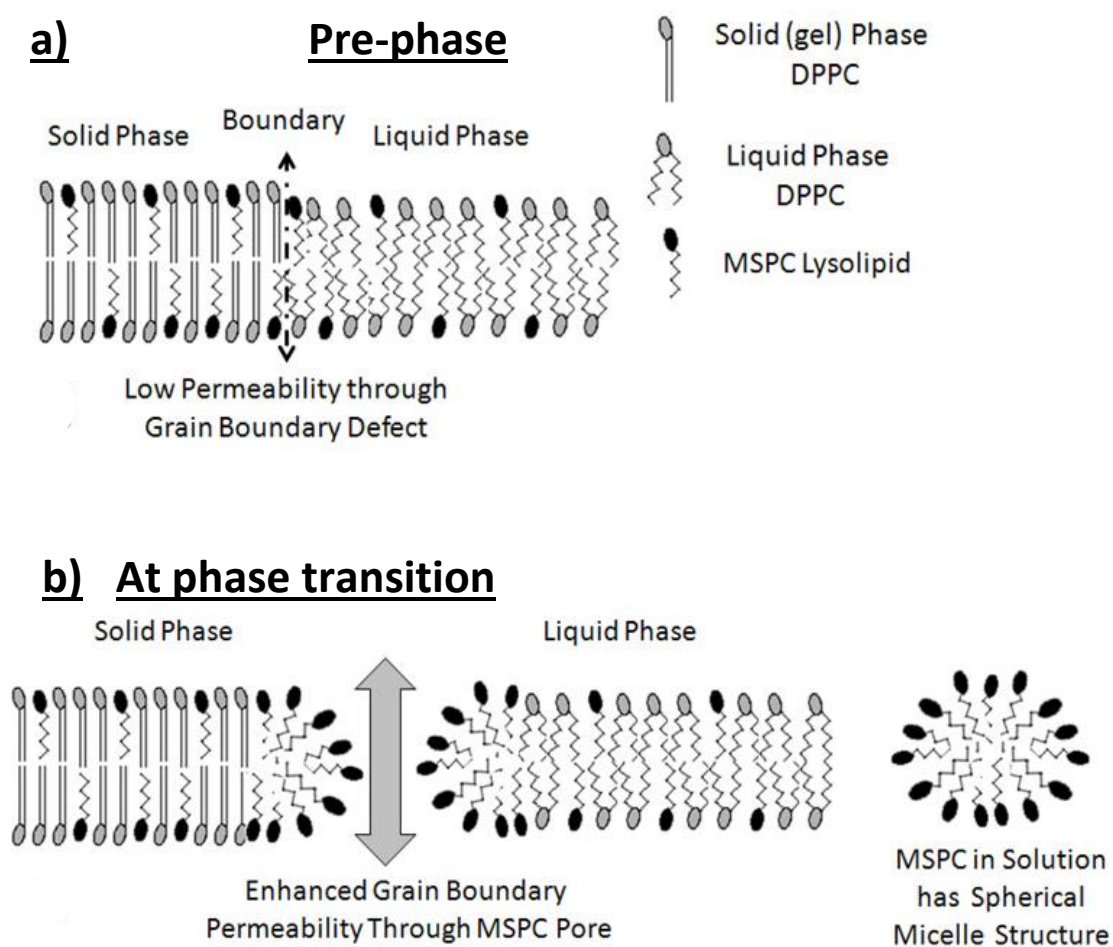


Figure 1.9 The mechanism of enhanced grain boundary permeability through the use of pore-stabilising MSPC in the ThermoDox[®] formulation liposome. **a)** stable bilayer pre-phase transition, **b)** rapidly stabilised pore formation at phase transition. (Adapted

expense of a release profile favourable for tumour therapy. This provokes the investigation into other temperature sensitive elements, which may increase the release profile without decreasing the serum stability.

1.6.2 Theranostic liposomes

Theranostic as previously mentioned is a coalescence of the terms therapeutic and diagnostic, and serves to describe a new generation of medicine in which liposomes are very much included. The potential for a medicine to both diagnose and treat bodes for a much more effective cancer therapy. If one was able to monitor the liposomal delivery of a drug to the site of a tumour, and trigger its release at the point of peak tumour accumulation, this will allow the peak potential to be gained from the therapy¹⁵¹. Building on this basis, with the further development of liposome technologies, it can be possible to incorporate a mind-boggling array of different modalities and functions into a single treatment. Liposomes as we know are highly versatile platforms, which have never been limited strictly to therapeutic ends. The additional non-lipid components range from quantum dots¹⁵² to SPIONs for magnetoliposomes¹⁵³ along with an extensive range of other metallic nanoparticles^{154,155}, dyes^{90,156}, photosensitisers¹⁵⁷ and radiotracers. For the effective upgrade of a liposomes to a multimodal theranostic, there are many factors to consider. The charge of the component, method of incorporation, toxicity, effect on bilayer stability and desired function are but a few. A number of theranostic systems are in development with *in vivo* applications as displayed in **Table 1.3**.

The most predominant drug encapsulated is DOX, most probably as a result of its effective loading mechanism and release upon bilayer compromisation through destruction or phase transition. The next class of therapeutic element most prominently used are PDT photosensitisers which induce cell death through the generation of cytotoxic singlet oxygen under irradiation¹⁵⁸. Due to the low fluorescent properties of these elements, they can be used for optical imaging as well as therapy, however the wavelengths and optical fluorescences do not provide enough light for very effective imaging. Visudyne®, liposomal verteporfin is an example of an approved liposomal photosensitiser for the treatment of age related macular degeneration¹⁵⁹. Peptides and nucleic acid based therapies have also been used successfully along with imaging agents.

There is a wide variety of imaging elements which have been trialled, utilising several different imaging modalities alongside therapeutic entities¹⁶⁰. Gd³⁺ is a popular MRI contrast agent and constitutes one of the first widely used agents Magnevist®. Gd³⁺ ions are highly

toxic, but when chelated to DTPA or DOTA, are stable and relatively safe¹⁶¹. Their chelation to these molecules also allows ligation to nanoparticles such as phospholipids¹⁶² making it a versatile label. Quantum dots are highly fluorescent nanocrystals, ubiquitous in the field of optoelectronics, and have been used to label liposomes allowing the use of IVIS systems to track them *in vivo*. The wide selection of these entities and narrow spectral bands allow their use alongside other optical agents such as dyes for cell labelling and *in vivo* applications¹⁶³. Radionuclides have long been used to tag distinct molecules within liposomes and are a near essential tool for truly quantitative biodistribution studies⁷⁸. ¹⁸F, ⁶⁴Cu and ^{99m}Tc can be incorporated into liposomes and act as highly sensitive PET tracers. Combined with CT or MRI, these elements provide excellent temporal and spatial information of transport through the body, and can even provide functional information when targeted to activated peptides⁷⁹. Dyes such as rhodamine and IRDye can be easily conjugated or incorporated into liposomes and allow detection through the means of fluorescent imaging.

Table 1.3 Theranostic liposomes designed for cancer applications

Drug	Diagnostic	Imaging Technique	Application	Outcome		Ref
				Therapeutic	Diagnostic	
DOX	Gd ³⁺	MRI	<i>In vitro</i>	10% Improved cell killing over DOX	41% increase in T ₁ relaxivity	164
DOX	IRDye-DSPE, Gd ³⁺ , ⁶⁴ Cu & ^{99m} Tc	Optical, PET & MRI	<i>In vivo</i>	Unreported	Trimodal Imaging of tumour accumulation	165
Suicide gene	Quantum Dot	Fluorescent	<i>In vivo</i>	Cessation of tumour growth	Imaging of Tumour accumulation	166
DOX	SPION	MRI	<i>In vivo</i>	Reduction in tumour growth	Imaging of tumour accumulation	167
siRNA (Survivin)	Gd ³⁺ & Rho-DOPE	MRI & Optical	<i>In vivo</i>	Reduction in tumour growth & surviving RNA	Imaging of tumour accumulation & fluorescent cryosection	168
DOX	ICG	MSOT	<i>In vivo</i>	Unreported	Imaging of tumour accumulation	90
DOX	ICG	Optical	<i>In vitro</i> & <i>in vivo</i>	<i>In vitro</i> cell killing under heating	<i>In vivo</i> imaging of tumour accumulation	169
ICG	ICG	Optical	<i>In vivo</i>	PDT mediated retardation of tumour growth	<i>In vivo</i> imaging of tumour accumulation	170
siPLK1	AuNR ₇₈₀ & NIR-787	MSOT & Optical	<i>In vivo</i>	Increased apoptosis visualised by TUNEL	Imaging of tumour accumulation & fluorescent cryosection	88
Benzoporphyrin	Benzoporphyrin	Optical	<i>In vivo</i>	Near cessation of tumour growth	Imaging of uptake via IVIS	171
Naphthalocyanine	Naphthalocyanine	Optical	<i>In vivo</i>	Increase in tumour necrosis	Not displayed	172
Zn-phthalocyanine	Zn-phthalocyanine	Optical	<i>In vivo</i>	Increased damage to tumour circulation	Imaging of tumour uptake	173
APT _{EDB} peptide	Rhod	Optical	<i>In vivo</i>	Retardation of tumour growth	Imaging of tumour uptake	156

The cyanine dye ICG has successfully been used in liposomes alongside therapeutic elements for both fluorescent imaging as well as photoacoustic such as MSOT, due to its previously described aptitude as a contrast agent resulting from its photothermal properties. ICG is the only FDA approved¹⁷⁴ near infra-red absorbing dye. It is amphiphilic and although not highly soluble in high salt buffers, absorbs well in hydrophobic environments. Its low toxicity has resulted in its use in liver function tests for sufferers of severe cirrhosis¹⁷⁵. It has so far been used in liposomes for imaging purposes and only once for therapeutic¹⁷⁰, and has been present in theranostic systems just a couple of times^{90,176}. As well as imaging potential, ICG is a photosensitizer producing singlet oxygen as well as concentration dependent heat generation upon excitation. This gives ICG on top of imaging, both photodynamic (300 μ J/pulse of a single band 804 nm¹⁷⁰) and photothermal (808 nm 1W continuous wave radiation¹⁷⁷) properties¹⁷⁸. The combination of PTT (808 nm 1W for 1 minute) using free ICG (5 μ M) and doxorubicin has a significant effect on cancer cell sensitisation to doxorubicin¹⁷⁹.

In combination with multispectral optoacoustic tomography imaging, it has been possible to carry out live high spatial resolution imaging of the circulation dynamics of tumours providing information about its heterogeneity¹⁸⁰. The imaging resolution is even more notable as upon intravenous injection, ICG rapidly binds plasma proteins such as albumin and lipoproteins and is cleared from the bloodstream. Considering the efficacy of MSOT imaging using free ICG, the potential imaging capabilities of liposomal ICG with the benefit of extended circulation times are exciting. Liposomal ICG is a fairly novel idea, with just a few publications reporting it. They have been used for imaging lymphatic function with fluid non-thermosensitive liposomes⁸⁷ *in vivo* tumour imaging with thermosensitive formulations¹⁸¹, imaging of choroidal angiogenesis with cationic liposomes¹⁸², and lipid grafted ICG for tumour imaging¹⁷⁸.

Chapter 2

2 Project aims and hypotheses

Cancer progression is directly proportional to its lethality, and thus requires fast and effective intervention for successful treatment. This translates to rapid treatment as well as accurate imaging for monitoring of disease progression and therapeutic response. Theranostics are systems which carry both therapeutic and imaging qualities allowing one to simultaneously treat, monitor drug delivery and response to therapy on successive treatments.

The goal of this work was to develop a theranostic system using a liposome based nanocarrier. This liposome would have to both deliver active chemotherapeutics at a therapeutic concentration to the tumour site, but contain high enough levels of an imaging agent to allow successful imaging of the treatment and response.

2.1 Thermosensitivity

Thermosensitive liposomes release their payload in response to heating. The lipid DPPC is well characterised as a low temperature thermosensitive lipid of choice with a T_m close of 41.3°C to 41.9°C⁴³. Phase transition of this lipid population at this temperature opens up grain boundaries in the bilayer releasing the payload. Liposome bilayer constitution can be carefully designed to undergo phase transition at specific temperatures based on the combination of phospholipids selected. It is important to tailor liposomes to release at 42°C, as heating above this temperature risks damage to surrounding tissues through protein denaturation.

ThermoDox^{®183} is the most clinically advanced thermosensitive PEGylated liposome currently undergoing phase III clinical trials. It is a DPPC based liposome also incorporating the lysolipid MSPC, comprising a single acyl chain and a propensity toward stabilised pore formation at the T_m , accelerating doxorubicin release¹⁴⁷. The liposome when combined with radio frequency ablation (RFA) has shown a 58% increase in overall survival of HCC in comparison to RFA alone¹⁵⁰. Some side effects were observed, the most common being grade 3, leukopenia and grade 2 neutropenia. Myelosuppression is an indication of DOX uptake by the RES and bone marrow. This indicates poor colloidal stability resulting in release of free doxorubicin into the circulation. This was confirmed *in vitro* under incubation at 37°C in 50% mouse serum as reported in **Figure 4.3a**. This therefore called for the development of a new

thermosensitive liposome, with better serum stability at physiological temperatures, but also with release triggerable at 42°C.

The aims for the initial stage of this project, were to first increase the serum stability of the system, as it would be less likely to produce doxorubicin related side-effects such as myelosuppression and cardiotoxicity, and also increase the resultant DOX concentration in the tumour site. However this may be at the expense of a release profile favourable for tumour therapy. Thus the continuation of the work would seek to generate a number of liposomes of different compositions in order to better understand the relationship between composition and DOX release kinetics. The initial goal would therefore be the development of a liposome with a high serum stability at 37°C and a controllable release profile over an hour of heat treatment.

Aims 1

The first section of this project aimed to:

1. Improve upon the serum stability at 37°C of the most clinically advanced thermosensitive liposome ThermoDox®.
2. Gain tuneable control over the doxorubicin release rate at 42°C, through modification of the constituent lipid ratios.

2.2 Theranostics

The development of theranostic liposomes will follow the initial optimisation of the lipid composition of the therapeutic liposomal DOX, through the addition of the imaging agent ICG.

ICG is the only FDA approved¹⁷⁴ near infra-red absorbing dye. It demonstrates enhanced light absorbance in hydrophobic environments and presents very low toxicity. It is a powerful imaging agent when combined with the right modality, however it is rapidly cleared from the bloodstream following intravenous administration when unencapsulated in a nanocarrier, limiting its utility for cancer imaging. In combination with multispectral optoacoustic tomography imaging, nanoparticle encapsulated ICG has successfully been used

to carry out high spatial resolution imaging of the circulation dynamics of tumours providing information about their structural heterogeneity^{89,180}.

MSOT imaging works through near infra-red LASER irradiation of a tissue with ultra-short optical pulses. The light absorption by a near-infrared light absorbing, optoacoustic contrast agent results in thermoelastic expansion of tissues generating acoustic waves. It has been used in tissue imaging for resolving vascular contrast and the corresponding physiological changes particularly haemoglobin oxidation state. Introduction of ex/endogenous reporter agents such as fluorescent probes/proteins allows further propagation of the technique toward molecular imaging applications¹⁸⁴. The near infra-red region of the electromagnetic spectrum lies between 750 nm and 1400 nm. Biomedical imaging in this light region is preferable due to the reduced scattering effect observed from chromophores such as melanin and haemoglobin¹⁸⁵, resulting in the highest level of tissue transmittance of this wavelength specifically in the region of 800 nm. MSOT detection of absorbance depends on many factors, examples being depth of target and tissue density. An OD of 1.25/12.5 mM liposomes has been suggested as a minimum value for reliable imaging.

In what is already a niche field of ICG comprising liposomal therapeutics, the subsequent aim of the project is to develop a viable theranostic liposome. One which can encapsulate therapeutic concentrations of doxorubicin, and incorporate ICG at concentrations high enough for imaging purposes. The initial part of theranostic liposome development will determine the most effective method of ICG incorporation, and its effects on the physicochemical characteristics of a rigid formulation liposome. The liposomal lipid composition selected is based on the widely used and first FDA approved nanodrug DOXIL®/Caelyx^{®124}. This system was chosen due to its robust composition comprising HSPC:Cholesterol:DSPE-PEG₂₀₀₀, and its extensive history of development and clinical use^{94,123,186}. So far, ICG has been incorporated into the same lipid formulation through one methodology, however in the absence of therapeutic concentrations of DOX⁹⁰. The optimum protocol would incorporate the highest ICG concentration possible to allow detection of liposomes at low concentrations, giving an OD above 1.25/12.5 mM lipid, as well as encapsulating therapeutic levels of DOX. The imaging potential must subsequently be proven through *in vivo* imaging of the liposomes via MSOT, and an indication of its theranostic potential must be realised through validation of co-localisation of both ICG and DOX accumulation in a tumour model.

Aims 2

The second section of this project aimed to:

1. Identify the optimum method of incorporating ICG, the FDA approved near-infrared dye into a rigid formulation liposome based on DOXIL®.
2. Demonstrate the construct's efficacy as a theranostic agent through temporal imaging of its tumour accumulation through high-resolution MSOT imaging, and co-localisation of DOX through fluorescent imaging.

2.3 Thermosensitive theranostics and the photothermal trigger

The final part of this project aimed to combine what was learnt from the initial thermosensitive liposome design, and optimisation of ICG incorporation protocols to develop thermosensitive theranostic liposomal DOX. The optimum liposome construction and ICG incorporation protocol derived from the work with the rigid formulation liposome will be tested on a number of thermosensitive lipid formulations. The focus will be put on the system which shows resilience to *in vitro* incubation in the presence of serum proteins at 37°C over 24 hours, as well as tuneable release at 42°C. As with the rigid system, transit and co-localisation of both drug and imaging agent at the tumour site will be assessed *in vivo* to prove the efficacy of the system as a theranostic agent.

The property of ICG which is exploited by MSOT for imaging purposes, is the dye's propensity to generate heat in response to irradiation with light at the appropriate wavelength. This property has previously been exploited for a number of applications both pre-clinical and clinical¹⁸⁷⁻¹⁸⁹ for the purposes of thermal ablation based cytotoxicity, most often using 1W continuous wave 800-808 nm lasers and reaching temperatures up to 60°C. Thermal ablation risks damage to surrounding tissue and necrosis, whilst far surpassing the 42°C which has so far been used to induce DOX release in *in vitro* release assays.

Instead of using the liposomal ICG for tissue destruction, it could potentially be used as a photothermal trigger to induce DOX release from the optimised thermosensitive liposomes. Through careful temperature control and power optimisation with the right light source, it should be possible to maintain the heating to within the low temperature hyperthermia range, not surpassing 43°C, whilst inducing DOX release with molecular precision. Due to the concentration dependency of the heating effect, enough ICG must be incorporated for a final tumour concentration of ~5 µM. Assuming ~10% tumour accumulation this would equate to a 50 µM [ICG] of the injected dose. Thus the final part of this project will be to validate the use of ICG's photothermal properties as a trigger to induce DOX release from the thermosensitive liposomes.

The benefit of using the dye as a liposome heating source under irradiation is that it will heat the liposomes directly rather than heating the surrounding tissue, which is often the case with conventional hyperthermia sources and can induce drug release in healthy tissues. Based on the EPR effect, peak accumulation in the tissue will be in the tumour site rather than the surrounding tissue, and thus the most enhanced photothermia should occur there. Conventional sources of hyperthermia are either invasive, expensive and or inaccessible. Lasers of the required power cost about £1000, and with the development of radial arrays¹⁸⁵, can be used to deliver controlled doses of light over 2-3 dimensional axes. As well as imaging potential, ICG carries photosensitizer-like traits, producing singlet oxygen¹⁹⁰ as well as concentration dependent heat generation upon excitation. The combination of PTT (808 nm 1W for 1 minute) using free ICG (5 µM) and doxorubicin has a significant effect on cancer cell sensitisation to doxorubicin *in vitro*¹⁹¹ and *in vivo*¹⁹².

Aims 3

The final section of this project aimed to:

1. Identify the optimum method of incorporating ICG, the FDA approved near-infrared dye into a thermosensitive formulation.
2. Demonstrate the constructs efficacy as a robust theranostic agent through *in vivo* tumour accumulation assays, and co-localisation of both drug and dye.
3. Achieve laser induced ICG-based photothermia to induce DOX release whilst maintaining the temperature within the low temperature hyperthermia range.

Chapter 3

3 Materials and Methods

3.1 Chemicals

HSPC, DPPC and DSPE-PEG₂₀₀₀ were kindly donated by Lipoid, (Ludwigshafen, Germany). Cholesterol, ammonium sulphate, 4-(2-hydroxyethyl)-1-piperazineethanesulfonic acid (HEPES), sodium chloride, sodium hydroxide, doxorubicin hydrochloride, tetrahydrofuran, 8-Anilino-1-naphthalenesulfonic acid (ANS), 1,6-diphenyl-1,3,5-hexatriene (DPH), ferric chloride hexahydrate and ammonium thiocyanate were all purchased from Sigma-Aldrich (UK). Indocyanine green (ICG) was obtained from Pulsion Medical Systems (Germany). Chloroform, methanol and hydrochloric acid (HCl) were purchased from Fisher (UK).

3.2 Liposome preparation.

HSPC, Cholesterol and DSPE-PEG₂₀₀₀ were solubilised in a 4:1 ratio solution of chloroform and methanol (Fisher, UK), at a ratio of 56:38:6 and concentration of 12.5 mM in a round bottomed flask. The solvent is then evaporated via rotary evaporation at 40°C. The film is flushed with air to remove any residual solvent, prior to hydration at 60°C with ammonium sulphate buffer (250 mM, pH 8.5). All buffers are filtered through Millex-HA 0.22 µm filters (Millipore) and pH adjusted using either HCl (Fisher) and/or NaOH solution before use. Small unilamellar liposomes are then formed through either water bath sonication for 30 minutes (water bath sonicator, VWR, UK) or extrusion at 60°C, an established technique for attaining a defined size distribution of liposomes⁴². For the extrusion step, the liposome suspension is forced 5 times through an 800 nm pore size membrane (Whatman, UK), 5 times through a 200 nm membrane, and finally 10 times through a 100 nm membrane using 1 ml glass syringes (Hamilton, US) and a mini-extruder (Avanti, US). The external buffer is then exchanged from ammonium sulphate to HEPES buffered saline (HBS) comprising 20 mM HEPES and 150 mM NaCl solubilised in diH₂O and buffered to pH 7.4. This process was facilitated through gel filtration via a sephadex G-50 column (150 mm x 15 mm column, Biorad, UK) (Sephadex G-50 resin, Sigma-Aldrich, UK), hydrated with HBS. The liposome suspension is then reconcentrated using a Vivaspin® 20 centrifugal

concentrator, at 6000RPM. The liposomes are then loaded with doxorubicin for 1.5 hours at 60°C via the established ammonium sulphate salt/pH gradient⁵, at a lipid concentration of 12.5 mM and a 20:1 lipid:DOX weight ratio. The residual unencapsulated doxorubicin is then removed through Zeba column purification. The Zeba column is placed in a 15 ml conical centrifuge tube and centrifuged at 1'000 RPM for 3 minutes at 4°C. Following removal of the storage buffer, the Zeba column is then equilibrated with the solvent excipient to the liposome suspension. This process is repeated until a constant weight and flow through volume is achieved post centrifugation. The liposome suspension is loaded into the column, and spun once to collect the first fraction. An equal volume of buffer is then introduced and spun through the column to collect the second fraction. When pooled, the first 3 fractions will contain the majority of the liposomes (85%-100%). A Vivaspin® 6 centrifugal concentrator (Sartorius Stedim UK Ltd.) is then used to reconcentrate the liposomes back to the initial starting concentration at 6000 RPM. Error calculations referring to liposome characterisation represent the standard deviation between repeats (n>3).

3.2.1 Film insertion protocol:

In this protocol, the 200 µM ICG is introduced through solubilisation amongst phospholipids and cholesterol in chloroform methanol (4:1). The lipid-ICG film forms as a result of rotary evaporation, and is hydrated at 60°C with a solution of ammonium sulphate, and periodically vortexed to facilitate its resuspension. The suspension is then sonicated or extruded directly, as per the previously described downsizing protocols. The liposomes are then purified from the unincorporated ICG using the zeba column as previously described.

3.2.2 Freeze fracture protocol:

This protocol introduces ICG during the film hydration stage solvated in ammonium sulphate at an ICG concentration of 200 µM. The ICG is initially solvated in 5% dextrose, before addition to the ammonium sulphate buffer. The lipid suspension is vortexed intermittently over a 20 minute period, before transfer to cryogenic vials (ThermoScientific, UK). The suspension is then subjected to 6 freeze-fracture cycles whereby the vials are frozen through immersion in liquid nitrogen for 3 minutes, followed by thawing in a water bath at 60°C. The unincorporated ICG is removed

through size exclusion chromatography 1 hours post extrusion using a Zeba Spin Desalting as previously described.

3.2.3 Post insertion protocol:

In this protocol, the ICG is introduced in the final stages of DOX loading. The 12.5 mM liposomes are loaded with doxorubicin for 110 minutes at 60°C, followed by addition of ICG in 5% dextrose to attain a final ICG concentration of 200µM and incubated for another 10 minutes also at 60°C. The free ICG and doxorubicin are then purified from the liposomes using a Zeba column at 1000RPM for 3 minute cycles at 4°C. The volume passed through the column is 1.8 ml. The liposomes are then reconcentrated to the starting lipid concentration 24 hours post purification.

3.2.4 Reheat insertion protocol:

Liposome-DOX was prepared via the sonication protocol as previously described and then kept overnight at 4°C. The liposomes were then heated to 60°C before a solution of ICG in 5% dextrose was added. The ICG-liposome mixture was incubated for a further 10 minutes at 60°C. The free ICG is then purified from the liposomes using a Zeba column at 1000RPM for 3 minute cycles at 4°C. The volume passed through the column is 1.8ml. The liposomes are then reconcentrated to the starting lipid concentration 24 hours post purification.

3.3 Phospholipid quantification

Phospholipid quantification was carried out using the Stewart assay, which is a colourimetric assay used to quantify phospholipid concentration.¹⁹³ Stewart reagent comprises 0.1 M ammonium ferrothiocyanate, which is produced through the mixture of 27.03 g ferric chloride hexahydrate 30.4g of ammonium thiocyanate and 1 L of ddH₂O. To perform the assay, a sample of the liposome dispersion is 100 times diluted in a 1:1 mixture of chloroform:ammonium ferrothiocyanate. The mixture is then vortexed for 20 seconds, followed by 6 minutes of centrifugation at 1'600 RPM. The hydrophobic chloroform fraction is removed and absorbance is read at 485 nm by a Cary winUV 50 Bio spectrophotometer (Varian, USA).

3.4 ICG incorporation efficiency

ICG incorporation efficiency was calculated using UV/Vis absorbance at 794 nm to quantify following its dilution in DMSO. The initial ICG concentration was calculated before addition to the lipid/liposome suspension. The post purification sample was concentrated back to the initial lipid concentration and solubilised in DMSO.

3.5 Encapsulation efficiency

Doxorubicin encapsulation efficiency was measured by comparing the total doxorubicin fluorescence intensity of the post incubation liposome-doxorubicin mixture, before and after the unincorporated doxorubicin is removed via Zeba column as previously described. Pre and post-purification samples are first diluted 1:40 (sample:HBS). Liposomes are broken following the addition of 0.1% Triton X-100 (Sigma Aldrich, UK) and vortexing for 10 seconds to release the intra-liposomal doxorubicin for the quantification of total doxorubicin fluorescence. At a high concentration of doxorubicin, such as that which is intra-liposomal, auto-quenching occurs resulting in negligible levels of fluorescence. Once the intra-liposomal doxorubicin is released into the surrounding buffer, this quenching effect no longer occurs, resulting in strong fluorescence emission at 593 nm following excitation at 480 nm (slit 10/20 nm). 200 μ l of sample is read from a quartz cuvette using a LS 50B fluorescence spectrometer (PerkinElmer,UK).

3.6 Dynamic light scattering and laser doppler micro-electrophoresis

Dynamic light scattering is a modality used to detect the liposome diameter and size distribution in solution. The instrument used was a Zetasizer Nano ZS (Malvern, UK) with the orientation of the light detector at 173° to that of the incident beam, the instrument incorporates non-invasive back scatter technology. The sample is introduced into the machine in a polystyrene cuvette (Malvern, UK). Laser Doppler Micro-electrophoresis is a technique used to measure the zeta-potential of a dispersion of charged particles so readings are made following the sample's dilution in dH₂O. For the measurement of zeta potential using the same instrument the dispersion is introduced into a zeta capillary cell (Malvern, UK).

3.7 Doxorubicin release and retention

Quantification of the release of the liposome encapsulated doxorubicin in response to heat is important for the initial characterisation of the liposomes stability in response to their constitutional alterations. Release studies are carried out at 37°C to mimic physiological temperature. The environments in which the liposomes are treated are HBS and 50% CD-1 mouse serum (Sera Lab International Ltd. UK) the latter as a simulation of proteins present *in vivo* following intravenous injection. 1 mM doxorubicin-loaded liposomes are diluted 1:1 in serum and incubated at 37°C for 24 hours. At specific time points, 20 µl of the liposome dispersion are removed and diluted in a further 380 µl of HBS. Fluorescence intensity is then read as previously described (slit 10/20 nm) and quantified against the 0 minute and 60 minute with triton as the 0 % and 100 % release values. Error bars represent S.D. between repeats.

3.8 Transmission electron microscopy

Liposomes of different compositions were visualised with transmission electron microscopy (FEI Tecnai 12 BioTwin). Samples were diluted to 1 mM lipid concentration, then a drop from each liposome suspension was placed onto a Carbon Film Mesh Copper Grid (CF400-Cu, Electron Microscopy Science), and the excess suspension was removed with a filter paper. Staining was performed using aqueous uranyl acetate solution 1%. Operation of the TEM was carried out by Dr. Aleksandr Mironov of the University of Manchester FLS TEM department.

3.9 Fluorescence anisotropy measurements.

Liposomes were prepared and diluted to 0.025 mM then divided into two 4 mL aliquots. DPH solution in tetrahydrofuran (0.8 mM, 2.5 µL) or an aqueous ANS solution (10 mM, 4 µL) was mixed with the liposomes at 500:1 lipid/DPH or 25:1 lipid/ANS. To allow the probes to be incorporated, the samples were shaken at room temperature for 2 h then left overnight before starting measurements. Fluorescence polarization was then measured by fluorescence spectrometer equipped with automated polarizer and thermostatic cell holder connected to a water bath to control the sample temperature. For the DPH experiment, the anisotropy measurements were carried out

at an excitation slit of 10 nm and emission slit of 10 nm and excitation and emission wavelengths of 361 and 425 nm, respectively. ANS anisotropy was measured at excitation and emission slits of 20 and 395 nm and 476 nm excitation and emission wavelengths, respectively. Measurements were started at 25°C, and then increased gradually up to 70°C. The samples were equilibrated for at least 6 min after each temperature change.

Fluorescence anisotropy was then measured automatically by the fluorimeter based on the following equation:

$$r = \frac{IVv - Glv}{IVv + 2GIVh}$$

Where r is the fluorescence anisotropy and IVv and IVh are the emission intensity excited with vertically polarized light and measured with emission polarizer oriented in a parallel or perpendicular direction to the plane of excitation, respectively. G is an instrument specific factor calculated to correct the instrument polarization, which is equal to IHV/IHH , and obtained by measuring the vertically and horizontally polarized emission intensities after excitation with horizontally polarized light.

3.10 4T1 murine tumour xenograft

5-6 week-old female C57BL6 mice (15–20 g) were purchased from Harlan (UK Limited, U.K) allowed to acclimatize for 1 week and kept under a 12-hour light/dark cycle under steady temperature and humidity with access to food and water *ad libitum*. Mice were housed in groups of 5 with free access to water and kept at a temperature of 19–22 °C and relative humidity of 45–65%. Animal procedures were performed in compliance with the UK Home Office Code of Practice for the Housing and Care of Animals used in Scientific Procedures. All experiments were conducted with prior approval from the UK Home Office under PPL 70/7763.). 4T1 murine mammary carcinoma (ATCC, USA) was established by subcutaneous injection of 0.8×10^5 4T1 cells in a volume of 20 μ L of PBS bilaterally into each flank using 26G needles. The tumour volume was estimated by measuring three orthogonal diameters (a , b , and c) with calipers; the volume was calculated as $(a \times b \times c) \times 0.5 \text{ mm}^3$. The experiments were performed when the tumour volume reached 200 mm^3 . (This was carried out by Zahraa Al-Ahmady).

3.11 IVIS biodistribution imaging

The fluorescence of the DOX and ICG from the liposomes following injection of 200 μ l at a lipid concentration of 12.5 mM was measured with an IVIS Lumina fluorescent imaging system (Caliper Life Sciences). The wavelength used for DOX was at an excitation of 465 nm and for the ICG at 745 nm. (This was carried out by Zahraa Al-Ahmady)

3.12 Blood stability of [14 C]-DOX liposomes in vivo

In order to study liposome biodistribution and in vivo stability, all liposomes were loaded with DOX comprising [14 C]Dox at a 20:1 lipid:Dox weight ratio. Unencapsulated Dox and 14 C-Dox were removed as previously described. C57BL6 Mice ($n = 4$) were anesthetized by inhalation of isoflurane and injected via the tail vein with 200 μ L of the liposomes suspension (equivalent to 0.2 μ Ci 14 C, 2.5 μ mol of lipids/200 μ L, Dox 5 mg/kg) in HBS. The animals were anesthetized by inhalation of isoflurane and the body temperature of the mice was monitored with a rectal thermocouple. At different time points, the mice were bled by tail vein puncture and 35 μ L of blood was collected using heparinized capillary tubes. Blood withdrawn did not exceed 10% of the mouse blood volume per day. Mice were killed after 24 h post-injection by cervical dislocation. Total radioactivity in the blood was calculated based on the assumption that the total blood volume is accounting for 7.3% of the total body weight¹⁹⁴. The results were represented as the percentage of the injected dose (%ID). (Animal handling was carried out by Zahraa Al-Ahmady)

3.13 Blood radioactivity measurements

Blood samples were transferred to 20 mL scintillation vials and solubilized with 1 mL of Soluene-350 tissue solubiliser (PerkinElmer, UK), and shaken overnight at 55 $^{\circ}$ C. Before adding the scintillation cocktail samples were decolorized by adding 0.3 mL of 30% H₂O₂ and isopropanol as an antifoaming agent. Samples were shaken at 55 $^{\circ}$ C for 1–3 h to expel H₂O₂ before adding the scintillation cocktail. Samples were then mixed with 20 mL of Optiphase “Safe” scintillation cocktail (Fisher Scientific, UK) acidified with 0.7% (v/v) glacial acetic acid to eliminate any chemiluminescence. 14 C

radioactivity was quantified for each sample using LS6500 multipurpose scintillation counter (Beckman, USA).

3.14 Photothermal release experiments

Liposomes were diluted to a specified ICG concentrations and transferred to a transparent 96-well plate at a volume of 250 μL per well with a 50% mouse serum concentration. The plate was kept at a constant temperature of 37°C atop a hot plate with temperature control. Once reaching the correct temperature, the laser was engaged irradiating the sample for 5 minutes. The CW fibre coupled laser system (Laser Components UK) was initially aligned via its 10 mW 650 nm aiming beam, then set to a power density of 0.3w/cm² at a wavelength of 808 nm with a spot size 6.5 mm in diameter. The system was enclosed in a black foil protected fume hood fitted with an interlock safety system connected to the main beam of the laser. Following irradiation, samples were removed, diluted and fluorescence measurements at 593 nm following excitation at 480 nm (slit 10/20 nm) for comparison to the non-irradiated samples.

3.15 *In vivo* MSOT imaging

MSOT measurements were carried out using a whole-body mouse imaging MSOT system as previously described⁸⁹. Briefly, optical excitation was provided by a Q-switched Nd: YAG pulsed laser with a 10 ns pulse duration at a repetition rate of 10Hz. Light at a tuneable range of 680-900 nm wavelengths, was homogeneously delivered to the animal through a fibre bundle split into 10 output arms. The subsequent ultrasound signal that was generated, was detected by a 64 element transducer array in a radial orientation generating a central frequency of 5MHz, allowing acquisition of transverse plane images. The fibre bundle and transducer array were stationary, and the animal could be moved to acquire different imaging planes using a moving stage. Measurements were taken in a temperature controlled water bath at 34 °C for the purposes of acoustic coupling. The animal was kept dry using a thin clear polyethylene membrane attached to the sample holder. The animal imaging was performed under anaesthesia using 1.8% isoflurane in oxygen. Measurements were acquired along the animal, acquiring cross-sectional images of the tumour region. 20 averages were acquired per wavelength at 680, 710, 740, 770, 800, 830, 860 and 900 nm. Images

were acquired before and after intravascular tail vein injection of 200 μ L of liposome. Images following injection were acquired at different time points at 10 min, 1 h, 4 h and 24 h. Images acquired in advance to liposome administration were used as control measurements, to ensure accuracy of the spectral unmixing method to indicate the liposome's presence. All MSOT imaging experiments were undertaken by Dr. Antonio Nunes from the Technical University of Munich.

Chapter 4

4 Optimisation of the Composition of Thermosensitive Liposomes

4.1 Introduction

Scientists have exploited the facility of liposomes to encapsulate therapeutic and imaging entities, circulate and passively target areas of disease, greatly enhancing the therapeutic potential of their payload^{54,55,56}. Due to the EPR effect¹⁶, injected nanoparticles are preferentially uptaken and retained in tumour tissue as proven using radiolabelled liposomes¹⁵. Following substantial work and optimisation^{64,69,68}, the glycolipid DSPE-PEG formed of polyethylene glycol conjugated to DSPE was developed to improve circulation half-lives by reducing uptake by the reticuloendothelial system⁴⁴.

DOX a close relative of daunomycin¹¹⁹, is an effective and long established chemotherapeutic^{179,120,121}. However due to its lack of targeting as a free agent, it causes leukopenic and cardiotoxic side effects⁹². DOX was encapsulated into liposomes, significantly reducing the side effects them whilst greatly increasing the survival of the murine tumour model challenged over equivalent DOX concentrations⁹². Despite these improvements in safety, the liposome did not produce a clinical therapeutic improvement in terms of efficacy in prolonging overall survival in the intervention of metastatic breast cancer which was 21 months for liposomal DOX and 22 for DOX alone¹²⁷. Stabilising the circulation half-life of DOX through its encapsulation within a rigid, PEGylated liposome allows more drug to accumulate in the tumour site, but doesn't necessarily make it readily available to the cells of the cancer tissue itself. This beckoned the development of an environmentally responsive system which would act to retain its payload until its release is induced by an external stimulus.

Many release triggering strategies are under development¹⁹⁵, with the most clinically advanced system responds to low temperature hyperthermia to achieve controlled release. This refers to heating above physiological temperature of 37°C but below 45°C which risks tissue damage. through altering the membrane composition

from the rigid 55°C T_m HSPC:Chol:DSPE-PEG₂₀₀₀, to a more fluid system with a 41.3°C⁴⁹ T_m comprising DPPC:MSPC:DSPE-PEG₂₀₀₀. The use of low temperature hyperthermia was designed to fall into a window by which it is higher than the body temperature of the patient, but not so high that the heating would destroy the tissue which may lead to necrosis. The MSPC, a single acyl chain comprising phospholipid acts to stabilise pore formation upon phase transition facilitating DOX release¹⁴⁵ as displayed in **Figure 4.1**.

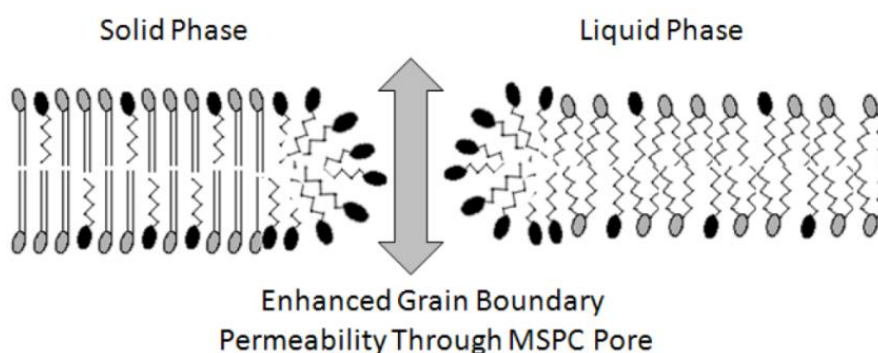


Figure 4.1 Mechanism of MSPC mediate pore formation at grain boundaries between gel and liquid phase lipid populations. Figure adapted from²⁸.

The strategy behind the use of such a rapid burst release upon the application of hyperthermia was to target the tumour vasculature, thus stemming the lifelines to the tumour and subsequently inhibiting tumour growth. This strategy has proven effective *in vivo* murine human tumour xenograft models¹⁴⁸, however failed phase III clinical trials against hepatocellular carcinoma as it did not reach the target of 33% increase in lifespan^{196,197}. Side effects can be attributed to the rapid release rate in the presence of serum proteins^{142,148}, as demonstrated during circulation under clinical trials¹⁹⁸. These side effects included immunosuppression, along with alopecia, a tell-tale sign of free circulating DOX and third degree burns resulting from the application of hyperthermia^{183,199}. Also the liposomes will not necessarily have the time to enter the cells before the trigger is pulled as the heating is carried out during infusion, thus releasing the drug in the vascular lumen, targeting the tumour vasculature but not penetrating deeply into the tumour tissue. Thus a strategy to stabilise the system

during circulation allowing time for the liposomes to extravasate into the tumour tissue may increase the local drug concentration whilst reducing observed side effects.

A number of strategies have been tested to modify the release kinetics of ThermoDox, changing the MSPC, and DSPE-PEG₂₀₀₀ content²⁰⁰. However, in this work the mono-stearoyl comprising MSPC was replaced with the di-stearoyl DSPC increasing the T_m and eliminating the pore stabilisation effect. The ratios between the DPPC and DSPC were modified, in order to modify the liposome T_m and further investigate the effect this had on the rate of DOX release under simulated *in vitro* physiological and low temperature hyperthermic conditions. This would result in the development of a repertoire of liposomes of differing release kinetics, which also show a higher stability at 37°C in the presence of serum proteins than the MSPC comprising system.

The final study investigated the inclusion of a chemical imaging moiety into the liposome. Following the systematic investigation into the modification of lipid ratios, and the incorporation of a thermosensitive peptide, the near infrared absorbing dye ICG was incorporated into the liposome, as displayed in **Figure 4.2**. Due to the amphiphilic and zwitterionic nature of the dye, one hypothesis is that it could act as molecular mortar. Theoretically by filling the defects within the bilayer, whilst interacting with the hydrophobic stearoyl chains, the phosphate and choline groups within the phospholipids, it should act to rigidify the bilayer, reducing the penetration of serum proteins into the bilayer at lower temperatures, and reduce the propensity for lateral movement upon phase transition. In addition to the bilayer rigidifying effect, it would also add an optical imaging element to the liposomes, generating a theranostic system. Upon successful incorporation into liposomes, the absorbance signal was found to be very stable and the OD greatly increased over unincorporated dye solubilised in buffer. It successfully stabilised the release profiles of the majority of the systems. The proposed final system for this study is exemplified in **Figure 4.2**.

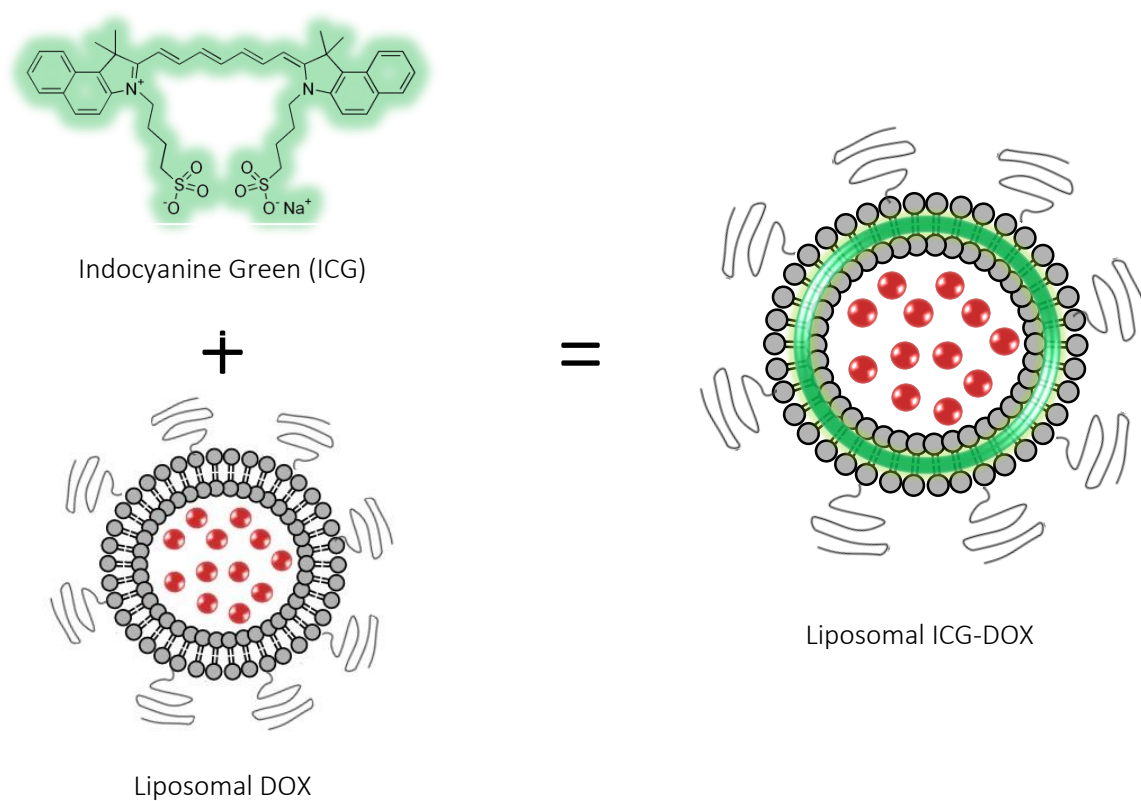


Figure 4.2 Combination of Liposomal DOX with ICG upgrading therapeutic liposomes to theranostic systems with which it would be possible to both image and treat cancer patients simultaneously.

4.2 Results

4.2.1 Probing Membrane Rigidity Through Modulation of DPPC:DSPC ratio

The concept behind the following study was to alter the composition of the constituent lipids in the low temperature thermosensitive formulation of the DPPC:DSPC:DSPE-PEG₂₀₀₀ platform. The hypothesis was that if the ratio of DPPC to DSPC was altered from the initial 90:10 as previously utilised¹⁴², it would be possible to alter the system's physicochemical characteristics. The specific characteristics would be, the transition temperature of the system, its relative bilayer fluidity and subsequent stability, in terms of doxorubicin release in HBS and 50% mouse serum at 37°C and 42°C in a controlled and proportionate manner. Through the development of the facility to alter the release profiles in such a controlled manner, it could be possible to tailor the liposome to release the doxorubicin at differing rates depending on the requirements of the treatment protocol. For example, a burst release profile would better target the vasculature of a tumour, and a more gradual release profile would allow deeper penetration into tumour tissue and more gradual dissemination of the doxorubicin throughout the lesion in question.

Looking to **Table 4.1**, the initial liposomes DPPC:MSPC:DSPE-PEG₂₀₀₀ (LTSL) and HSPC:Cholesterol:DSPE-PEG₂₀₀₀ (NTSL) were prepared using sonication. This method is often used for the preparation of these formulations of liposomes²⁰¹. From the representative liposomes displayed in the table, the LTSL are smaller than the NTSL following sonication with the average diameter residing around 70 nm in comparison to the 95 nm of the NTSL. This can be attributed to the higher rigidity of the NTSL at 60°C due to the cholesterol and generally higher transition temperature than that of the LTSL resulting in less dynamic dissociation of MLVs-SUVs. Another reason for the difference in size is the MSPC within the LTSL which is a monostearoyl comprised phosphocholine, rather than a distearoyl, such as the HSPC in its NTSL counterpart. This indicates that the tessellation of the lipids in the gel phase will be tighter on a steric level between the DPPC, MSPC and DSPE-PEG₂₀₀₀ over the HSPC, Cholesterol and DSPE-PEG₂₀₀₀, thus reducing the overall diameter of the liposome. The polydispersity

index between 0.20 and 0.25, is reflective of the sonication technique inducing more variation in the mean particle size than, for example, extrusion. The zeta potential of both liposomes lies between -5 mV and -10 mV due to the largely zwitterionic nature of the constituent lipids and the association of the sulphate ions with the choline in the phospholipid head groups. The doxorubicin loading efficiency was high for both formulations as expected (>80% EE).

Table 4.1 Characterisation of non-thermosensitive and thermosensitive liposomes

Formulation	Size (nm)	PDI	Zeta-Potential in AS ¹ (mV)	Doxorubicin EE ² (%)
DPPC:MSPC:DSPE-PEG₂₀₀₀ (86:10:4) LTSL	71.6	0.250	-9.4	83.6
HSPC:DSPC:DSPE-PEG₂₀₀₀ (56.3:38.2:5.5) NTSL	97.0	0.210	-7.0	93.3
DPPC:DSPC:DSPE-PEG₂₀₀₀				
90:10:5	139.1	0.073	-9.6	98.8
80:20:5	134.4	0.094	-9.3	94.7
70:30:5	136.8	0.073	-9.3	97.6
60:40:5	133.6	0.085	-10.4	96.8
50:50:5	141.0	0.100	-4.6	100.0

¹AS: Ammonium Sulphate pH 8.5 ²EE: Encapsulation Efficiency

The subsequent DPPC:DSPC:DSPE-PEG₂₀₀₀ based liposomes were prepared using the extrusion technique as previously utilised in our lab for the production of thermosensitive liposomes¹⁴². This technique is often used for the preparation of this composition of this basis of liposome, especially when anticipating its use *in vivo*²⁰². For assays that are not *in vivo*, moderate standard deviation in liposome particle size is not especially important, for example in the case of doxorubicin release studies. This is

due to the observation of release of DOX from the overall population and thus slight differences in release rate over the range of size will not have a substantial effect on the overall result. However *in vivo*, this characteristic can very much affect the liposome's function as a drug delivery vehicle, and its subsequent biodistribution. For example in the case of tumour perfusion, uptake by the RES system and vascular extravasation⁶⁶. This technique was therefore used to maintain consistency in the preparation method, which can also affect the physicochemical properties of the bilayer, in anticipation of future *in vivo* work.

With the extrusion protocol as previously described the liposome size remained 130 nm to 140 nm for all formulations. The polydispersity index remained between 0.07 and 0.1, as is expected by the more tightly controlled nature of size regulation depending on membrane pore diameter associated with this technique. The zeta potential slightly negative, between -4 mV and -10 mV and very high doxorubicin encapsulation efficiency of 95% to 100 %.

Differential scanning calorimetry (DSC) was used to monitor the effects of changing the DPPC:DSPC ration in the composition of the DPPC:DSPC:DSPE-PEG₂₀₀₀ composition liposome.

Considering the relative characterization observed in **Table 2**, with the size, surface charge and encapsulation efficiency showing negligible variance, the changes in the T_m of the system can be held accountable to the ratio alterations. DPPC has a transition temperature of 41.4°C and DSPC 54.9°C⁴³. It is thus expected that by decreasing the DPPC and increasing the DSPC contents of the liposome composition, a higher transition temperature would be achieved imparting a higher T_m and increased rigidity to the liposome.

As can be appreciated in **Figure 4.3**, as the DSPC content was increased from a 80:20 → 50:50 DPPC: DSPC ratio, as expected the T_m increased from 44.70°C at 80:20 to 46.43°C at 70:30, 47.20°C at 60:40 and finally 48.54°C at 50:50. This demonstrates the possibility of tuning the T_m of the system through altering this ratio.

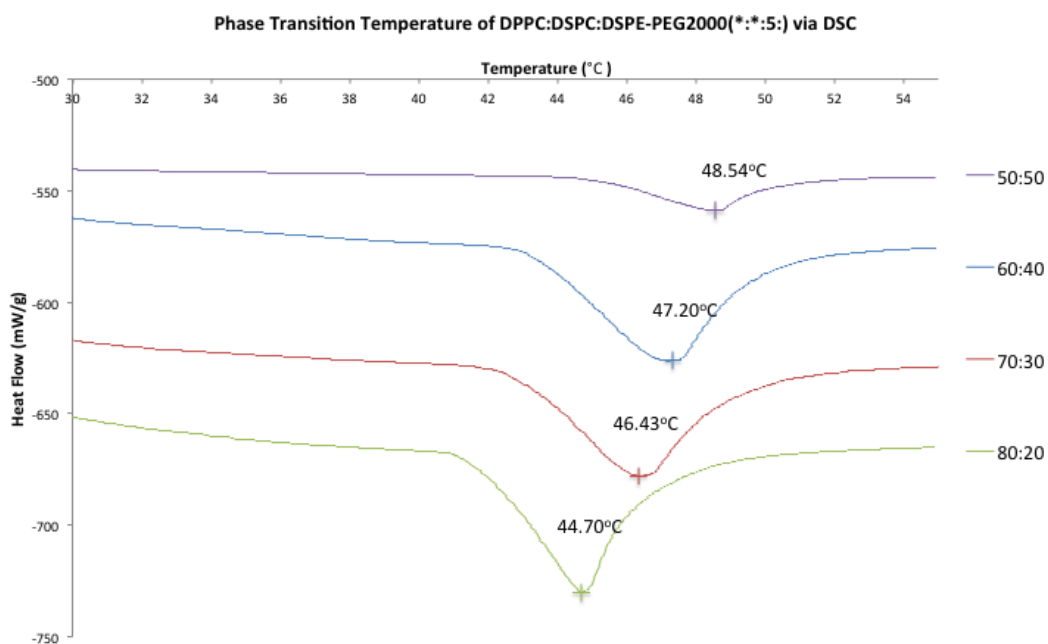


Figure 4.3. The variance in phase transition temperature of DPPC: DSPC: DSPE-PEG₂₀₀₀ based liposomes as the DPPC: DSPC ratio is modified.

The natural progression of this study was to contextualize the value this platform's tunability in the spectrum of thermosensitive doxorubicin encapsulating liposomes. This was performed through doxorubicin release studies at 37°C and 42°C in HBS and 50% mouse serum. **Figure 4.4** shows the characteristic release profiles of two of the most characterised doxorubicin encapsulating liposome compositions as a comparison to the system in question. **Figure 4.4 a) and b)** display the doxorubicin release profiles of the LTSL; DPPC: DSPC: DSPE-PEG₂₀₀₀ (86:10:4) composite, with a T_m of 41.3°C⁴⁹. In HBS, the system is stable at 37°C but shows a burst release profile at 42°C releasing almost 90% of its contents after 5 minutes. In 50% mouse serum, the liposome releases 100% of its encapsulate after 5 minutes at 37°C and 1 minute at 42°C. **Figure 4.4 c) and d)**, display the doxorubicin release profiles of the NTSL;

HSPC:Chol:DSPE-PEG₂₀₀₀ (56.3:38.2:5.5) composite, with a T_m above 55°C. In both HBS and 50% mouse serum, the system is stable at 37°C and 42°C.

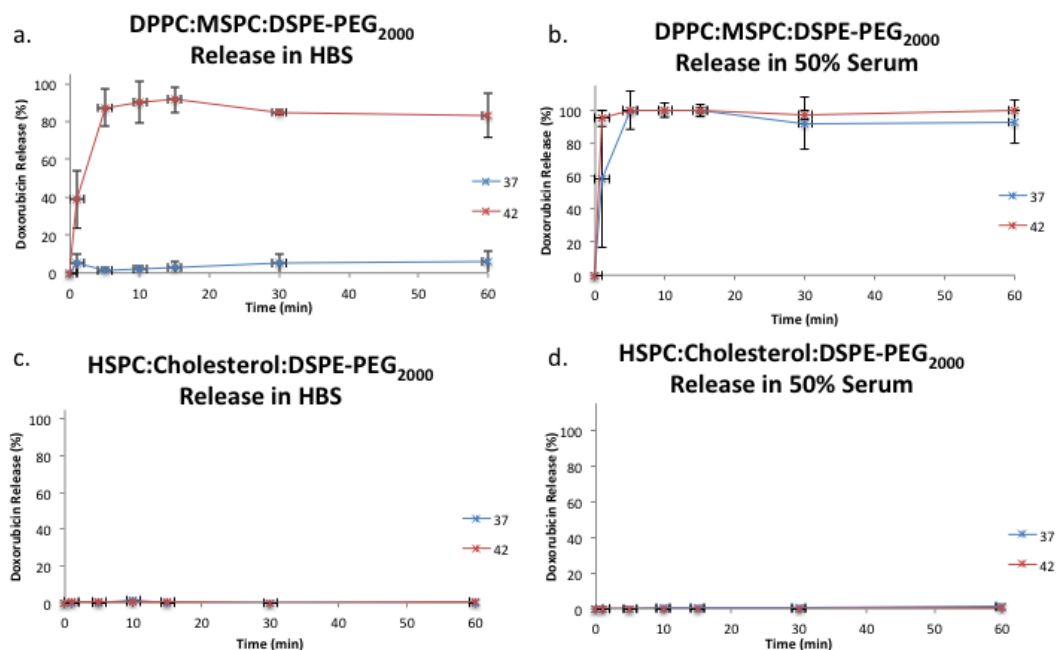
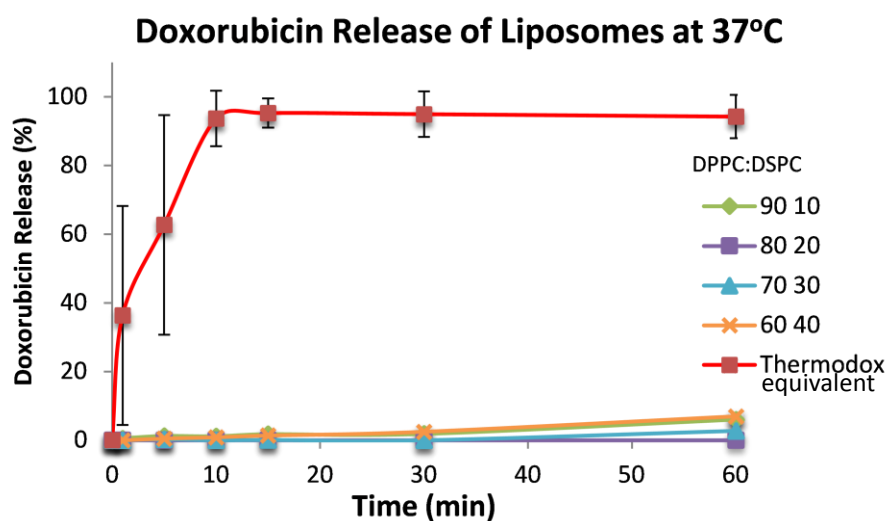


Figure 4.4 Doxorubicin release profiles at 37°C and 42°C for a) DPPC:MSPC:DSPE-PEG₂₀₀₀ in HBS and b) in 50% mouse serum, c) HSPC:Cholesterol:DSPE-PEG₂₀₀₀ in HBS and d) in 50% mouse serum.

With the profiles of **Figure 4.4**, in mind, the next step is to investigate the doxorubicin release profiles of the DPPC:DSPC:DSPE-PEG₂₀₀₀ platform. With the substitution of the pore forming monostearoyl MSPC with the distearoyl DSPC, the hypothesis is to increase the stability and release of the liposome over the DPPC:MSPC:DSPE-PEG₂₀₀₀ but retain more fluidity than that of the HSPC:Chol:DSPE₂₀₀₀. The resultant release profiles as displayed in **Figure 4.5 a)**, displays the stability of the most fluid system in question DPPC:DSPC 90:10 at 37°C in 50% mouse serum. In these conditions, only 7% release of the encapsulated doxorubicin is observable after an hour, with more rigid systems showing 5% (60:40) and 2% (50:50) respectively. **Figure 4.5 b)**, shows stabilisation of the system in an effect proportional to the increase of constituent DSPC within the system when incubated at 42°C in 50% mouse serum. In the DPPC:DSPC 90:10 liposome, 100% release of doxorubicin is observed after 5

minutes, whereas an increase in DSPC to a 70:30 ratio reduces this % release to just 43%, exhibiting 100% release after an hour. An increase to a DPPC:DSPC 50:50 ratio renders release after 5 minutes to just 11% with just 32% release after an hour.

a.



b.

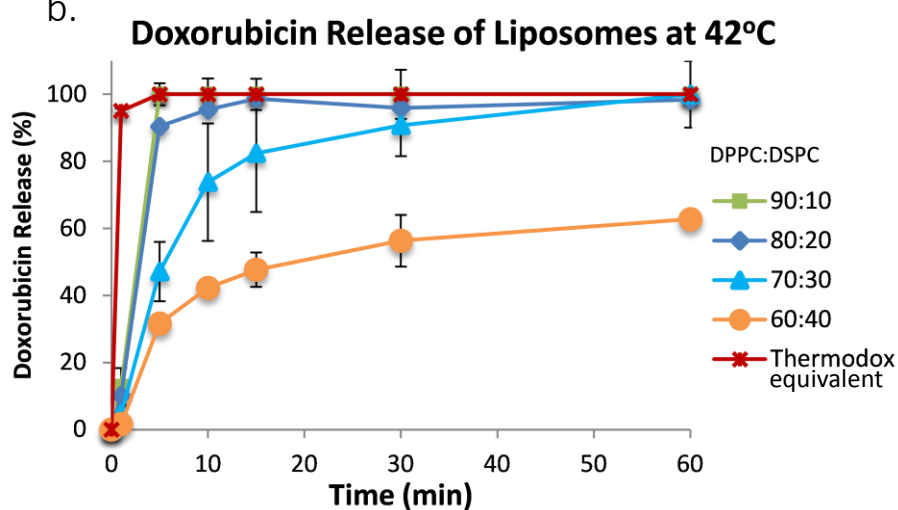


Figure 4.5. Doxorubicin release profiles of extruded DPPC:DSPC:DSPE-PEG₂₀₀₀ at differing DPPC:DSPC ratios represented in the legend at **a)** 37°C and **b)** 42°C in 50% mouse serum.

In conclusion, changing one of the constituent lipids, MSPC, from the DPPC:MSPC:DSPE-PEG₂₀₀₀, to DSPC, has provided the system with increased stability in terms of T_m and doxorubicin release at 37°C in 50% mouse serum. As a simulation for physiological conditions, it is important that the thermosensitive liposome does not release before it reaches its target site upon which it is triggered with heating to 42°C. This is an essential factor to control for its implications *in vivo*. Moving to the change in DPPC:DSPC ratio itself, through the increase in DSPC content, it has been possible to alter the T_m as well as the speed with which the doxorubicin leaks from the liposome, in a proportional manner.

Firstly, this provides vehicles for doxorubicin delivery which would theoretically be more stable at physiological conditions than previous thermosensitive liposomes.

Secondly this provides vehicles which release doxorubicin at different rates over an hour, which may be tested against each other to investigate preferential strategies in thermosensitive liposome based tumour therapies. This can be described as boost versus gradual release.

Thirdly, by developing several platforms displaying different levels of rigidity depending on the lipid ratio, it provides several bases from which one can develop more complex liposomes. This would allow easier countering of the destabilising/stabilising effects of future iterations, such as the incorporation of imaging agents or release triggering mechanisms.

4.2.2 Utilisation of sonication rather than extrusion for liposome preparation

To monitor the effect of the initial downsizing protocol and the resultant liposomes generated, sonication for 30 minutes at 60°C was used for initial liposome downsizing in place of extrusion. As can be observed in **Table 4.2**, the particle size generated through the use of sonication is much smaller than the extrusion protocol implemented. As expected the polydispersity index is higher due to the lack of membrane pores which narrow the size variability. The zeta-potential was measured at the end of the production protocol following buffer exchange to HBS resulting in a more negative surface charge due to the absence of choline-neutralising ammonium ions. Little difference was observed in the doxorubicin encapsulation efficiency.

Table 4.2 Characterisation of sonicated thermosensitive liposomes.

Formulation (DPPC:DSPC:DSPE-PEG ₂₀₀₀)	Size (nm)	PDI	Zeta-Potential in HBS (mV)	DOX EE (%)
60:40:5	81.0 ± 4.1	0.245 ± 0.02	-23.4 ± 0.9	97.4 ± 1.9
50:50:5	77.7 ± 1.7	0.228 ± 0.011	-22.9 ± 0.8	97.5 ± 3.5

The DOX release kinetics are substantially different in the sonicated liposomes in **Figure 4.6** in comparison to the extruded liposomes in **Figure 4.5**. At 37°C, the liposomes release 15% DOX after 1 hour, increasing and plateauing at 70% after 8 hours. At 42°C, the 50:50 system release 50% DOX after 5 minutes, 5% more than the extruded 70:30 system, eventually reaching 85% release after an hour. The 60:40 system displays a burst release profile, releasing 85% DOX in the first 5 minutes, reaching a plateau of 90% release after 30 minutes, much like the extruded 80:20 ratio system.

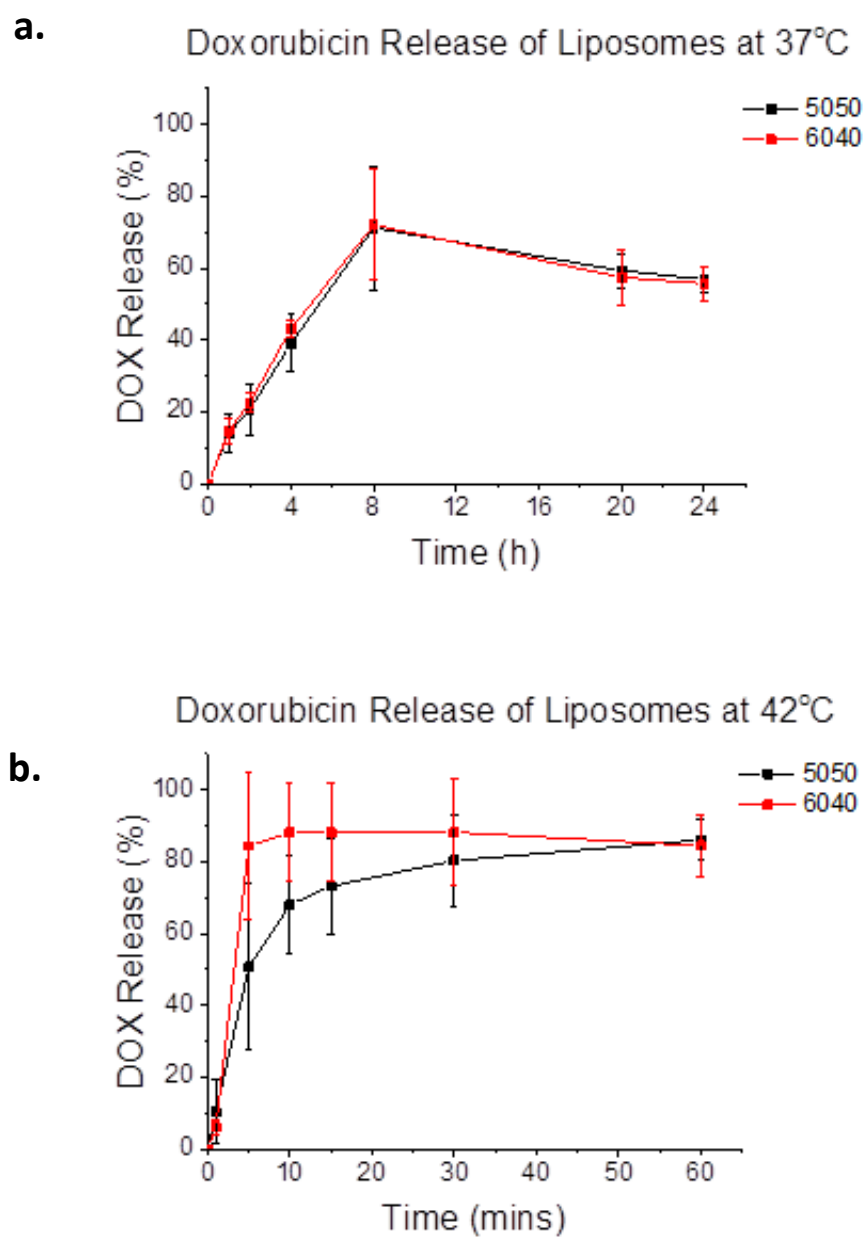


Figure 4.6 Doxorubicin release profiles of sonicated DPPC:DSPC:DSPE-PEG₂₀₀₀ at differing DPPC:DSPC ratios as represented in the legend at **a)** 37°C and **b)** 42°C in 50% mouse serum.

4.3 Addition of Indocyanine Green (ICG) as a bilayer stabilising and imaging agent

The scope of this study is that through the incorporation of ICG into the thermosensitive liposome, it will be possible gain temporal and spatial characterisation of the drug delivery to the tumour tissue in future *in vivo* studies. On top of the imaging potential, it will be possible to better optimise the temporal aspects of the induction of hyperthermia at the point at which peak liposome accumulation is observed at the tumour site, to attain the highest possible delivery of doxorubicin to the tumour. The understanding of the fluidity of the lipid composition in terms of doxorubicin release of the relative platforms tested provides an important basis to work from in tailoring the platform to suit the effects of the ICG incorporation.

4.3.1.1 Incorporation of ICG into the DPPC:DSPC:DSPE-PEG₂₀₀₀ (60:40:5) Liposome

The hypothesis for the initial part of this study, is that it will be possible to incorporate ICG into the bilayer of the chosen composition of liposome whilst retaining similar physicochemical characteristics and doxorubicin encapsulation efficiency. Liposomes were prepared via the extrusion protocol. This method of ICG incorporation is different to what has been previously reported in literature, for example encapsulation during film hydration¹⁸¹. The reasons for this are that ICG is more soluble in chloroform:methanol (4:1) than ammonium sulphate as notable from Figure 4.7. As the polarity of the solvent is reduced, the OD increases, which is a readout of the solubility and thus the extent to which the molecule interacts with the excipient media, allowing efficient absorbance of light. The peak at the ICG Amax in the region of 780-820 nm increased in comparison to the shoulder (H-peak) around 720-740 nm. This shows a reduction in aggregation. In highly polar conditions, the hydrophobic regions of the ICG find a more entropically favourable state by stacking upon each other which reduces the absorbance intensity, and affects a hypsochromic shift in the wavelength of light²⁰³. Film-hydration based ICG Incorporation will result in the ICG localising in the aqueous cavity, and is therefore likely to either be lost when the

membrane is compromised during the extrusion process, or to aggregate due to the intraliposomal AS. By mixing the ICG into the chloroform, methanol and lipid

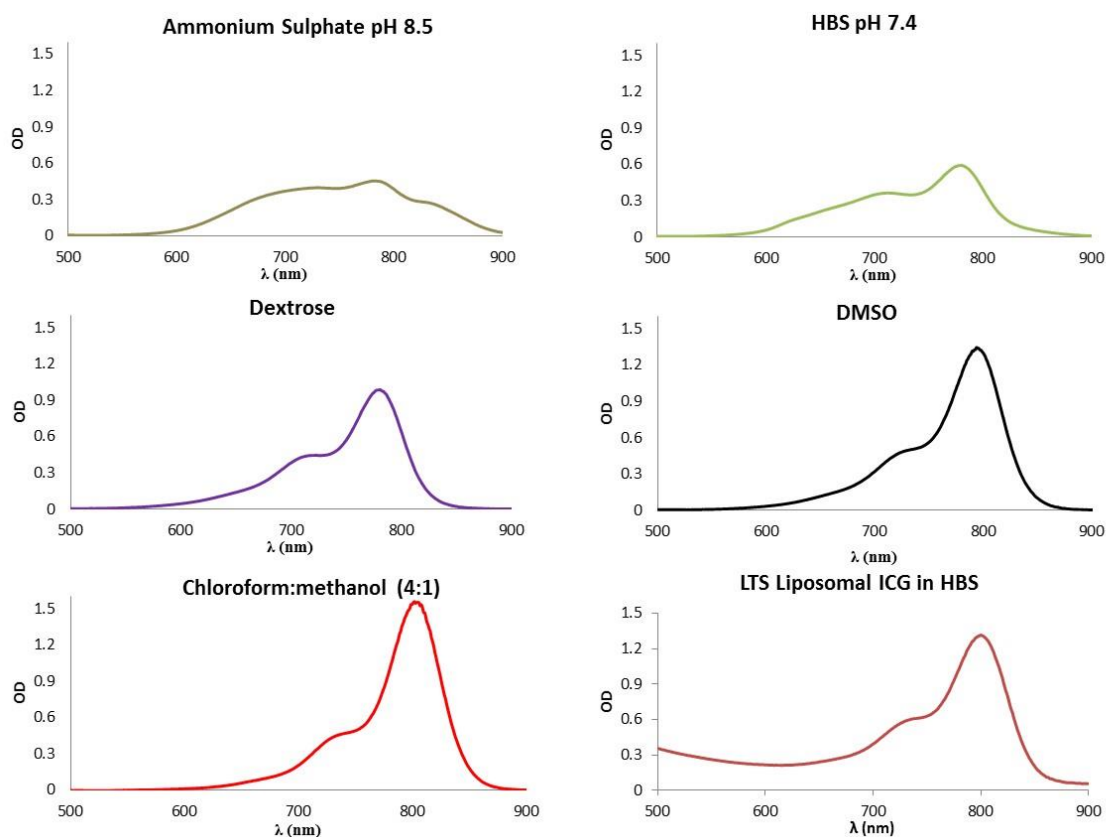


Figure 4.7 Optical spectra of 7.5 μ M ICG in various solvents.

mixture, the ICG will be less aggregated and thus should attain a tighter association to the lipids following film formation and is thus more likely to be integrated into the liposomal bilayer than through the encapsulation protocol.

Table 4.3 shows the physicochemical effects of ICG incorporation into the DPPC:DSPC:DSPE-PEG₂₀₀₀ (60:40:5) liposome at different ICG concentrations. This formulation of liposome was chosen due to the uncertainty over how the liposomal bilayer would react upon ICG incorporation, in terms of a stabilising or destabilising effect regarding doxorubicin release. This system was chosen for this pilot experiment and representative liposomes displayed, as its release profile appears about half way between the 90:10:5 LTS liposome and the HSPC:Cholesterol:DSPE-PEG₂₀₀₀ NTS liposome. At 200 μ M ICG, the size is 210 nm, which is higher than the usual 133 nm

observed with the plain liposome, and the PDI is 0.295, which is also very high for this protocol, which generally limits PDI to about 0.1. It appears that either the integration of the ICG or the presence of unincorporated ICG has destabilized the liposome bilayers leading to flocculation. The other concentrations of ICG incorporated displayed slightly smaller than normal with sizes of 115-133 nm and PDI of 0.13. The ICG incorporation did not affect the surface charge of the system, with all liposomes yielding about -12 mV. The ICG incorporation efficiency, following initial gel filtration/buffer exchange, was calculated at 68.2% for the 150 μ M system, 67.1% for the 100 μ M system and 69.3% for the 50 μ M system. This was carried out using absorbance at 793 nm, however it was not controlled for lipid loss.

Table 4.3 Characterisation of DPPC:DSPC:DSPE-PEG₂₀₀₀ (60:40:5) incorporating ICG

Size (nm)	PDI	Zeta-Potential (mV)	DOX Encapsulation Efficiency (%)	Initial [ICG] (μ M)	Final [ICG] (μ M)
210.2	0.295	-13.7	3.7	200	153.0
119.9	0.127	-10.3	2.3	150	102.3
133.3	0.133	-11.3	3.8	100	67.1
114.5	0.135	-13.8	3.8	50	34.7
133.6	0.085	-10.4	96.8	0	0

The most significant difference in physicochemical characteristics observed was the reluctance of each ICG incorporating system to encapsulate doxorubicin at 42°C over 2 hours. The encapsulation efficiency was between 2% and 4%. This is indicative of a stabilization effect of the ICG, which may have increased the system's T_m rendering 42°C no longer suitable for loading.

As hypothesised, it was possible to integrate ICG into the liposome, without grossly changing the size, PDI and zeta-potential for the 50 μ M-150 μ M ICG liposomes. However the presence of ICG at these concentrations did preclude doxorubicin

loading. The logical progression was therefore to investigate the differences in T_m between the systems incorporating different concentrations of ICG, using DSC. This serves to prove the hypothesis that the incorporation of ICG stabilises the liposome bilayer, raising the T_m , thus rendering the previously described doxorubicin loading protocols invalid. **Figure 4.8**, displays the calorimetry curves and the relative T_m of each system incorporating 0-150 μM ICG. The T_m did fall from 47.21 $^\circ\text{C}$ in the ICG free system to 46.69 $^\circ\text{C}$ in the 150 μM system, 46.89 $^\circ\text{C}$ in the 100 μM and 47.14 $^\circ\text{C}$ in the 50 μM system. The difference in terms of T_m is not high enough to explain such poor encapsulation efficiency due to too high an incubation temperature of 42 $^\circ\text{C}$, considering that the 70:30 system with a T_m of 46.43 $^\circ\text{C}$ could encapsulate 92.6% doxorubicin at 45 $^\circ\text{C}$ over two hours. This does not agree with the hypothesis that suggests the change in T_m to be the factor impeding doxorubicin encapsulation.

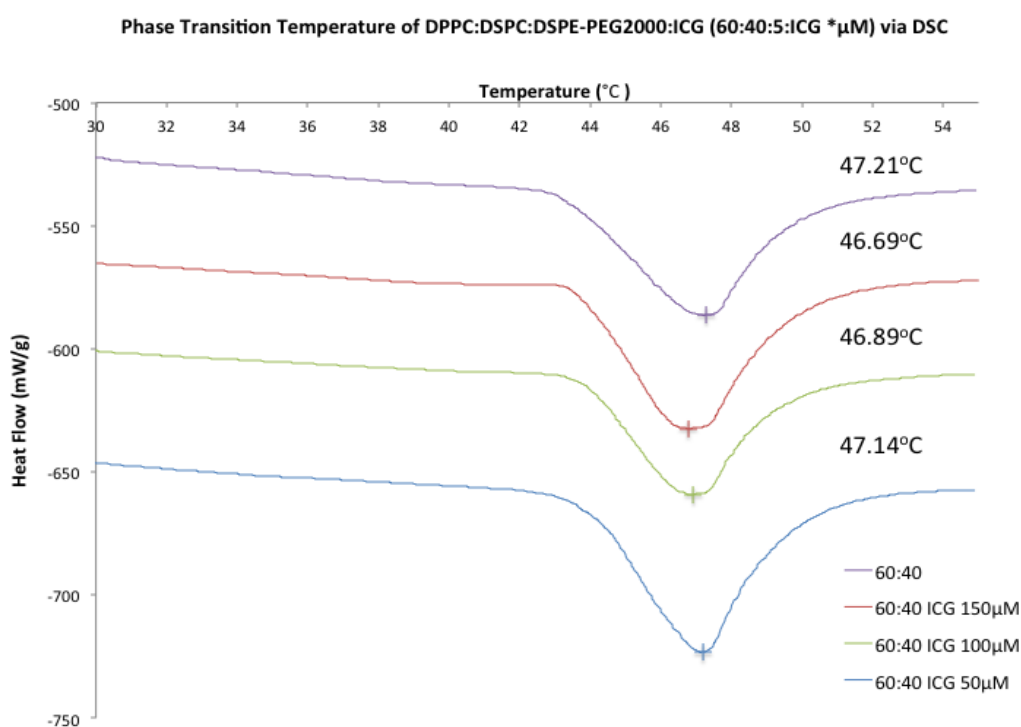


Figure 4.8 Variance in phase transition temperatures of the 60:40 liposome system when the ICG concentration is altered. 0 μM ICG $T_m=47.21^\circ\text{C}$ at 34.6 μM ICG $T_m= 47.14^\circ\text{C}$, at 67.1 μM ICG $T_m= 46.89^\circ\text{C}$ and at 102.3 μM ICG $T_m= 46.69^\circ\text{C}$.

Through the incorporation of ICG into the liposomal bilayer, the hypothesis is that the absorbance signal will be better retained over the ICG alone. The theory behind this is that ICG

is less likely to aggregate when incorporated into the bilayer as well as being less reactive with components of the surrounding medium. **Figure 4.9**, displays the absorbance spectra generated by the ICG when incorporated into liposomes at different starting concentrations. For the liposome-ICG systems spectra were taken at 4 days and 7 days following liposome preparation. What is important to note is that all of the ICG concentrations of the liposomes analysed have been corrected to 2.5 μM in order to compare the relative OD and optical stability in comparison to free ICG at the same concentration.

In **Figure 4.9 a)**, the 50 μM ICG liposome generates a characteristic ICG spectra after 4 days, with a well-defined peak at approximately 796 nm with an absorbance maxima of 0.57 and the characteristic shoulder at 740 nm after 7 days, the spectra is almost superimposable, with an absorbance maxima a fraction higher. In **b)**, the 100 μM ICG liposome displays a similar spectra, with a slightly broader peak and a shorter main absorbance peak in comparison to the shoulder, indicating slightly less ICG stability in the bilayer. A decrease in the difference between the peak and the shoulder is indicative of dimerization and eventual precipitation of the ICG. The absorbance maxima is 796 nm with a lower value of 0.47. The spectra for the liposome-ICG at 150 μM as observed in **c)**, displays a distinct difference in shape in comparison to the previous. Despite the superimposition of the spectra for the 4 day and 7 day values, the difference between the peak and the shoulder has significantly decreased along with the absorbance maxima showing a marginal blue shift to 785 nm and a value of 0.28. The blue shift is also indicative of a loss of ICG from the bilayer as it is closer to the absorbance maxima of free doxorubicin in HBS of approximately 780 nm. This progression continues in **d)**, where the difference has reduced to the extent that the shoulder and the peak are almost indistinguishable. The absorbance maxima is at 786 nm and the value is 0.26. The spectra corresponding to day 4 and day 7 are still however superimposable. Finally **e)**, displays the absorbance spectra for the free ICG at a concentration of 2.5 μM . As soon as the ICG was solubilized in HBS, the ICG displayed an absorbance spectra, the peak and shoulder shape of which was indicative of well dispersed ICG. The absorbance maxima is at 780 nm rather than at 796 nm as observed in **a)**, and the value is 0.32. After a single day, this value drops by over half, to 0.135, and after 5 days there is no distinguishable peak. After 11 days, a peak of 0.11 appears at 889 nm (J-peak), which is indicative of aggregation of the ICG²⁰³.

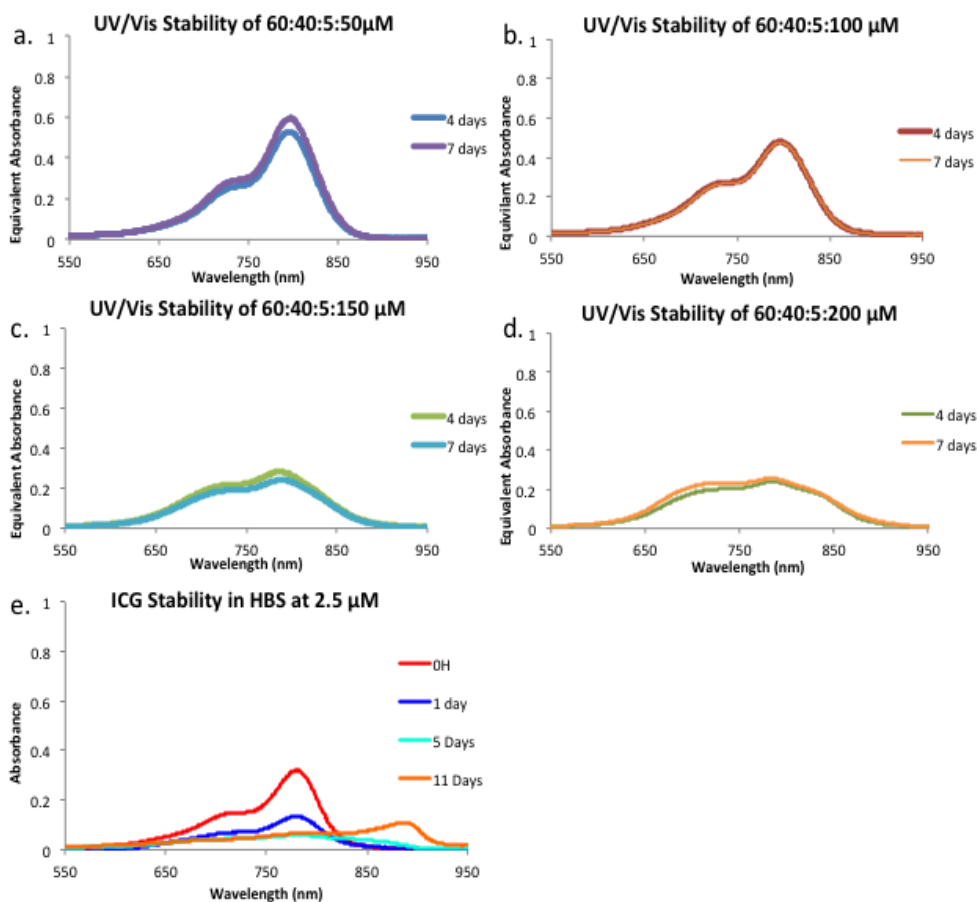


Figure 4.9 Stability of ICG absorbance spectra over a week in DPPC:DSPC:DSPE-PEG₂₀₀₀ (60:40:5) liposomes incorporating ICG in comparison to free 2.5 μM ICG in HBS. **a)** 50 μM initial [ICG] liposome **b)** 100 μM **c)** 150 μM **d)** 200 μM **e)** free ICG. (Absorbance was read at dilutions generating a final ICG content of 2.5 μM in order to compare between systems of varying final [ICG]).

What can be concluded from this study is that the incorporation of ICG at high concentrations into the 60:40 liposome, appears efficient with the ICG-lipid film integration protocol as previously described. The ICG does appear to sequester doxorubicin loading into the liposome, however it is not as a result of considerably altering the T_m of the system. Through incorporation of ICG into the liposome, it was not only possible to stabilise the signal to the extent of no loss of signal being observed between 4 days and a week after formulation, but it was possible to boost the absorbance to almost twice that of freshly solubilised free ICG, when read a week after liposome preparation. It was also observed that the liposome incorporating the lowest concentration of ICG showed the highest relative absorbance values whilst retaining the stability of signal over the temporal design of the assay.

Through phantom experiments, the detection limit for MSOT was found to be 0.3 μM ICG for the injected sample⁸⁹. This considered, 200 μM / 1ml of 5 mM liposomes or 200 nM ICG is excessive in terms the required amount of ICG for imaging using liposome ICG conjugate considering the hindrances observed in terms of doxorubicin encapsulation using such high concentrations. This brings the continuation of the study to consider lower concentrations of ICG for a future theranostic system.

4.3.1.2 Incorporation of Low Concentration ICG into differing lipid ratios of the DPPC:DSPC:DSPE-PEG₂₀₀₀ Liposome

Figure 4.9 a), demonstrates that 2.5 μM ICG when incorporated into a liposome gives an absorbance of at worst 0.26 and at best 0.57. With this in mind, an ICG concentration of 5 μM was trialled. The hypothesis of this study was that by reducing the ICG concentration, incorporating close to the bare minimum of ICG required for imaging, it should be possible to attain the required OD, reduce the adverse effect of the inability to encapsulate doxorubicin and hopefully minimise any potential problems that may affect the doxorubicin release profiles.

Table 4.4, displays some of the physicochemical characteristics of representative liposomes following incorporation of 5 μM ICG. As a follow on from the previous work carried out in 4.1, the same five different lipid ratios were chosen. Although little differences were seen in the characteristics displayed in **Table 4.1** with the ICG free systems at the same lipid ratios, this would not necessarily mean the same would occur with the ICG incorporating systems. However, it did. The size was consistent from 125-134 nm in size, the PDI was similarly consistent varying between 0.07 and 0.1. The zeta-potential was between -5.7 mV and -10.4 mV, and the doxorubicin encapsulation efficiency was very high, between 95% and 98%. The same doxorubicin loading protocol was used for the ICG incorporating liposomes as the plain ones prepared for study 4.1.

Table 4.4 Characterisation of DPPC:DSPC:DSPE-PEG₂₀₀₀:ICG 5 μ M at differing Lipid Ratios

Formulation	Size (d.nm)	PDI	Zeta-Potential (mV)	DOX EE (%)	ICG Concentration (μ M)
90:10:5:ICG	130.5	0.100	-6.3	98.4	5
80:20:5:ICG	125.1	0.086	-5.7	95.9	5
70:30:5:ICG	131.4	0.069	-7.1	94.5	5
60:40:5:ICG	133.6	0.085	-10.4	96.8	5
50:50:5:ICG	132.0	0.087	-10.1	96.8	5

The high doxorubicin encapsulation efficiency is encouraging, as the lack of it was the main hindrance observed in the high concentration ICG-liposomes. With one of the goals of this hypothesis achieved, the study moved on to test the other hypothesis that 5 μ M ICG was sufficient to achieve an OD of at least 0.5. **Figure 4.10**, denotes the OD of the two of the ICG incorporating liposomes through different stages of their preparations in order to monitor retention of the ICG signal. The spectra were read the day after liposome preparation of the fractions before gel filtration was used to purify the unincorporated ICG (pre-gel filtration), the fraction after ICG purification (post-gel filtration) and the fraction post doxorubicin loading and subsequent gel filtration to remove unencapsulated doxorubicin (post-doxorubicin loading. **a**) displays the OD of the 90:10 ratio liposome. Pre-gel filtration, the OD is 0.77, which remains similar after removal of the free ICG at 0.81. Following doxorubicin loading, this value falls by over half to 0.33. In **b**), a similar profile is observed in the 80:20 ratio ICG incorporating liposome with an OD value of 0.91 before free ICG removal, 0.90 after free ICG removal and a decline to 0.50 after doxorubicin was encapsulated.

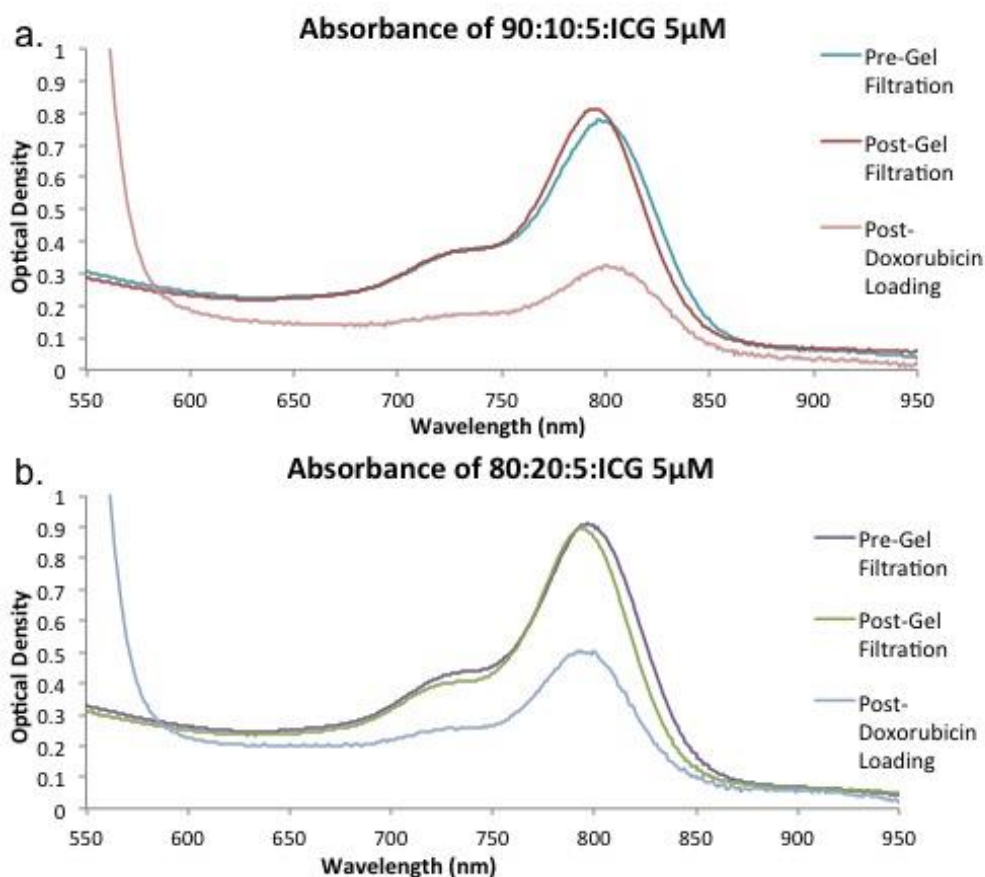


Figure 4.10 Absorbance spectra of liposomal ICG of two differing lipid compositions based on DPPC:DSPC;DSPE-PEG₂₀₀₀ at an [ICG] of 5 μ M. Spectra were read at different points of the liposome production protocol, before and after gel filtration, and after DOX loading for **a)** the 90:10 and **b)** the 80:20 DPPC:DSPC ratio systems.

Although we can conclude that 5 μ M ICG is sufficient to achieve an OD above 0.5 in the early stages of liposome preparation, which in itself suffices to achieve a second goal from the hypothesis. It does however appear that some of this ICG has been lost through the process of doxorubicin loading. The lipid concentration of these samples was not however controlled for, but is an issue that will be addressed later in this study. The conventional way to quantify the ICG concentration of the sample was previously through an ICG DMSO calibration curve as used for calculation of ICG incorporation efficiency of the high concentration ICG-liposomes. However, using the low concentration of 5 μ M, using the same dilution ratio would render the absorbance value too low to properly quantify, and at low dilution ratios, the dispersion was

too turbid to identify the ICG absorbance spectra at all. This issue will also be addressed later in the study.

4.3.1.3 Pushing the boundaries of ICG incorporation into the more fluid lipid ratios of the DPPC:DSPC:DSPE-PEG₂₀₀₀ Liposome

The next step in this study follows on from these two discoveries. Firstly, by lowering the ICG concentration in these lipid constitutions of liposomes to 5 μM , evaded the conundrum of the lack doxorubicin encapsulation in the high concentration ICG liposomes. Secondly, that 5 μM may not be a high enough concentration to allow for the loss of signal following the final doxorubicin loading and purification step. The hypothesis for this next step is that if the ICG concentration was marginally increased, the limit of how much ICG is too much for efficient doxorubicin loading will be tested. If the concentration can be increased and the absorbance maintained, the previously mentioned obstacles in this work may be outmanoeuvred.

Table 4.5, displays the physicochemical properties of representative liposomes of the same lipid ratio as previously tested, the 90:10 and the 80:20, but of different low ICG concentrations. Initially the ICG concentrations tested were 0 μM , 5 μM , 7.5 μM and 10 μM . There was some differences observed in the sizes, but without correlation to the ICG concentration as they ranged from 114 nm to 143 nm, the smallest diameter being the 7.5 μM ICG liposome and the largest being the 10 μM . The PDI was consistently around 0.095. The zeta-potential of the systems did show some correlation with the ICG concentration, increasing marginally from -7.45 mV to -5.7 mV between the 10 μM and the 5 μM liposome but decreasing to -9.3 mV in the ICG free liposome. This is likely due to chance as a similar concentration dependent fall in charge was not observed in the high ICG concentration liposomes, where the differences between ICG concentrations were much larger. In terms of doxorubicin encapsulation efficiency, although the range was not previously defined, the prediction of an inversely proportional relationship between ICG concentration and doxorubicin encapsulation was proved. At 10 μM ICG, it was only possible to incorporate 40% Doxorubicin. At 7.5 μM ICG an improvement is observed with 92% doxorubicin encapsulation. At 5 μM ICG, as previously reported, encapsulation increases to 95.9%, and levels off with a similar 94.7% encapsulation without ICG.

Table 4.5 Characterisation of thermosensitive and non-thermosensitive liposomes incorporating higher ICG concentrations

Formulation	Size (d.nm)	PDI	Zeta-Potential (mV)	DOX EE (%)	Final [ICG] (μM)
DPPC:DSPC:DSPE-PEG ₂₀₀₀					
80:20:5	142.8	0.104	-7.5	40.1	10
80:20:5	113.8	0.086	-6.7	91.8	7.5
80:20:5	125.1	0.086	-5.7	95.9	5
80:20:5	134.4	0.094	-9.3	94.7	0
90:10:5	129.1	0.091	-6.7	89.4	7.5
90:10:5	130.5	0.100	-6.3	98.4	5
90:10:5	139.1	0.073	-9.6	98.8	0
HSPC:Chol:DSPE-PEG ₂₀₀₀ (56.3:38.2:5.5)	128.7	0.046	-7.1	91.8	20
HSPC:Chol:DSPE-PEG ₂₀₀₀ (56.3:38.2:5.5)	149.6	0.049	-10.6	91.8	5

In the 90:10 liposome, 0 μM , 5 μM and 7.5 μM ICG concentrations were tested. Little variation in size was observed averaging at about 135 nm with the PDI varying between 0.073 and 0.100. The zeta-potential, as in the previous 80:20 formulation, showed a slight correlation with ICG content, increasing from -6.68 mV to -6.30 mV looking from the 7.5 μM to the 5 μM ICG liposomes, falling back to -9.60 mV in the ICG free system. In terms of doxorubicin encapsulation efficiency, the same inverse proportionality was observed as in the previous system. 89% doxorubicin was encapsulated in the system incorporating 7.5 μM ICG,

increasing to 98% in the 5 μM ICG system and finally 98.8% in the ICG free system. For these liposomes it appears that increasing the ICG concentration to 7.5 μM is acceptable, but from what has been observed in the 80:20 liposomes at 10 μM ICG, there is a sharp drop off, following the increase of ICG concentration past 10 μM .

A short investigation was performed into whether this relationship was true in the HSPC:Chol:DSPE-PEG₂₀₀₀ system. Interestingly, even at a starting concentration of 200 μM ICG, it was still possible to encapsulate 91.8 % doxorubicin with no difference observed upon decreasing the ICG content to 5 μM .

Following the elucidation of the limits of ICG concentration for efficient doxorubicin loading in the DPPC:DSPC:DSPE-PEG₂₀₀₀ liposomes, the next obstacle to overcome was the loss of ICG absorbance through the preparation.

Figure 4.11, denotes the OD of 90:10:5 ICG 7.5 μM liposome through the different stages of its preparation through the same methodology as was portrayed in **Figure 4.10**. The hypothesis was that by increasing the starting ICG concentration, it would be possible to maintain a higher absorbance value following the final steps of its preparation. Before purification of the free ICG, the peak ICG OD value was 1.41. this remained at 1.41 following the gel filtration. After doxorubicin loading and the subsequent removal of the free chemotherapeutic, the OD fell to 0.96. This was a 32% loss in OD, in comparison to the 59% loss in the same platform incorporating 5 μM ICG and a 44% loss in the 80:20:ICG 5 μM system. On top of this, the retained absorbance is still above the 0.5 OD threshold required for *in vivo* MSOT imaging.

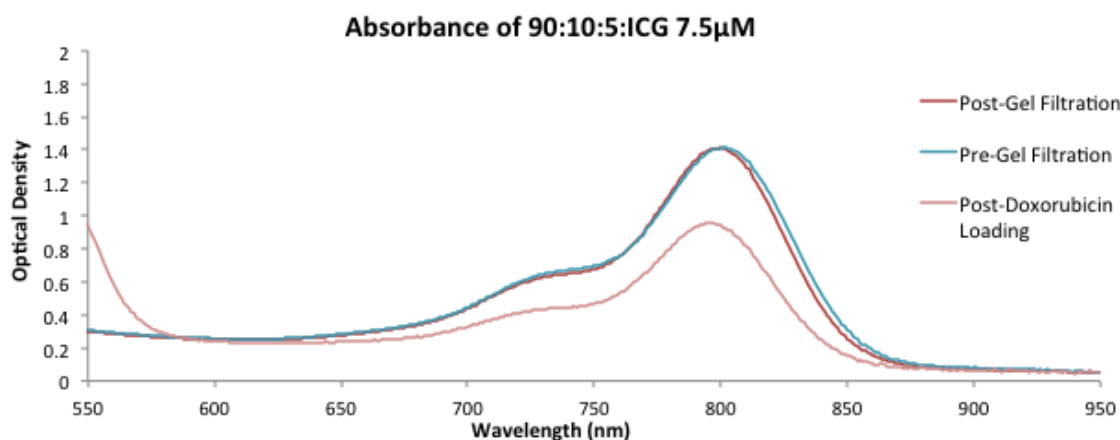


Figure 4.11 Absorbance spectra of liposomal ICG of the 90:10 system at an [ICG] of 7.5 μM . Spectra were read at different points of the liposome production protocol, before and after gel filtration, and after DOX loading.

Using ICG absorbance spectra is fine for the purposes of measuring ICG at high concentrations, as well as validation of the absorbance of the final liposome. However, its use in the quantification of ICG loss at low concentrations it is fraught with setbacks. For example, to measure loss of overall ICG, the liposomes should be dissolved in the same buffer to avoid any effects that the different constituents may have on the ICG. At such low ICG concentrations, it is not possible to dilute the liposomes into the same buffer, as the ICG signal will be below detection limits. The innate absorbance of the liposome can skew the calculation of total ICG loss. This is noticeable in the difference between the OD at 950 nm and 550 nm, which is not present with the ICG alone. Not quantifying for lipid loss throughout the preparation protocol is also a factor, independent of the ICG quantification modality.

The solution to these issues is to use fluorescence. Using fluorescence is a much more sensitive ICG quantification modality than absorbance. Absorbance can reliably detect as low as 5 μM free ICG in DMSO, whereas fluorescence can detect as low as 0.025 μM . This allows dilution of the system in DMSO, and the use of a calibration curve to accurately quantify the ICG present.

Transmission electron microscopy was used to investigate morphological changes resulting from the integration of ICG into the liposomes. **Figure 4.12**, shows micrographs generated from the DPPC:DSPC:DSPE-PEG₂₀₀₀ (80:20:5) liposomes with and without 5 μM ICG, at the post-extrusion, pre-gel filtration stage. The liposomes in **a)**, are without ICG, have an average size of 124 nm and a PDI of 0.111. **b)** displays the ICG-liposomes with a similar average size of 125 nm and a lower PDI of 0.086. Apart from a higher variation in sizes as described by the differences in PDI, there do not appear to be significant morphological differences between the two liposomes. In **a)**, the liposomes appear slightly rounder however there does not appear to be a difference in the thickness of the bilayer following ICG incorporation.

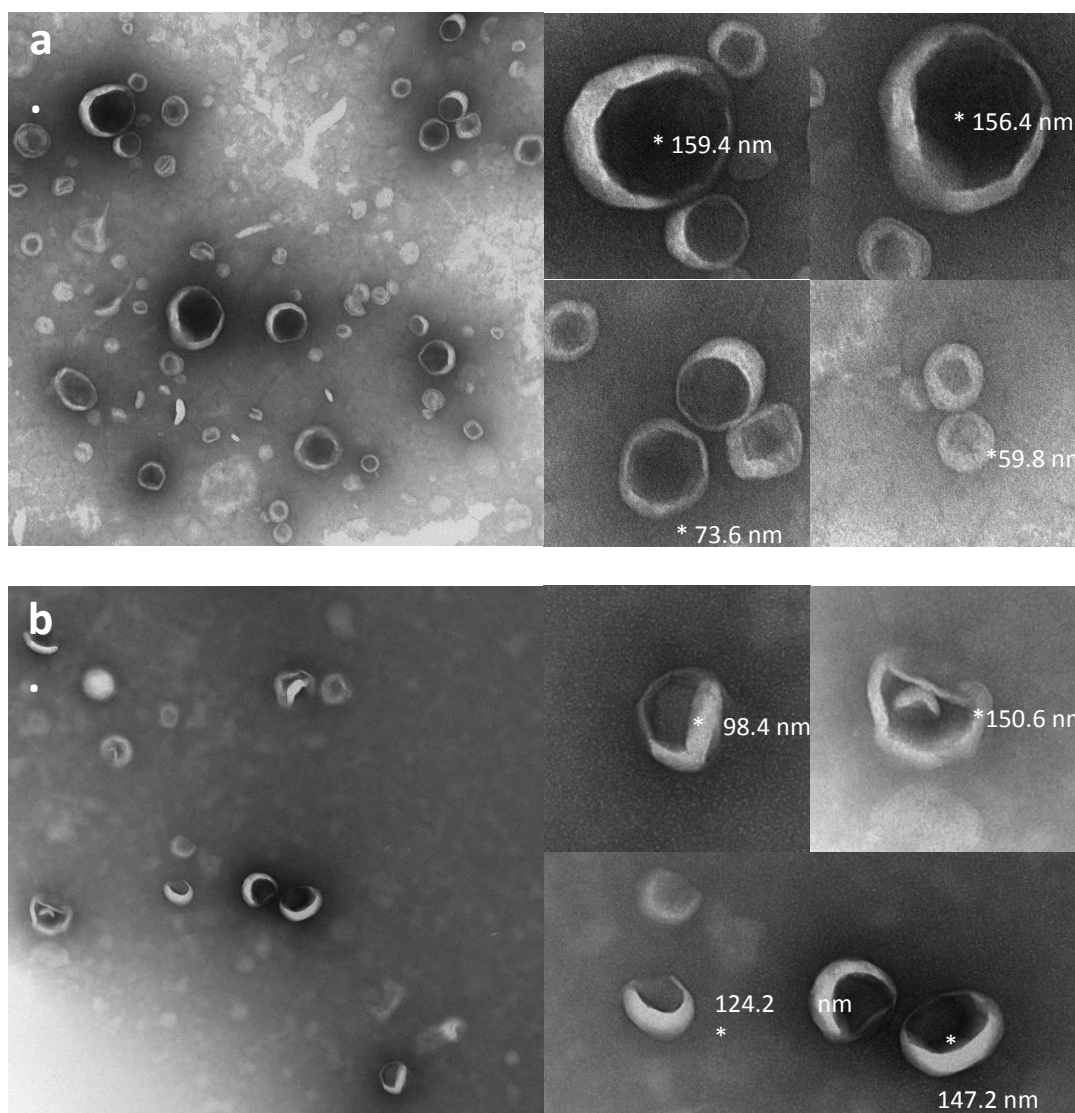


Figure 4.12 TEM micrographs of DPPC:DSPC:DSPE-PEG₂₀₀₀ (80:20:5) Liposomes in **a)** without ICG and in **b)** with 5 μ M ICG.

Considering the effect of ICG on doxorubicin loading, the hypothesis was that there would be a stabilisation effect by the ICG, slowing the rate of release. Liposomes were incubated at 37°C and 42°C in 50% mouse serum. As reported in **Figure 4.13**, at 37°C, as expected, the liposomes released low amounts of doxorubicin, the maximum release after an hour was the 90:10 liposome with a release of 5.9% in comparison to 6.0% in the ICG free 90:10 liposome.

At 42°C, there are significant stabilisation effects observed in the 90:10, 70:30 and 60:40 ratio liposomes. The ICG free 90:10 liposome had released 100% doxorubicin after 10 minutes, but with 5 μ M ICG, 60% was released at this time point, taking 1 hour to reach 99%. The ICG free 70:30 liposome had released 74% doxorubicin after 10 minutes taking 1 hour to

reach 100%. With 5 μM ICG, 28% was released at this time point, taking 1 hour to reach 55%. The ICG free 60:40 liposome had released 42% doxorubicin after 10 minutes taking 1 hour to reach 63%. With 5 μM ICG, 12% was released at this time point, taking 1 hour to reach 27%. The only exception to this significant stabilisation effect was when testing the 80:20 liposome. The ICG free 80:20 liposome had released 95% doxorubicin after 10 minutes taking 1 hour to reach 98%. With 5 μM ICG, 91% was released at this time point, taking 1 hour to reach 98%. This rate of release was significantly higher than the more fluid 90:10 ICG liposome.

The hypothesised stabilization effect of the ICG integration into the bilayers has been demonstrated through the reduced rate of release observable at 42°C in 50% mouse serum. This should also translate to the stability at 37°C over 24 hours, which would be preferential for therapy by avoiding uncontrolled drug release. However this experiment is yet to be completed. The next question to ask in the spectrum of this study is whether or not ICG concentration has a proportional effect to the rate of doxorubicin release. Considering the constraints observed during doxorubicin loading from 10 μM ICG and above, the study into varying ICG concentration was limited to just 5 μM and 7.5 μM ICG.

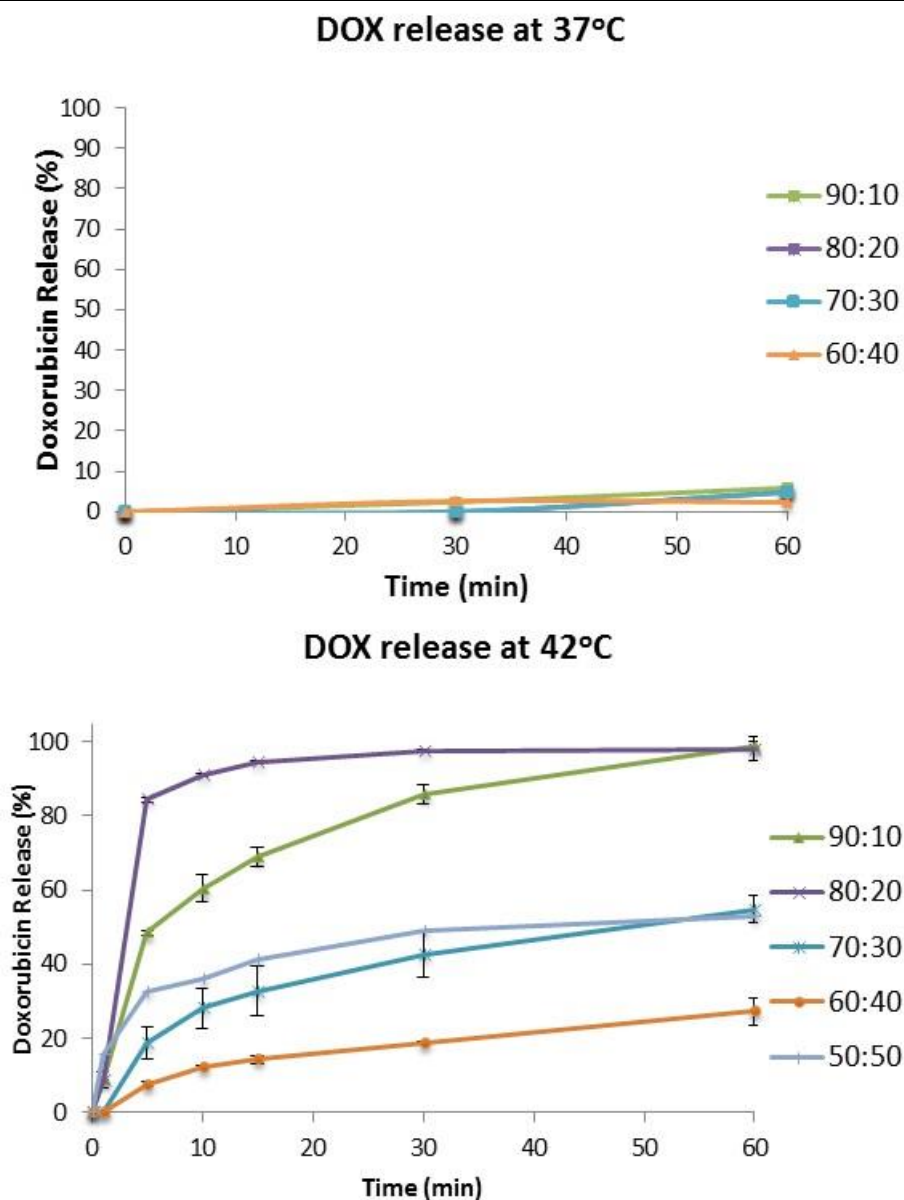


Figure 4.13 DOX release profiles of DPPC:DSPC based liposome-ICG-DOX systems at **a)** 37°C and **b)** 42°C in the presence of 50% mouse serum.

Figure 4.14, displays doxorubicin release profiles for the 90:10 and 80:20 DPPC:DSPC ratio liposomes with 5 μM and 7.5 μM ICG. The 90:10 ratio liposome incorporating 7.5 μM ICG did not have a substantially different release profile to the 5 μM ICG incorporating liposome. Initially the rate of release was higher releasing 75% of the drug after 5 minutes and increasing to 94% after an hour, in comparison to 48% after 5 minutes and 99% after an hour in the 5 μM ICG liposome. In the case of the 80:20 liposome, there was not a substantial difference between the 3 liposomes. At 15 minutes the ICG free liposome shows 96% release in comparison to the 94% of the 5 μM and the 91% of the 7.5 μM ICG liposomes.

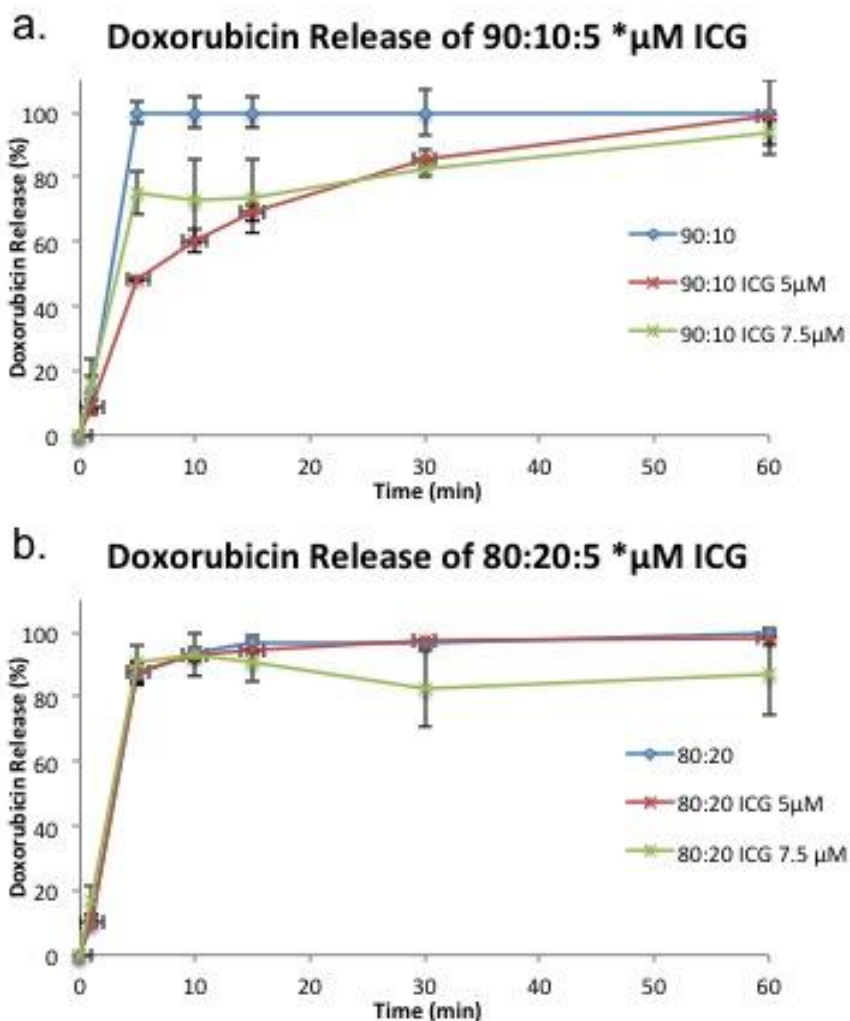


Figure 4.14 DOX release profiles of DPPC:DSPC based liposome-ICG-DOX systems at 42°C at differing [ICG] for **a)** 90:10 and **b)** 80:20 in the presence of 50% mouse serum.

As hypothesised, the ICG did have a stabilising effect on the liposomes in terms of rate of doxorubicin release however the effect was not concentration dependent at ICG concentrations low enough to allow initial doxorubicin encapsulation.

The post insertion protocol was also tested on the 6040 formulation liposomes as an attempt to increase the ICG concentration whilst retaining therapeutic concentrations of DOX. ICG concentrations started at 50 and 100 μ M. The insertion did not particularly effect the particle size or the surface charge, however the DOX encapsulation efficiency was below 60%. Exploration of this protocol was subsequently discontinued.

4.4 Discussion

The thermosensitive liposome known by its trade name ThermoDox™ is the most clinically advanced environmentally responsive nanocarrier under clinical trials. However, despite initial encouraging clinical data emanating from Celsion's phase III clinical trials for HCC intervention, the drug failed as it did not reach the target of 33% increase in lifespan^{196,197}. Although there are a number of reasons it failed regarding trial design, the logistics of heating during administration of the chemotherapy complicated the provision of this therapy by the clinicians. Improving upon the stability of the system whilst maintaining thermosensitivity would thus allow a number of heating protocols to be trialled, as well as potentially improving delivery of intact liposomal DOX to the tumour site without the risk of rapid leakage upon injection. The aforementioned rapid release rate in the presence of serum proteins^{142,148}, generating plethora of side effects due to the free circulating doxorubicin and heat application^{183,198,199}. This caveat of a system designed to rapidly release DOX under low temperature hyperthermia, is based on bilayer composition brilliantly designed specifically to target the tumour vasculature, without consideration for the side-effects of DOX release under physiological conditions. The DOX release profile stems from an exceptionally fluid bilayer, bolstered with a membrane pore stabilising lyso-lipid (MSPC). This chapter aimed to recreate this release profile whilst stabilising DOX leakage under physiological conditions. Through a systematic investigation into the lipid composition of the liposome bilayer, along with the inclusion of non-lipid entities, this ambition became a reality.

4.4.1 Probing Membrane Rigidity Through Modulation of DPPC:DSPC ratio

The initial aim of this study was reduce DOX release at 37°C in comparison to ThermoDox™, whilst maintaining a similar burst release profile. This was possible through the replacement of the monostearoyl MSPC with its distearoyl counterpart DSPC at the same ratio, reducing leakage at 37°C in the presence of serum proteins from >90% at 10 minutes to just 7% after 1 hour. Through the introduction of an additional stearoyl chain, the inter-stearoyl Van der Waals interactions will be doubled in this initial 10% of the lipid population. By reducing the void space in this hydrophobic region of the bilayer, and rigidifying the membrane through these increased lipid interactions, the liposomes were expected to show more resilience to serum protein destabilisation and increased temperature in comparison to the MSPC comprising system. Elimination of the conical lyso-lipid also rid the system of the stabilised pore formation, resulting in release becoming dependent on the extent of grain boundary formation in the specific formulation. Liposome serum interactions have been

extensively studied^{204,205,206,207}. The interaction between the vesicle surface and physiological environment is dependent on the radius of curvature/size, surface charge and chemistry. Several defined modes of protein bilayer interaction have been reported^{58,50,208,209}, simple charge based interactions such as ribonucleases or proteins rich in poly-lysine domains which interact with the negatively charged phosphate headgroups. Due to their superficial nature, they do not have much effect on the stability or permeability of the bilayer. It is the interaction of membrane penetrating proteins which have the propensity to destabilise the bilayer through membrane expansion, and decrease of the T_m . These include apolipoproteins, the most abundant proteins found adsorbed to liposomes, and complement proteins (C6-9) following interaction with serum proteins *in vitro* and *in vivo*²¹⁰. These lipoprotein subunits first dock through charge based interactions, then insert their hydrophobic domains into the bilayer. Intrinsic membrane proteins such as the myelin proteolipid, associate based on hydrophobic forces, contributing to increased permeability less so to reduction in T_m . The lower the radius of curvature, the more loosely the lipids are packed and thus the facility of protein-bilayer penetration is increased. The higher the level of irregularities, the more proteins interact with the bilayer. This is especially relevant when considering the grain boundary formation at the T_m of liposomes comprising multiple lipid compositions such as the DPPC:DSPC based system, and the pore stabilisation seen in the ThermoDox™ system²¹¹. Protein association is thus extremely important when considering *in vivo* release characteristics of these systems as is most notable in section 4.2.2.

The maintenance of the high DPPC content of the 90:10 DPPC:DSPC system allowed the retention of a similar burst release profile, with 100% DOX release after 5 minutes at 42°C in the presence of serum in comparison with 90% after 1 minute for the lysolipid comprising system. It was also possible to achieve the primary objective of stabilising the system at 37°C in the presence of serum proteins in comparison to the ThermoDox™.

As expected, as the DSPC content of the system was increased in comparison to the DPPC content, the T_m increased as the rate of DOX release at 42°C reduced. This is due to the higher concentration of a higher T_m lipid, which stabilises the overall system at 42°C. Through systematic investigation of a number of different lipid ratios, it was possible to generate a repertoire of systems with varying release kinetics at 42°C based on the ratio between DPPC and DSPC content.

4.4.2 Utilisation of sonication rather than extrusion for liposome preparation

When extrusion was replaced with sonication, as the initial single unilamellar vesicle formation mechanism, the liposomes appeared less stable in the presence of serum proteins both at 37°C and 42°C. As the sonicated liposomes are significantly smaller than the extruded, as is their radius of curvature. This increases the amount of void space and defects within the bilayer, the available surface area for protein interaction, the disparity between inner and outer lipid concentrations, and thus the propensity for proteins to become embedded and destabilise the structure of the bilayer, thus permeabilising it to the disruption of the pH/salt gradient thus encouraging efflux of the intraliposomal DOX. Due to the apparatus available, it was not possible to generate liposomes of the same size, and so it is not possible to say whether the sonication process truly disrupt the formation of the liposome structure to a higher extent than extrusion. Using liposomes comprised of the highly fluid lipid dioleoylglycerolphosphocholine (DOPC), extrusion and sonication were compared against each other using both anisotropy which measures the fluidity of the bilayer based on the rotational ability of the fluorescent probe, and fluorescence recovery after photobleaching, which measures the lipid diffusion coefficient based on the translational diffusion of fluorophore ligated lipids. Although similar differences in size and PDI were also observed, there did not appear to be a particular difference in bilayer fluidity between the two preparation protocols for these extremely fluid systems²¹². This further substantiates the theory that the differences in DOX release kinetics may just be down size as a result of bilayer permeability by serum proteins.

4.4.3 Addition of Indocyanine Green (ICG) as a bilayer stabilising and imaging agent

As hypothesised, it was possible to incorporate ICG into liposomes through film insertion, at high efficiencies (66-76%), with notable physicochemical characteristics only observed at a starting concentration of 200 µM where the size almost doubled, along with the polydispersity. The absorbance spectra also signalled high levels of aggregation as the initial concentration was increased. Up to an initial [ICG] of 150 µM, DSC did not elucidate any particular differences in the phase transition temperature of the 60:40 system in comparison to lower concentrations or the liposome alone. Despite this, the [ICG] was crucial to the system's ability to encapsulate DOX with this threshold subsequently falling to 7.5 µM where the system maintains encapsulate ~90%. The composition also seemed to play a role in terms

of the system's ability to encapsulate DOX, as when a DOXIL[®] formulation system was tested, this low ICG threshold did not seem to apply. As previously hypothesised, the inclusion of ICG at low concentrations did succeed in reducing the rate of DOX release at 42°C in the presence of serum, even though the DSC data did not indicate any change in the T_m of the liposomes at high [ICG].

This applied to each formulation to a significant degree apart from the 80:20 system which mysteriously and reproducibly showed a much lower reduction in release rate than the other compositions. At 37°C over one hour in the presence of serum little difference in DOX leakage was observed as a result of ICG incorporation. Under TEM, there was little difference in the morphology of the 80:20 formulations with and without 5 μ M ICG. In the more fluid 90:10 system, pushing the [ICG] up to 7.5 μ M from 5 μ M seemed to reduce this stabilisation effect, whereas in the 80:20 system, little differences between either formulations were observed.

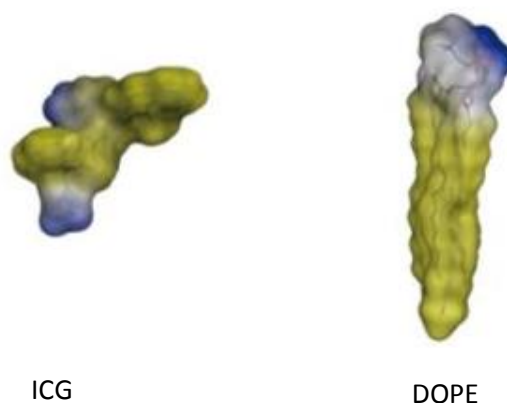


Figure 4.15 Mathematically modelled structures of ICG and DOPE (dioleoylphosphoethanolamine) annotated with relative polar regions in blue, and hydrophobic regions in yellow. Adapted from¹⁷⁸.

What was very apparent was the stabilisation of the optical absorbances of the ICG when incorporated into the liposomes which show very little decrease in the OD over a week, in comparison to the signal of the free ICG which deteriorates rapidly in HBS. Based on mathematical models of ICG and DOPE²¹³, (a phospholipid which differs from DSPC through the incorporation of a double bond in each acyl chain), in **Figure 4.15**, one can surmise the interaction between both entities based on their relative charges and hydrophobicities. The sulphonate groups are likely to interact with the choline in the polar head of the phospholipid,

with the aromatic portions interacting with the acyl chains assumably localising in the more peripheral portions of the liposomal bilayer.

Through the production process of the liposomes which are heated above the T_m of all lipid populations, the ICG will orientate itself in the most entropically favourable position within the bilayer. It does appear that ICG is lost from the bilayer between initial production and characterisation of the final DOX loaded system. Most likely adulteration of the liposome-ICG bilayer in terms of repeated heating steps above and around the transition temperature, induces increased lateral diffusion of the lipids and stresses upon the interactions between the ICG and lipid populations. It is quite likely that the loss of ICG during DOX loading may be as a result of the ICG's orientation along the grain boundaries of the system. As one lipid population reaches phase transition, as happens to the DPPC during DOX loading, the ICG may localise between the fluid and rigid phase DSPC lipids. This may be the reason for the effect the incorporation of ICG has on the DOX release rate of the composite systems. A way to test this would be to test the efficiency of ICG incorporation and the threshold concentration limiting DOX encapsulation, on liposome compositions with different lengths of grain boundary. The hypothesis is that if the ratios between lipid populations are closer to equal, then the grain boundaries will be longer and thus the efficiency of ICG incorporation should be higher.

Another consideration would be an adaptation of the ICG incorporation protocol to minimise the levels of lipid-ICG composite heating. For example the inclusion of the ICG towards the end of the liposomal DOX preparation protocol would limit this and possibly allow a higher ICG incorporation efficiency. An insertion protocol of ICG has been used for the inclusion of ICG into erythrocyte 'ghosts', which involves the insertion of ICG into pre formed membranes²¹⁴. Apart from the film insertion protocol, a version of which has been reported once before²¹⁵, a freeze fracture protocol exists. This involves hydrating the lipid film with an ICG solution, solubilisation and repeated freeze fracturing, which breaks and reforms the lipid membranes, exposing the edges of bilayer fragments to the free ICG in order to promote its interaction and incorporation. This is the most reported method if liposomal incorporation of ICG^{87,89,90,216}, however due to the use of highly polar AS, and ICG's relative solubility in that media, it is likely that the level of ICG aggregation may be too high to allow effective incorporation of monodisperse ICG into the bilayer of the liposomes.. Another consideration is to test the incorporation of ICG into sonicated systems. During extrusion, the liposomes are maintained and extruded at 60°C in order to downsize them over a 60-80 minute period. Sonication is generally a faster process for liposome formation, and would limit the time spent

above the transition temperature of the liposome. In addition to this, due to the smaller liposome size and thus the lower curvature radius, the lipids are more loosely associated together. This may allow deeper penetration and easier interaction of ICG with the constituent hydrophobic and polar lipid domains. The higher surface area, also give the ICG more available bilayer with which to interact, which may allow a higher incorporation efficiency with the retention of DOX.

Serum stability at 37°C over 24 hours is a very important factor to address, as it is one of the best *in-vitro* methods by which to simulate conditions of the circulation and test the stability of the liposomes in the circulation. Although it is difficult to tell the rate of blood clearance of the liposomes without *in vivo* biodistribution studies, liposomes of different rigidities have been shown to accumulate in tumour tissue, as well as be cleared via the liver over 24 hours⁷⁸. It is thus important, for an effective liposome to be stable at 37°C in serum over this time period to allow deeper penetration into the tumour, higher tissue accumulation of doxorubicin as well as evading the problem of doxorubicin releasing in the circulation resulting in immunosuppression through leakage into the bone marrow. This will also illuminate differences in the stability of the ICG and peptide liposomes over the plain, along with differences between the liposomes formed of different lipid ratios.

DPH/ANS fluorescence anisotropy, incorporates fluorescent probes into the bilayer of the liposome in both the

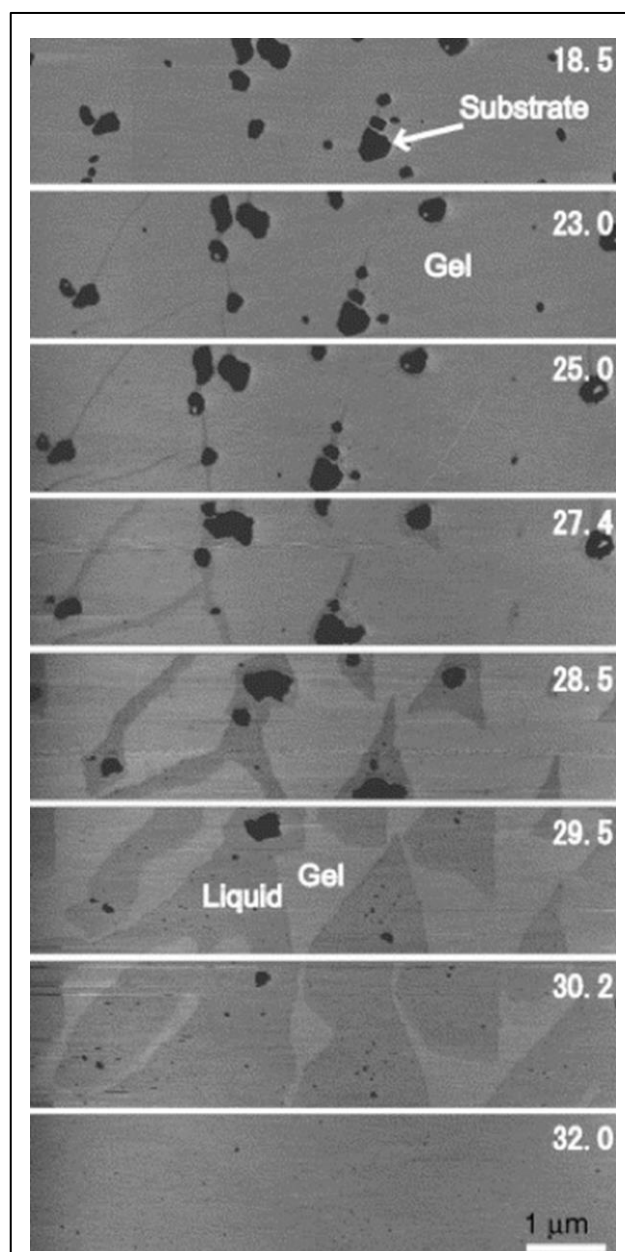


Figure 4.16. AFM micrographs showing increased lateral mobility of DMPC lipids from a bilayer to monolayer, following gel to liquid phase transition. Image from²⁸⁹.

hydrophobic (DPH) and hydrophilic (ANS) portions. This allows the monitoring of bilayer fluidity through the relative fluorescent of the probes. When static, the polarised light used to excite the fluorophores is constrained to a particular range of angles, with the emitted light confined to the same range. When the lipid bilayer undergoes phase transition above its T_m adopting a liquid crystal state as seen in **Figure 4.16**, the bilayer associated fluorophores become dynamic. The movement of the fluorophores between excitation and emission relinquishes the constraints to the same particular angles of polarized light. This results in less emitted light being detected the more fluid the bilayer is, allowing a functional readout of the dynamics of the phase transition over a certain temperature range following alterations to the composition. This was carried out in previous work which investigate the structural changes to the bilayer as a result of leucine-zipper peptide incorporation, providing important information about the rigidifying effect it had¹⁴². This information also compliments data obtained from DSC regarding the level of fluidity attained around the T_m as well as the loading and release characteristics. Fluorescence anisotropy would also be useful in characterising the effect that ICG incorporation has on the liposome bilayer, considering the little differences in phase transition temperature put against the substantial differences in release profiles.

The ICG-liposome system has additional therapeutic and functional properties, which can be further investigated *in-vitro*. ICG is a photosensitizer with both photodynamic therapy (PDT) and photothermal therapy (PTT) capabilities¹⁷⁸. Photodynamic refers to the production of a number of reactive oxygen species in response to irradiation of a photosensitiser, and generally seeks to maximise the production of singlet oxygen as a potent cytotoxic agent. Photothermal refers to the production of heat in response to irradiation, based on an agent's intrinsic photophysical properties. Combining the photothermal effect along with doxorubicin has been shown to have powerful effects on inhibiting cancer cell growth *in-vitro*¹⁷⁹. The theory behind this is that the local heating increases the permeability of the cell membrane to the DOX, thus increasing uptake and permeation into the nucleus¹⁷⁷. In addition to this, in multi-drug resistant cell types, hyperthermia can deregulate their p-glycoprotein efflux pumps which confer their drug resistance, improving cytotoxicity. Liposomes have been used for the intracellular delivery of photosensitisers in the past, more than doubling tumour tissue accumulation and therapeutic effect¹⁵⁷. Although using ICG for this purpose is not novel, and neither is the combination of it with doxorubicin, or incorporated into a liposome. However the combination of the FDA approved ICG, the doxorubicin, the temperature sensitive liposome, for a theranostic cancer chemotherapeutic, photodynamic and photothermal agent, is novel. Laser fluence, pulse frequency, irradiation time and ICG concentration, varies

between studies and would have to be optimized for the ICG liposome and cell type. There are several studies that can develop from the conception of this liposome.

Although PTT has shown efficacy in *in-vitro* cell kill assays, photothermal therapy shares the same downsides as thermal ablation. These downsides include the non-specific dissipation of heat into surrounding tissues resulting in non-specific tissue damage, resulting in the induction of necrosis, rather than apoptosis²¹⁷. Due to the physical destruction of the cell rather than signal mediated programmed cell death, cell contents leak into the surrounding tissue. This initiates an inflammatory response, and is slower for macrophages to clear than the apoptotic bodies produced as a result of apoptosis^{218,219}. This can lead to a build-up of necrotic tissue leading to surrounding tissue damage as well as tissue infections. However, instead of using the PTT as an adjuvant to the doxorubicin, considering the thermosensitivity of the liposome, it should be possible to induce drug release in response to PTT ICG mediated hyperthermia of the liposome bilayer to above the T_m rather than reliance on HIFU or RFA. This would avoid non-specific tissue heating, heating just the liposome, and it should also allow the use of a more rigid bilayer system due to the localized heating effect, allowing the use of a more serum stable therapeutic.

Considering average tumour accumulation of an injected liposome is anywhere between 0.5-11.3% of the injected dose^{220,221} depending on relative levels of tumour angiogenesis, and that the minimal final concentration to induce heating from 37°C to 42°C *in vitro* is 5 μM ¹⁷⁹, the liposomes must incorporate at least 44 μM ICG to attain a final tumour accumulation of 5 μM . Thus, there is still some optimisation work to attain the optimum ICG incorporation protocol into the system of optimal lipid composition to attain these ICG concentrations. A higher ICG concentration would allow the induced release of liposomes in a larger number of tumours of differing vascularities along with boosting their imaging potential and relative contrast.

4.5 Conclusion

In conclusion, it has been possible to attain thermosensitive liposomes which are stable at 37°C and rapidly release DOX at 42°C in the presence of serum, in comparison to the most clinically advanced thermosensitive liposome under trial. This should prove more effective *in vivo* in terms of safety, and tumour DOX accumulation. Following the liposomes stabilisation, through the systematic investigation into lipid composition, it was possible to generate a repertoire of liposomes which appear stable at 37°C and release DOX at a number

of different rates. These provide alternatives to a burst release protocol, and may allow deeper penetration into the tumour tissue, rather than strictly targeting the tumour vasculature. Sonication reduced the liposome size to a larger extent than extrusion, and it is likely that the smaller size was responsible for an increased dox release rate of lipids comprising the same lipid composition. This is expected to be as a result of the reduction in curvature radius and thus a looser packing and higher surface area with which serum proteins may interact.

The incorporation of a thermosensitive leucine zipper peptide, had already been reported to stabilise 90:10 (DPPC:DSPC) ratio PEGylated liposomes at 37°C over 24 hours¹⁴², however the functional effect of DOX release through protein dissociation had not been demonstrated. It took the trial of a number of different lipid ratios to establish this effect over a peptide with a higher denaturation temperature, and provided a system with a differing release rate and a more rigid lipid composition.

Finally it was possible to effectively incorporate ICG into thermosensitive liposomes. This effectively stabilised the majority of lipid ratios tested. However there appeared to be a fairly low [ICG] threshold which would allow the encapsulation of DOX at high efficiencies (>90%) of around 7.5 µM. Nonetheless, it has been possible to revamp the most clinically advanced thermosensitive liposome, and with the addition of ICG, generate a number of potential novel theranostics setting a solid foundation for the further optimisation of these systems to both maintain their DOX loading capacity and increase their levels of ICG incorporation.

Chapter 5

5 Optimisation of liposomal ICG Incorporation into non temperature sensitive (NTS)-Liposomes

5.1 Introduction

Theranostics is a rapidly developing field in the spectrum of cancer therapy, providing the facility of simultaneous imaging and treatment, with nearly 6'000 publications in 2016 alone. The purpose of this is to allow therapy and imaging to allow monitoring of both drug delivery to the tumour site as well as response to therapy. Cancer mortality is proportional to disease progression, thus the development of theranostic systems for rapid intervention and monitoring of the response of the disease is essential for the increment of survival rates.

Doxorubicin (DOX) is used against a plethora of tumour types^{222,223}, it does however carry toxicity related setbacks such as cardiotoxicity due to its lack of targeting. Through its encapsulation into liposomes it was possible to reduce the associated cardiotoxicity as well as improving efficacy of treatment of the leukaemia model tested⁹². Following iterations of PEGylated liposomes demonstrated success in preclinical trials and resulted in the development of DOXIL[®], which rapidly passed through clinical trials for the treatment of AIDS related kaposi's sarcoma based on its efficacy and a much improved safety profile over free DOX. This resulted in FDA approval of DOXIL[®], for the treatment of this cancer type in 1995, exhibiting an impressive circulation half-life of 79 hours¹⁸⁶

Subsequent steps taken, forming the crux of this paper sought to incorporate the near-infrared (NIR) absorbing/fluorescing dye indocyanine green (ICG) to turn this well-established drug into a theranostic system. Since FDA approval in the late 50's, ICG has been used for a plethora of biomedical applications such as cardiac output²²⁴, hepatic function⁸, and ophthalmologic angiography²²⁵. It's high fluorescence and rapid clearance by the liver through binding to blood serum proteins, was exploited to image the disrupted neovasculature in lesions of age related macular degeneration, monitor the cardiac output over a specified arterial distance and assess the efficacy of its hepatic clearance. ICG's low toxicity²²⁷, FDA approval, and absorbance/fluorescence in the NIR region, (the region of peak tissue transmittance²²⁸) denotes ICG a powerful imaging tool. A number of optical imaging modalities have been used for *in vivo* imaging of ICG²²⁹⁻²³¹. Optical imaging, does however have setbacks associated with light scattering and absorbance of light from the tissue's endogenous chromophores, generally restricting its penetration depth to sub-centimetre range, thus

limiting the sensitivity and resolution of the technique²³². Photoacoustic imaging exploits the photoacoustic effect by which upon NIR laser irradiation, a probe such as ICG carrying photothermal properties induces local heating induced pressure changes which when pulsed at the correct frequency, generates transducer detectable ultrasound waves. This technique allows non-invasive, live imaging of the probe through more than a centimetre of tissue⁸¹. Incorporation of multiple wavelengths of illumination has improved the signal to noise ratio and allowed compensation for movements during acquisition, resulting in the development of the Multispectral Optoacoustic Tomography system, (MSOT)²³³.

ICG-nanoparticle drug combinations have proved effective theranostic systems in terms of their constitutive efficacy. However as intravenously administered drug delivery vehicles these formulations are somewhat lacking. At 37°C in saline buffer, nanoparticles rapidly release ICG, losing between 40%^{234,235} and 65%²³⁶ in the first 4 hours, and in the case of DOX, 40%²³⁷ to 45%²³⁵ after 4 hours. In order to maximise tumour accumulation, liposomes as well established, long circulating drug delivery vectors have been under investigation for the housing of theranostic components for cancer intervention, in the last 5 years with the incorporation of ICG. This has been achieved through a few different protocols achieving a variety of different ICG/lipid ratios; lipid film hydration followed by direct lipid film incorporation through co-solubilisation of ICG with phospholipids in chloroform²³⁸, *freeze fracture*^{87,89,90,216}, lipid film hydration followed by sonication²³⁹ and ICG conjugation to a phospholipid, followed by addition to phospholipids in organic solvent at the film formation stage^{213,240}. So far, there have been two attempts to incorporate therapeutic entities to ICG incorporating liposomes: The incorporation of cetuximab targeted liposomes against EGFR for molecular imaging purposes²⁴¹, and the other for the purposes of targeted cancer therapy incorporated an anti-MUC1 targeted MAb into DOXIL® equivalent formulation⁹⁰, however at an efficiency attaining just 5% DOX of that of the clinical system. This is quite a shortfall in terms of the achievement of a viable theranostic rather than simply a profoundly effective photoacoustic contrast agent.

The previous chapter demonstrated relative success in the incorporation of ICG into thermosensitive extruded liposome systems. Through the film insertion of ICG, based on the dye's high solubility in chloroform:methanol (4:1), it was possible to incorporate high concentrations of ICG at high efficiencies. However, following ICG incorporation into the liposomal bilayer, the liposomes lost the ability to encapsulate ICG at therapeutic concentrations. Thus, a threshold [ICG] was established at 7.5µM, which is a concentration which is too low to likely achieve photothermal based heating up to the low temperature

hyperthermia range of 42°C under irradiation, and may be too low to gain well contrasting MSOT images based on the concentrations used in previous MSOT studies^{89,90}.

For the circumvention of this obstacle concerning [ICG], the protocol of ICG incorporation was analysed. Reported here are several techniques through which it is possible to incorporate the near-infrared imaging probe, ICG into the DOX encapsulating HSPC, cholesterol and DSPE-PEG₂₀₀₀ comprised liposome known by its trade name DOXIL[®]. ICG was chosen for its low toxicity and its excellent photoacoustic properties, and the DOXIL[®] formulation for its established clinical efficacy and reduced toxicity over free DOX in the treatment of vascularised tumours.

The three differing protocols, elements of which have previously succeeded in the incorporation of ICG into lipid bilayers, were selected with consideration of the intrinsic amphiphilicity of the dye. The techniques differ in the chronology of ICG's incorporation into the liposome. The first, named the *freeze fracture protocol*, introduces the ICG as a solution in ammonium sulphate during the film hydration of the pre-formed lipid film following evaporation of the excipient organic solvents. The second, coined as the *film insertion protocol* (as previously used in **Chapter 4**), inserts the dye into the lipid film following its introduction into the phospholipid-chloroform-methanol solution in the initial stages of the liposome production process. The third and most efficient ICG incorporation protocol, known as the *post insertion protocol*, introduces ICG to pre-formed DOX encapsulating liposomes in the final stages of liposome production, specifically in the last 10 minutes of the DOX loading process. Through the development of the dye post insertion protocol, it was possible to substantially increase the efficiency of dye incorporation as well as the yield of the final product.

The initial liposome downsizing was varied between two methodologies; sonication and extrusion, in order to investigate the contribution the method of liposome formation had on the resultant system. This is based on the theory of increased defects and bilayer permeability due to the lower radius of curvature of smaller sonicated liposomes over the larger extruded systems. This theory was proved correct, in terms of allowing a higher concentration of ICG, as well as allowing the encapsulation of therapeutic concentrations for each protocol tested.

The resultant system carries much potential through stabilisation of the optical properties of ICG, which as a free agent, rapidly aggregates in aqueous solutions resulting in a substantial drop in optical density. The protocol also allows the maintenance of therapeutic levels of the drug DOX, indicative of sustained therapeutic potential. A temporal description of

liposomal tumour accumulation in orthotopic 4T1 tumour bearing mice was generated through the detection of ICG through multispectral optoacoustic tomography, (MSOT). This was verified through fluorescence cryosection which colocalised both ICG and DOX thus realising the novel construct's imaging potential, paving the way for *in vivo* therapeutic studies. This work demonstrated a number of different methodologies for the development of a theranostic liposome based on the DOXIL[®] formulation. The DOXIL[®] formulation was used as it had already been established and in use for its clinical efficacy and reduced toxicity over free DOX in the treatment of vascularised tumours.

5.2 Results

Following production of these DOXIL-ICG liposomes through a number of different protocols, the systems were extensively characterised and compared at a fixed lipid concentration of 12.5 mM to assess the relative efficiency of the production processes in terms of the yield of the constituents.

5.2.1 Protocols for the incorporation of ICG into liposomal DOX

Figure 5.1 depicts the three protocols used and the chronology of ICG's incorporation at an initial 200 μ M to 12.5 mM lipids in each of the systems. The *film insertion protocol* (**Figure 5.1a**) as previously reported²³⁸, co-dissolves the ICG with the constituent phospholipids in organic solvent in the initial stages of liposome preparation before film formation. The lipid ICG film is then formed through rotary evaporation prior to hydration with ammonium sulphate and solubilisation at 60°C followed by extrusion/sonication. The liposome-ICG then undergoes buffer exchange, replacing the excipient buffer with HEPES buffered saline pH 7.4, to establish a pH/salt gradient. This allows subsequent DOX loading at 60°C resulting in the formation of liposome-ICG-DOX. The *freeze fracture protocol* (**Figure 5.1b**) is the most established protocol for incorporation of ICG into liposomes^{87,89,90,216} introduces the dye solvated in ammonium sulphate, during the film hydration step at the initial stages of liposome preparation following film formation. The lipid film is solubilised, and subsequently freeze thawed before sonication/extrusion to form liposomes. The buffer is then exchanged then DOX is loaded. In the novel *post insertion protocol* proposed here (**Figure 5.1c**) for the incorporation of ICG into liposomes, the empty liposomes are formed through film formation, hydration and extrusion/sonication. The buffer is then exchanged and the DOX loaded. In the final 10 minutes of DOX loading, ICG is introduced to the liposome-DOX suspension resulting in its insertion into the lipid bilayer to form the liposome-ICG-DOX.

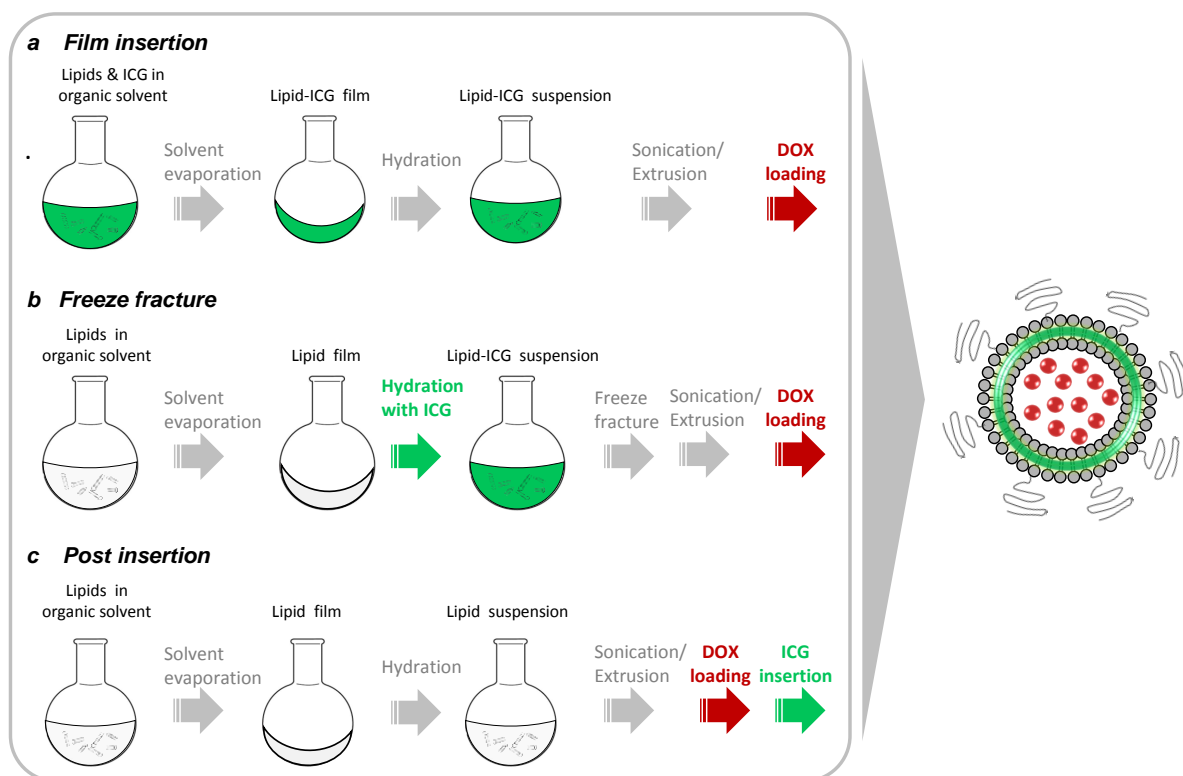


Figure 5.1. Schematic representation of the three liposome-ICG-DOX construction methodologies and relative differences in chronology of ICG incorporation. **(a)** Film insertion protocol, whereby ICG is incorporated within the phospholipids in organic solvent prior to lipid film formation. **(b)** Freeze fracture protocol, in which the ICG is incorporated during the hydration of the lipid film. **(c)** Post insertion protocol, during which ICG is incorporated in the final stages of DOX loading of the preformed liposome-DOX

5.2.2 Physicochemical characterisation of liposomes

In the consideration of the various physicochemical properties displayed in **Table 5.1**, one begins to understand the advantages of one protocol over the other. The lipid concentration was fixed to 12.5 mM and the properties characterised were; the size (d.nm) Polydispersity, surface charge (mV), lipid yield (%) and relative DOX and ICG concentrations attained (μM and % incorporated). Applying extrusion rather than sonication in the liposome-ICG, the lipid recovery was lowest for the *freeze fracture protocol* at 50%, with the *film insertion* generating a yield of 67% and the *post insertion* highest with 79%. There was little difference between the majority of the ICG alone and DOX loaded systems in terms of almost all of the physicochemical parameters. In terms of ICG incorporation efficiency of the liposome-ICG systems, the *freeze fracture* incorporated the least with 15% efficiency. The *film insertion* protocol incorporated marginally more at 23%, and the *post insertion* the most at 33%. The liposome-ICG-DOX systems appeared similar to the DOX exclusive systems for the *freeze fracture* and *post insertion* systems, incorporating 16% and 33% respectively, however the *film insertion* system incorporated 31%, 8% more than its DOX lacking counterpart. In terms of the size of these systems, the *freeze fracture* and *film insertion* systems showed little difference residing around 130 nm with or without the encapsulated DOX. The *post insertion* system had a larger size of about 150 nm.

Each system had a narrow polydispersity (PDI) of around 0.055, which is unsurprising based on the method of preparation. In terms of the relative zeta potential, all the systems displayed negative charge, differing little when inclusive of DOX. Between the preparations, the *freeze fracture* system showed the highest charge of -15 mV with the *film insertion* slightly lower at -19 mV and *post insertion* the most negative at -25 mV. When the extrusion step was substituted with sonication, a number of the physicochemical characteristics change. Between the DOX encapsulating systems and those incorporating ICG alone, there is little difference in the characteristics, only the *film insertion* protocol which achieved marginally higher ICG incorporation in the system incorporating ICG alone with an efficiency of 46% compared to 41% in the DOX inclusive system. In comparison between the three protocols, there is a similar trend to the extruded samples in terms of the relative ICG incorporation efficiency with the *freeze fracture protocol* incorporating the least ICG at 27% and the *post insertion protocol* incorporating the most at 64%. Considering the superior ICG incorporation efficiency, different starting concentrations of ICG were tested to push the ICG loading potential of the system (**Figure 5.2**). By increasing the concentration above 200 μM , there was a higher level of aggregation observed by the decreasing ratio between the absorbance maxima (A_{max}) at 805

nm and the aggregation peak at 740 nm (**Figure 5.2c**). This meant that despite the increased ICG concentration there was not a substantial increase in OD, hence 200 μ M was fixed as the starting concentration.

Comparing the extruded liposomes, sonication increased the ICG incorporation efficiency by about 100% in each of the protocols tested. In terms of the lipid yield, it appeared that the *freeze fracture* and *film insertion* protocols relinquished a larger proportion of lipids during the extrusion process, with an average yield of 82% for the sonicated *freeze fracture* in comparison to 50% for the extruded *freeze fracture*. For the *film insertion* the average lipid yield was 88% for the sonicated systems and 62% for those which underwent extrusion. The *post insertion protocol* does not follow the same trend. The average yield for the sonicated liposomes is 71%, in comparison to 79% for the extruded systems. The relative yields of the liposome-DOX whereby the yield of the extruded system is lower than the sonicated, 69% and 91% respectively. It was possible to load a higher concentration of DOX into each of the sonicated systems than the extruded. The sonicated *freeze fracture* system could incorporate 97% in comparison to 81% in the extruded, the *film insertion* encapsulates 94% in comparison to 83% and the *post insertion* encapsulates 98% in comparison to 90%.

Without the incorporation of ICG there was little difference in the DOX loading potential between the two liposome formation protocols, with the sonicated loading 100% to the extruded liposome's 97%. In terms of the resultant sizes incorporating sonication; the *freeze fracture* and *post insertion* protocols resided around 97 nm in diameter, with a PDI of about 0.15. The *film insertion* protocol displayed a larger resultant size of about 122 nm with a PDI of 0.27. Through the use of sonication, in general, the sizes generated were smaller than with the selected extrusion protocol, and the PDI was much larger. The zeta potential for the *sonicated freeze fracture* and *film insertion* systems was lower than the extruded, at about -30 mV in comparison to -15 mV for the extruded *freeze fracture* and -20 mV for the *film insertion*. For the *post insertion protocol*, the zeta potential changed negligibly between the extrusion and sonication protocol, with a value of -23 mV for the sonicated and -24 mV for the extruded. To understand the contribution of the methodology to the zeta potential, one considers the ICG free liposome-DOX systems, which showed a lower value of -35 mV for the sonicated system over -27 mV for the extruded.

a

Initial [ICG] μM	Lipid Recovery	Final ICG		Lipid:ICG	Hydrodynamic diameter, \varnothing (nm)	Polydispersity Index, PDI	Zeta Potential, ζ (mV)
		μM	IE [†]				
0	96%	0	0	-	100.3 \pm 1.43	0.222 \pm 0.016	-21.0 \pm 1.0
50	97%	29	58	431:1	105.0 \pm 1.8	0.241 \pm 0.003	-18.4 \pm 0.6
100	96%	58	58	215:1	106.3 \pm 2.8	0.237 \pm 0.006	-18.1 \pm 0.3
200	96%	126	63	99:1	105.8 \pm 2.5	0.248 \pm 0.026	-19.7 \pm 1.2
400	97%	162	41	77:1	104.3 \pm 1.7	0.240 \pm 0.015	-20.1 \pm 1.0
600	96%	189	32	66:1	106.3 \pm 1.6	0.232 \pm 0.018	-18.4 \pm 1.5
800	96%	228	29	55:1	105.8 \pm 2.1	0.247 \pm 0.015	-18.7 \pm 1.1

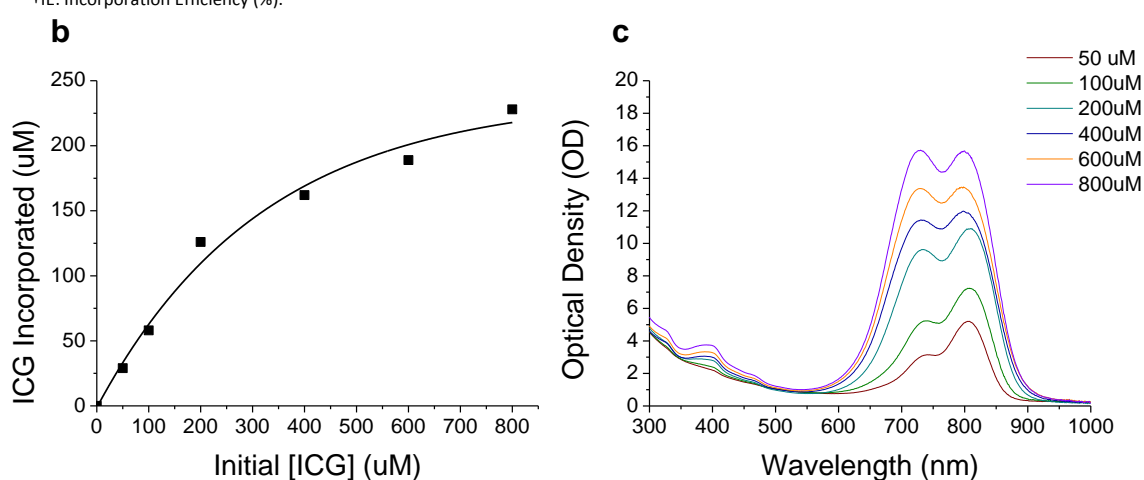
[†]IE: Incorporation Efficiency (%).

Figure 5.2. Testing ICG integration during the post insertion protocol by varying the initial ICG concentration between 0 and 800 μM . **(a)** Tabulated physicochemical characterisation of liposomes prepared via post Insertion protocol with a starting lipid concentration of 12.5mM. **(b)** ICG incorporation vs initial ICG concentration of liposomes of 12.5mM starting lipid concentration. **(c)** Absorbance spectra of liposome-ICG, to monitor the concentration vs OD, and relative aggregation.

Table 5.1. Tabulated physicochemical characterisation of each of the liposome systems constructed comprising; liposome-ICG, liposome-DOX and liposome-ICG-DOX at a 12.5 mM lipid concentration.

System	Lipid	ICG		Lipid:ICG Ratio	Doxorubicin		Hydrodynamic diameter Ø (nm)	Polydispersity Index, PDI	Zeta Potential ζ (mV)
	Recovery (%)	μM	IE†		μM	EE‡			
Liposome-ICG									
<i>Extruded</i>									
Film Insertion	67	47	23	267:1	-	-	131.3 ± 0.7	0.067 ± 0.024	-18.4 ± 0.5
Freeze Fracture	50	30	15	422:1	-	-	127.1 ± 1.3	0.048 ± 0.004	-14.5 ± 1.1
Post Insertion	79	66	33	189:1	-	-	150.7 ± 0.8	0.065 ± 0.004	-25.2 ± 0.9
<i>Sonicated</i>									
Film Insertion	86	92	46	136:1	-	-	124.3 ± 1.9	0.275 ± 0.005	-29.6 ± 0.9
Freeze Fracture	77	55	28	227:1	-	-	99.0 ± 2.4	0.171 ± 0.009	-31.0 ± 1.8
Post Insertion	69	126	63	99:1	-	-	95.5 ± 0.9	0.153 ± 0.006	-22.7 ± 0.1
Liposome-DOX									
<i>Extruded</i>	69	-	-	-	776	97	137.6 ± 4.2	0.025 ± 0.020	-26.8 ± 0.9
<i>Sonicated</i>	91	-	-	-	800	100	100.6 ± 1.6	0.162 ± 0.002	-34.6 ± 0.1
Liposome-ICG-DOX									
<i>Extruded</i>									
Film Insertion	56	62	31	201:1	664	83	128.7 ± 0.8	0.046 ± 0.016	-20.1 ± 0.4
Freeze Fracture	51	31	16	402:1	648	81	128.4 ± 1.0	0.056 ± 0.007	-15.3 ± 0.6
Post Insertion	78	66	33	188:1	720	90	148.0 ± 0.7	0.058 ± 0.016	-24.0 ± 0.2
<i>Sonicated</i>									
Film Insertion	89	83	41	151:1	750	94	121.8 ± 1.2	0.243 ± 0.011	-29.9 ± 0.1
Freeze Fracture	87	52	26	240:1	718	97	94.2 ± 0.7	0.132 ± 0.012	-29.7 ± 0.2
Post Insertion	73	128	64	98:1	784	98	98.4 ± 0.8	0.141 ± 0.007	-23.5 ± 1.6

†IE: Incorporation Efficiency (%). ‡EE: Encapsulation Efficiency (%)

5.2.3 DOX retention at 4°C and release at 37°C in 50% serum

Retention of doxorubicin over time was measured to discern the stability of the composite systems (**Figure 5.3a, 5.3b**). There were negligible changes in the level of DOX leakage in almost all of the formulations. The extruded *freeze fracture* liposome which showed and maintained a 6% decrease after 3 days with the *post insertion*, the *film insertion* and the *freeze fracture* retaining their total doxorubicin content at 4°C in HBS over the 16-18 days monitored. To emulate *in vivo* conditions during circulation, the liposomes were incubated at 37°C in 50% serum. For the extruded systems (**Figure 5.3c**), the *freeze fracture* showed the lowest level of release of 6% over 24 hours, the *film inserted* liposome showed 11% and the *post inserted* vectors displayed the highest level of release of 22%. This may be as a result of the relative ICG concentrations and aggregation status, or the positioning of the ICG within the bilayer. When considering the sonicated liposomes (**Figure 5.3d**), the *freeze fracture* liposomes again showed the lowest level of release of 11%, the *film insertion* liposome released 18%, and the *post insertion protocol* liposome appeared similar to its extruded counterpart releasing 21% over 24 hours. The level of release does appear to be consistent between protocols, in terms of the *freeze fracture* being the most stable and the *post insertion* releasing the most, whether extruded or sonicated.

Overall extrusion resulted in the formation of more stable liposomes than sonication for the *freeze fracture* and *film insertion* in terms of DOX retention in these conditions. However, the method of downsizing did not effect the *post inserted* liposomes in terms of release. To further understand the differential extents of release, fluorescence anisotropy was used to probe the relative fluidity of the different bilayer components (**Figure 5.4**). DPH and ANS probe the hydrophobic acyl chain segments and polar headgroups respectively, using a fluorescent readout of relative probe motility over a defined temperature ramp to define the fluidity of the bilayer. Simply, the higher the anisotropic value, the more stable the bilayer component. Overall, the extruded liposomes appeared more rigid over the temperature ramp in comparison to the sonicated systems in terms of the polar ANS component. In terms of the DPH anisotropy, there was little difference observed between sonication and extrusion for the *freeze fracture* and *film insertion* preparations, a slight increase in fluidity at the higher end of the temperature ramp for the sonicated systems, and an overall increase in fluidity for the liposome-DOX prepared through sonication over extrusion. However, the relative observed increase in fluidities did not particularly correlate with the relative release at 37°C.

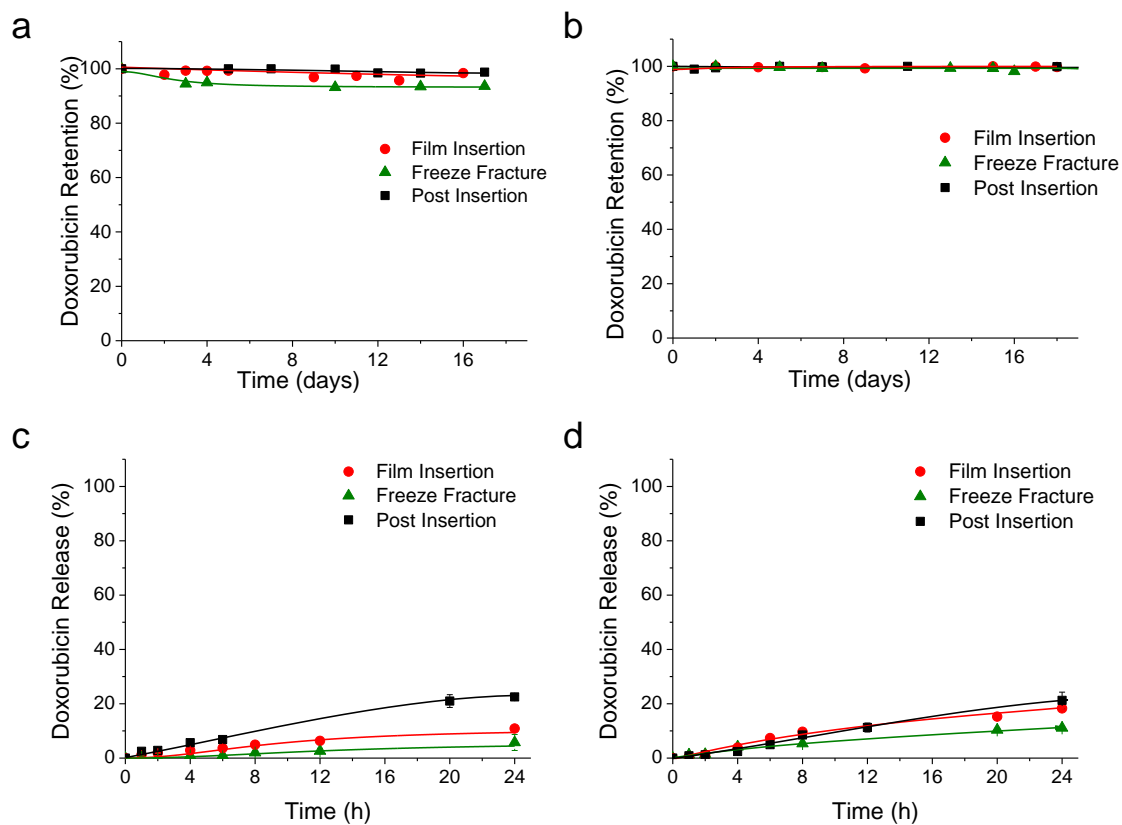


Figure 5.3. DOX retention and release of liposome-ICG-DOX systems prepared via each of the three protocols, via film insertion (red), freeze fracture (green) and post insertion liposomes (black). **(a)** DOX retention at 4°C in HBS of 12.5mM liposomes formed initially using extrusion, or **(b)** sonication. **(c)** DOX release at 37°C in the presence of 50% serum of liposomes formed initially via extrusion, or **(d)** sonication.

5.2.4 DPH/ANS anisotropy of each liposome–ICG–DOX system prepared via the differing protocols

DPH/ANS fluorescence anisotropy was tested (**Figure 5.4**) to investigate whether the difference in preparation protocol affected the intrinsic fluidity of the bilayer and whether it would be possible to localise the ICG within the aforementioned bilayer. Via DPH anisotropy the DPH probed the disruption in Van der Waals forces which maintain the hydrophobic region of this colloidal system, it appears that there is almost complete overlap between the ICG free and incorporating systems initially formulated via extrusion and sonication respectively. This indicates that there is more significant interaction of the ICG with the polar head group portion of the bilayer than the acyl chain portion in the *post insertion* system than in the *film insertion* and *freeze fracture* systems, which is logical considering the method of entry and relative exposures of the ICG to the hydrophobic regions of the liposomes.

ANS anisotropy indicated higher values and thus a more rigid bilayer for the extruded liposomes over the sonicated, which correlates with the relative size differences. However the relative fluidity demonstrated by the ANS anisotropy did not correlate with the relative rates of release at 37°C. Overall, there was not a substantial change in the relative fluidity of the bilayers in response to ICG incorporation. The effect of cholesterol on the stabilisation and structure of the bilayer indicates increased steric hindrance and reduction of void spaces through the tessellation of the molecule between the phospholipids. ICG has a much higher binding affinity to phospholipids than cholesterol²⁴², so it is most likely that ICG mainly interacts with the phospholipid component. It has been observed that ICG increases the critical micelle concentration of surfactant micelles indicating that within the phospholipid, the ICG disrupts the traditional conical spatial occupation of the molecule critical to the formation of micelles themselves.

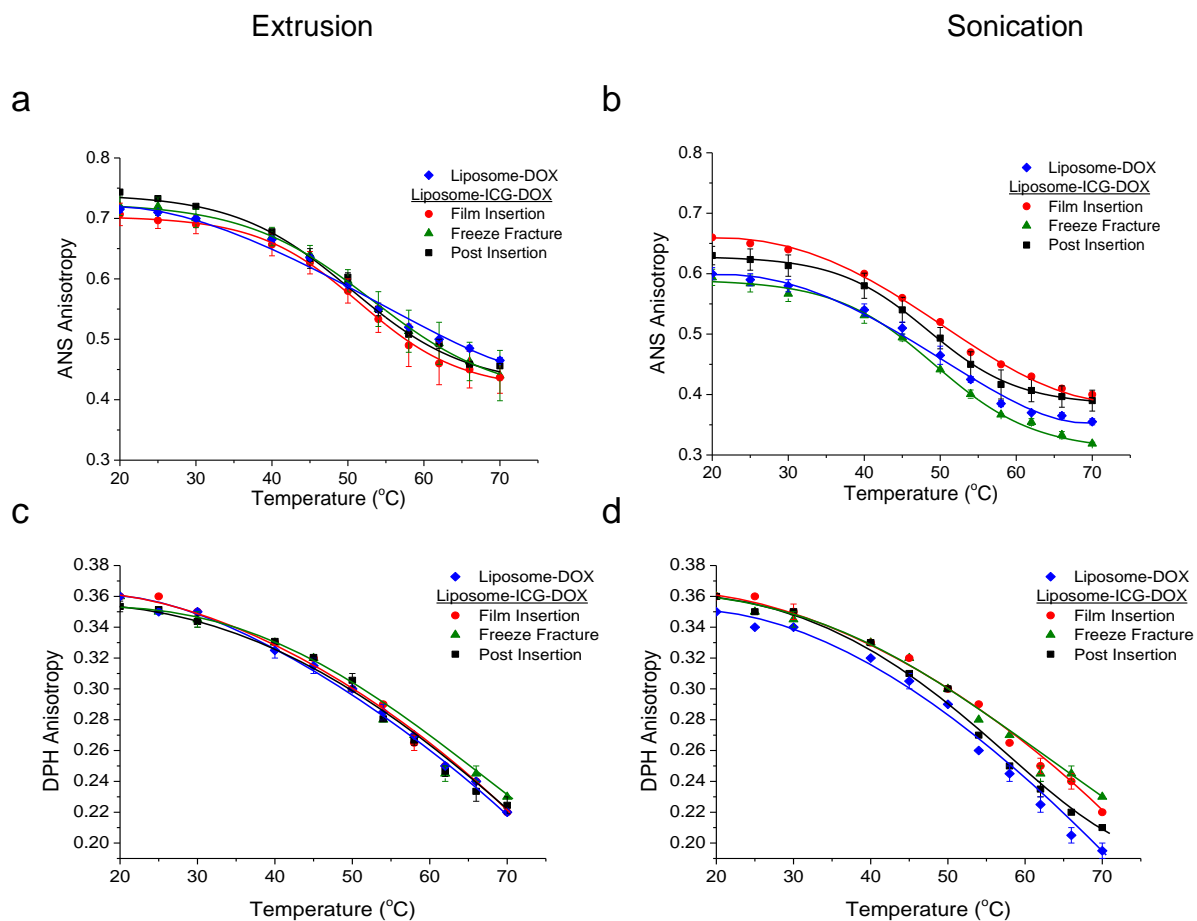


Figure 5.4. DPH/ANS fluorescence anisotropy of each of the liposome-ICG-DOX formulations prepared via film insertion (red), freeze fracture (green), post insertion liposomes (black) and liposome-DOX (blue). ANS anisotropy of liposome-ICG-DOX formed **(a)** by extrusion, or **(b)** via sonication. DPH anisotropy of liposome-ICG-DOX formed by **(c)** extrusion or **(d)** via sonication.

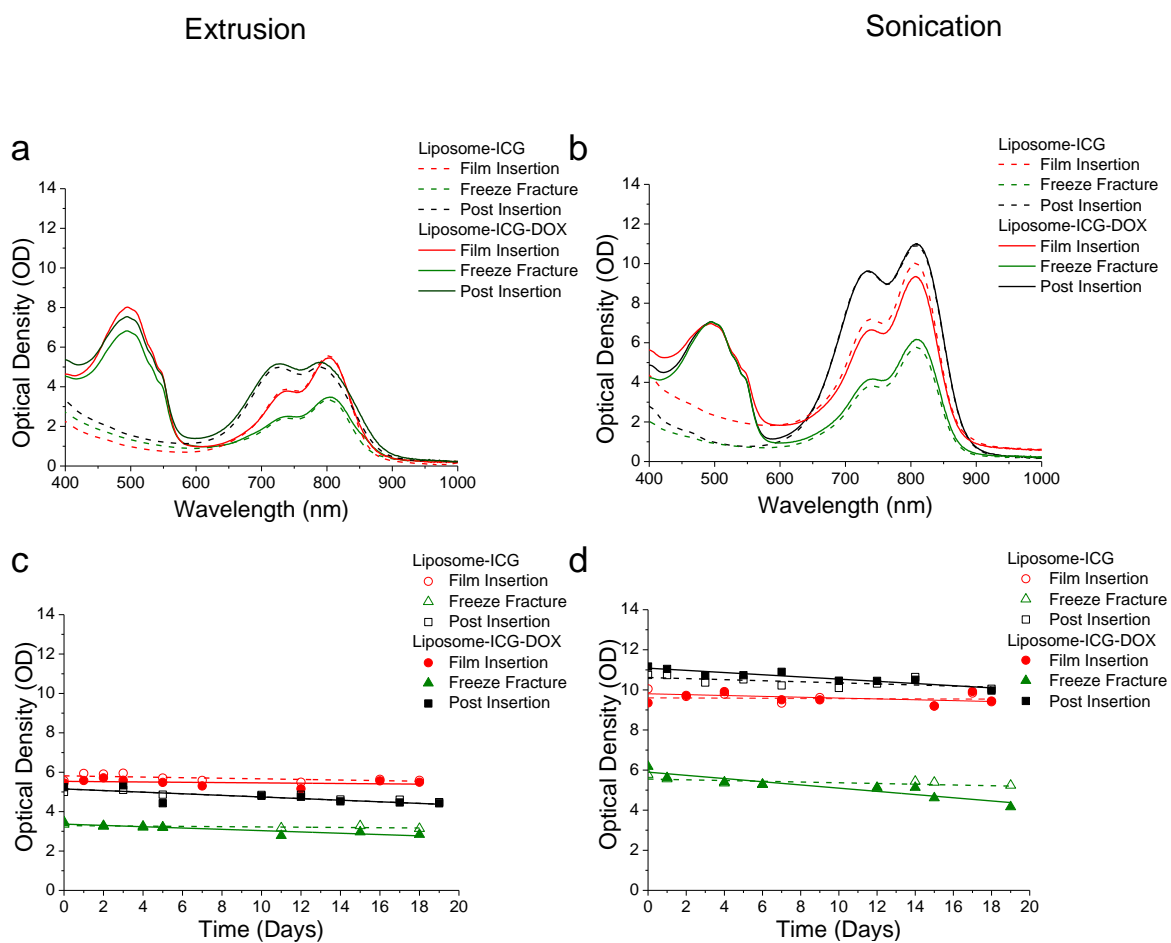
5.2.5 Optical density and stability of the liposome-ICG-DOX systems prepared via differing protocols.

To better predict the utility of liposome systems for imaging purposes the optical density and relative stability were monitored over time (**Figure 5.5**). The absorbance spectra of each of the liposome systems comprise 3 major peaks (**Figure 5.5a & b**); the λ_{max} of the monomeric ICG at 790-810 nm, the characteristic shoulder at 750 nm indicates early stages of aggregated ICG finally the peak of the DOX present in the liposome-ICG-DOX systems at 500 nm. As expected the ICG optical density (OD) of the extruded liposomes (**Figure 5.5a**) in overall were much lower than the sonicated liposomes (**Figure 5.5b**), as a result of the relative ICG concentrations. The extruded *freeze fracture* system displayed the lowest OD of all the systems, with both DOX inclusive and exclusive spectra overlapping apart from the DOX peak at 500 nm. Through the substitution of the extrusion step with sonication, the ICG OD increases from 3 to 6, with the ratio of the monomeric and aggregate peaks appearing consistent, varying in the relative amplitude only. The extruded *film insertion* system has an OD of 5 for the ICG alone system and 6 for that comprising DOX.

When sonication is employed the OD increases to 10 for both DOX inclusive and free systems. Like the *freeze fracture* system, the relative amplitude changes with little change in the shape of the peak itself. The extruded post insertion system displays an OD of 5 for both DOX inclusive and exclusive systems, with an almost equal contribution from the monomeric and aggregate peaks. When sonication is applied, both DOX present and absent spectra superimpose. The OD rises to 11 and the ratio between the monomeric and aggregate peak increases over the sonicated system. However, the ratio between the peaks of the absorbance maxima and the shoulder at 750 nm for the sonicated *film insertion* and *freeze fracture* is higher than that of the post insertion, indicating a lower level of aggregation of the constituent dye, either as a result of the lower concentration, or the production protocol. In terms of the optical stability over time as seen in **Figure 5.5c & d**, all the systems appears fairly stable over the 18 days monitored. For the extruded systems in **Figure 5.5c**, each system shows around a 0.5 (± 0.3) decrease in OD within 20 days.

In terms of the sonicated systems in **Figure 5.5d**, there is a higher level of fluctuation in OD. The *freeze fracture* system comprising ICG alone displays a 0.5 OD decrease and comprising DOX, shows a 2.0 OD decrease. The *film insertion* system comprising ICG alone shows a decrease in OD of 0.6, however in the presence of DOX, there is no overall decrease in OD. In the post inserted system, there is a 0.7 decrease in OD of the system comprising ICG alone, and in the presence of DOX, there is a 1.2 OD decrease. Regardless of the drop in OD,

the sonicated *post insertion* system still displays the highest OD of 10 after 18 days, marginally more than the 9.4 OD of the film inserted system.



5.2.6 *In vivo* MSOT Imaging of liposome-ICG-DOX

Following the development of the liposome ICG incorporation protocol, sonicated *film inserted* and *post inserted* liposome-ICG-DOX are both promising systems to take forward. Here, the sonicated *post inserted* system was selected for *in vivo* MSOT tumour imaging (**Figure 5.6a**) based on its superior optical density. The Initial scan at 800 nm provides an anatomical view of the section of the mouse in the form of a greyscale image with the source of contrast emanating from endogenous tissue chromophores, particularly oxy and deoxyhaemoglobin²⁴³. This can be substantiated by the signal which emanates from the major tumour supplying blood vessels indicate dby the number 2. This provides a reference upon which the signal emanating from the ICG within the liposomes can be superimposed. Following IV injection of 200µl of 12.5mM liposome into a 4T1 orthotopic tumour bearing mouse, a spike in the optoacoustic signal was observable from the vasculature supplying the tumour after just 10 minutes. At 24 hours, a peak arose from the periphery of the tumour, as well as from the major blood supply to the lesion. There is also a diffuse signal spread throughout the tumour tissue itself with a very low level of background observable from the rest of the section.

When DOX and ICG tumour uptake was validated by fluorescence cryosection (**Figure 5.6b**), low levels of DOX accumulation and negligible levels of ICG were noted after 1 hour in the tumour site, with some diffuse levels of background fluorescence from each constituent. However, at 24 hours, a very high level of both dye and drug could be observed from the tumour tissue, with some emission detected from the tissues of the adjacent hind limb. Similarly, the distribution of liposome-ICG-DOX throughout the whole body revealed that initial detected signal was diffusely spread throughout the body with broad signal emanating from the liver and spleen, with low levels specifically emanating from the tumour. After 24 hours, some specific organ accumulation, with lower signal than in the 1 hour scan observed emanating from the spleen, liver, gallbladder, and a high signal detected from the entire tumour mass, clearly showing tumour accumulation of the liposome system (**Figure 5.6c & 5.8**).

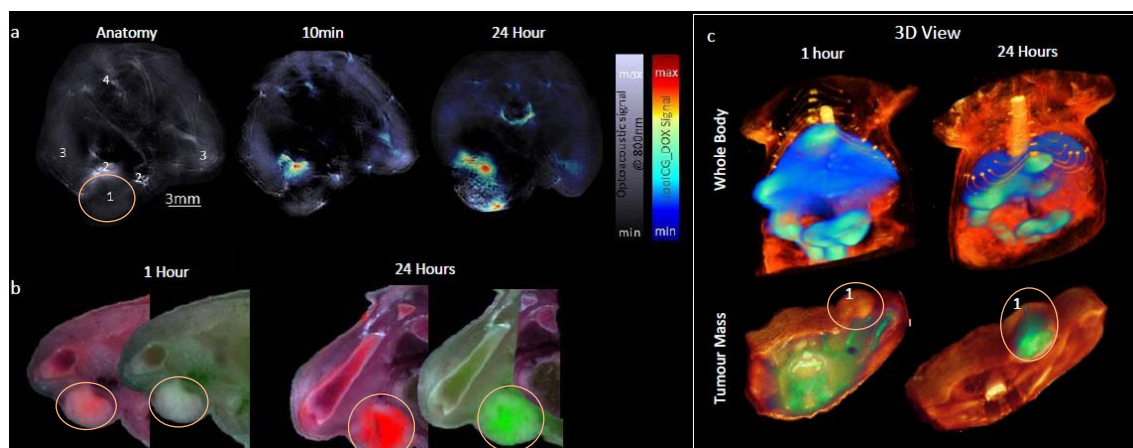


Figure 5.6. *In vivo* validation of tumour accumulation of liposome-ICG-DOX prepared via the *post-insertion* protocol. (a) Temporal description of tumour accumulation as displayed through MSOT at 10 minutes and 24 hours. (b) Fluorescence cryosection image for validation of the MSOT signal derived from the ICG at 800 nm and validation of co-localisation of doxorubicin at 593 nm, both overlapped in a colour photograph. (c) 3D reconstruction of the fluorescence cryosection image from the ICG signal (green) of the whole mouse body (top) and tumour mass region (bottom). (1: 4T1 orthotopic tumour encircled in orange; 2: tumour feeding blood vessels; 3: muscle hindlimb; 4: spinal cord). (Imaging experiments undertaken by Dr. Antonio Nunes from the Technical University of Munich.)

5.3 Discussion

Presented are three protocols which not only allow the incorporation of DOX at therapeutic levels but also have resulted in the development of the protocol which incorporates ICG at efficiencies almost 10 fold of that which has been reported by other groups^{87,238}.

The *film insertion protocol* introduces the dye with the constituent lipids in organic solvent, exploiting ICGs high solubility in these conditions. It endeavored to most directly incorporate ICG into the bilayer promoting interaction of the dye with the solubilised constituent phospholipids prior to its inclusion into the lipid film, and subsequent liposome formation. Through this methodology, the ICG would have less exposure to the excipient buffer than the freeze-fracture protocol, and would theoretically aggregate less. This is likely to have been the factor which reduced the stiffness of the extrusion process in comparison to the previous protocol, thus increasing the yield, as well as facilitating the incorporation of a higher concentration of well tessellating, monomeric ICG as realised in the observed increased incorporation efficiency. The process is also shorter than the previous protocol due to the omission of the freeze fracture cycles as well as the easier extrusion when incorporated in place of sonication, meaning that the liposome-ICG would have spent less time in the liquid crystal state. The well incorporated ICG would also manifest itself in stable OD over time, as well as resilience to doxorubicin leakage during storage as well as when incubated in serum, all of which have been observed. Although the extrusion process was less stiff than with the previous protocol, through comparison with the sonication protocol, the reduced lipid yield and ICG incorporation efficiency continues to indicate a similar loss of ICG during extrusion. Following liposome formation, the liposomes undergo the same steps to facilitate active loading of DOX through establishment of a transmembrane pH/salt gradient for each protocol.

The well established *freeze fracture* protocol hydrates the lipid film with ICG in ammonium sulphate, the lipid ICG suspension is repeatedly frozen and thawed. The tactic of this protocol was to incorporate ICG into the lipid bilayer through its repeated fissuring and reformation, allowing the dye to stack amongst the phospholipids themselves. However due to the poor solubility of the dye in aqueous salts, particularly ammonium sulphate, much of the dye is likely to have aggregated following its solubilisation at concentrations above 100 μ M²⁰³. Increasing the temperature to around 60°C has also been reported to increase the levels of aggregation²⁴⁴. Following its aggregation it would have made it more difficult for the majority of it to incorporate, as well as a proportion of it being encapsulated into the liposomes rather than being intercalated into the bilayer.

The subsequently stiff extrusion is likely to have been as a result of these aggregates clogging the extrusion pores following its sifting from the liposomes themselves, and is likely to be the source of the lipid loss during the protocol. This can be justified when comparing the generally meagre lipid yield following extrusion in comparison to when sonicated. By prolonging this process through the increased effort required for downsizing, a proportion of the monomeric ICG sat within the bilayer is likely to have been released due to the increased length of time spent at 60°C. At this temperature, the bilayer is in a liquid crystal state at which point the ICG would have been more loosely associated with the liposomes themselves. Removal of these aggregates, and more loosely associated ICG would be concurrent with the lower ICG incorporation efficiency attained through this incorporation protocol when inclusive of extrusion rather than sonication. Sonication involves the passage of ultrasound waves through the lipid suspension above the bilayer phase transition temperature. This disturbs the solubilised lipid films resulting in the destruction of the higher order packing of phospholipids in the lipid film and subsequent reformation, downsizing them to the liposome subgroup of single unilamellar vesicles. Extrusion involves the forced passage of the lipid suspension, above the phase transition temperature, through membranes comprising pores of defined sizes sequentially reducing the membrane pore size through every set of passages. This process forces the lipid membranes to deform and dissociate in a highly size resolved manner resulting in liposomes of a highly defined size and low polydispersity. The dye which remained is likely to have been less aggregated and better incorporated into the bilayer itself. It has been trialed but not previously possible to incorporate therapeutic concentrations of doxorubicin in the past in addition to ICG⁹⁰.

The *post insertion* methodology is novel for ICG incorporation into liposomes, but takes elements similar to those techniques used for the incorporation of phospholipid ligated antibodies to pre-formed liposomes^{90,245} requiring co-incubation of the liposomes and dye close to the liposome transition temperature. The protocol also takes points from the co-incubation of erythrocyte ghosts with ICG²¹⁴ where the free dye successfully incorporates into the plasma membrane without necessitating incorporation in the initial stages through *freeze fracture* cycles or co-dissolution with phospholipids in organic solvent. This protocol attempted to address the issues mentioned in the previously described protocols by reducing the level of adulteration of the liposome-ICG, likely to be responsible for the low incorporation efficiency of ICG into the system. Specifically, the dye was added in the final stages of DOX loading, while the liposome bilayer was still in a liquid crystal state, to try to facilitate its inclusion into the bilayer. This sought to exploit the intrinsic properties of the dye through its propensity to fall into the most entropically favourable environment, satisfying both hydrophobic and

hydrophilic elements of the dye interacting within the lipid bilayer, as well as facilitating favourable charge interactions between the dye and the polar head group of the constituent phospholipids. Subsequently the time which ICG spends at 60°C in buffer is just 10 minutes. Due to the lack of ICG in the initial stages, this protocol yielded the most lipid following extrusion. As the liposome and ICG spends just 10 minutes at 60°C during incorporation and there are no additional heating steps imposed on the composite system, the highest ICG incorporation was expected and subsequently realised. Due to the difference in chronology of ICG incorporation, the aggregated ICG dimers and poorly associated ICG would not have been sifted out of the bilayer, resulting in the lower ratio between the absorbance peaks at 800 nm:750 nm as observed in the extruded iteration. This higher aggregate contribution resulted in a higher ICG concentration but a lower OD than the film inserted systems, due to the lower quantum yield of aggregated ICG over monomeric.

The OD of the post inserted system is lower per unit of ICG incorporated in comparison to the other systems. This may have resulted in the highest DOX release at 37°C between the extruded systems. When comparing the extruded to the sonicated *post inserted* systems, the reasons behind the improvement in optical density and relative ICG incorporation efficiency is not initially obvious when based on the extrusion ICG aggregate sifting effect. Sonication below the phase transition temperature (T_m) of a system can induce defects in the bilayer²⁴⁶. The sonication step is carried out at 60°C, above the T_m of the major constituent lipid HSPC ($T_m \sim 55^\circ\text{C}$), This is as a result of the inclusion of cholesterol at a molar ratio of 38%, as above 33% there is an elimination of a specific T_m negating the use of differential scanning calorimetry on these systems⁷⁸. This results in a phase transition of gel to intermediate fluid state over the temperature range rather than a clear cut gel to liquid phase transition. However, above 33% molar ratio, cholesterol's inhibition of phase transition, it is likely that there will be an increased number of defects in the sonicated systems over the extruded.

Cholesterol orientates itself to allow hydrophobic interactions of the hydrocarbon chain as well as the sterol head group resulting in a deep insertion into the bilayer. The hydroxyl group forms a hydrogen bond with the terminal phosphate of the adjacent phospholipids, and as a result causes a steric hindrance to the glycerol regions without a specific interaction with them²⁴⁷. Another possibility arises when one considers the relative size difference between the sonicated and extruded systems. The sonicated system is 50 nm smaller in diameter than the extruded. This means that the relative curvature of the liposome is much higher, thus the fluidity of the bilayer due to the reduction in concinnity of the respective constituents, disrupting polar and hydrophobic interactions between them, as well

as increasing the relative void space within the membrane. The relative increase in distance between the polar head groups will potentially reduce the propensity of the hydroxyl to phosphate bond formation providing an increased opportunity for electrostatic interactions between the encroaching ICG and the polar head groups. This vacant space may also logically increase the porosity of the bilayer to *post insertion* of ICG.

Another justification for the increased ICG incorporation based on size is that the suspension of smaller liposomes will have a higher available surface area with which the ICG may interact as well as a lower surface charge facilitating possible charge interactions between the ICG and the lipid polar head groups. This can be justified by the consistently high ICG incorporation results in the system being more effective and efficient than the other protocols. The DOX encapsulation efficiency was also slightly higher, likely due to the DOX having entered the liposome already rather than having to contend with an ICG-incorporating bilayer. This may also be to do with the increased fluidity of smaller liposomes. Despite these potential qualms, the OD is still consistently higher with the *post insertion* than each of the other protocol. The DOX retention over time was also very stable with negligible loss observed over 18 days for almost every system. DOX release at 37°C in 50% serum was monitored to simulate conditions during *in vivo* circulation. 24 hours was the time-point selected as it has been established as the point of peak tumour accumulation of DOXIL amongst other liposomes⁷⁸.

The same work also demonstrated no DOX release from DOXIL over this time period. The extruded *film insertion* and *freeze fracture* appeared released the least likely due to the lower ICG concentration and higher ratio of monomeric vs aggregated ICG, which would have applied less stress on the tessellation of the constituent phospholipids in comparison to the extruded post inserted liposomes. The release increased in the sonicated systems for the *freeze fracture* and *film insertion* protocols, likely due to a combination of higher surface area due to the reduced size of the liposomes facilitating a higher level of heat conduction, and protein absorption than would be observed in larger liposomes. Reduction in size has been shown to increase relative release of carboxyfluorescein from thermosensitive liposomes²⁴⁸. However the only system which correlates with this is the *freeze fracture* with the increased release of the sonicated over extruded system. Otherwise, rate of release and size appear unrelated when comparing the other systems. The increased ICG concentration may have also caused more stress on the bilayer. The *post insertion* did not appear to react in the same way, remaining fairly unchanged between the extruded and sonicated systems in terms of DOX release. It is likely that a combination of reduced capacity of ICG incorporation in the extruded system due to the relative size/curvature, and the higher ICG incorporation in the post-

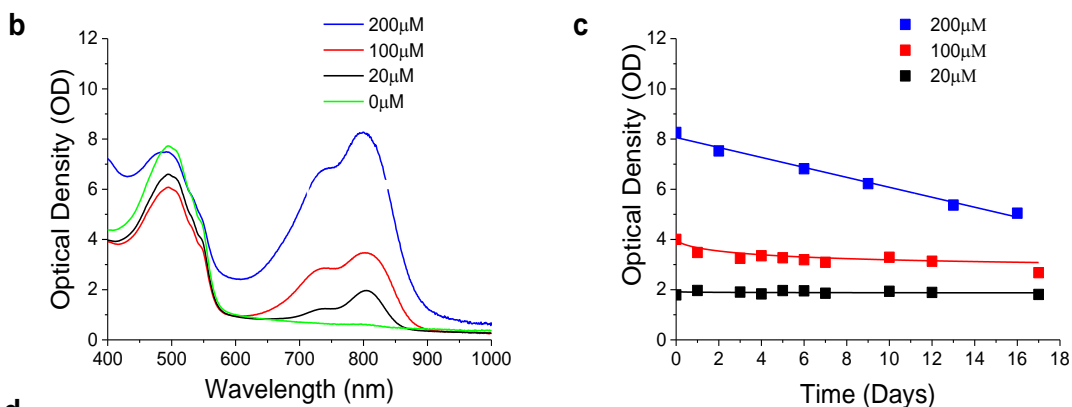
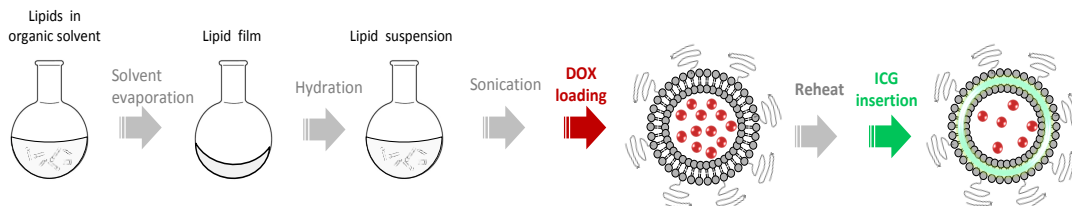
insertion system may have both had relative denigrating effects in terms of the permeability of the bilayer and thus facilitated a more rapid release for different reasons.

The disruption of ICG self-aggregation through phospholipid interaction is lipid charge independent²⁴⁹. This is likely to have resulted in the increased particle size of the sonicated *film insertion* preparation over the other sonicated liposomes. The bathochromic shift observed following liposome incorporation also indicates that the ICG has moved to a more hydrophobic environment. However it is important to consider that the dye is quite a complex amphiphile, comprising two heterocyclic groups providing the propensity to form hydrophobic interactions, one of which contains a pyrrolidine contributing a positive charge and two sulphonate groups contributing a negative charge each. The most logical conclusion to draw from further understanding this molecule is that the ICG sits in the partition between the hydrophobic and hydrophilic regions of the bilayer, with the *film insertion* and *freeze fracture* liposomes having the ICG more deeply embedded than the *post insertion* liposomes where there is more interaction with the polar lipid head groups. This can be explained by the mode of incorporation where in the *film insertion protocol*, the ICG is able to freely interact with solubilised phospholipids in organic solvent, and further during the evaporation and film formation, allowing the most entropically favourable orientation of the dye. With the *freeze fracture protocol*, the lipid film is hydrated then undergoes multiple freeze fracture steps, breaking and reforming the lipid bilayers allowing interaction and intercalation of the ICG amongst both regions of the phospholipids. With the *post insertion* protocol, the ICG is not exposed to the hydrophobic portion, but incorporates into the bilayer via the polar portion resulting in more superficial embedding into the bilayer, however, embedding deeply to negate further interaction with the excipient buffer, and attaining the same bathochromic shift and most of the optical stability over time as observed through the other protocols.

To facilitate the protocol of ICG incorporation for healthcare practitioners using commercial DOXIL[®], the *reheat insertion protocol* was also trialed (**Figure 5.7**). The difference between this protocol and the *post insertion* was an overnight stabilisation at 4°C between DOX purification and ICG insertion. This acts to emulate the condition of the DOXIL[®] as available from the relevant healthcare provider. The resultant system, comparing at the same initial ICG concentration of 200µM, only encapsulated 22% of DOX (**Figure 5.7d**) and exhibited a size increase of almost 40% (150 nm). Reducing half the initial ICG concentration, maintained about 80% of the encapsulated DOX and resulted in a system incorporating 37µM ICG with an OD of 4. In general, the physicochemical characteristics of this system were very similar to that produced through the sonicated liposome-DOX-ICG protocol. Although the resultant OD may

not be as high as the optimum systems, this does not necessarily negate its value for a wealth of other imaging modalities especially considering its ease of production.

a Reheat insertion



d

Initial [ICG] (μM)	Lipid		ICG		Lipid:ICG Ratio	Doxorubicin		Hydrodynamic diameter, ϕ (nm)	Polydispersity Index, PDI	Zeta Potential, ζ (mV)
	Recovery (%)		μM	IE \ddagger		μM	EE \ddagger			
0	100		-	-	-	768	96	110.2 ± 1.4	0.242 ± 0.003	-34.5 ± 1.4
20	88		13	65	960:1	710	89	108.3 ± 1.8	0.197 ± 0.011	-22.0 ± 0.7
100	90		37	37	334:1	665	83	110.7 ± 1.7	0.166 ± 0.003	-21.2 ± 1.1
200	69		80	40	157:1	176	22	147.6 ± 1.5	0.193 ± 0.011	-27.3 ± 1.9

\ddagger IE: Incorporation Efficiency. \ddagger EE: Encapsulation Efficiency

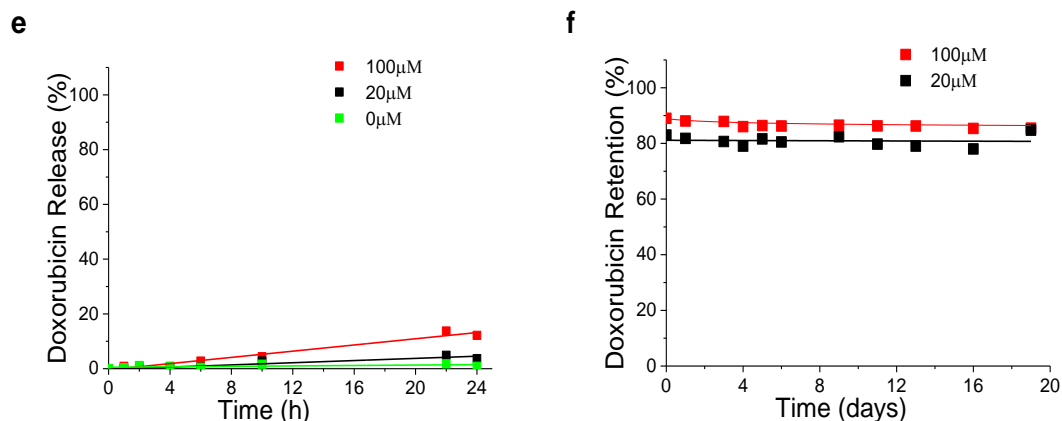


Figure 5.7. Characterisation of the reheat insertion protocol of ICG and DOX incorporation into HSPC:cholesterol:DSPE-PEG₂₀₀₀ liposome. **(a)** Schematic representation of liposome preparation protocol. **(b)** Optical density (OD) spectra of 200 μM (blue), 100 μM (red), 20 μM ICG (black) and 0 μM (green). **(c)** Peak optical density over time of 200 μM (blue), 100 μM (red), 20 μM DOX (black)). **(d)** Tabulated values following physicochemical characterisation of all liposomes. **(e)** DOX retention over 24 hours at 37°C in 50% mouse serum. **(f)** DOX retention over time of liposomes at 4°C.

There is quite a large variation in tumour uptake of DOXIL[®] which relies on the enhanced permeation and retention effect. This variation is dependent on the level of poorly constructed vascularisation of the tumour tissue resulting in leakage of injected nanoparticles into the lesion. Anything between 0.5% and 11.3% of the injected dose is expected to reach the tissue after 72 hours^{220,221}. With a high ICG incorporation efficiency via this protocol, the sonicated post insertion liposome system is an ideal candidate for the purposes of biomedical imaging of vascularised tumours. Although relatively it did show one of the highest DOX releases at 24 hours, but actually this was still a low level of release compared to other DOX/ICG nanoparticles previously mentioned^{235,250}, and considering the efficacy of DOX delivery to tumour sites via the TTSL system, which has been shown to release 60% over 24 hours, this did not appear a particular hindrance.

The *in vivo* imaging was carried out in a highly vascularised orthotopic tumour comprised of the 4T1 cell line. The level of vascularisation of this tumour has in the past resulted in its choice to model the effects of inhibitors of vascular endothelial growth factor receptor inhibitors²⁵¹. The MSOT imaging data, confirms the efficacy of tumour accumulation of the post-insertion liposome-ICG-DOX system, with a high optoacoustic signal emanating from the tumour tissue at 24 hours, which was confirmed via fluorescence cryosection. A 3D reconstruction of a number of fluorescence cryosections in **Figure 5.6c**, show a transverse view of the relative biodistribution of the ICG from the liposomes at 1 and 24 hours. This view clearly shows a reduction in the diffuse signal emanating from the body at 1h and localising in the liver, spleen and in the tumour site which specifically generates a high signal at 24 hours. With the combination of the imaging modality and the potent levels of this photoacoustic contrast agent accumulating in the tissue, the signal to noise ratio is minimal providing excellent resolution of liposome distribution. Raw coronal fluorescence cryosections at different locations in the mouse gives a temporal description of the liposome's biodistribution showing the diffuse ICG fluorescence at 10 minutes and 24 hours in **Figure 5.8**. These sections are colour photographs, upon which the green fluorescent signal has been superimposed. In addition to the sections, the transverse sections are also displayed, further substantiating the aforementioned distribution of the liposome incorporated ICG (**Figure 5.8**). These sections provide a detailed insight into the very early stages of the liposome's biodistribution post injection with the liver, kidneys and spleen showing high contrast due to the high blood supply, with little signal emanating from the tumour mass. After 24 hours, the residual signal from these organs fades and is most prominent in the tumour site. The kidneys lose near all of the contrast with residual signal in the liver and spleen as expected due to the uptake by resident macrophages of the RES tissues. The gall bladder's signal marks the biliary clearance of a

portion of the liposomes from the body via the liver. The biodistribution based on the ICG signal does appear to correlate with that of DOXIL[®] as previously reported, with peak accumulation being observed after 24 hours.⁷⁸

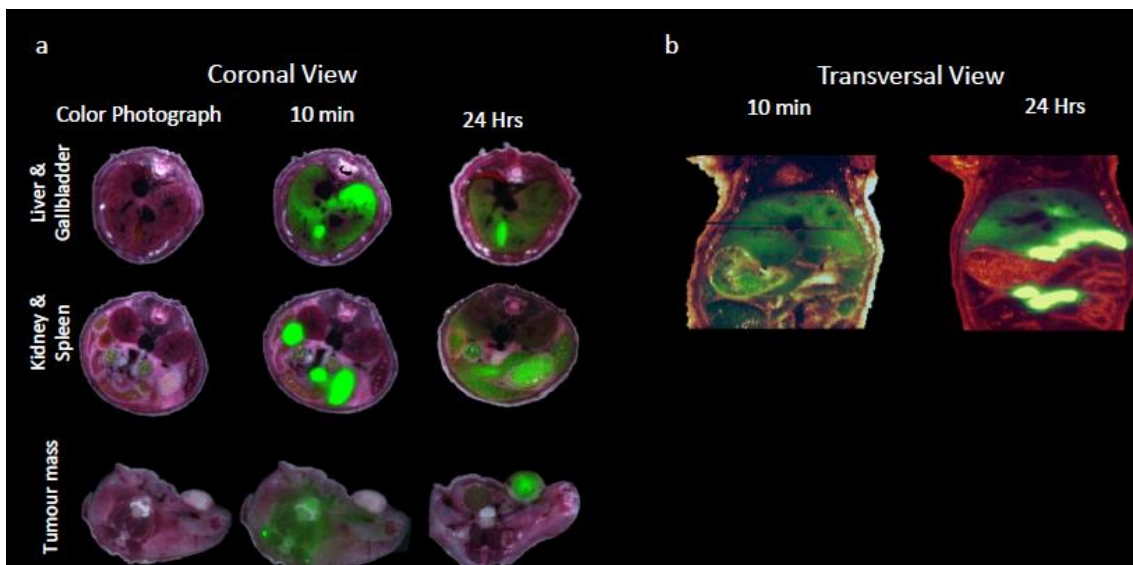


Figure 5.8. Fluorescence cryosection image for validation of the MSOT signal derived from the ICG at 800 nm. **(a)** Coronal view at different organ regions of a color photograph (left panel) overlapped with ICG 800 nm signal after 10 minutes (middle panel) and 24 hours (right panel). **(b)** 2D reconstruction of transversal fluorescence cryosection image from ICG signal (green) of the whole mouse body view. (Images courtesy of Dr. Antonio Nunes from the Technical University of Munich.)

5.4 Conclusion

This work has not only introduced the first liposome system incorporating both ICG and therapeutic concentrations of DOX suitable for intravenous administration, but a number of different protocols to boost the incorporation of both components, with relative ease. With the liposomal composition tested, preparation formation of the liposomes via sonication rather than extrusion led to approximately a doubling in the incorporation efficiency of ICG with the *film insertion and post insertion* protocols demonstrating the highest incorporation efficiency. The relative DOX encapsulation efficiency did not dramatically change between protocols and the physicochemical properties analysed did not show dramatic differences. The development of the *reheat insertion* protocol demonstrates a fast and easy methodology by which healthcare practitioners may develop this liposome-ICG-DOX from commercially available DOXIL[®]. Considering the different techniques reported, integrating ICG in different manners and polarity of solvents, extrapolation of the techniques to incorporate dyes of different relative hydrophobicities may be possible. Due to the lack of chemical modification of these two FDA approved entities and their widespread use as standalone agents, the potential for translation to clinical use is also evident. Finally, with the validation of tumour accumulation of the highest OD *post insertion* liposome-ICG-DOX system, the case for progression to therapeutic studies is evident.

Chapter 6

6 Design and optimisation of theranostic thermosensitive Liposomes

6.1 Introduction

Externally triggerable, theranostic, drug delivery vehicles form an important and interesting area of development in the field of cancer therapy. Survival rates for cancer, like many illnesses decrease with disease progression, and thus effective imaging is extremely important to monitor disease progression, response to therapy, and successful accumulation of the drug in the target site. The sooner the healthcare provider appropriates such information, the sooner an appropriate therapy may be prescribed. Theranostic agents streamline this process by providing both therapeutic and non-invasive diagnostic elements. There is a cornucopia of drug, trigger, vector conjugates in development^{154,155,252,253} however very few exist on the market. Debatably Zevalin®(ibritumomab tiuxetan) an anti-CD20 radioimmunoconjugate comprising either the radionuclide Y-90 for therapy^{254,255,256} or In-111 for imaging²⁵⁷, as well as ¹³¹I and ⁶⁸Ga-DOATOC for thyroid cancer are the only *in vivo* theranostic systems clinically approved. There are also a number of MABs which are sold with diagnostic kits exist which claim to be theranostics due to the drug's active role in *in vitro* biomarker detection such as Herceptin® and HercepTest®²⁵⁸.

The inclusion of ICG into the bilayer of thermosensitive liposomes was trialed amongst a varying number of differing lipid compositions in **Chapter 4**. This was successful at high ICG concentrations attaining 150 µM, however it was not possible to attain such high ICG concentrations without sacrificing the construct's ability to load therapeutic levels of DOX loading. Thus once elucidating the threshold ICG concentration that would allow efficient DOX loading, the final constructs attained a maximum of just 7.5 µM ICG. At this concentration, whilst assuming ~10% as an average proportion of the IV injected dose to accumulate in the tumour site, the potential for imaging and photothermal based induction of payload release is limited, especially for optimised imaging contrast and effective release.

In the previous chapter (5), the NTSL Liposome-ICG-DOX, was demonstrated as an effective MSOT contrast agent, providing a readout of tumour tissue perfusion and a temporal description of optimal tissue accumulation. At an optical density of 11 and an injected dose at a concentration of 128 μM , this was significantly higher than previously published literature using liposomal ICG as an MSOT contrast agent at a concentration of 75 μM which also provided detailed MSOT images of a highly vascularised tumour type⁸⁹. In terms of concentrations required for effective heat generation for enhancement of tumour cytotoxicity in the presence of DOX, one previous study directly injected nanoparticles comprising DOX alongside ICG at a concentration of 71 μM and effectively rid the animals of their xenograft tumours following laser irradiation¹⁹². Therefore the range of increase in ICG concentrations in thermosensitive liposomal DOX would be about a ten fold increase to ~ 75 μM to enhance both imaging and therapeutic potential.

Following the development of a number of differing ICG incorporation protocols as described in chapter 5, other methodologies for ICG insertion into thermosensitive liposomes were tested. The theories alluded to in the previous chapter regarding the difference in sonication over extrusion were that sonication generates more defects in the surface of the liposomal bilayer as well as generating smaller nanoparticles. Both these factors should therefore result in lower interlipidic pressure due to the defects and increased curvature of the particles generating more dead space within the bilayer, furthermore a higher surface area will be exposed with which the ICG may interact. The lack of the bulky cholesterol present in the NTSL should also allow deeper penetration of the dye into the bilayer itself. Using sonication as a downsizing technique demonstrated increased ICG loading capacity whilst allowing the retention of a higher concentration of ICG for the NTSL system. So to circumvent the low threshold of 7.5 μM , this is what was tested using the 2 most efficient protocols as seen in the NTSL work: the film Insertion and the post Insertion as depicted in **Figure 6.1**. Due to the increased release rate seen with the sonicated systems incorporating doxorubicin alone over the extruded systems as shown in chapter 4, the most rigid formulations were tested comprising: 50:50, 60:40 and 70:30 DPPC:DSPC.

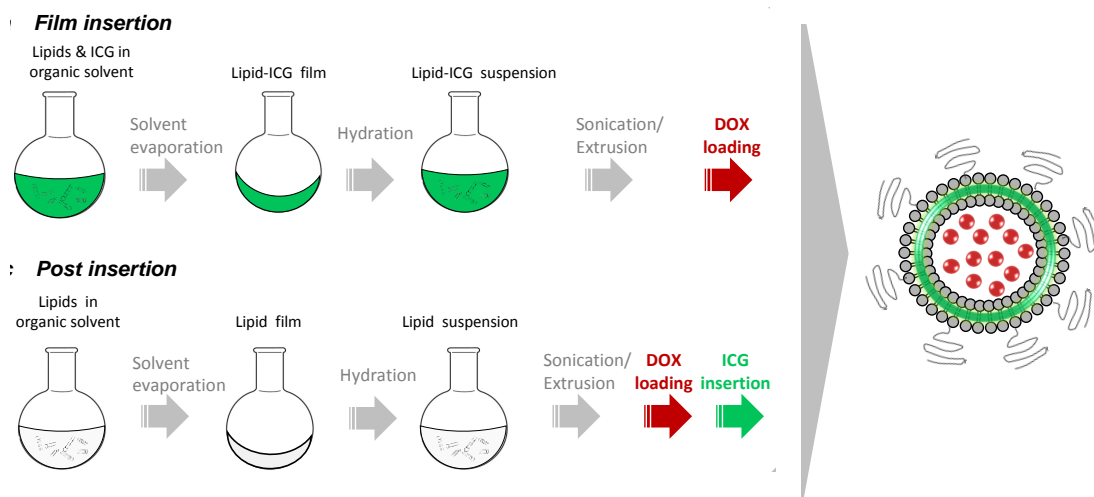


Figure 6.1. Liposomes were prepared via sonication. ICG incorporation was achieved through either the film insertion (top) or post insertion (bottom) protocol.

6.2 Results

6.2.1 Physicochemical liposome characterisation

Physicochemical characterisation of each of the systems analysed is displayed in **Table 6.1**. The film insertion protocol coupled with sonication based downsizing yielded much higher ICG incorporation efficiency along with loading with therapeutic concentrations of doxorubicin in comparison to the extruded liposomes. After testing an initial ICG concentration of 200 μM in the more rigid 50:50 system (50:50 i200) which yielded only 12% DOX encapsulation (data not shown), the starting concentration was based around 100 μM . The 50:50 i100 system showed impeccable reproducibility, incorporating an average of 78.5 μM ICG and generating an optical density of 11.8. The DOX encapsulation was 97.5%, and the average diameter was 89 nm with a surface charge of -23.2 mV and a polydispersity of 0.22. This indicates a ICG concentration threshold between 100 and 200 μM for the retention of DOX at therapeutic concentrations. Due to the irreproducibility of the 60:40 i100 system, a number of different initial ICG concentrations were tested. Between i70 and i110, there was little difference observed in terms of the final OD. As expected the final ICG concentration of the i70 system was lowest at 58 μM and the highest 76 μM when starting at 110 μM .

The sizes and surface charges are also very similar with diameters around 90 nm, with PDIs of 0.20-0.22 and Zeta-potentials between -16 and -23 mV. Each show a very slight size increase over the ICG free counterparts of 5-10 nm. What is appreciable is the differences in DOX encapsulation efficiency which is close to 100% for the i70 and i90, however at i100 the average encapsulation is 73% with an s.d. of almost 30%. This trend continues to the i110 system which encapsulates 75%. What can be concluded is that with this 60:40 system, the ICG concentration threshold which will allow reproducible DOX EE of close to 100% is somewhere around 100 μM thus the optimum concentrations is the i90. Due to the observed limitations in terms of ICG incorporation whilst maintaining therapeutic concentrations of DOX, with the more rigid 50:50 system maintaining a higher threshold than the more fluid 60:40 system, the 70:30 system was not explored for this protocol.

The post insertion sonication protocol yielded promising results also in comparison to the previously described film insertion extrusion. The 50:50 showed resilience to each starting ICG concentration, incorporating ICG at a high efficiency; 69% at 200 μM , 87% at 100 μM and 100% at 50 μM . This is a slightly higher average than in the film insertion protocol, however the optical density remains similar at 12.3 in comparison to the film insertion at 11.8. The 50:50 systems did not display a particular size increase over their ICG free counterparts, residing at 78 nm in diameter. This shows an element of colloidal resilience to the potential surfactant action of ICG and or a neater ICG packing strategy within the bilayer. The polydispersity of 0.2 remains acceptable for sonicated systems, and the surface charge is similar for each system at -27 mV, very slightly lower than the ICG free counterpart of -23 mV. The 60:40 systems tell a similar threshold story to the film inserted liposomes, showing both poor ICG incorporation at 200 μM of 48% with a low OD of 10.8 for that high an ICG concentration.

The DOX encapsulation efficiency was just 18%. This was coupled with a size increase of about 10 nm from that which was seen in the other 60:40 systems and the 50:50, with a similar polydispersity of 0.24 and a surface charge of -30 mV. The 60:40 i100 system displayed good ICG incorporation efficiency of 85% with an OD of 12. The DOX encapsulation efficiency was vastly improved at 95%, and the size was unchanged at 81 nm. The polydispersity was 0.22 and the surface charge -27 mV. Reducing the ICG concentration to 50 μM , as in the 50:50 system did not provide much benefit, lowering both the final ICG concentration and OD. The DOX encapsulation efficiency remained at 95%, the size at 80 nm polydispersity at 0.23 and surface charge of -24 mV. The final ICG concentration appeared as 61 μM and OD at 10. The ICG concentration is obviously erratic however due to the success and improvement of the 60:40 i100 over the i50, this system was not repeated. The liposomes incorporating DOX alone from the 50:50 to the 70:30 appeared similar, each encapsulating near 100% DOX. They each attained a diameter of about 80 nm, a PDI between 0.23 and 0.27, and a surface charge of -23 mV.

Table 6.1 Physicochemical characterisation of sonicated liposomes comprising various proportions of DPPC:DSPC along with DOX and ICG.

System	ICG		Lipid:ICG	Doxorubicin		Hydrodynamic diameter, ϕ (nm)	Polydispersity Index, PDI	Zeta Potential, ζ (mV)
	μ M	OD		μ M	EE \ddagger			
Film insertion Sonication								
6040i110	76.0 \pm 2.8	10.4 \pm 0.5	164:1	720 \pm 6.8	74.5 \pm 0.7	88.8 \pm 2.8	0.196 \pm 0.062	-19.1 \pm 3.1
6040i100	66.7 \pm 18.3	9.3 \pm 2.7	187:1	707 \pm 277	73.2 \pm 28.7	89.7 \pm 7.6	0.225 \pm 0.040	-19.7 \pm 4.8
6040i90	72.0 \pm 3.6	10.5 \pm 0.6	174:1	934 \pm 29.9	96.7 \pm 3.1	90.0 \pm 7.2	0.220 \pm 0.013	-21.0 \pm 4.7
6040i70	58.0 \pm 2.8	9.3 \pm 0.1	216:1	966 \pm 0	100.0 \pm 0	85.8 \pm 9.3	0.223 \pm 0.029	-16.1 \pm 0.2
5050i100	78.5 \pm 10.4	11.8 \pm 1.3	160:1	941 \pm 26.1	97.5 \pm 2.7	89.3 \pm 5.3	0.217 \pm 0.026	-23.0 \pm 4.8
Post insertion Sonication								
7030i200	125.1 \pm 4.0	14.9 \pm 2.8	100:1	394 \pm 122	41.0 \pm 12.7	138.8 \pm 28.8	0.279 \pm 0.055	-25.8 \pm 0.4
7030i100	80.5	11.2	155:1	874	91.0	124.5 \pm 0.4	0.289 \pm 0.030	-26.5 \pm 0.8
7030i50	36.8	6.1	340:1	924	96.3	80.9 \pm 1.5	0.276 \pm 0.027	-31.2 \pm 2.1
6040i200	95.0	10.8	132:1	173	17.9	91.6 \pm 1.3	0.240 \pm 0.010	-29.7 \pm 1.0
6040i100	84.6 \pm 20.6	12.2 \pm 2.6	148:1	913 \pm 82.1	94.5 \pm 8.5	80.9 \pm 5.4	0.221 \pm 0.010	-26.9 \pm 4.6
6040i50	61.3	9.8	204:1	923	95.6	79.7 \pm 2.4	0.228 \pm 0.027	-24.2 \pm 1.3
5050i200	137.0 \pm 24.5	16.9 \pm 1.3	91:1	937 \pm 28.9	97.1 \pm 3.0	78.1 \pm 2.15	0.236 \pm 0.003	-25.7 \pm 2.3
5050i100	87.0 \pm 14.3	12.3 \pm 2.1	144:1	930 \pm 27.0	96.4 \pm 2.8	77.5 \pm 2.0	0.220 \pm 0.011	-25.2 \pm 1.7
5050i50	53.8	8.8	232:1	965	100.0	78.6 \pm 1.3	0.226 \pm 0.037	-27.5 \pm 0.8
7030SONi0	0	0	0	953 \pm 10.6	99.3 \pm 1.1	78.5 \pm 0.5	0.269 \pm 0.002	-22.6 \pm 0.8
6040SONi0	0	0	0	941 \pm 18.4	97.4 \pm 1.9	81.0 \pm 4.1	0.245 \pm 0.020	-23.4 \pm 0.9
5050SONi0	0	0	0	941 \pm 33.8	97.5 \pm 3.5	77.7 \pm 1.7	0.228 \pm 0.011	-22.9 \pm 0.8

i: initial ICG concentration (μ M). \ddagger IE: Incorporation Efficiency (%). \ddagger EE: Encapsulation Efficiency (%)

6.2.2 Optical liposome properties

Graphically portrayed in **Figure 6.2**, the relationship between lipid composition and initial [ICG] has profound effects on the final composition of the system. In **Figure 6.2 a & b**, one may observe the contribution initial [ICG] makes to the efficacy of DOX loading. For the post inserted systems in **a.**, each composition encapsulates >90% DOX when the initial ICG concentration is kept at 100 μ M and below. However at 200 μ M we see a sharp decrease in DOX EE to 41% in the case of the 70:30 system and 18% in the 60:40 system. The 50:50 system appears resilient to the higher ICG concentration and maintains close to 100% encapsulation indicating a rigidity based resilience to the ICG insertion at this concentration. The film inserted liposomes in **b.**, appeared less resilient to ICG with the 50:50 unable to load more that 12% DOX at 200 μ M initial

[ICG] and the 60:40 i110 system encapsulating an average of 75% DOX and the i100 73% with a standard deviation of almost 30%. I90 and below proved within the threshold limit for >90% DOX encapsulation for the 60:40 system. When considering the relationship between initial [ICG] and final OD in **Figure 6.2 c & d**, the OD was not directly proportional to the concentration over those tested as similarly observed in chapter 5. This is somewhat related to the reduction in ICG incorporation efficiency as the starting concentration increases at the higher concentrations, along with the lack of linearity in terms of the resultant OD/ μM ICG. Commencing with the post inserted systems, in the 70:30 system, the resultant OD of the i50 is 6.1 following the incorporation of 36 μM ICG. At i100 the [ICG] increases by 125% to 80.5 μM however the OD increases to 11.2, just an 84% increase. When the concentration is increased to i200, the [ICG] increases to 125 μM , a 55% increase in ICG concentration and almost a 20% decrease in ICG incorporation efficiency, but the OD only rises by 33% to 14.9. The 60:40 system shows a higher than expected incorporation efficiency of ICG from the i50 of 61.3 μM resulting in an OD of 9.8. When this is increased to i100, the [ICG] rises to 84.6, a 40% increase, however the resultant OD is just 12.2, about a 20% increase. When the [ICG] rises to i200, there is just a 10 μM increase in final [ICG] but a slight reduction in OD to 10.8, indicating aggregation based reduction of A_{max} . For the 50:50 system, the i50 incorporates slightly higher than expected ICG at 53.8 μM generating an OD of 8.8. When this is increased to i100, the concentration increases to 87, roughly 60% however the OD increases to just 12.3, a 40% increase. When this is further increased to i200, the concentration increases to 137 μM , almost another 60% increase, however the OD increases to just 16.9, an increase of less than 40%. In **Figure 6.2 b**, a lower range of initial [ICG] were tested as a result of the observed threshold. For the 60:40 system at i70, the ICG incorporated amounts to 58 μM generating an OD of 9.3. When this concentration is increased to i90, the final [ICG] increases to 72 μM a 24% increase increasing the OD to 10.5, a 13% increase. When the initial [ICG] is increased to i100 the final [ICG] is 67, showing a large s.d. of 18.3, and the OD returns back to 9.3 an s.d. of 2.7. This is also the point at which the system does not reproducibly encapsulate >90% DOX. Increasing the [ICG] concentration to i110 does push the final [ICG] to 76 μM but does not increase the OD above what was observed in the reproducible i90 system reaching an OD of just 10.4. The more resilient 50:50 i100

system encapsulates 78.5 μM ICG generating an OD of 11.8, higher than any of the film inserted 60:40 systems.

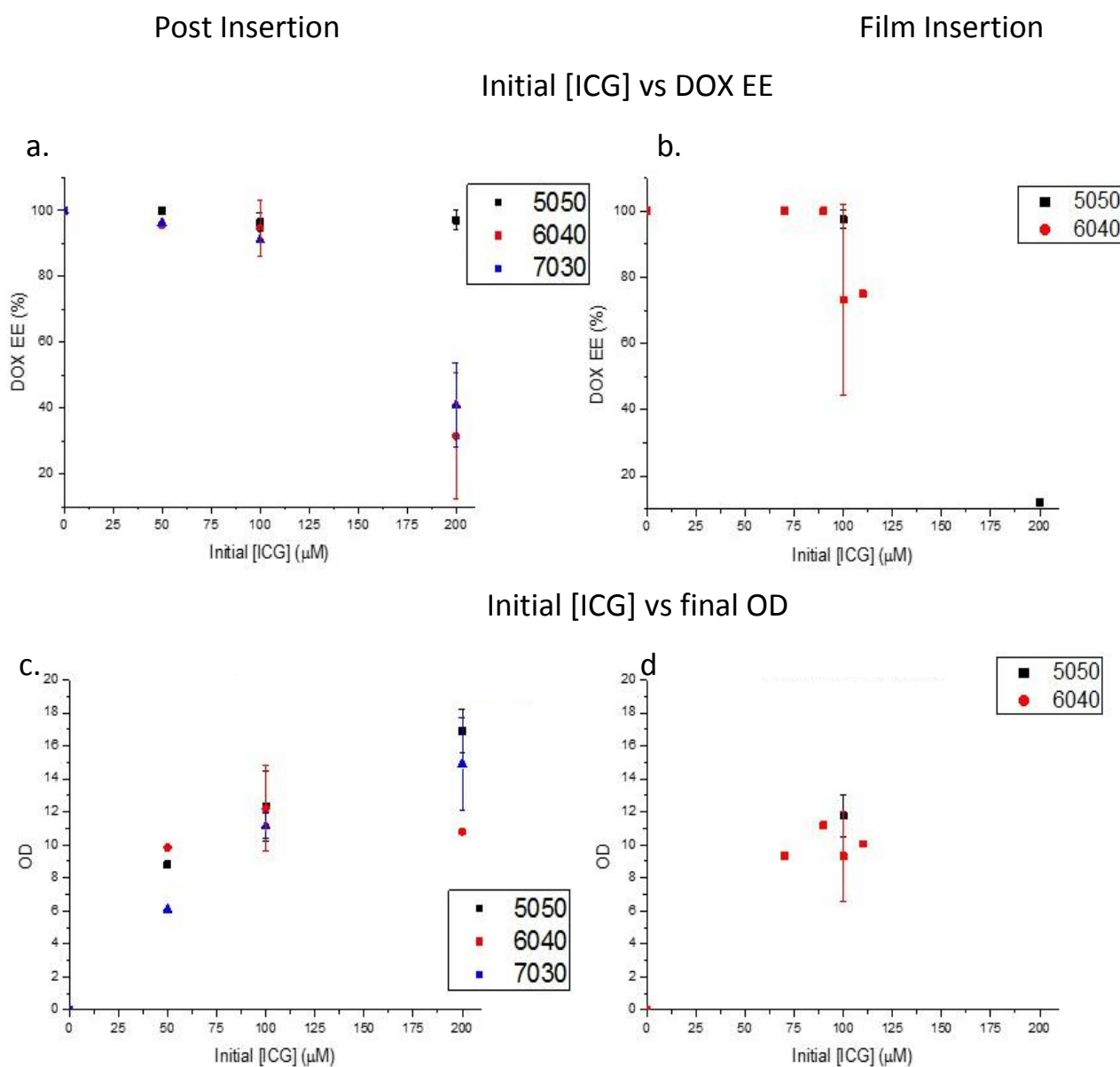


Figure 6.2 Relationships between initial ICG concentration and final DOX EE (a,b) or OD (c,d). For the post inserted systems (a,c) and film inserted (b,d) at varying DPPC:DSPC lipid ratios as represented in the legends.

6.2.3 Physical Liposome Properties

Figure 6.3, depicts the physical attributes of liposomes of varying lipid compositions and initial [ICG], specifically the resultant size and charge. The post insertion protocol (**a**) does not appear to induce a size alteration for any of the liposomes up to i50, remaining at approximately 80 nm in diameter. At i100, just the 70:30 ratio liposome increases in size to 125 nm showing a destabilisation of the vesicular structure, whereas the 60:40 and 50:50 systems retain their size. At an initial [ICG] of 200 μM , the 70:30 system increases in size to near 140 nm in diameter. The 60:40 system increase to 92 nm, indicative of a destabilisation and subsequent loss of DOX encapsulation efficiency. The 50:50 system retains its size at 78 nm. The case with the film inserted systems (**b**), there is an overall size increase between 5 and 9 nm for the 60:40 systems across each ICG concentration tested, regardless of their capacity to withhold DOX.

The same is seen with the 50:50 system which exhibits an 11 nm size increase. In the case of the surface charge the post inserted systems (**c.**), show a decrease upon the incorporation of ICG. In the case of the 70:30 system, the charge decreases from -23 mV to -31 mV upon the incorporation of 50 μM ICG, which then decreases to -27 mV at i100 and further to -26 mV at i200. In the case of the 60:40 system, the charge decreases from -23 mV to -24 mV upon the incorporation of 50 μM ICG, and further to -27 mV at i100, finally decreasing to -30mV at i200. The 50:50 system displays an initial decrease from -23 mV to -28 mV upon the incorporation of 50 μM ICG, returning to -25 mV at i100 and a finally -26 mV at i200. The same general trend of progressive decrease is not followed by the film inserted systems (**d**). The 50:50 system does not show a change in surface charge upon the incorporation of ICG at i100, maintaining at -23 mV. The 60:40 system shows an increase from -23 mV to -16 mV at i70. It decreases to -21 mV at i90 and further to -23 at i100. At i110 it increases to -19 mV. Between i90 and i110, the S.D. ranges from 3 mV to 5 mV, thus the overlap does not show a significant difference in charges between the 3 systems.

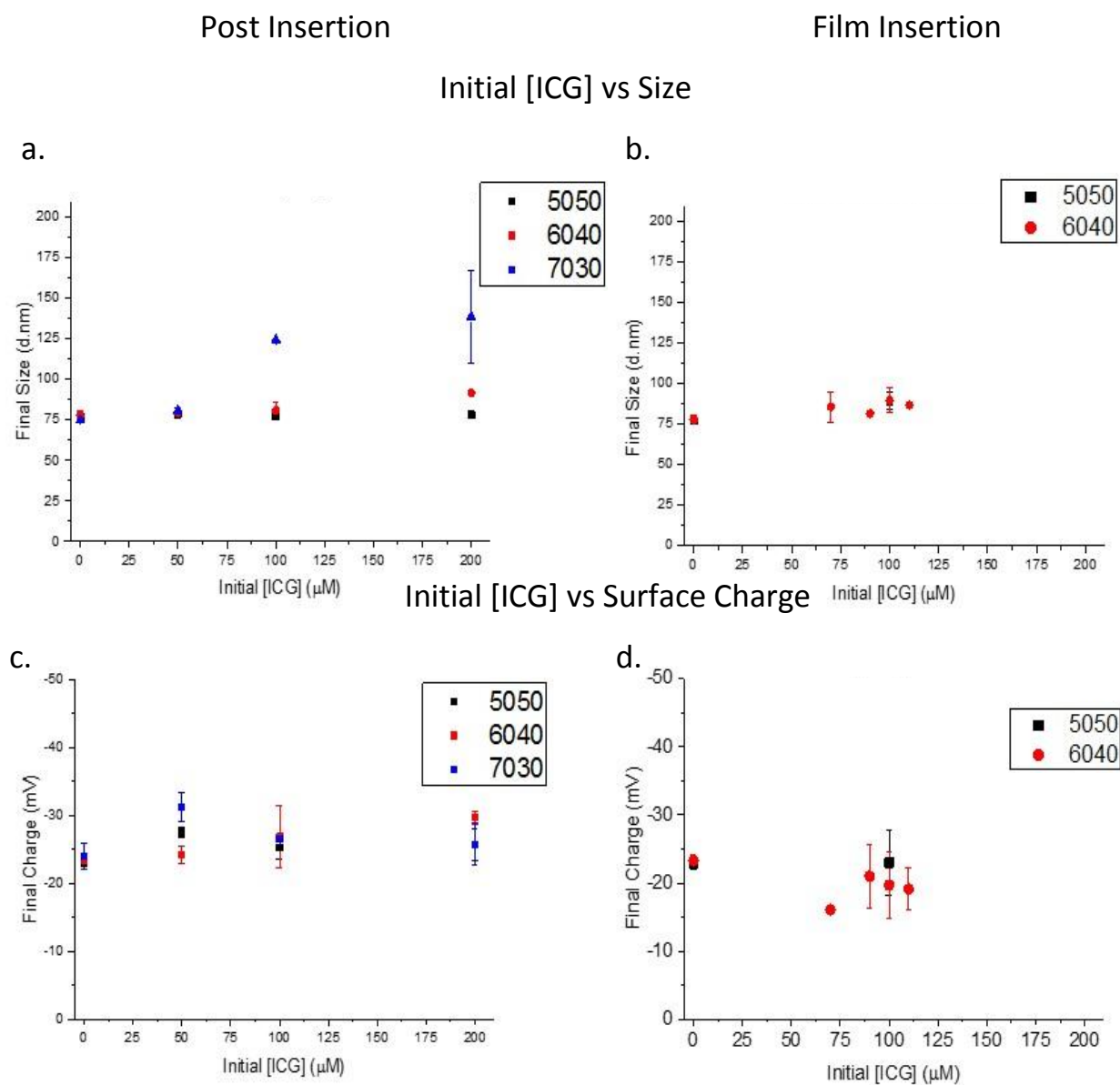


Figure 6.3 Relationships between initial ICG concentration and final size (**a,b**) or surface charge (**c,d**). For the post inserted systems (**a,c**) and film inserted (**b,d**) at varying DPPC:DSPC lipid ratios as represented in the legends.

6.2.4 IVIS based murine xenograft biodistribution

Due to the chronology of liposome development, the 50:50 post inserted system was selected for the initial thermosensitive liposome biodistribution experiment on a murine 4T1 invasive mammary carcinoma xenograft model. The purpose of this experiment was to elucidate the temporal dynamics of liposome accumulation into the tumour site, based on the fluorescence signal emanating from the ICG and DOX as monitored by IVIS. The mice were inoculated bilaterally to induce tumour growth on each flank so as to economise on animals sacrificed, and to gain repeats within the same animal as a measure of reproducibility. The tumour growth profiles as seen in **Figure 6.4**, display a tumour volume of 65mm^3 with a low standard deviation of 10mm^3 . As the tumours grow further, the standard deviation increases. After 9 days, an average volume of 130mm^3 is reached with a standard deviation of 30mm^3 , and after 11 days they average 180mm^3 with a standard deviation of 60mm^3 .

4T1 Tumour Xenograft Growth Profile

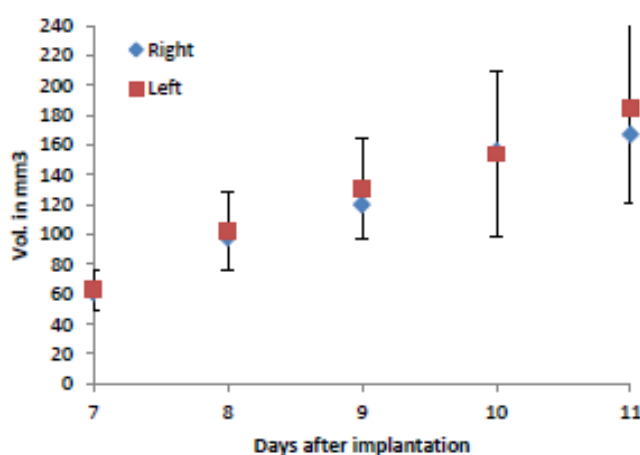


Figure 6.4 4T1 Tumour growth profiles following inoculation with 0.8×10^6 cells in $50\mu\text{l}$ PBS bilaterally into either flank of the mice.

The liposomes prepared for injection in **Table 6.2**, were representative of the previously characterised preparations seen in **Table 6.1**. Each of the liposomes had a size between 77 and 80 nm in diameter, polydispersities around 0.2. The empty liposomes without ICG had a surface charge of -31mV. This decreased to -23mV with the incorporation of DOX alone, -26 mV following ICG post insertion into empty liposomes, and -24 mV with the combination of the two. When loaded with DOX alone, the encapsulation efficiency was 99%. With the addition of ICG at the final stages of DOX loading, the encapsulation efficiency dropped to 93%, and the ICG incorporation efficiency was 93%, equating to 93 μ M. When ICG was inserted alone, the incorporation efficiency was 83%.

Table 6.2 Physicochemical characterisation of sonicated post inserted liposomes comprising DOX, ICG and a combination of the two.

System	ICG		Lipid:ICG	Doxorubicin		Hydrodynamic diameter, \varnothing (nm)	Polydispersity Index, PDI	Zeta Potential, ζ (mV)
	μ M	IE†		μ M	EE‡			
50:50 HBS	-	-	-	-	-	78.5 \pm 0.8	0.208 \pm 0.011	-30.7 \pm 0.8
50:50 DOX	-	-	-	956	99	76.6 \pm 0.3	0.229 \pm 0.014	-22.6 \pm 0.4
50:50 ICG	83	83	160:1	-	-	80.2 \pm 0.7	0.237 \pm 0.013	-25.7 \pm 1.2
50:50 ICG-DOX	93	93	142:1	898	93	78.0 \pm 0.6	0.235 \pm 0.003	-23.9 \pm 0.6

†IE: Incorporation Efficiency (%). ‡EE: Encapsulation Efficiency (%)

The 50:50 post inserted liposome system was injected via the tail vein of the murine models after 11 days of tumour growth. IVIS images were taken, 2 hours, 4 hours and 24 hours post injection, as displayed in **Figure 6.5**. In the left and middle panels, the mice from left to right have been injected with, PBS, 50:50-ICG-DOX 1, 50:50-ICG-DOX 2, 50:50-DOX, and 50:50-ICG. These are the raw images displaying the fluorescence of either ICG on the left and DOX in the middle panels. The right hand images, the autofluorescence from the control mice has been subtracted and thus shows the contribution of the DOX fluorescence over the background. In **a.**, in the left panel, the fluorescence observed 2 hours post injection emanating from the ICG signal shows accumulation in the liver of a portion of the injected dose as expected for the ICG containing liposomes, due to the high blood concentration of the organ, as well as the metabolism of a portion of the liposomes cleared by the spleen, and processed by

the organ. There was no autofluorescence observed in the PBS control. The middle panel displays the fluorescence emanating from the DOX. Some autofluorescence is observed from the PBS control, however, slightly more can be observed in the tumour site of the ICG-DOX liposome injected mice. No signal can be observed from the DOX, or ICG liposomes. In the right panel, the DOX fluorescence is plotted over images of the mice with the autofluorescence of the control mice subtracted. The mice have been injected with the following: from left to right, PBS, 50:50-ICG-DOX 1, 50:50-ICG-DOX 2, PBS, 50:50-DOX, 50:50-ICG. The most prominent fluorescent signal is emanating from the tumour sites of the 50:50-ICG-DOX injected animals, possibly as a result of increased DOX release in the tumour site over the liposomal DOX alone. Some patches of fluorescence were observed around the ears, most probably due to the thin skin and fur and thus the higher light penetration from the circulating system. The rapidly formed and highly fenestrated vasculature at the periphery of the tumour has been inundated with circulating liposomes, and with the stretching of the skin and proximity to the skin's surface, the fluorescence can easily penetrate through. No fluorescence is observed in the other mice, apart from a little autofluorescence in the ear of the PBS control.

In **b.**, in the left panel, the ICG fluorescence indicates prolonged clearance from the blood into the liver for the circulating liposomes. As free ICG is cleared from the blood and liver in a matter of minutes²⁵⁹, this indicates uptake of liposomes by the liver Kupffer cells.. No fluorescence can be observed from the DOX in the middle panel, this is indicative of a high level of clearance of the liposomes from the blood between the 2 hour and 4 hour time points. Due to higher rates of scattering and absorbance of the endogenous chromophores of light at 465 nm in the DOX channel, the level of penetration is much lower than in the infrared range, attributing to lower sensitivity than in the ICG channel. This, as well as the autoquenching of DOX at high intraliposomal concentrations would explain why the liposomes would give off a higher signal in the liver from the ICG channel than the DOX channel at this depth within the tissue. There is no indication of DOX fluorescence in the right panel, confirming that which has been observed in the middle panel. The 24 hour timepoint, **c.**, shows ICG fluorescence emanating from the tumour, liver and spleen in the left panel, most prominently in the 50:50-ICG-DOX injected animals, with fluorescence also present in

the 50:50-ICG animal. DOX fluorescence in the middle panel, is observed mainly from the tumour site of the animals administered with liposomes containing DOX alone and DOX-ICG. The diffuse signal emanating from the animal is most likely caused by autofluorescence as it is present in the liposome-ICG animal as well. The tumour fluorescence readout is confirmed, in the right panel, with high DOX signal emanating from the tumours of the mice injected with the DOX containing liposomes. There is some fluorescence emanating from the liposome comprising ICG alone, but the intensity is minimal. The control mice show a little autofluorescence around the ear. This study indicates that although high liposome concentrations appear in the tumour site after 2 hours, it is most probably as a result of their circulation through the bloodstream. However, peak tumour liposome accumulation appears to occur at 24 hours, as was seen with the more rigid NTSL-DOX-ICG system.

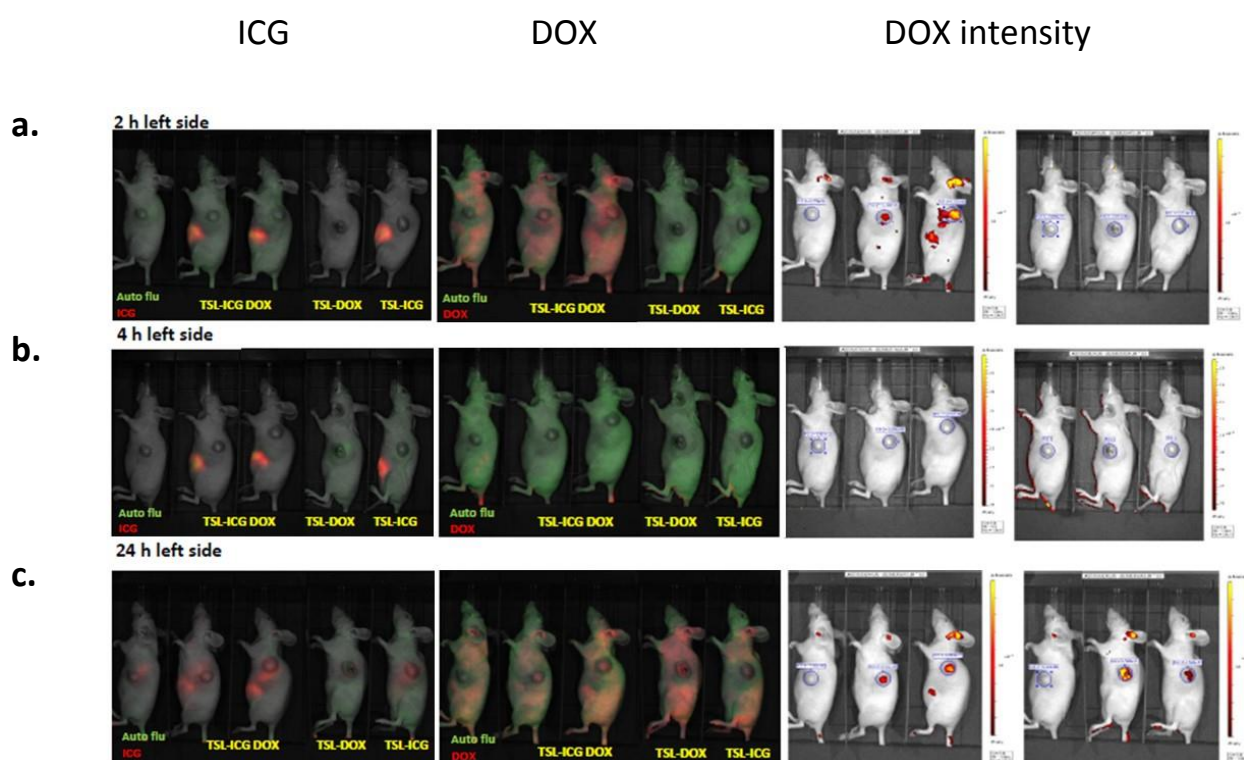


Figure 6.5. *in vivo* imaging system (IVIS) mediated murine 4T1 tumour xenograft 50:50 DPPC:DSPC ratio liposome biodistribution assay displaying ICG and DOX fluorescence as well as DOX fluorescence intensity following correction for background autofluorescence. **a)** at 2 hours, **(b)** at 4 hours and **(c)** at 24 hours. Imaging was undertaken by Dr. Zahraa Al-Ahmady

6.2.5 Water-bath heated DOX release

In **Figure 6.6**, the liposomes were subjected to a temperature of 37°C in the presence of 50% mouse serum to emulate conditions during circulation. This was carried out for 24 hours to monitor the release rate during passage to the tumour and its clearance from the blood. The temperature was also increased to 42°C to monitor the effects of this temperature, widely used for the triggering of low temperature sensitive liposomes, high enough to induce release but not so high as to damage tissues peripheral to the tumour site itself. This was carried out for an hour to emulate what is clinically used for other thermosensitive systems.

The assays provide a useful comparison between the tested systems, of their relative thermosensitivity and colloidal stability under the challenge of heat and serum proteins. The displayed systems were selected based on their ability to encapsulate therapeutic levels of DOX, and maximum ICG incorporation. The systems were tested without ICG as a benchmark to monitor the effect of its incorporation on the environmental responsiveness. Initially considering the post inserted systems, the 70:30 system was excluded due to the aforementioned size increase. The 50:50 system was tested at i100 and i200, and the 60:40 at just i100. Out of the film inserted systems, the 50:50 i100 was selected alongside the 60:40 i90. As this appeared to be the initial [ICG] threshold for the effective loading of >90% DOX. The optimum system would exhibit minimal release at 37°C. At 42°C, rapid burst release would allow targeting of the tumour vascular if triggered *in situ*, whereas a more gradual rate of release would allow the vasculature to heat up, inducing vasodilation, and allow the system to penetrate further into the tumour stroma whilst releasing DOX. As both strategies appear beneficial, it would be ideal to attain 2 systems, with these 2 differing release profiles, of which to monitor the effects for an *in vivo* therapeutic study.

In the absence of ICG, both 50:50 and 60:40 systems behave similarly at 37°C, releasing 17% DOX in the first hour, 22% by the second, and peaking at 70% at 8 hours. At 42°C, the systems released DOX at a much higher rate than seen in the extruded systems, but maintaining an expected trend with the 60:40 system releasing faster

than the 50:50 system due to the higher concentration of the low T_m lipid DPPC. The 50:50 system releases 10% DOX after 1 minute of heating, climbing to 50% after 5 minutes at which point release begins to plateau reaching 80% after 1 hour. The 60:40 system releases 5% after 1 minute, rapidly climbing to 83% after 5 minutes, at which point it plateaus for the remainder of the hour. Upon the incorporation of ICG via the post insertion method, at 37°C, the 50:50 i200 system releases 10% DOX after 2 hours, climbing to 45% after 8 hours. At this point it begins to plateau, releasing a total of 60% after 24 hours. Reducing the initial [ICG] to 100 μ M makes little impact on the release kinetics at this temperature, again releasing 10% DOX after 2 hours, increasing to 45% after 8 hours, and reaching a total release of 70% after 20 hours. The value appears to decrease at 24 hours, most likely due to aggregation and autoquenching of the free DOX fluorescence, due to its aggregation.

The 60:40 i100 system releases more rapidly at 37°C, reaching 25% at 2 hours and reaching a plateau of 60% after 6 hours. At 37°C, the 50:50 systems show a slight reduction in release rate over the ICG free system, and the 60:40 system appears fairly similar. When ICG was incorporated via the film insertion method, the systems appear far more stable at 37°C with little difference observed between the 50:50 i100 and 60:40 i90 systems. Releasing 5% DOX after 2 hours, slowly increasing to 10% for the 50:50 system and 15% for the 60:40 finally reaching just under 30% after 24 hours. At 37°C it appears that the film insertion method generates liposomes more resilient to the conditions emulated in this assay, and thus are more likely to deliver a higher level of DOX to the tumour site *in vivo* than the post inserted liposomes which release DOX more rapidly. The relative side effects from the free DOX released should also be decreased through the use of the more resilient systems.

At 42°C, the post insertion 50:50 i200 system shows a gradual release of 7% after 1 minute, increasing to 25% after 10 minutes, and 60% at 30 minutes. The system continues to release to 75% at 1 hour. When the initial [ICG] is reduced to 100 μ M the rate of release increases, releasing 6% after 1 minute, rapidly increasing to 58% after 10 minutes and 65% after 30. At this point the rate plateaus reaching a final release of 72% after 1 hour. As expected, the 60:40 i100 system exhibits a more rapid rate of release of 8% after 1 minute, 78% after 10 minutes, reaching a plateau of 90% after 30

minutes, which persists until the 1 hour mark. The film inserted systems, have a reduced rate of release in comparison to the post inserted systems. The 50:50 i100 liposome releases 2% DOX after 1 minute, increasing to 26% after 10 minutes and 50% after 30 minutes of heating. The 60:40 i90 system, releases 1% after 1 minute, rapidly increasing to 40% after 10 minutes of heating. The system reaches a final release of 58% after 1 hour. minutes and 65% after 30 reaching a final release of 70%.

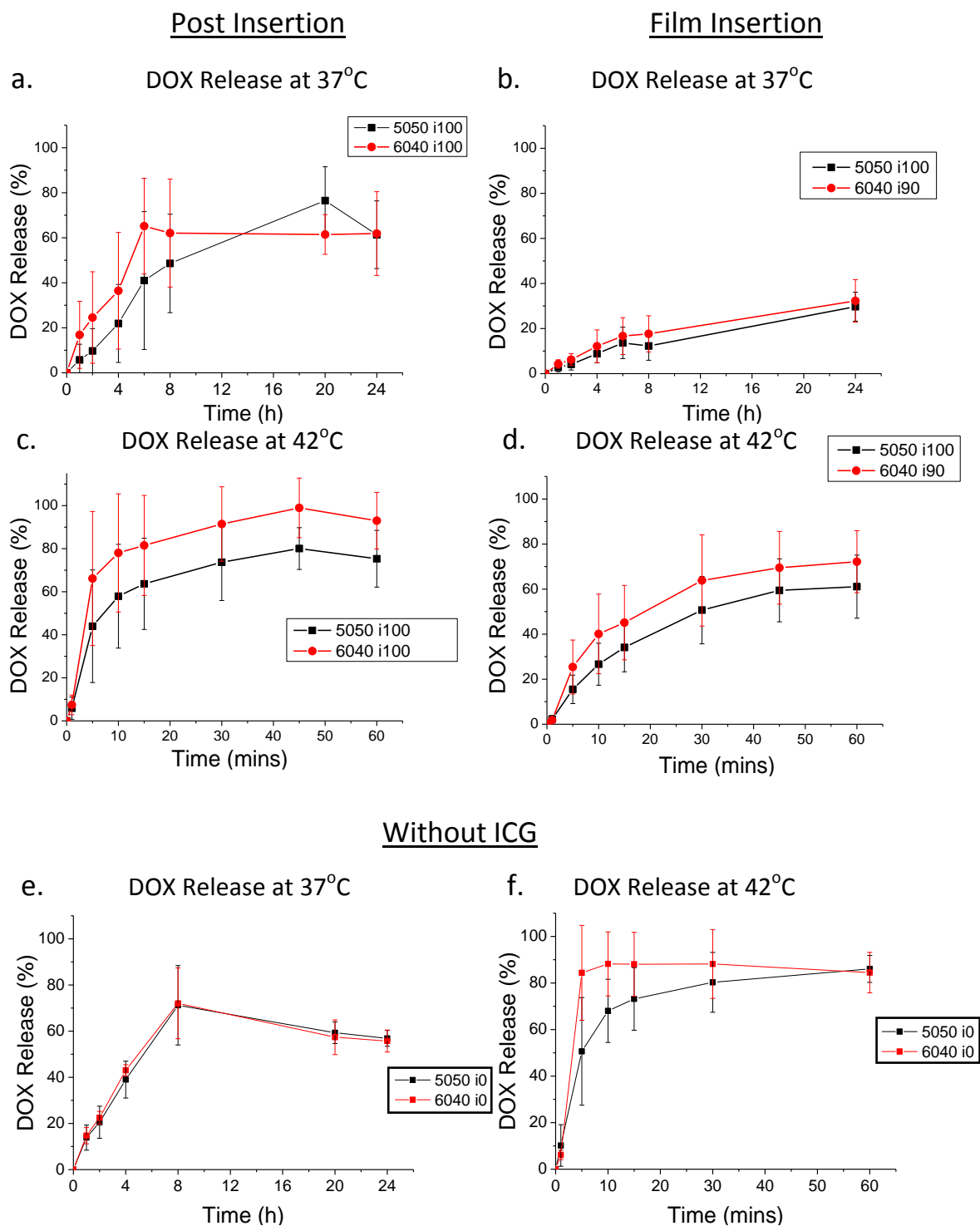


Figure 6.6 DOX release profiles in 50% mouse serum of 50:50 and 60:40 formulations comprising DOX and ICG (a-d) or DOX alone (e,f). Post insertion systems at 37°C (a) and 42°C (c) and film insertion systems at 37°C (b) and 42°C (d). Systems encapsulating DOX alone were tested at 37°C (e) and 42°C (f). Legends represent DPPC:DSPC ratio followed by ICG concentration.

6.2.6 ICG as a trigger for the photothermoinductive release of DOX

A number of different triggering modalities exist for thermosensitive constructs, both experimentally and clinically. The most commonly used are high intensity focused ultrasound (HIFU)²⁶⁰, radio frequency ablation (RFA)^{261,262}, microwave radiation²⁶³ and water-bath based heating^{78,202,264}. The major problems of these existing modalities are the lack of heating specificity across the tumour tissue and heat induction in healthy rather than malignant tissue. HIFU utilises ultrasound, transducing acoustic waves through the tissue. A proportion of the ultrasound is absorbed inducing a heating effect as the tissue resonates. Curvature of the applicator results in a point of convergence where ultrasound waves concentrate to a focal point allowing accurate direction to the tumour site. This modality is often MRI guided. The disadvantages are the risk of cavitation which can destroy tissue through thermocoagulation inducing necrosis, and the lack of clinical HIFU centres as less than 200 exist worldwide. The mechanism which induces bulk heating of a zone of tissue is directed toward the tumour, however it is the site which is heated rather than the drug specifically, and cannot guarantee that healthy tissue will not be effected. It is the choice low temperature hyperthermia induction mechanism for 4/6 of Celsion's© Clinical trials involving ThermoDox®, the other 2/6 involving RFA, which is a more commonly used heating modality. RFA is an invasive procedure, requiring the introduction of an RF probe into the centre of the tumour thus requiring coupling with an imaging modality such as CT or MRI. Radio waves are then passed through the probe inducing a heating effect. Due to the heat radiating from a single element, a gradient of heating radiates from this and thus does not generate homogenous heating across the tissue. Tissue burning can result from misuse inducing necrosis. Water bath based heating is mostly used in pre-clinical models where a tumour can easily be induced on easily submergible animal extremities. Lesions are generally localised on the limbs of the animals which are submerged in their entirety. Following combination of LTSL and heating, due to the lack of targeted heating, the animals develop high levels of toxicity induced atrophy within the limb.

Photothermotherapy using ICG acts as a molecular heating mechanism specific to the liposome. Much like molecular imaging⁷⁹ in comparison to modalities such as CT

or MRI, it is the presence of the liposomal construct at appropriate concentrations which propagates molecular heat generation via photothermia under laser irradiation.

As seen in **Figure 6.7 a)**, the laser was carefully set-up at one end of our open plan lab within the confines of a fume hood. The front of the fume hood was covered with opaque black foil, and the sliding window was fitted with an interlock device which cut the power supply to the main beam of the laser when the window was open. A web-cam was carefully set up to provide an overview of the laser irradiation. The laser was secured and aligned using a red pilot beam. The liposomes were mixed with 50% serum to a final ICG concentration of 10 μM and contained in a 96-well plate, atop a hot plate, which kept them at 37°C using an external temperature controller. The liposomes were irradiated at a power density of 0.3W/cm² for 5 minutes during which the temperature was recorded, and after which DOX release was calculated.

NTSL (DOXIL equivalent) formulation systems as introduced in **Chapter 5**, were compared with the 50:50 systems developed in this chapter for photothermic heating response and DOX release. Each system was prepared via the film insertion protocol, utilising sonication as a downsizing method. In **c)**, the heat increase in response to laser irradiation is shown for the NTSL systems. The serum alone did not rise more than 1°C, and the liposome-DOX rose to just 38°C. The ICG alone rose in temperature to 44°C. The NTSL-ICG and NTSL-ICG-DOX displayed superimposing temperature profiles, reaching a final temperature of 43°C. In **d)**, the heat increase in response to laser irradiation is shown for the 50:50 thermosensitive systems. Neither the serum alone nor the 50:50-DOX rose more than a few tenths of 1°C. The ICG alone rose in temperature to 44°C. The 50:50-ICG system rose in temperature rapidly, reaching a final temperature of 45°C, and the 50:50-ICG-DOX system was the least responsive of the 3 liposomes, rising to 43°C. Each irradiation of ICG comprising samples appeared to begin plateauing after 180 seconds. Following calculation of DOX fluorescence following irradiation **b)**, there was no DOX release from either of the NTSL systems. The 50:50 system comprising DOX alone released just 2.5% DOX, however the 50:50 system comprising both DOX and ICG, released its complete payload.

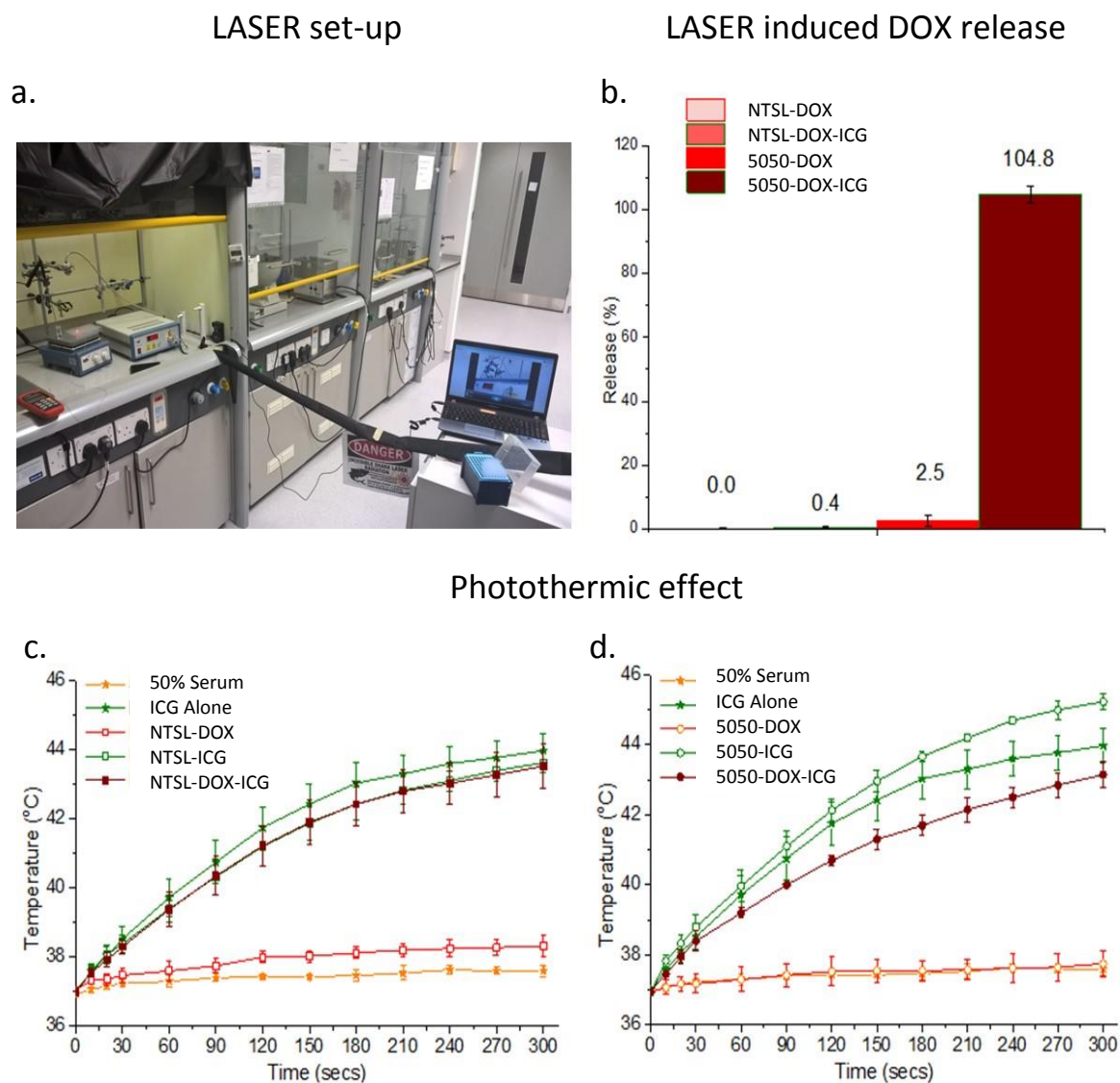


Figure 6.7 Laser based photothermia of liposomal DOX in NTSL and thermosensitive constructs with and without incorporated ICG. **a)** displays the laser set-up, **(b)** the DOX release following irradiation of photothermia, **(c & d)** heat increases in the NTSL constructs and the 50:50 thermosensitive construct. (n=3)

TEM was used to monitor differences in liposome morphology as a result of irradiation. The 50:50 systems comprising either DOX alone or a combination of ICG and DOX were combined with mouse serum, negatively stained and imaged. **Figure 6.8 a)** shows the 50:50-DOX system prior to irradiation, well dispersed and exhibiting a round morphology one expects from intact liposomes, with a size distribution correlating with the DLS of these sonicated systems. After irradiation, little difference is observed, apart from one or two deformed vesicles. **b)** presents the 50:50-ICG-DOX systems. The vesicles again are round and well dispersed exhibiting a size distribution correlating to the DLS measurements. Most noticeable is the visualisation of DOX crystals within a few of the systems, something which is usually only seen in cryo-EM. Following irradiation, there are significant morphological changes. The liposomes appear almost melted, adopting elongated morphologies and some rod/disk type structures representative of collapsed liposomes.

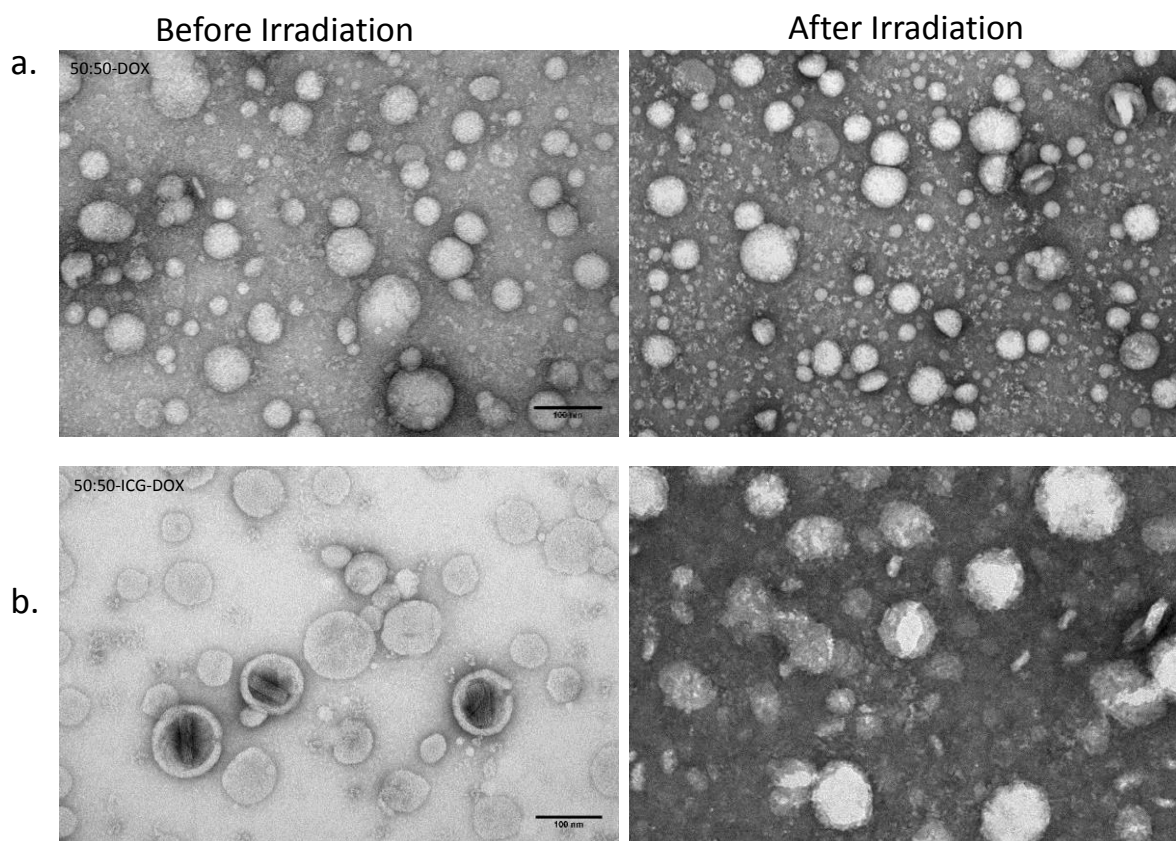


Figure 6.8 TEM micrographs of 50:50 formulation liposomes before and after irradiation at $0.3\text{W}/\text{cm}^2$ for 5 minutes at 808 nm. Liposomes comprised DOX alone (**a**) or combined ICG and DOX (**b**). (TEM operated by Dr. Aleksandr Mirinov)

6.2.7 [^{14}C]-DOX liposome Blood Circulation profile of film insertion sonicated system

The purpose of measuring the persistence of the liposome's circulation through the blood was to monitor the improvement of DOX encapsulation in this liposome in terms of circulation half life over free DOX as well as other liposome formulations. Another factor was also whether the DOX is remaining encapsulated within the systems, as free DOX is rapidly cleared by the kidneys.

Initially, [^{14}C]-DOX was serially diluted, and the radioactivity read following processing as previously stated. This allows correlation between the radioactivity and the DPM as a confirmation of the functionality of the scintillation counter as displayed in **Figure 6.9**.

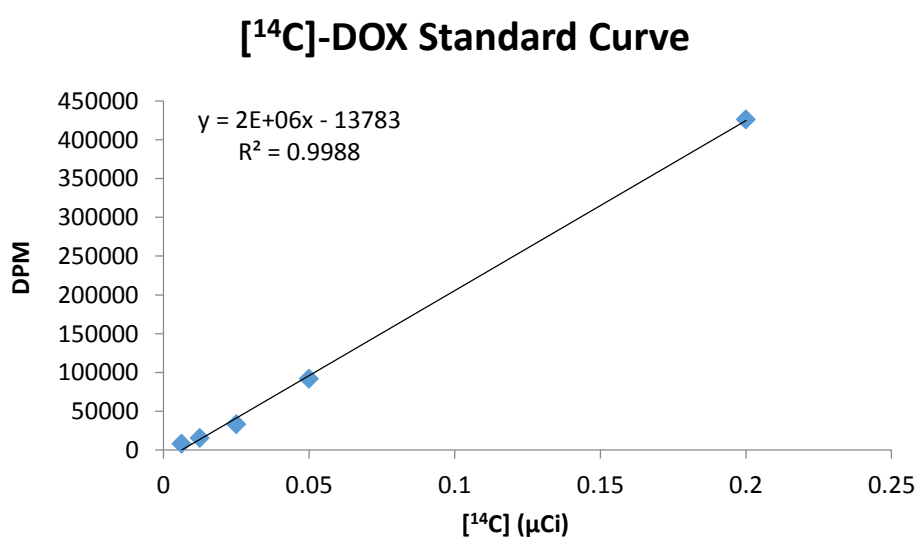


Figure 6.9 [^{14}C]-DOX standard curve equating radioactivity with DPM following serial dilution.

Figure 6.10 demonstrates the blood stability of the circulating 5050-ICG-DOX system as prepared via film insertion sonication. Following administration, circulating free DOX drops to just 2.4% after 30 minutes, dropping further to 0.9% after an hour. In comparison, after half an hour, 91% of the 50:50-ICG-DOX system persists to circulate, maintaining 83% in the bloodstream after 1 hour. After 6 hours, this concentration drops to 7.6%, and to 0.9% after 24 hours.

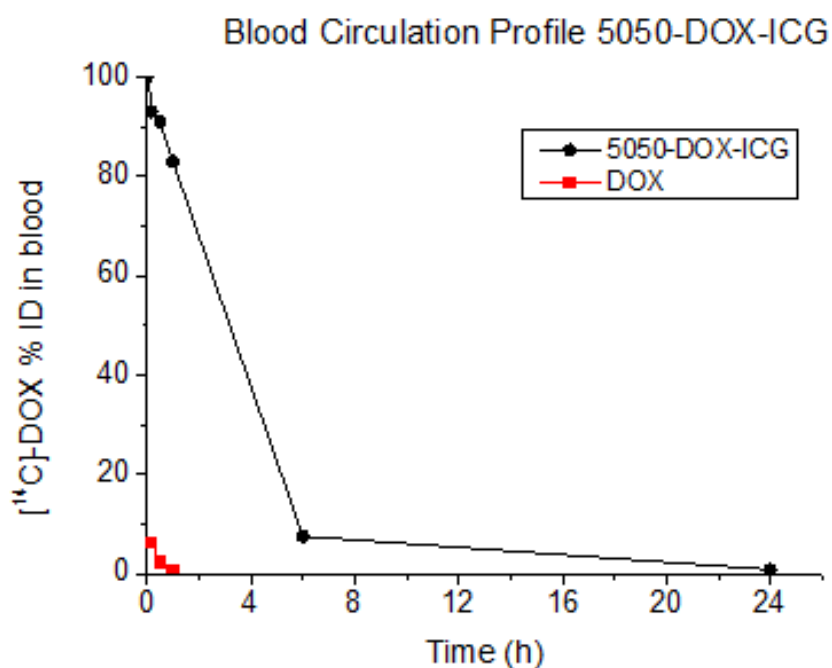


Figure 6.10 Blood stability profile of the film inserted, sonicated 50:50-ICG-DOX system vs free DOX. (n=4, SEM included).

6.3 Discussion

Following initial success in incorporating ICG into thermosensitive liposomal DOX in **Chapter 4**, albeit at low concentrations, this chapter presents the optimisation leading to the development of improved thermosensitive systems. The previously attained ICG concentrations limit the potential utility of the system as a theranostic agent. Through the use of information gained from the thorough investigation into ICG incorporation protocols in **Chapter 5**, it was possible to incorporate tenfold the concentrations of ICG previously attained without the disruption of the system's ability to encapsulate DOX. The two protocols which showed the highest levels of ICG incorporation into NTSL, with the maintenance of therapeutic DOX concentrations were applied to thermosensitive liposomal constructs. These were the film and post insertion protocols incorporating sonication as the liposome downsizing methodology. This did contribute to a higher polydispersity as is expected with the use of sonication in place of extrusion. The film insertion protocol incorporated ICG in the initial stages of liposome preparation, being co-solubilised amongst the constituent lipids and evaporated down to form a lipid-ICG film. The post insertion protocol incorporates ICG in the final stages of DOX loading, where the pre-formed liposome-DOX is still above the phase transition temperature. Sonication proved to effectively double the ICG incorporation efficiency and OD of each system when exchanged with extrusion as an initial downsizing technique. The systems were optimised for maximum ICG incorporation, and characterised to discern how the differing preparation protocols affected the performance between them.

The initial goal was to establish the threshold ICG concentration which would allow DOX encapsulation at therapeutic concentrations.

The post insertion methodology was initially tested at initial [ICG] ranging between 50 and 200 μM . The 50:50 system effectively incorporated ICG at each concentration tested whilst maintaining DOX at >95% EE. The 60:40 failed to do so at 200 μM initial [ICG] achieving just 18% DOX EE, but was uncompromised at lower [ICG], despite a slight size increase from 80 to 90 nm at an initial [ICG] of 100 μM . The 70:30 system also failed at 200 μM , with DOX EE dropping to 41%. Notably the size increased dramatically at an initial [ICG] of 100 μM from 80 to 125 nm. The ICG

threshold for the post insertion protocols appear to be somewhere above 200 μM for the 50:50 system, between 100 and 200 μM for the 60:40 and based on the large size increase, between 50 and 100 μM for the 70:30.

These composition specific ICG incorporation thresholds substantiate the theory that the ICG initially localises along the grain boundaries of the liposomes. As the relative lipid composition of the systems move closer to parity between the DPPC and DSPC, the lengths of the grain boundaries between the lipids increase at the loading temperature. The DPPC will be close to the phase transition temperature, whereas the DSPC will still be in the gel phase. The largest region of defects, and the poorest lipid packing in this state will be at these boundaries^{265,266}, as imaged in **Figure 6.11**. This allows the flux of DOX to enter the liposomes as the porosity of the bilayer in this region increases. It is thus a valid assumption based on these composition dependent thresholds that ICG exploits these defects to insert and reach the most entropically favourable conformation. It would provide access to more hydrophobic areas, the acyl chains into which the benzindole groups of the ICG may interact whilst maintaining the polar sulphonate-choline interaction with the polar head groups of the lipids.

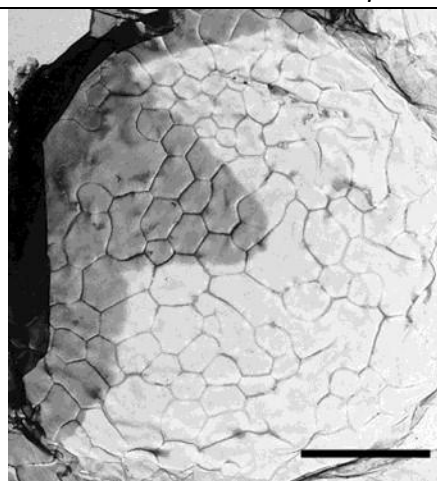


Figure 6.11. TEM micrograph of an air filled phosphatidylcholine based 5 μm microparticle displaying grain boundary structure. (Scale bar = 1 μm). Adapted from²⁶⁶.

Surfactant type effects have been observed when exposing free ICG to erythrocytes and retinal pigment epithelium^{267,268}. ICG has been shown to modify the superficial tension of water, and in the presence of differing surfactants, effectively increases their cmc²⁴⁹. Addition of surfactants to liposomes has been shown to increase vesicle size²⁶⁹. In the initial stages of low concentration surfactant addition to liposomes, surfactants incorporate into the bilayer forming mixing with the constituent lipids, associating between hydrophobic and hydrophilic environments with little overall effect upon the integral structure. As the surfactant concentration increases and the bilayer becomes saturated, membrane permeability increases, and the

vesicular structure begins to transform into micelles²⁷⁰. It appears that following the saturation of the grain boundaries of the tested formulations at their relative saturation points, the ICG begins to act as a surfactant, integrating into the bulk fluid lipid populations, and like SDS into a monolipidic liposome bilayer, increases the size and permeability. Seemingly, the ICG and lipid concentrations used appear to be around the brink of saturation for the thermosensitive systems, with the DOX encapsulating providing readout of surfactant like permeabilisation.

A lower range of ICG concentrations were tested for the film insertion, sonication prepared liposomes. Initially, 200 μM initial [ICG] was used in the preparation of the 50:50 system, however this did not allow effective DOX loading, so the concentration was dropped to 100 μM and tested in the 50:50 and 60:40 formulations. It appears that this protocol showed more sensitivity to ICG in terms of the threshold concentrations which allowed efficient DOX loading. The threshold for the 50:50 system appeared to be between 100 and 200 μM ICG, and the 60:40 system between 90 and 100 μM . Due to the repeated heating and cooling cycles, the ICG-liposomes undergo due to the chronology of ICG addition in the film insertion protocol, it is likely that the most poorly associated and sterically unstable ICG is lost as the bilayer becomes fluid during phase transition, and the free ICG is purified through chromatographic means. A 10 nm size difference occurs during DOX loading of these systems, which is not observed at the same ICG concentrations in the post-insertion protocol. The film insertion sonication systems excluding either DOX or ICG maintain a size around 80 nm in diameter. This average consistently increases to around 90 nm following DOX loading. This may be as a result of the influx of DOX through the grain boundaries, and reorientation/reinsertion of the ICG.

The IVIS based biodistribution study was carried out with the 50:50-ICG-DOX post inserted sonicated system as this was the most attractive liposomes in terms of ICG content and stability at the time of development. ICG signal emanating from the liver and spleen was as expected, based on the liposome biodistribution and macrophage uptake reported in previous studies using thermosensitive liposomes at 15 minutes¹⁸¹, 30 minutes²⁷¹, 1 hour and 24 hours⁷⁸. Peak DOX tumour accumulation at 24 hours was observed as was seen in the DOXIL[®]-ICG-DOX formulation as resolved

my MSOT and fluorescent cryosection in **Chapter 5** despite the radically different composition and bilayer properties. It was also as expected in comparison to the published literature on biodistribution of thermosensitive liposomes^{78,272,123,273}. As the mechanism of tumour accumulation of these liposomes is based on the EPR effect^{15,16}, up to a point the longer the circulation time the better. This allows increased numbers of passages through the tumour microvasculature and thus increased potential for extravasation. However, strategies to stabilise the system such as the inclusion of cholesterol would increase the size of the vehicles reducing the level of penetration into the tumour tissue and increasing uptake by the RES. It would also reduce the level of thermosensitivity. An increase in the level of PEGylation may further reduce interaction with RES associated macrophages and other lymphocytes, but would also limit interaction with tumour cells thus reducing uptake. There is a fine line in designing a thermosensitive liposome with the optimum characteristics of drug release, tumour accumulation and evasion of RES tissues without considering the inclusion of ICG.

The integrity of the liposomal bilayer was tested during DOX release studies at 37°C in the presence of 50% serum. This tested the permeability of the bilayer as well as the propensity for lipoproteins, specifically those amphiphilic ones to insert into the bilayer inducing membrane expansion, disrupting the vesicular structure and membrane integrity below the liposome phase transition temperature²¹¹. The rate of release would reflect the accommodation of the ICG within the vesicle and demonstrate either a stabilising effect if the total ICG is well incorporated, or destabilising if the concentration is too high for the structure, and it applies a surfactant like effect inducing defects pertaining to increased permeabilisation, which serum proteins may further exploit.

The 70:30 ratio system was discarded due to the low ICG incorporation threshold for effective DOX loading. The 90 µM initial [ICG] 60:40 film insertion system was carried forward over the 100 µM, due to the proximity to the threshold for dye incorporation which resulted in irreproducibility. The post insertion prepared 60:40 system appeared very similar to the ICG exclusive system in terms of release kinetics, while the 50:50 system showed a slight stabilisation when ICG was incorporated at 100

μM and a slightly higher stabilisation effect at $200 \mu\text{M}$. The film insertion systems showed a gross stabilisation effect for both systems releasing the same amount after 24 hours as the post insertion systems did after just 4 hours, which in turn showed little difference between their relative release kinetics. At 42°C , the systems are heated above the transition temperature of DPPC, which in turn opens grain boundaries, and makes this fluid lipid population especially vulnerable to the advances of membrane destabilising lipoproteins. The liposomes follow the same trend as observed at 37°C , with marginal reductions in DOX release rate for the post insertion systems, and significant for the film insertion systems. The 10 nm size difference is unlikely to radically effect the release kinetics. Larger liposomes are more stable than smaller ones seemingly regardless of composition, but the effect of higher size differences is minor in comparison to what has been observed between these formulations²⁴⁸.

These results appear to indicate a more entropically favourable configuration with which the ICG localises in the bilayer to give rise to this stabilisation. Despite the lower [ICG] thresholds which allow DOX encapsulation, especially with the close proximity to the threshold of the 60:40 system, it appears the incorporation protocol promotes a more favourable orientation of the dye. It is likely that due to the repeated heating steps the dye is given a longer time, above the DPPC T_m to allow the dye to find a more entropically favourable situation within the bilayer. Also, as the dye is initially mixed with the monomeric phospholipids, the absence of steric hindrances and requirement for penetration into the bilayer would logically favour a more optimal interaction of the two constituents prior to liposome formation.

The post insertion protocol relies on the dye penetrating the bilayer, and forcing itself into the membrane of pre-formed liposomes in an ionic aqueous medium in which it is not highly soluble. Over 10 minutes of interaction slightly above the transition temperature of the DPPC component, it is unlikely that the dye will find as entropically favourable an orientation as the film insertion methodology. It is likely that the post insertion will allow a more superficial association of the ICG with the liposomal bilayer than the film insertion based on the access the ICG has to the constituent lipids. This would favour interactions at the grain boundaries and more

superficial interactions with the DPPC populations. As seen with cholesterol^{142,274,275}, fatty alcohols²⁷⁶, carotenoids²⁷⁷, and certain peptides^{142,278}, interaction and localisation with the hydrophobic element of the bilayer consistently generates a membrane rigidifying effect. The acyl chains form a more loosely packed network than the polar headgroups, based on the relative sizes, charges and thus packing. Due to the access the film insertion protocol allows the ICG to the hydrophobic region of the bilayer, it is likely that there is a stronger interaction with the acyl chains in the film inserted liposome than the post inserted, giving rise to a more pronounced stabilisation effect, along with the increased density the lipid bilayers would pertain from a more optimum ICG seating within the bilayer.

The investigation into photothermia mediated induction of DOX release was a resounding success. The theory that the incorporation of ICG into a thermosensitive liposomal bilayer for its use as a photothermal triggering mechanism is completely novel. The distinct differences in resultant release between the 50:50-DOX with 2.5% and the 50:50-ICG-DOX with 100% release. 104.8% release was calculated as a result of low levels of evaporation during the maintenance of the systems at 37°C and the subsequent photothermia. This release displayed significant responsiveness to the photothermia which spent just 2 minutes between 42°C and 43°C. The decision to run release in 50% mouse serum acted to emulate as closely as possible the comparative conditions of the water-bath based hyperthermia, and *in vivo* circulation. Current clinical hyperthermia application methods are expensive, invasive, scarce, and or do not provide homogenous heating of the tumour site. For example, there are less than 200 healthcare centres which provide HIFU treatment worldwide, none of which are in the UK²⁷⁹. The use of a laser which can be procured for less than £1'500, the light of which can be delivered through a variety of applicators, would certainly make the photothermic triggering of drug release significantly cheaper as well as being specific to the site of drug accumulation. Photodynamic therapy is already widely used on the NHS as a treatment for oesophageal, skin, lung and mouth cancers as well as worldwide throughout Europe, Japan and the USA²⁸⁰. Laser based drug activation is therefore a widely practiced technology and its subsequent uptake using this NIR light activation would not be a particular burden upon healthcare providers.

The blood stability profile of DOX was tested using radiolabelled [^{14}C]-DOX. Free DOX has a circulation half-life of about 5 minutes¹²³ and ThermoDox[®] 0.5²⁸¹-1.3 hours²⁸². The film inserted 50:50-ICG-DOX system had a DOX circulation half-life of around 3.5 hours which is a major improvement. This is not surprising considering the rapid release rate observed when ThermoDox[®] is incubated in 50% serum at 37°C as mentioned in **Chapter 4**. DOXIL has a circulation half-life of 73.9h in comparison, due to the rigid bilayer composition and presence of cholesterol¹²⁷. To better understand the contribution *in vivo* release had on the half-life, [^3H]-phosphocholine can be used to detect lipid circulation which can be compared to the circulation of [^{14}C]-DOX as has been previously reported using tritiated cholesterol⁷⁸. A full biodistribution study would shed light on the efficacy of the film inserted 50:50 system as an effective drug delivery vehicle. It would take into account the radionuclide content of organs related to the reticuloendothelial system such as the lungs, liver and spleen, as well as tumour uptake in tumour bearing animals.

6.4 Conclusion

Following the relative success of ThermoDox[®] reaching phase III clinical trials, this work continued to investigate the more stable thermosensitive compositions as reported in **Chapter 4**. Following the successful incorporation of ICG through a number of different protocols in **Chapter 5**. This work successfully merged the lipid compositions and dye insertion techniques to increase the ICG loading into thermosensitive formulations up to a range which has produced effective imaging of 75-128 μM . Importantly whilst retaining therapeutic levels of DOX >90% EE (at a 20:1 Lipid:DOX mass ratio). The liposomes demonstrated impressive stability of just 30% DOX release over 24 hours in simulated *in vivo* conditions, incorporating 72-79 μM ICG and retaining 97-98% DOX EE. With liposomes of a lower stability in serum (the post insertion system), it was possible to demonstrate successful tumour accumulation with both DOX and ICG colocalising in tumour xenografts at 24 hours post injection as visualised via IVIS. Following further serum stabilisations of the system (the film insertion system), the liposomes showed an improved blood circulation profile over DOX alone, and ThermoDox[®]. With this performance *in vivo* and the relative ICG

concentrations attained, the intrinsic photothermal properties were tested under irradiation of a near infrared LASER. Upon light application, the ICG within the liposomes generated a bulk heat increase to the low temperature hyperthermia range in *in vitro* assays. Despite just 5 minutes under photothermia, the ICG comprising thermosensitive liposomes demonstrated 100% DOX release while the ICG free and NTSL systems showed minimal to no release. These convincing results prompts the imminent continuation of this system into *in vivo* therapeutic studies.

Chapter 7

7 Conclusions and perspectives for future work

The goal of this work was to develop a theranostic system using a liposome based nanocarrier. It would both deliver active chemotherapeutics at a therapeutic concentration to the tumour site whilst containing high enough levels of a light responsive imaging agent to allow successful imaging of the treatment and response, in addition to light induced drug release.

The field of theranostics is a rapidly developing area of research in the field of future medicine. A very limited selection of theranostics have reached clinics however this does not reflect the extensive number of projects currently focusing on this field. Nanomedicine in drug delivery endeavours to use constructs at a nanometric scale to improve the therapeutic index, safety and delivery of APIs to target sites. This size limit concerning functionality does vary in the range of a few hundred nanometres depending on the material. Complexation of proprietary compounds within versatile nanoscopic vectors makes it possible to greatly improve circulation half-lives, and facilitate the delivery of molecules and concentrations otherwise too potent for IV-administration as free agents. Cancer therapy is one of the biggest fields in nanomedicine research in addition to anti-microbials and cardiovascular disorders¹. The EPR effect allows passive targeting of injected nanoparticles to the tumour site due to the inherently leaky tumour vasculature. Through the co-complexation of both therapeutic and imaging agents into nanoscopic delivery vectors, it is possible to track the delivery of the system to the tumour site, as well as monitor response to intervention. Cancer requires early and effective intervention, and thus is a suitable subject for theranostic applications.

Nanoparticles for cancer intervention are not limited to imaging and delivery of proprietary compounds. With careful design, there are a number of additional

functions that are possible to impart upon nanoscopic delivery vectors. Controlled payload release is an example of this. This allows induction of drug release in response to external stimulation. This is necessary, as the payload is only effective if it is free to interact with its target. Robust nanoparticulate vectors such as liposomes have shown great efficacy in improving the safety profile of many active molecules, and effectively improving drug delivery to the tumour site. However, long circulating, rigid liposomes such as DOXIL[®], have previously shown little differences in therapeutic efficacy over free DOX despite these increased tumour concentrations in some cancers. In response to this, thermosensitive liposomes were developed, allowing the use of externally applied hyperthermia to induce drug release in the target site, in order to improve its efficacy against a larger variety of tumour types. This was achieved through the use of thermosensitive lipids which undergo phase transition around 42°C. ThermoDox[®], the most clinically developed thermosensitive liposomes currently in stage III clinical trials is extremely thermosensitive and unstable in physiological environments. ThermoDox[®] was designed to release rapidly upon heating within the tumour vasculature, targeting the vascular endothelial cells in order to limit the blood supply to the tumour. Heating should be applied to the tumour site via RFA or HIFU to ensure that it has reached 42°C by the time the construct reaches the vasculature. It has shown improved efficacy over DOX alone but has been shown to elicit side effects such as alopecia, cardiotoxicity and myelosuppression typically associated to free DOX. Due to separate departments being responsible for the administration of the chemotherapeutics and provision of hyperthermia, poor results in previous trials have hindered the progression of this system. The heating protocol required evidently adds logistical limitations for the application of this therapy as a result of its intrinsic stability.

This is the fundamental context from which this PhD developed. It initially endeavoured to improve upon the shortfalls of previous liposomal-DOX based systems. The next step was to turn these systems into effective theranostic agents through the incorporation of an imaging agent. *In vivo* validation of co-localisation of both the drug and the dye would validate the system as a successful theranostic.

Aims 1

The first section of this project aimed to:

Improve upon the serum stability at 37°C of the most clinically advanced thermosensitive liposome ThermoDox®.

Gain tuneable control over the doxorubicin release rate at 42°C, through modification of the constituent lipid ratios.

7.1 Stabilising the ThermoDox® composition at 37°C

ThermoDox® was carefully designed to rapidly release its payload within the first minute of heat application for the purposes of vascular targeting. This was achieved through the inclusion of the conical single acyl chain lysolipid MSPC's inclusion in the lipid composition along with the majority 41-42°C T_m DPPC population. The mechanism by which it facilitated release was the induction of pore formation, stabilising grain boundaries formed upon phase transition, effectively doing so in aqueous media. Due to the single acyl chain component of the MSPC, the density of acyl chains in the bilayer was reduced, along with the stability due to the reduction in Van der Waals interactions between them. This increases the void space in the bilayer increasing its permeability to serum proteins resulting in its poor stability at 37°C in the presence of serum proteins. The strategy to replace the MSPC with the diacyl version of the lipid DSPC eliminated the pore formation mechanism resulting in DOX release occurring through the established grain boundaries. It also increased the density of the hydrophobic portion of the liposomal bilayer, as well as stabilising the bilayer through increased Van der Waal interactions.

7.2 Gain tuneable control over the doxorubicin release rate at 42°C

Following the development of the DPPC:DSPC based formulation maintaining the same 90:10 ratio as used in the ThermoDox® DPPC:MSPC composition, it was possible to maintain similar release properties without the caveat of destabilisation in emulated physiological conditions. This thermosensitive system achieved near 100% DOX release within the first 5 minutes rather than during the first minute. Rapid release rates were designed to target the tumour vasculature, however slower release rates emanating from more rigid systems were thought to allow further penetration into the tumour stroma allowing deeper drug delivery into the lesions rather than peripheral. Thus, a number of systems based on the same core phospholipids were designed to release at different rates. This was achieved through the systematic variation in DPPC:DSPC. DPPC T_m at 41-42°C is significantly lower than DSPC at 55°C. So the higher the DSPC content the slower the DOX release rate.

Considering the differences in release rate observed through liposomes downsized via extrusion vs sonication, it would be interesting to further expand the study with the inclusion of sonicated systems covering the same ratios. Additional ratios may also be tested with an inversion of the ratios, containing a higher DSPC content in comparison to DPPC. Considering peak accumulation of thermosensitive liposomes observed 24 hours following administration as elucidated in **Chapter 6**, stability studies for each system over 24 hours at 37°C in 50% serum would be useful for further characterisation of liposome stability. An investigation into the addition of low cholesterol concentrations as seen in the traditional thermosensitive liposome (TTSL) systems may allow further stabilisation at 37°C whilst maintaining thermosensitivity at 42°C.

Aims 2

The second section of this project aimed to:

- Identify the optimum method of incorporating ICG, the FDA approved near-infrared dye into a rigid formulation NTS liposome.
- Demonstrate the constructs efficacy as a theranostic agent through temporal imaging of its tumour accumulation through high-resolution MSOT imaging, and co-localisation of DOX through fluorescent imaging.

7.3 Optimising ICG incorporation into the DOXIL® formulation liposome

The near infrared imaging agent ICG was selected for liposomal incorporation in order to turn this FDA approved, frequently used nanomedicine into a theranostic system with which it would be possible to both image and treat simultaneously. ICG was chosen due to its efficacy as a photoacoustic contrast agent, its low toxicity, FDA approval and most importantly at the initial stages, its amphiphilic nature. Its solubility in both aqueous and hydrophobic environments gives it a high level of versatility in incorporation protocol design. Initial studies into ICG incorporation into the thermosensitive DOX encapsulating liposomes designed in the previous section proved difficult due to the disruption of the vesicles leading to poor DOX loading even at low dye concentrations (>10 μM). The ICG had been incorporated in the initial stages of film formation, co-solubilising the dye with the lipids in the organic solvent. The liposomes had been prepared using extrusion for their initial downsizing. With such low dye concentrations, the chances of successful imaging and photothermal heating was slim to none.

This predicament drove the investigation into two additional dye incorporation strategies. The first was the freeze fracture protocol which was taken from previous literature on the subject of ICG lipid incorporation. In this protocol the film was hydrated with an ammonium sulphate based ICG solution prior to solubilisation and

several cycles of freeze fracturing. The second was the post insertion protocol, developed from a method used for ICG incorporation into erythrocyte ghosts. In this protocol the ICG is introduced to pre-formed and DOX loaded liposomes in the final stages of DOX loading, allowing the ICG to insert from the excipient media into the liquid phase liposomal bilayer above the composition's T_m . In addition to the 3 differing incorporation protocols, the method of downsizing was also varied between extrusion, as previously used, and sonication. Sonication generates liposomes of a smaller diameter than what was possible using extrusion. The smaller the liposomes, the higher the available surface area for interaction and vesicle curvature. The higher curvature increases the void space in the bilayer reducing the level of steric hindrances in the outer layer, theoretically increasing the ease of penetrance and integration of the dye into the bilayer. It also reduced the time that the liposomes are kept above their T_m in the presence of ICG in the case of the film insertion and freeze fracture protocols. This time reduction was considered important to minimise the possibility of ICG loss following initial bilayer incorporation, as well as reducing the propensity for dye aggregation which occurs rapidly in the polar ammonium sulphate excipient media.

The optimal downsizing technique in terms of ICG incorporation was via sonication. The most efficient incorporation protocol was post insertion closely followed by film insertion. Notably the dye incorporation efficiency with this protocol increased the lipid:dye ratio 6.8 fold from 666:1 to 98:1 resulting in a final concentration of 128 μM , a vast improvement over the incorporation threshold into the thermosensitive liposomes in **Chapter 4**.

7.4 Demonstrating the imaging potential of the NTS liposome-ICG-DOX via MSOT

MSOT provides non-invasive temporal and spatial imaging of appropriate photoacoustic contrast agents, of which ICG is the optimal⁸⁹. Previous attempts to incorporate ICG into thermosensitive liposomes were too inefficient to provide a high enough dye concentration for viable use in imaging. With the optimisation of the incorporation protocol, the dye concentration was substantially increased for the justification for its use in *in vivo* imaging. The system was tested in an orthotopic 4T1

tumour bearing mouse model. Following IV administration, the liposomes reached peak tumour accumulation after 24 hours, with a prominent, well disseminated signal emanating from across the tumour tissue. The ICG signal was successfully co-localised with that from the DOX via fluorescence cryosection, validating the system as an effective theranostic nanodrug.

Despite successful imaging at this ICG concentration, it would be interesting to establish the upper threshold for initial [ICG] for the sonicated film insertion protocol.

Aims 3

The final section of this project aimed to:

- Identify the optimum method of incorporating ICG, into a thermosensitive formulation.
- Demonstrate the constructs efficacy as a robust theranostic agent through *in vivo* tumour accumulation assays, and co-localisation of both drug and dye.
- Achieve laser induced ICG-based photothermia to induce DOX release whilst maintaining the temperature within the low temperature hyperthermia range.

7.5 Identifying the optimum method of incorporating ICG into thermosensitive liposomes

Following the optimisation of dye incorporation protocol into the NTS-liposome in **Chapter 5**, the most efficient methodologies were tested in thermosensitive formulation liposomes. The necessity of the use of these more fluid formulations stems from the lack of therapeutic efficacy over free DOX of rigid systems, inferring the lack of drug bioavailability when encapsulated in these NTS formulation, and thus emphasising the requirement of triggerable drug release. Several lipid ratios were

tested ranging from 50:50 to 70:30 DPPC:DSPC ratios in order to discern which will provide the best stability over 24 hours at 37°C in 50% serum, whilst displaying effective release over 1 hour at 42°C. The two most successful ICG incorporation protocols were also tested, the film insertion and post insertion, relying on sonication as the choice downsizing strategy. Following extensive trials and stability studies, the optimum system was prepared using the 50:50 composition, applying the film insertion ICG incorporation protocol. This system showed 79% ICG incorporation efficiency with a threshold initial [ICG] of 100 µM, achieving ample ICG concentrations and OD for imaging purposes when compared to reported liposome-ICG systems used in MSOT. Although this protocol didn't have the highest incorporation efficiency, OD or threshold, achieved by the 50:50 post insertion system, it's shown substantially the highest stability at 37°C, alongside ~60% DOX release at 42°C. Stability at 37°C over 24 hours is crucial for the optimal levels of tumour accumulation, expected to peak at this time-point following IV administration.

Considering the differing thresholds for initial [ICG] was very much lipid ratio dependent, it would be interesting to test additional, more rigid ratios to increase final [ICG], and elucidate the effects different concentrations have on the relative vesicle stability under heating.

7.6 Demonstrating the constructs efficacy as a theranostic agent through *in vivo* imaging and stability

IVIS was used for the analysis of tumour accumulation and biodistribution studies for the thermosensitive 50:50 system. Due to the chronology of development and time constraints, the 50:50 system prepared via post insertion was administered IV to 4T1 invasive mammary carcinoma bearing mice. This system demonstrated a substantially lower stability than the film insertion system developed at a later stage. Despite this, it was possible to co-localise the fluorescence of both DOX and ICG, peaking 24 hours post administration. This validated this theranostic as a drug delivery system, proving its imaging potential whilst successfully delivering its payload. The film insertion 50:50 system was subjected to a blood stability study to compare its relative circulation half-life in comparison to other liposome compositions and free DOX. This

was performed using [^{14}C]-DOX loaded liposomes. The circulation half-life was 3.5 hours, which compared to the 5 minute half-life of free DOX, and the 0.5-1.3 hour half-life of ThermoDox[®], was a clear improvement. The longer the circulation half-life, the higher the EPR effect mediated tumour accumulation. This is considered an improvement in terms of this therapeutic strategy by facilitating a higher uptake of liposomes in the tumour site and maintaining a higher concentration of intra-liposomal DOX during the liposome's transport to the tumour site. From a safety perspective, the increased stability at 37°C would allow the facilitation of targeted release whilst reducing the risks of DOX related side effects due to its low stability in simulated physiological conditions.

It would be preferable to have been able to attain MSOT images of the thermosensitive constructs, considering the photoacoustic properties of the ICG, and the higher resolution and sensitivity of the instrument over IVIS. The blood stability study provided interesting data on DOX circulation stability, and the difference observed in comparison to free DOX and ThermoDox[®] is testament to the improvements in liposomal formulation. However the study could be improved with the use of tritiated phospholipids along with the radiolabelled DOX. This would shed light on the stability of the liposome in terms of DOX leakage during circulation, allowing the deconvolution of clearance between the lipid and the DOX. This would allow validation of the *in vitro* release data at 37°C in 50% serum, and provide more accurate stability characterisation for future *in vivo* studies

7.7 Achieving laser induced ICG-based photothermia to induce DOX release

One of the advantages of using ICG as an imaging agent in thermosensitive liposomes, is its aptitude as a photothermal agent. Photothermia is the mechanism which provides the pulses of thermoelastic expansion through which it acts as a photoacoustic contrast agent. However, with the right irradiation at the correct ICG concentration, it should be possible to use a non-thermal infra-red laser as a light source to induce substantial heating for the triggering of DOX release. The conditions of this would be to maintain the heating to <43°C, so as to maintain the system in the low temperature hyperthermia range. This was realised through the use of 0.3 W/cm²

800 nm laser irradiation over 5 minutes in the presence of 50% serum. Under these conditions, the 50:50-ICG-DOX liposome prepared via film insertion reached 43°C from a starting temperature of 37°C, releasing 100% of the encapsulated payload. When tested on the ICG free liposomal DOX, just 2.5% release was observed. This resounding success opens up huge potential for the use of near infra-red light as a release induction strategy. Previous work has focused on the use of water bath based hyperthermia which is untargeted and induces substantial tissue damage in pre-clinical *in vivo* applications. Using a non-thermal laser allows molecular heating of the liposomes themselves rather than direct bulk heating of the tumour region as used pre-clinically and clinically through RFA, HIFU and microwave based applicators. In addition to the targeted heating potential, photothermal induced heating in the presence of DOX has shown to sensitise even resistant cells to the effects of DOX, increasing the system's therapeutic potential.

The next steps in the validation of the liposomes designed in this thesis is of course therapeutic studies on murine tumour models. Following the validation of these systems as effective drug delivery vehicles and imaging agents in tumour models, it is essential to understand the tumour response to the applied therapy. It is mandatory that the relative power and time of laser irradiation be optimised. Further investigation into the laser induced release rates at differing powers would allow thorough investigation into the optimum strategy for tumour destruction. Whether the burst release strategy in the initial stages post administration to target the vasculature, or release 24 hours following peak tumour accumulation would be most effective. With the powers studied up to now, it has been possible to induce 100% DOX release at 0.2 and 0.3 W/cm² within 5 minutes. It would be useful to better characterise the DOX release in these early irradiation time-points, along with developing a strategy which would slow the release rate down to what is observed during water bath mediated heating. The advantage of having such a responsive release system using the lipid ratios tested, is that it should be possible to achieve rapid release in more rigid systems which may show improved stability at 37°C. The NTSL formulation does not release at all, but with an increase in DSPC content, it may be possible to slightly improve upon the systems designed for photothermia mediated release.

7.8 Limitations and Future Work

A number of effective methodologies have been used for the incorporation of ICG into a number of DOX encapsulating liposomes. However, this small scale liposome formulation is quite different to those methods used for industrial scale production. Upscaling of the sonication protocol is difficult, and although high pressure industrial extrusion is feasible, the film evaporation phase prior to both processes are difficult to upscale. The most common technique is known as ethanol injection²⁸³, which injects a lipid ethanol solution into an aqueous phase rapidly forming planar bilayer fragments²⁸⁴. The fragments are then broken down by ultrasonication or stirring, inducing exposure and reformation of the bilayers to reduce exposure of the hydrophobic acyl chains to the aqueous excipient. This results in the adoption of increasing curvature of the bilayers subsequently forming the liposomes. Through a reduction in pressure of the solution, the ethanol is evaporated leaving an aqueous liposome suspension. Although the liposome formulation process differs greatly to those methodologies used in this work, there is no reason why elements of the ICG incorporation would not be successful. The film insertion methodology would be difficult due to the lack of film formation in this methodology. Co-solubilisation of the lipids and ICG to force an interaction between the two would depend on the solubility of the ICG in the ethanol, and subsequent aqueous phase, in comparison to the strength of interaction the ICG has when associated with the phospholipids. ICG could be introduced to the aqueous phase prior to bilayer downsizing to allow interaction with the hydrophobic elements of the lipids, but would only work assuming the interaction was not disrupted by the bilayer downsizing. The post insertion methodology seems to be the most transferrable to ethanol injection as it involves interacting with the pre-formed liposomes following their preparation.

Although ICG and DOX have been effectively delivered to the tumour sites using both non-thermosensitive and thermosensitive formulations, to truly understand the theranostic potential of the liposome-DOX-ICG constructs, therapeutic efficacy in a representative tumour bearing *in vivo* model must also be demonstrated in addition to effective imaging and tumour co-localisation of both constituents. In addition to this, a full biodistribution of tritiated phospholipids and [¹⁴C]-DOX would allow

quantification of tumour uptake, as well as understanding the *in vivo* DOX leakage through changes observed in the ratio between both constituents.

High fluorescence and optoacoustic signals are observed in the liver, which is expected as a result of liposome-ICG uptake by resident Kupffer cells of this RES tissue. However, this effect may also mask the uptake of free ICG following its binding to serum proteins. It is important to know that the ICG is still fully associated to the liposomes during circulation, and if a portion of the dye becomes dissociated, exactly how much. The *in vivo* data presented does show co-localisation of both ICG and DOX, however to achieve effective photothermia, it is important to know the proportion of ICG which provides the contrast is still associated to induce effective release. This could be achieved through the quantification of tritiated lipids of radiolabelled liposomes, and the comparative ICG concentration in the tumour site. *In vitro* analysis could also monitor the concentration of free ICG following incubation of the liposomes in simulated physiological conditions following separation of the liposomes from the excipient media. This could also be applied to liposomes which have undergone heating at 42°C to monitor the effect this has on the liposome's constitution.

7.9 Final thoughts

In summary, the goal of this work has been realised following extensive optimisation. It has been possible to develop a number of liposomes with theranostic potential, which show excellent stability at 37°C in comparison to other systems. Through the testing of a number of ICG incorporation protocols, it was possible to revamp this DOXIL®-equivalent formulation, successfully demonstrating its utility as a theranostic agent via MSOT. Following the stabilisation of the ThermoDox® formulation with the replacement of the lysolipid, it was possible to significantly stabilise the system at 37°C whilst displaying a number of differing release rates from a repertoire of differing thermosensitive systems. Through optimisation of ICG incorporation, it was possible to demonstrate successful imaging of thermosensitive liposome tumour accumulation in murine models, and demonstrate improved circulation half-life over ThermoDox®. In addition to this, through the exploitation of ICG's photothermal attributes it was possible to demonstrate rapid release under

irradiation at a maximum temperature of 43°C of 100% after 5 minutes. This system demonstrates exciting potential as a novel theranostic. It successfully transports therapeutic levels of DOX to the tumour site whilst proving itself as an effective imaging agent when combined with the use of MSOT. It has shown thermosensitivity under simulated physiological conditions in the presence of serum, releasing DOX when heated to 42°C through water-bath based hyperthermia, whilst demonstrating good stability at 37°C. The effective photothermal response under near-infrared laser irradiation beckons a novel and effective way to target DOX release in a targeted manner, demonstrating an exciting new addition to the field of thermosensitive theranostics.

8 Bibliography

1. Etheridge, M. L. *et al.* The big picture on nanomedicine: the state of investigational and approved nanomedicine products. *Nanomedicine Nanotechnology, Biol. Med.* **9**, 1–14 (2013).
2. Efeyan, A. & Serrano, M. p53: guardian of the genome and policeman of the oncogenes. *Cell cycle* **6**, 1006–1010 (2007).
3. Nagaich, A. K. *et al.* p53-induced DNA bending and twisting: p53 tetramer binds on the outer side of a DNA loop and increases DNA twisting. *Proc. Natl. Acad. Sci.* **96**, 1875–1880 (1999).
4. Pathway Commons. TP53 Interactome as visualised by PCViz. Available at: <http://www.pathwaycommons.org/pcviz/#neighborhood/TP53>.
5. Bos, J. L. *et al.* Prevalence of ras gene mutations in human colorectal cancers. *Nature* **327**, 293–297 (1987).
6. Brose, M. S. *et al.* BRAF and RAS mutations in human lung cancer and melanoma. *Cancer Res.* **62**, 6997–7000 (2002).
7. Knudson, A. G. Two genetic hits (more or less) to cancer. *Nat. Rev. Cancer* **1**, 157–162 (2001).
8. Folkman, J. Tumor angiogenesis factor. *Cancer Res.* **34**, 2109–2113 (1974).
9. Vander Heiden, M. G., Cantley, L. C. & Thompson, C. B. Understanding the Warburg effect: the metabolic requirements of cell proliferation. *Science (80-)*. **324**, 1029–1033 (2009).
10. Jordan, C. T., Guzman, M. L. & Noble, M. Cancer stem cells. *N. Engl. J. Med.* **355**, 1253–1261 (2006).
11. Kim, J., Tchernyshyov, I., Semenza, G. L. & Dang, C. V. HIF-1-mediated expression of pyruvate dehydrogenase kinase: a metabolic switch required for cellular adaptation to hypoxia. *Cell Metab.* **3**, 177–185 (2006).
12. Forsythe, J. A. *et al.* Activation of vascular endothelial growth factor gene transcription by hypoxia-inducible factor 1. *Mol. Cell. Biol.* **16**, 4604–4613 (1996).
13. Tannock, I. F. Population kinetics of carcinoma cells, capillary endothelial cells, and fibroblasts in a transplanted mouse mammary tumor. *Cancer Res.* **30**, 2470–2476 (1970).
14. Chang, Y. S. *et al.* Mosaic blood vessels in tumors: Frequency of cancer cells in contact with flowing blood. *Proc. Natl. Acad. Sci.* **97**, 14608–14613 (2000).
15. Iwai, K., Maeda, H. & Konno, T. Use of Oily Contrast Medium for Selective Drug Targeting to Tumor : Enhanced Therapeutic Effect and X-Ray Image Use of Oily Contrast Medium for Selective Drug Targeting to Tumor : Enhanced Therapeutic Effect and X-Ray Image1. 2115–2121 (1984).
16. Maeda, H., Wu, J., Sawa, T., Matsumura, Y. & Hori, K. Tumor vascular permeability and the EPR effect in macromolecular therapeutics: a review. *J. Control. release* **65**, 271–284 (2000).
17. Fang, J., Nakamura, H. & Maeda, H. The EPR effect: unique features of tumor blood

- vessels for drug delivery, factors involved, and limitations and augmentation of the effect. *Adv. Drug Deliv. Rev.* **63**, 136–151 (2011).
18. Hare, J. I. *et al.* Challenges and strategies in anti-cancer nanomedicine development: An industry perspective. *Adv. Drug Deliv. Rev.* (2016). doi:10.1016/j.addr.2016.04.025
 19. Lammers, T., Kiessling, F., Hennink, W. E. & Storm, G. Drug targeting to tumors: principles, pitfalls and (pre-) clinical progress. *J. Control. release* **161**, 175–187 (2012).
 20. Anttila, M. A. *et al.* High Levels of Stromal Hyaluronan Predict Poor Disease Outcome in Epithelial Ovarian Cancer. *Cancer Res.* **60**, 150–155 (2000).
 21. Pietras, K. & Östman, A. Hallmarks of cancer: Interactions with the tumor stroma. *Exp. Cell Res.* **316**, 1324–1331 (2010).
 22. Cook, J. & Hagemann, T. Tumour-associated macrophages and cancer. *Curr. Opin. Pharmacol.* **13**, 595–601 (2013).
 23. Jones, S. W. *et al.* Nanoparticle clearance is governed by Th1/Th2 immunity and strain background. *J. Clin. Invest.* **123**, 3061–3073 (2013).
 24. Stix, G. A malignant flame. *Sci. Am.* **297**, 60–67 (2007).
 25. Caino, M. C. *et al.* Metabolic stress regulates cytoskeletal dynamics and metastasis of cancer cells. *J. Clin. Invest.* **123**, 2907–2920 (2013).
 26. Yang, J. & Weinberg, R. A. Epithelial-Mesenchymal Transition: At the Crossroads of Development and Tumor Metastasis. *Dev. Cell* **14**, 818–829 (2008).
 27. Curran, S. & Murray, G. I. Matrix metalloproteinases in tumour invasion and metastasis. *J. Pathol.* **189**, 300–308 (1999).
 28. Reya, T., Morrison, S. J., Clarke, M. F. & Weissman, I. L. Stem cells, cancer, and cancer stem cells. *Nature* **414**, 105–111 (2001).
 29. Bertolini, F., Shaked, Y., Mancuso, P. & Kerbel, R. S. The multifaceted circulating endothelial cell in cancer: towards marker and target identification. *Nat. Rev. Cancer* **6**, 835–845 (2006).
 30. Chaffer, C. L. & Weinberg, R. A. A perspective on cancer cell metastasis. *Science (80-)*. **331**, 1559–1564 (2011).
 31. Green, M. R. *et al.* Abraxane®, a novel Cremophor®-free, albumin-bound particle form of paclitaxel for the treatment of advanced non-small-cell lung cancer. *Ann. Oncol.* **17**, 1263–1268 (2006).
 32. Jordan, A. NanoTherm® Therapy. *Biomed Tech* **56**, 1 (2011).
 33. Sanna, V., Pala, N. & Sechi, M. Targeted therapy using nanotechnology: focus on cancer. *Int. J. Nanomedicine* **9**, 467 (2014).
 34. Bangham, A. D. & Horne, R. W. Negative staining of phospholipids and their structural modification by surface-active agents as observed in the electron microscope. *J. Mol. Biol.* **8**, 660–IN10 (1964).
 35. Goltsov, A. N. & Barsukov, L. I. Synergetics of the membrane self-assembly: a micelle-to-vesicle transition. *J. Biol. Phys.* **26**, 27–41 (2000).
 36. Yoshimura, T., Ohno, A. & Esumi, K. Mixed micellar properties of cationic trimeric-type quaternary ammonium salts and anionic sodium n-octyl sulfate surfactants. *J. Colloid*

Interface Sci. **272**, 191–196 (2004).

37. Israelachvili, J. N., Mitchell, D. J. & Ninham, B. W. Theory of self-assembly of lipid bilayers and vesicles. *Biochim. Biophys. Acta - Biomembr.* **470**, 185–201 (1977).
38. Rawicz, W., Olbrich, K. C., McIntosh, T., Needham, D. & Evans, E. Effect of Chain Length and Unsaturation on Elasticity of Lipid Bilayers. *Biophys. J.* **79**, 328–339 (2000).
39. Alexandridis, P., Olsson, U. & Lindman, B. A Record Nine Different Phases (Four Cubic, Two Hexagonal, and One Lamellar Lyotropic Liquid Crystalline and Two Micellar Solutions) in a Ternary Isothermal System of an Amphiphilic Block Copolymer and Selective Solvents (Water and Oil). *Langmuir* **14**, 2627–2638 (1998).
40. Chapman, D. Phase transitions and fluidity characteristics of lipids and cell membranes. *Q. Rev. Biophys.* **8**, 185–235 (1975).
41. Anderson, M. & Omri, A. The Effect of Different Lipid Components on the In Vitro Stability and Release Kinetics of Liposome Formulations. *Drug Deliv.* **11**, 33–39 (2004).
42. Jacobson, K. & Papahadjopoulos, D. Phase transitions and phase separations in phospholipid membranes induced by changes in temperature, pH, and concentration of bivalent cations. *Biochemistry* **14**, 152–161 (1975).
43. Mabrey, S. & Sturtevant, J. M. Investigation of phase transitions of lipids and lipid mixtures by sensitivity differential scanning calorimetry. *Proc. Natl. Acad. Sci.* **73**, 3862–3866 (1976).
44. Allen, T. M., Hansen, C., Martin, F., Redemann, C. & Yau-Young, A. Liposomes containing synthetic lipid derivatives of poly (ethylene glycol) show prolonged circulation half-lives in vivo. *Biochim. Biophys. Acta (BBA)-Biomembranes* **1066**, 29–36 (1991).
45. Simons, K. & Ehehalt, R. Cholesterol, lipid rafts, and disease. *J. Clin. Invest.* **110**, 597–603 (2002).
46. Briuglia, M.-L., Rotella, C., McFarlane, A. & Lamprou, D. A. Influence of cholesterol on liposome stability and on in vitro drug release. *Drug Deliv. Transl. Res.* **5**, 231–242 (2015).
47. Avanti Lipids. Avanti Lipid Structures. Available at: <https://avantilipids.com/product-category/products/phospholipids/pc-lpc/saturated-fatty-acid/>.
48. Winter, N. D. & Schatz, G. C. A Coarse Grained Molecular Dynamics Study of Permeability Enhancement in DPPC Bilayers by Incorporation of Lysolipid. *J. Phys. Chem. B* **114**, 5053–5060 (2010).
49. Mills, J. K. & Needham, D. Lysolipid incorporation in dipalmitoylphosphatidylcholine bilayer membranes enhances the ion permeability and drug release rates at the membrane phase transition. *Biochim. Biophys. Acta - Biomembr.* **1716**, 77–96 (2005).
50. Papahadjopoulos, D., Cowden, M. & Kimelberg, H. Role of cholesterol in membranes effects on phospholipid-protein interactions, membrane permeability and enzymatic activity. *Biochim. Biophys. Acta (BBA)-Biomembranes* **330**, 8–26 (1973).
51. Kinsky, S. C. Antibiotic interaction with model membranes. *Annu. Rev. Pharmacol.* **10**, 119–142 (1970).
52. Haxby, J. A., Kinsky, C. B. & Kinsky, S. C. Immune response of a liposomal model membrane. *Proc. Natl. Acad. Sci.* **61**, 300–307 (1968).

53. Kinsky, S. C. Antibody-complement interaction with lipid model membranes. *Biochim. Biophys. Acta (BBA)-Reviews Biomembr.* **265**, 1–23 (1972).
54. MAGEE, W. E. & MILLER, O. V. Liposomes containing Antiviral Antibody can protect Cells from Virus Infection. *Nature* **235**, 339–341 (1972).
55. Tyrrell, D. A., Ryman, B. E., Keeton, B. R. & Dubowitz, V. Use of liposomes in treating type II glycogenosis. *Br Med J* **2**, 88 (1976).
56. Patel, H. M. & Ryman, B. E. Oral administration of insulin by encapsulation within liposomes. *FEBS Lett.* **62**, 60–63 (1976).
57. Gregoriadis, G., Swain, C. P., Wills, E. J. & Tavill, A. S. DRUG-CARRIER POTENTIAL OF LIPOSOMES IN CANCER CHEMOTHERAPY. *Lancet* **303**, 1313–1316 (1974).
58. Kimelberg, H. K. Protein-liposome interactions and their relevance to the structure and function of cell membranes. *Mol. Cell. Biochem.* **10**, 171–190 (1976).
59. Hoekstra, D. & Scherphof, G. Effect of fetal calf serum and serum protein fractions on the uptake of liposomal phosphatidylcholine by rat hepatocytes in primary monolayer culture. *Biochim. Biophys. Acta (BBA)-Biomembranes* **551**, 109–121 (1979).
60. Jonah, M. M., Cerny, E. A. & Rahman, Y. E. Tissue distribution of EDTA encapsulated within liposomes of varying surface properties. *Biochim. Biophys. Acta (BBA)-Biomembranes* **401**, 336–348 (1975).
61. Allen, T. M. & Everest, J. M. Effect of liposome size and drug release properties on pharmacokinetics of encapsulated drug in rats. *J. Pharmacol. Exp. Ther.* **226**, 539–544 (1983).
62. Woodruff, J. J. & Gesner, B. M. The effect of neuraminidase on the fate of transfused lymphocytes. *J. Exp. Med.* **129**, 551–567 (1969).
63. Greenberg, J. P. *et al.* Survival of rabbit platelets treated in vitro with chymotrypsin, plasmin, trypsin, or neuraminidase. *Blood* **53**, 916–927 (1979).
64. Allen, T. M. & Chonn, A. Large unilamellar liposomes with low uptake into the reticuloendothelial system. *FEBS Lett.* **223**, 42–46 (1987).
65. Allen, T. M., Hansen, C. & Rutledge, J. Liposomes with prolonged circulation times: factors affecting uptake by reticuloendothelial and other tissues. *Biochim. Biophys. Acta (BBA)-Biomembranes* **981**, 27–35 (1989).
66. Nagayasu, A., Uchiyama, K. & Kiwada, H. The size of liposomes: a factor which affects their targeting efficiency to tumors and therapeutic activity of liposomal antitumor drugs. *Adv. Drug Deliv. Rev.* **40**, 75–87 (1999).
67. Vonarbourg, A., Passirani, C., Saulnier, P. & Benoit, J.-P. Parameters influencing the stealthiness of colloidal drug delivery systems. *Biomaterials* **27**, 4356–4373 (2006).
68. Beauchamp, C. O., Gonias, S. L., Menapace, D. P. & Pizzo, S. V. A new procedure for the synthesis of polyethylene glycol-protein adducts; Effects on function, receptor recognition, and clearance of superoxide dismutase, lactoferrin, and α 2-macroglobulin. *Anal. Biochem.* **131**, 25–33 (1983).
69. Klibanov, A. L., Maruyama, K., Torchilin, V. P. & Huang, L. Amphipathic polyethyleneglycols effectively prolong the circulation time of liposomes. *FEBS Lett.* **268**, 235–237 (1990).

70. Runge, V. M., Dickey, K. M., Williams, N. M. & Peng, X. Local tissue toxicity in response to extravascular extravasation of magnetic resonance contrast media. *Invest. Radiol.* **37**, 393–398 (2002).
71. Martina, M.-S. *et al.* Generation of superparamagnetic liposomes revealed as highly efficient MRI contrast agents for in vivo imaging. *J. Am. Chem. Soc.* **127**, 10676–10685 (2005).
72. Mulder, W. J. M., Strijkers, G. J., van Tilborg, G. A. F., Griffioen, A. W. & Nicolay, K. Lipid-based nanoparticles for contrast-enhanced MRI and molecular imaging. *NMR Biomed.* **19**, 142–164 (2006).
73. Kokuryo, D. *et al.* Evaluation of thermo-triggered drug release in intramuscular-transplanted tumors using thermosensitive polymer-modified liposomes and MRI. *Nanomedicine Nanotechnology, Biol. Med.* **11**, 229–238 (2015).
74. Ghaghada, K., Hawley, C., Kawaji, K., Annapragada, A. & Mukundan, S. T1 relaxivity of core-encapsulated gadolinium liposomal contrast agents—effect of liposome size and internal gadolinium concentration. *Acad. Radiol.* **15**, 1259–1263 (2008).
75. Huang, S. *et al.* Improving ultrasound reflectivity and stability of echogenic liposomal dispersions for use as targeted ultrasound contrast agents. *J. Pharm. Sci.* **90**, 1917–1926 (2001).
76. Dijkmans, P. A. *et al.* Microbubbles and ultrasound: from diagnosis to therapy. *Eur. Hear. Journal-Cardiovascular Imaging* **5**, 245–246 (2004).
77. Zheng, J. *et al.* Liposome contrast agent for CT-based detection and localization of neoplastic and inflammatory lesions in rabbits: validation with FDG-PET and histology. *Contrast Media Mol. Imaging* **5**, 147 (2010).
78. Al-Jamal, W. T., Al-Ahmady, Z. S. & Kostarelos, K. Pharmacokinetics & tissue distribution of temperature-sensitive liposomal doxorubicin in tumor-bearing mice triggered with mild hyperthermia. *Biomaterials* **33**, 4608–4617 (2012).
79. Nguyen, Q. D. *et al.* Temporal and spatial evolution of therapy-induced tumor apoptosis detected by caspase-3-selective molecular imaging. *Clin. Cancer Res.* **19**, 3914–3924 (2013).
80. Oku, N. *et al.* PET imaging of brain cancer with positron emitter-labeled liposomes. *Int. J. Pharm.* **403**, 170–177 (2011).
81. Ma, R., Taruttis, A., Ntziachristos, V. & Razansky, D. Multispectral optoacoustic tomography (MSOT) scanner for whole-body small animal imaging. *Opt. Express* **17**, 21414–21426 (2009).
82. Ntziachristos, V. & Razansky, D. Molecular imaging by means of multispectral optoacoustic tomography (MSOT). *Chem. Rev.* **110**, 2783–2794 (2010).
83. Burton, N. C. *et al.* Multispectral Opto-acoustic Tomography (MSOT) of the Brain and Glioblastoma Characterization. *Neuroimage* **65**, 522–528 (2013).
84. Taruttis, A. & Ntziachristos, V. Advances in real-time multispectral optoacoustic imaging and its applications. *Nat Phot.* **9**, 219–227 (2015).
85. Li, M.-L. *et al.* Simultaneous molecular and hypoxia imaging of brain tumors in vivo using spectroscopic photoacoustic tomography. *Proc. IEEE* **96**, 481–489 (2008).
86. Alander, J. T. *et al.* A review of indocyanine green fluorescent imaging in surgery. *J.*

Biomed. Imaging **2012**, 7 (2012).

87. Proulx, S. T. *et al.* Quantitative Imaging of Lymphatic Function with Liposomal Indocyanine Green. *Cancer Res.* **70**, 7053–7062 (2010).
88. Lozano, N. *et al.* Liposome-gold nanorod hybrids for high-resolution visualization deep in tissues. *J. Am. Chem. Soc.* **134**, 13256–8 (2012).
89. Beziere, N. *et al.* Dynamic imaging of PEGylated indocyanine green (ICG) liposomes within the tumor microenvironment using multi-spectral optoacoustic tomography (MSOT). *Biomaterials* **37**, 415–424 (2015).
90. Lozano, N., Al-Ahmady, Z. S., Beziere, N. S., Ntziachristos, V. & Kostarelos, K. Monoclonal antibody-targeted PEGylated liposome-ICG encapsulating doxorubicin as a potential theranostic agent. *Int. J. Pharm.* doi:http://dx.doi.org/10.1016/j.ijpharm.2014.10.045
91. Nerenz, D. R., Leventhal, H. & Love, R. R. Factors contributing to emotional distress during cancer chemotherapy. *Cancer* **50**, 1020–1027 (1982).
92. Forssen, E. A. & Tökès, Z. A. Use of anionic liposomes for the reduction of chronic doxorubicin-induced cardiotoxicity. *Proc. Natl. Acad. Sci.* **78**, 1873–1877 (1981).
93. Torchilin, V. Tumor delivery of macromolecular drugs based on the EPR effect. *Adv. Drug Deliv. Rev.* **63**, 131–135 (2011).
94. James, N. D. *et al.* Liposomal doxorubicin (Doxil): An effective new treatment for Kaposi's sarcoma in AIDS. *Clin. Oncol.* **6**, 294–296 (1994).
95. Vemulapalli, S. *et al.* Phase I study of ATI-1123, a novel human serum albumin-stabilized docetaxel liposomal formulation, in patients with advanced solid malignancies. in *ASCO Annual Meeting Proceedings* **29**, 2609 (2011).
96. Kim, E. S. *et al.* A phase II study of STEALTH cisplatin (SPI-77) in patients with advanced non-small cell lung cancer. *Lung Cancer* **34**, 427–432 (2001).
97. Lay, M. *et al.* Cationic lipid/DNA complexes (JVRS-100) combined with influenza vaccine (Fluzone®) increases antibody response, cellular immunity, and antigenically drifted protection. *Vaccine* **27**, 3811–3820 (2009).
98. Bressler, N. M. & Bressler, S. B. Photodynamic therapy with verteporfin (Visudyne): impact on ophthalmology and visual sciences. *Invest. Ophthalmol. Vis. Sci.* **41**, 624–628 (2000).
99. Thomas, S. M. *et al.* Tissue distribution of liposome-mediated epidermal growth factor receptor antisense gene therapy. *Cancer Gene Ther.* **10**, 518–528 (2003).
100. Jordan, M. A. Mechanism of action of antitumor drugs that interact with microtubules and tubulin. *Curr. Med. Chem. Agents* **2**, 1–17 (2002).
101. McGrogan, B. T., Gilmartin, B., Carney, D. N. & McCann, A. Taxanes, microtubules and chemoresistant breast cancer. *Biochim. Biophys. Acta (BBA)-Reviews Cancer* **1785**, 96–132 (2008).
102. Xu, X. *et al.* Clinical comparison between paclitaxel liposome (Lipusu®) and paclitaxel for treatment of patients with metastatic gastric cancer. *Asian Pacific J. Cancer Prev.* **14**, 2591–2594 (2013).
103. Fan, Y. & Zhang, Q. Development of liposomal formulations: from concept to clinical

- investigations. *Asian J. Pharm. Sci.* **8**, 81–87 (2013).
104. Forssen, E. A. & Ross, M. E. Daunoxome® treatment of solid tumors: preclinical and clinical investigations. *J. Liposome Res.* **4**, 481–512 (1994).
 105. Domínguez, A. R., Hidalgo, D. O., Garrido, R. V. & Sánchez, E. T. Liposomal cytarabine (DepoCyt®) for the treatment of neoplastic meningitis. *Clin. Transl. Oncol.* **7**, 232–238 (2005).
 106. Silverman, J. A. & Deitcher, S. R. Marqibo®(vincristine sulfate liposome injection) improves the pharmacokinetics and pharmacodynamics of vincristine. *Cancer Chemother. Pharmacol.* **71**, 555–564 (2013).
 107. DiGiulio, S. FDA Approves Onivyde Combo Regimen for Advanced Pancreatic Cancer. *Oncol. Times* (2015).
 108. Deitcher, S. R., Cullis, P., Wong, M. & Choy, G. S. Vinorelbine liposomes injection results in greater tumor drug exposure compared to conventional vinorelbine in tumor-bearing nude mice. *Liver* **1668**, 1–6 (2007).
 109. Aleku, M. *et al.* Atu027, a liposomal small interfering RNA formulation targeting protein kinase N3, inhibits cancer progression. *Cancer Res.* **68**, 9788–9798 (2008).
 110. Prud'homme, R. K. & Svenson, S. in *Multifunctional Nanoparticles for Drug Delivery Applications* 1–5 (Springer, 2012).
 111. Infante, J. R. *et al.* Phase I and pharmacokinetic study of IHL-305 (PEGylated liposomal irinotecan) in patients with advanced solid tumors. *Cancer Chemother. Pharmacol.* **70**, 699–705 (2012).
 112. Gokhale, P. C. *et al.* Improved safety, pharmacokinetics and therapeutic efficacy profiles of a novel liposomal formulation of mitoxantrone. *Anticancer Res.* **21**, 3313–3321 (2000).
 113. Ghamande, S. A. *et al.* A phase I study of the novel DNA topoisomerase-1 inhibitor, TLC388, administered intravenously to patients with advanced solid tumors. in *ASCO Annual Meeting Proceedings* **29**, e13618 (2011).
 114. Fasol, U. *et al.* Vascular and pharmacokinetic effects of EndoTAG-1 in patients with advanced cancer and liver metastasis. *Ann. Oncol.* mdr300 (2011).
 115. Lin, Y.-Y. *et al.* Size effect on tumor treatment with PEGylated liposomal drugs in a tumor-bearing mouse model. *J. Nucl. Med.* **52**, 1737 (2011).
 116. Bernstein, Z. P. *et al.* A MULTICENTER, PHASE II/III STUDY OF ATRAGEN™(Tretinoin Liposomal) IN PATIENTS WITH AIDS-ASSOCIATED KAPOSI'S SARCOMA. *JAIDS J. Acquir. Immune Defic. Syndr.* **17**, A24 (1998).
 117. Nagasawa, M. *et al.* Evaluation of cancer-targeting, pharmacokinetics and antitumor activity of liposomal methotrexate with transferrin ligand, MBP-Y003. *Cancer Res.* **67**, 5650 (2007).
 118. Yousefpour, P. & Chilkoti, A. Co-opting biology to deliver drugs. *Biotechnol. Bioeng.* **111**, 1699–1716 (2014).
 119. Calendi, E., Di Marco, A., Reggiani, M. di, Scarpinato, B. & Valentini, L. On physico-chemical interactions between daunomycin and nucleic acids. *Biochim. Biophys. Acta (BBA)-Nucleic Acids Protein Synth.* **103**, 25–49 (1965).

120. Di Marco, A. *et al.* Daunomycin', a new antibiotic of the rhodomycin group. *Nature* **201**, 706–707 (1964).
121. Tan, C., Tasaka, H., Yu, K., Murphy, M. L. & Karnofsky, D. A. Daunomycin, an antitumor antibiotic, in the treatment of neoplastic disease. Clinical evaluation with special reference to childhood leukemia. *Cancer* **20**, 333–353 (1967).
122. Haran, G., Cohen, R., Bar, L. K. & Barenholz, Y. Transmembrane ammonium sulfate gradients in liposomes produce efficient and stable entrapment of amphipathic weak bases. *Biochim. Biophys. Acta - Biomembr.* **1151**, 201–215 (1993).
123. Gabizon, A. *et al.* Prolonged circulation time and enhanced accumulation in malignant exudates of doxorubicin encapsulated in polyethylene-glycol coated liposomes. *Cancer Res.* **54**, 987–992 (1994).
124. FDA. FDA DOXIL Approval. <https://www.accessdata.fda.gov/scripts/cder/drugsatfda/index.cfm?fuseaction=Search.DrugDetails> (1995).
125. Nunez, M. *et al.* Response to liposomal doxorubicin and clinical outcome of HIV-1-infected patients with Kaposi's sarcoma receiving highly active antiretroviral therapy. *HIV Clin. Trials* **2**, 429–437 (2001).
126. Rose, P. G. Pegylated liposomal doxorubicin: optimizing the dosing schedule in ovarian cancer. *Oncologist* **10**, 205–214 (2005).
127. O'Brien, M. E. R. *et al.* Reduced cardiotoxicity and comparable efficacy in a phase III trial of pegylated liposomal doxorubicin HCl (CAELYX™/Doxil®) versus conventional doxorubicin for first-line treatment of metastatic breast cancer. *Ann. Oncol.* **15**, 440–449 (2004).
128. Zamboni, W. C. *et al.* Systemic and tumor disposition of platinum after administration of cisplatin or STEALTH liposomal-cisplatin formulations (SPI-077 and SPI-077 B103) in a preclinical tumor model of melanoma. *Cancer Chemother. Pharmacol.* **53**, 329–336 (2004).
129. Peleg-Shulman, T., Gibson, D., Cohen, R., Abra, R. & Barenholz, Y. Characterization of sterically stabilized cisplatin liposomes by nuclear magnetic resonance. *Biochim. Biophys. Acta (BBA)-Biomembranes* **1510**, 278–291 (2001).
130. Barenholz, Y. Amphipathic weak base loading into preformed liposomes having a transmembrane ammonium ion gradient: From the bench to approved DOXIL. *Liposome Technol. Entrapment drugs other Mater. into liposomes* **2**, 1–25 (2007).
131. Silverman, L. & Barenholz, Y. In vitro experiments showing enhanced release of doxorubicin from Doxil® in the presence of ammonia may explain drug release at tumor site. *Nanomedicine Nanotechnology, Biol. Med.* **11**, 1841–1850 (2015).
132. Ishida, T., Kirchmeier, M. J., Moase, E. H., Zalipsky, S. & Allen, T. M. Targeted delivery and triggered release of liposomal doxorubicin enhances cytotoxicity against human B lymphoma cells. *Biochim. Biophys. Acta (BBA)-Biomembranes* **1515**, 144–158 (2001).
133. Kale, A. A. & Torchilin, V. P. Enhanced transfection of tumor cells in vivo using 'Smart' pH-sensitive TAT-modified pegylated liposomes. *J. Drug Target.* **15**, 538–545 (2007).
134. Yamada, Y. *et al.* Mitochondrial delivery of mastoparan with transferrin liposomes equipped with a pH-sensitive fusogenic peptide for selective cancer therapy. *Int. J. Pharm.* **303**, 1–7 (2005).

135. Shigeta, K. *et al.* Novel histidine-conjugated galactosylated cationic liposomes for efficient hepatocyte-selective gene transfer in human hepatoma HepG2 cells. *J. Control. release* **118**, 262–270 (2007).
136. Sarkar, N. R. *et al.* ‘Uncorking’ of liposomes by matrix metalloproteinase-9. *Chem. Commun.* 999–1001 (2005).
137. Balakirev, M., Schoehn, G. & Chroboczek, J. Lipoic acid-derived amphiphiles for redox-controlled DNA delivery. *Chem. Biol.* **7**, 813–819 (2000).
138. Yavlovich, A., Singh, A., Blumenthal, R. & Puri, A. A novel class of photo-triggerable liposomes containing DPPC: DC 8, 9 PC as vehicles for delivery of doxorubicin to cells. *Biochim. Biophys. Acta (BBA)-Biomembranes* **1808**, 117–126 (2011).
139. Ueno, Y. *et al.* Combination of ultrasound and bubble liposome enhance the effect of doxorubicin and inhibit murine osteosarcoma growth. *Cancer Biol. Ther.* **12**, 270–277 (2011).
140. Yatvin, M. B., Weinstein, J. N., Dennis, W. H. & Blumenthal, R. Design of liposomes for enhanced local release of drugs by hyperthermia. *Science (80-)*. **202**, 1290–1293 (1978).
141. Katagiri, K. *et al.* Magneto-responsive On-Demand Release of Hybrid Liposomes Formed from Fe₃O₄ Nanoparticles and Thermosensitive Block Copolymers. *Small* **7**, 1683–1689 (2011).
142. Al-Ahmady, Z. S. *et al.* Lipid–Peptide Vesicle Nanoscale Hybrids for Triggered Drug Release by Mild Hyperthermia in Vitro and in Vivo. *ACS Nano* **6**, 9335–9346 (2012).
143. Park, S. M. *et al.* Novel temperature-triggered liposome with high stability: Formulation, in vitro evaluation, and in vivo study combined with high-intensity focused ultrasound (HIFU). *J. Control. Release* **170**, 373–379 (2013).
144. Hayashi, H., Kono, K. & Takagishi, T. Temperature-controlled release property of phospholipid vesicles bearing a thermo-sensitive polymer. *Biochim. Biophys. Acta (BBA)-Biomembranes* **1280**, 127–134 (1996).
145. Landon, C. D. Nanoscale Drug Delivery and Hyperthermia: The Materials Design and Preclinical and Clinical Testing of Low Temperature-Sensitive Liposomes Used in Combination with Mild Hyperthermia in the Treatment of Local Cancer. *Open Nanomed. J.* **3**, 24–37 (2011).
146. Nemcek Jr, A. A. Complications of radiofrequency ablation of neoplasms. in *Seminars in interventional radiology* **23**, 177 (Thieme Medical Publishers, 2006).
147. Anyarambhatla, G. R. & Needham, D. Enhancement of the phase transition permeability of DPPC liposomes by incorporation of MPPC: a new temperature-sensitive liposome for use with mild hyperthermia. *J. Liposome Res.* **9**, 491–506 (1999).
148. Needham, D., Anyarambhatla, G., Kong, G. & Dewhirst, M. W. A new temperature-sensitive liposome for use with mild hyperthermia: characterization and testing in a human tumor xenograft model. *Cancer Res.* **60**, 1197–1201 (2000).
149. Gaber, M. H., Hong, K., Huang, S. K. & Papahadjopoulos, D. Thermosensitive sterically stabilized liposomes: formulation and in vitro studies on mechanism of doxorubicin release by bovine serum and human plasma. *Pharm. Res.* **12**, 1407–1416 (1995).
150. Celsion. http://celsion.com/docs/technology_thermodox. (2015).

151. Lammers, T., Kiessling, F., Hennink, W. E. & Storm, G. Nanotheranostics and image-guided drug delivery: current concepts and future directions. *Mol. Pharm.* **7**, 1899–1912 (2010).
152. Muthu, M. S., Kulkarni, S. A., Raju, A. & Feng, S.-S. Theranostic liposomes of TPGS coating for targeted co-delivery of docetaxel and quantum dots. *Biomaterials* **33**, 3494–3501 (2012).
153. Fattahi, H. *et al.* Magnetoliposomes as multimodal contrast agents for molecular imaging and cancer nanotheranostics. *Nanomedicine* **6**, 529–544 (2011).
154. Al-Jamal, W. & Kostarelos, K. Liposome-nanoparticle hybrids for multimodal diagnostic and therapeutic applications. (2007).
155. Janib, S. M., Moses, A. S. & MacKay, J. A. Imaging and drug delivery using theranostic nanoparticles. *Adv. Drug Deliv. Rev.* **62**, 1052–1063 (2010).
156. Saw, P. E. *et al.* Effect of PEG pairing on the efficiency of cancer-targeting liposomes. *Theranostics* **5**, 746 (2015).
157. Jiang, F. *et al.* Photodynamic therapy of U87 human glioma in nude rat using liposome-delivered photofrin. *Lasers Surg. Med.* **22**, 74–80 (1998).
158. Dougherty, T. J. *et al.* Photodynamic therapy. *J. Natl. Cancer Inst.* **90**, 889–905 (1998).
159. Chang, H.-I. & Yeh, M.-K. Clinical development of liposome-based drugs: formulation, characterization, and therapeutic efficacy. *Int J Nanomedicine* **7**, (2012).
160. Lammers, T., Aime, S., Hennink, W. E., Storm, G. & Kiessling, F. Theranostic nanomedicine. *Acc. Chem. Res.* **44**, 1029–1038 (2011).
161. Telgmann, L., Sperling, M. & Karst, U. Determination of gadolinium-based MRI contrast agents in biological and environmental samples: a review. *Anal. Chim. Acta* **764**, 1–16 (2013).
162. Choi, S.-Y., Kim, Y.-S., Seo, Y.-J., Yang, J. & Choi, K.-S. Gas-filled phospholipid nanoparticles conjugated with gadolinium play a role as a potential theragnostics for MR-guided HIFU ablation. *PLoS One* **7**, e34333 (2012).
163. Chan, W. C. W. & Nie, S. Quantum dot bioconjugates for ultrasensitive nonisotopic detection. *Science (80-.)*. **281**, 2016–2018 (1998).
164. Pitchaimani, A., Nguyen, T. D. T., Wang, H., Bossmann, S. H. & Aryal, S. Design and characterization of gadolinium infused theranostic liposomes. *RSC Adv.* **6**, 36898–36905 (2016).
165. Li, S., Goins, B., Zhang, L. & Bao, A. Novel multifunctional theranostic liposome drug delivery system: construction, characterization, and multimodality MR, near-infrared fluorescent, and nuclear imaging. *Bioconjug. Chem.* **23**, 1322–1332 (2012).
166. Shao, D. *et al.* Noninvasive theranostic imaging of HSV-TK/GCV suicide gene therapy in liver cancer by folate-targeted quantum dot-based liposomes. *Biomater. Sci.* **3**, 833–841 (2015).
167. Deng, L. *et al.* A MSLN-targeted multifunctional nanoimmunoliposome for MRI and targeting therapy in pancreatic cancer. *Int J Nanomedicine* **7**, 5053–5065 (2012).
168. Kenny, G. D. *et al.* Novel multifunctional nanoparticle mediates siRNA tumour delivery, visualisation and therapeutic tumour reduction in vivo. *J. Control. Release* **149**, 111–116

- (2011).
169. Kono, K. *et al.* Multifunctional liposomes having target specificity, temperature-triggered release, and near-infrared fluorescence imaging for tumor-specific chemotherapy. *J. Control. Release* **216**, 69–77 (2015).
 170. Maruyama, T. *et al.* Treatment of Near-Infrared Photodynamic Therapy Using a Liposomally Formulated Indocyanine Green Derivative for Squamous Cell Carcinoma. *PLoS One* **10**, e0122849 (2015).
 171. Tangutoori, S. *et al.* Simultaneous delivery of cytotoxic and biologic therapeutics using nanophotoactivatable liposomes enhances treatment efficacy in a mouse model of pancreatic cancer. *Nanomedicine Nanotechnology, Biol. Med.* **12**, 223–234 (2016).
 172. Cuomo, V., Jori, G., Rihter, B., Kenney, M. E. & Rodgers, M. A. Liposome-delivered Si (IV)-naphthalocyanine as a photodynamic sensitizer for experimental tumours: pharmacokinetic and phototherapeutic studies. *Br. J. Cancer* **62**, 966 (1990).
 173. van Leengoed, H. L. *et al.* In vivo fluorescence and photodynamic activity of zinc phthalocyanine administered in liposomes. *Br. J. Cancer* **69**, 840 (1994).
 174. FDA. FDA ICG Approval. <https://www.accessdata.fda.gov/scripts/cder/drugsatfda/index.cfm?fuseaction=Search.DrugDetails> (1959).
 175. Sheng, Q.-S. *et al.* Indocyanine green clearance test and model for end-stage liver disease score of patients with liver cirrhosis. *Hepatobiliary Pancreat Dis Int* **8**, 46–49 (2009).
 176. Portnoy, E., Lecht, S., Lazarovici, P., Danino, D. & Magdassi, S. Cetuximab-labeled liposomes containing near-infrared probe for in vivo imaging. *Nanomedicine Nanotechnology, Biol. Med.* **7**, 480–488 (2011).
 177. Tang, Y. & McGoron, A. J. Combined effects of laser-ICG photothermotherapy and doxorubicin chemotherapy on ovarian cancer cells. *J. Photochem. Photobiol. B* **97**, 138–44 (2009).
 178. Suganami, A. *et al.* Preparation and characterization of phospholipid-conjugated indocyanine green as a near-infrared probe. *Bioorg. Med. Chem. Lett.* **22**, 7481–7485 (2012).
 179. Tang, Y. & McGoron, A. J. Combined effects of laser-ICG photothermotherapy and doxorubicin chemotherapy on ovarian cancer cells. *J. Photochem. Photobiol. B Biol.* **97**, 138–144 (2009).
 180. Herzog, E. *et al.* Optical Imaging of Cancer Heterogeneity with Multispectral Optoacoustic Tomography. *Radiology* **263**, 461–468 (2012).
 181. Turner, D. C., Moshkelani, D., Shemesh, C. S., Luc, D. & Zhang, H. Near-infrared image-guided delivery and controlled release using optimized thermosensitive liposomes. *Pharm. Res.* **29**, 2092–2103 (2012).
 182. Hua, J. *et al.* In vivo imaging of choroidal angiogenesis using fluorescence-labeled cationic liposomes. *Mol. Vis.* **18**, 1045–1054 (2012).
 183. Zagar, T. M. *et al.* Two phase I dose-escalation/pharmacokinetics studies of low temperature liposomal doxorubicin (LTLD) and mild local hyperthermia in heavily pretreated patients with local regionally recurrent breast cancer. *Int. J. Hyperth.* **30**,

- 285–294 (2014).
184. Razansky, D. *et al.* Multispectral opto-acoustic tomography of deep-seated fluorescent proteins in vivo. *Nat Phot.* **3**, 412–417 (2009).
 185. Ntziachristos, V., Bremer, C. & Weissleder, R. Fluorescence imaging with near-infrared light: new technological advances that enable in vivo molecular imaging. *Eur. Radiol.* **13**, 195–208 (2003).
 186. Lyass, O. *et al.* Correlation of toxicity with pharmacokinetics of pegylated liposomal doxorubicin (Doxil) in metastatic breast carcinoma. *Cancer* **89**, 1037–1047 (2000).
 187. Chen, Q. *et al.* An albumin-based theranostic nano-agent for dual-modal imaging guided photothermal therapy to inhibit lymphatic metastasis of cancer post surgery. *Biomaterials* **35**, 9355–9362 (2014).
 188. Oz, M. C. *et al.* Indocyanine green dye enhanced vascular welding with the near infrared diode laser. *Vasc. Endovascular Surg.* **24**, 564–570 (1990).
 189. Tuchin, V. V *et al.* A pilot study of ICG laser therapy of acne vulgaris: photodynamic and photothermolysis treatment. *Lasers Surg. Med.* **33**, 296–310 (2003).
 190. Bäumlner, W. *et al.* Photo-oxidative killing of human colonic cancer cells using indocyanine green and infrared light. *Br. J. Cancer* **80**, 360 (1999).
 191. Tang, Y. & McGoron, A. J. Combined effects of laser-ICG photothermotherapy and doxorubicin chemotherapy on ovarian cancer cells. *J. Photochem. Photobiol. B.* **97**, 138–44 (2009).
 192. Zheng, M. *et al.* Single-Step Assembly of DOX / ICG Loaded Lipid À Polymer Nanoparticles for Highly E ff ective Chemo-photothermal. *ACS Nano* **7**, 2056–2067 (2013).
 193. Stewart, J. C. M. Colorimetric determination of phospholipids with ammonium ferrothiocyanate. *Anal. Biochem.* **104**, 10–14 (1980).
 194. Buiting, A. M. J., Zhou, F., Bakker, J. A. J., Van Rooijen, N. & Huang, L. Biodistribution of clodronate and liposomes used in the liposome mediated macrophage ‘suicide’ approach. *J. Immunol. Methods* **192**, 55–62 (1996).
 195. Ganta, S., Devalapally, H., Shahiwala, A. & Amiji, M. A review of stimuli-responsive nanocarriers for drug and gene delivery. *J. Control. Release* **126**, 187–204 (2008).
 196. Mura, S., Nicolas, J. & Couvreur, P. Stimuli-responsive nanocarriers for drug delivery. *Nat Mater* **12**, 991–1003 (2013).
 197. Liu, D., Yang, F., Xiong, F. & Gu, N. The Smart Drug Delivery System and Its Clinical Potential.
 198. Poon, R. T. P. & Borys, N. Lyso-thermosensitive liposomal doxorubicin: a novel approach to enhance efficacy of thermal ablation of liver cancer. *Expert Opin. Pharmacother.* **10**, 333–343 (2009).
 199. Wood, B. J. *et al.* Phase I study of heat-deployed liposomal doxorubicin during radiofrequency ablation for hepatic malignancies. *J. Vasc. Interv. Radiol.* **23**, 248–255 (2012).
 200. Needham, D., Park, J.-Y., Wright, A. M. & Tong, J. Materials characterization of the low temperature sensitive liposome (LTSL): effects of the lipid composition (lysolipid and

- DSPE–PEG2000) on the thermal transition and release of doxorubicin. *Faraday Discuss.* **161**, 515–534 (2013).
201. Sandström, M. C., Ickenstein, L. M., Mayer, L. D. & Edwards, K. Effects of lipid segregation and lysolipid dissociation on drug release from thermosensitive liposomes. *J. Control. release* **107**, 131–142 (2005).
 202. Li, L. *et al.* Triggered content release from optimized stealth thermosensitive liposomes using mild hyperthermia. *J. Control. Release* **143**, 274–279 (2010).
 203. Landsman, M. L., Kwant, G., Mook, G. a & Zijlstra, W. G. Light-absorbing properties, stability, and spectral stabilization of indocyanine green. *J. Appl. Physiol.* **40**, 575–583 (1976).
 204. Scherphof, G., Damen, J., Wilschut, J. & Gregoriadis, G. *Liposome Technology*, Vol. (1984).
 205. Morrisett, J. D., Jackson, R. L. & Gotto, Am. Lipid-protein interactions in the plasma lipoproteins. *Biochim. Biophys. Acta (BBA)-Reviews Biomembr.* **472**, 93–133 (1977).
 206. Juliano, R. L. &astro, M. J. *Liposomes*. (Elsevier Science Publishers, 1989).
 207. Caracciolo, G. Liposome–protein corona in a physiological environment: Challenges and opportunities for targeted delivery of nanomedicines. *Nanomedicine Nanotechnology, Biol. Med.* **11**, 543–557 (2015).
 208. Papahadjopoulos, D., Moscarello, M., Eylar, E. H. & Isac, T. Effects of proteins on the thermotropic phase transitions of phospholipid membranes. *Biochim. Biophys. Acta (BBA)-Biomembranes* **401**, 317–335 (1975).
 209. Nelsestuen, G. L., Kisiel, W. & Di Scipio, R. G. Interaction of vitamin K dependent proteins with membranes. *Biochemistry* **17**, 2134–2138 (1978).
 210. Hadjidemetriou, M. *et al.* In vivo biomolecule corona around blood-circulating, clinically used and antibody-targeted lipid bilayer nanoscale vesicles. *ACS Nano* **9**, 8142–8156 (2015).
 211. Scherphof, G., Morselt, H., Regts, J. & Wilschut, J. C. The involvement of the lipid phase transition in the plasma-induced dissolution of multilamellar phosphatidylcholine vesicles. *Biochim. Biophys. Acta (BBA)-Biomembranes* **556**, 196–207 (1979).
 212. Lapinski, M. M., Castro-Forero, A., Greiner, A. J., Ofoli, R. Y. & Blanchard, G. J. Comparison of liposomes formed by sonication and extrusion: rotational and translational diffusion of an embedded chromophore. *Langmuir* **23**, 11677–11683 (2007).
 213. Suganami, A. *et al.* Preparation and characterization of phospholipid-conjugated indocyanine green as a near-infrared probe. *Bioorganic Med. Chem. Lett.* **22**, 7481–7485 (2012).
 214. Bahmani, B., Bacon, D. & Anvari, B. Erythrocyte-derived photo-theranostic agents: hybrid nano-vesicles containing indocyanine green for near infrared imaging and therapeutic applications. *Sci. Rep.* **3**, (2013).
 215. Murata, M., Tahara, K. & Takeuchi, H. Real-time in vivo imaging of surface-modified liposomes to evaluate their behavior after pulmonary administration. *Eur. J. Pharm. Biopharm.* **86**, 115–119 (2014).
 216. Jeong, H.-S. *et al.* The effect of mannosylation of liposome-encapsulated indocyanine

- green on imaging of sentinel lymph node. *J. Liposome Res.* **23**, 291–297 (2013).
217. Sadick, N. S. Update on non-ablative light therapy for rejuvenation: A review. *Lasers Surg. Med.* **32**, 120–128 (2003).
218. Li, X. *et al.* Mechanism study of tumor-specific immune responses induced by laser immunotherapy. in *SPIE BiOS 790006* (International Society for Optics and Photonics, 2011).
219. Pattani, V. P., Shah, J., Atalis, A., Sharma, A. & Tunnell, J. W. Role of apoptosis and necrosis in cell death induced by nanoparticle-mediated photothermal therapy. *J. Nanoparticle Res.* **17**, 20 (2015).
220. Harrington, K. J. *et al.* Effective targeting of solid tumors in patients with locally advanced cancers by radiolabeled pegylated liposomes. *Clin. Cancer Res.* **7**, 243–254 (2001).
221. Hsu, C.-W. *et al.* Comparative therapeutic efficacy of rhenium-188 radiolabeled-liposome and 5-fluorouracil in LS-174T human colon carcinoma solid tumor xenografts. *Cancer Biother. Radiopharm.* **27**, 481–489 (2012).
222. Sarris, A., Dimopoulos, M., Pugh, W. & Cabanillas, F. Primary Lymphoma of the Prostate: Good Outcome with Doxorubicin-Based Combination Chemotherapy. *J. Urol.* **153**, 1852–1854 (1995).
223. Fidas, P., Carey, R. W. & Grossbard, M. L. Non-hodgkin's lymphoma presenting with biliary tract obstruction. A discussion of seven patients and a review of the literature. *Cancer* **75**, 1669–1677 (1995).
224. Imai, T., Takahashi, K., Fukura, H. & Morishita, Y. Measurement of cardiac output by pulse dye densitometry using indocyanine green: a comparison with the thermodilution method. *Anesthesiology* **87**, 816–822 (1997).
225. CM, L., Smith, F., Longueville, J., Paumgartner, G. & MM, H. Indocyanine green clearance as a test for hepatic function: Evaluation by dichromatic ear densitometry. *JAMA* **200**, 236–240 (1967).
226. Hayashi, K., Hasegawa, Y. & Tokoro, T. Indocyanine green angiography of central serous chorioretinopathy. *Int. Ophthalmol.* **9**, 37–41 (1986).
227. Luty, G. A. The acute intravenous toxicity of biological stains, dyes, and other fluorescent substances. *Toxicol. Appl. Pharmacol.* **44**, 225–249 (1978).
228. Phan, T. G. & Bullen, A. Practical intravital two-photon microscopy for immunological research: faster, brighter, deeper. *Immunol Cell Biol* **88**, 438–444 (2010).
229. Kim, T. *et al.* Evaluation of Temperature-Sensitive, Indocyanine Green-Encapsulating Micelles for Noninvasive Near-Infrared Tumor Imaging. *Pharm. Res.* **27**, 1900–1913 (2010).
230. van der Vorst, J. R. *et al.* Near-infrared fluorescence-guided resection of colorectal liver metastases. *Cancer* **119**, 3411–3418 (2013).
231. Ntziachristos, V., Tung, C.-H., Bremer, C. & Weissleder, R. Fluorescence molecular tomography resolves protease activity in vivo. *Nat Med* **8**, 757–761 (2002).
232. Stolik, S., Delgado, J. A., Pérez, A. & Anasagasti, L. Measurement of the penetration depths of red and near infrared light in human 'ex vivo' tissues. *J. Photochem. Photobiol. B Biol.* **57**, 90–93 (2000).

233. Razansky, D., Buehler, A. & Ntziachristos, V. Volumetric real-time multispectral optoacoustic tomography of biomarkers. *Nat. Protoc.* **6**, 1121–1129 (2011).
234. Ma, Y., Sadoqi, M. & Shao, J. Biodistribution of indocyanine green-loaded nanoparticles with surface modifications of PEG and folic acid. *Int. J. Pharm.* **436**, 25–31 (2012).
235. Manchanda, R., Fernandez-Fernandez, A., Nagesetti, A. & McGoron, A. J. Preparation and characterization of a polymeric (PLGA) nanoparticulate drug delivery system with simultaneous incorporation of chemotherapeutic and thermo-optical agents. *Colloids Surfaces B Biointerfaces* **75**, 260–267 (2010).
236. Saxena, V., Sadoqi, M. & Shao, J. Indocyanine green-loaded biodegradable nanoparticles: preparation, physicochemical characterization and in vitro release. *Int. J. Pharm.* **278**, 293–301 (2004).
237. Srinivasan, S. *et al.* Targeted nanoparticles for simultaneous delivery of chemotherapeutic and hyperthermia agents – An in vitro study. *J. Photochem. Photobiol. B Biol.* **136**, 81–90 (2014).
238. Murata, M., Tahara, K. & Takeuchi, H. Real-time in vivo imaging of surface-modified liposomes to evaluate their behavior after pulmonary administration. *Eur. J. Pharm. Biopharm.* **86**, 115–119 (2014).
239. Lopes, L. B. *et al.* Studies on the encapsulation of diclofenac in small unilamellar liposomes of soya phosphatidylcholine. *Colloids Surfaces B Biointerfaces* **39**, 151–158 (2004).
240. Hua, J. *et al.* In vivo imaging of choroidal angiogenesis using fluorescence-labeled cationic liposomes. *Mol. Vis.* **18**, 1045–54 (2012).
241. Portnoy, E., Lecht, S., Lazarovici, P., Danino, D. & Magdassi, S. Cetuximab-labeled liposomes containing near-infrared probe for in vivo imaging. *Nanomedicine Nanotechnology, Biol. Med.* **7**, 480–488 (2011).
242. Yoneya, S. *et al.* Binding properties of indocyanine green in human blood. *Investig. Ophthalmol. Vis. Sci.* **39**, 1286–1289 (1998).
243. Beard, P. Biomedical photoacoustic imaging. *Interface Focus* **1**, 602–631 (2011).
244. Rotermund, F., Weigand, R., Holzer, W., Wittmann, M. & Penzkofer, A. Fluorescence spectroscopic analysis of indocyanine green J aggregates in water. *J. Photochem. Photobiol. A Chem.* **110**, 75–78 (1997).
245. Moreira, J., Ishida, T., Gaspar, R. & Allen, T. Use of the Post-Insertion Technique to Insert Peptide Ligands into Pre-Formed Stealth Liposomes with Retention of Binding Activity and Cytotoxicity. *Pharm. Res.* **19**, 265–269 (2002).
246. Szoka Jr, F. & Papahadjopoulos, D. Comparative properties and methods of preparation of lipid vesicles (liposomes). *Annu. Rev. Biophys. Bioeng.* **9**, 467–508 (1980).
247. Bittman, R. & Blau, L. Phospholipid-cholesterol interaction. Kinetics of water permeability in liposomes. *Biochemistry* **11**, 4831–4839 (1972).
248. Hossann, M. *et al.* Size of thermosensitive liposomes influences content release. *J. Control. Release* **147**, 436–443 (2010).
249. Devoisselle, J.-M., Soulie-Begu, S., Mordon, S. R., Desmettre, T. & Maillols, H. Fluorescence properties of indocyanin green: I. In-vitro study with micelles and liposomes. in **2980**, 453–460 (1997).

250. Srinivasan, S. *et al.* Targeted nanoparticles for simultaneous delivery of chemotherapeutic and hyperthermia agents - An in vitro study. *J. Photochem. Photobiol. B Biol.* **136**, 81–90 (2014).
251. Prewett, M. *et al.* Antivascular endothelial growth factor receptor (fetal liver kinase 1) monoclonal antibody inhibits tumor angiogenesis and growth of several mouse and human tumors. *Cancer Res.* **59**, 5209–5218 (1999).
252. Al-Jamal, W. & Kostarelos, K. Liposomes: from a clinically established drug delivery system to a nanoparticle platform for theranostic nanomedicine. *Acc. Chem. Res.* **44**, 1094–1104 (2011).
253. Terreno, E., Uggeri, F. & Aime, S. Image guided therapy: the advent of theranostic agents. *J. Control. release* **161**, 328–337 (2012).
254. Witzig, T. E. *et al.* Randomized controlled trial of yttrium-90–labeled ibritumomab tiuxetan radioimmunotherapy versus rituximab immunotherapy for patients with relapsed or refractory low-grade, follicular, or transformed B-cell non-Hodgkin’s lymphoma. *J. Clin. Oncol.* **20**, 2453–2463 (2002).
255. Witzig, T. E. *et al.* Treatment with ibritumomab tiuxetan radioimmunotherapy in patients with rituximab-refractory follicular non-Hodgkin’s lymphoma. *J. Clin. Oncol.* **20**, 3262–3269 (2002).
256. Morschhauser, F. *et al.* Phase III trial of consolidation therapy with yttrium-90–ibritumomab tiuxetan compared with no additional therapy after first remission in advanced follicular lymphoma. *J. Clin. Oncol.* **26**, 5156–5164 (2008).
257. Iwamoto, F. M. *et al.* Study of radiolabeled indium-111 and yttrium-90 ibritumomab tiuxetan in primary central nervous system lymphoma. *Cancer* **110**, 2528–2534 (2007).
258. Nicolaidis, N. C., O’Shannessy, D. J., Albone, E. & Grasso, L. Co-development of diagnostic vectors to support targeted therapies and theranostics: essential tools in personalized cancer therapy. *Drug-Diagnostics Co-Development Oncol.* **48** (2014).
259. Zhang, G. *et al.* Imaging of pharmacokinetic rates of indocyanine green in mouse liver with a hybrid fluorescence molecular tomography/x-ray computed tomography system. *J. Biomed. Opt.* **18**, 40505 (2013).
260. Grüll, H. & Langereis, S. Hyperthermia-triggered drug delivery from temperature-sensitive liposomes using MRI-guided high intensity focused ultrasound. *J. Control. Release* **161**, 317–327 (2012).
261. Pennathur, A. *et al.* Image-guided radiofrequency ablation of lung neoplasm in 100 consecutive patients by a thoracic surgical service. *Ann. Thorac. Surg.* **88**, 1601–1608 (2009).
262. Abbas, G., Pennathur, A., Landreneau, R. J. & Luketich, J. D. Radiofrequency and microwave ablation of lung tumors. *J. Surg. Oncol.* **100**, 645–650 (2009).
263. Colombo, R. *et al.* Multicentric study comparing intravesical chemotherapy alone and with local microwave hyperthermia for prophylaxis of recurrence of superficial transitional cell carcinoma. *J. Clin. Oncol.* **21**, 4270–4276 (2003).
264. Al-Ahmady, Z. S., Scudamore, C. L. & Kostarelos, K. Triggered doxorubicin release in solid tumors from thermosensitive liposome-peptide hybrids: Critical parameters and therapeutic efficacy. *Int. J. Cancer* n/a-n/a (2015). doi:10.1002/ijc.29430

265. Mouritsen, O. G. & Zuckermann, M. J. Model of interfacial melting. *Phys. Rev. Lett.* **58**, 389 (1987).
266. Kim, D. H., Costello, M. J., Duncan, P. B. & Needham, D. Mechanical properties and microstructure of polycrystalline phospholipid monolayer shells: Novel solid microparticles. *Langmuir* **19**, 8455–8466 (2003).
267. Kirchherr, A.-K., Briel, A. & Mäder, K. Stabilization of indocyanine green by encapsulation within micellar systems. *Mol. Pharm.* **6**, 480–491 (2009).
268. Ikagawa, H. *et al.* Chemical toxicity of indocyanine green damages retinal pigment epithelium. *Invest. Ophthalmol. Vis. Sci.* **46**, 2531–2539 (2005).
269. de la Maza, A. & Parra, J. L. Changes in phosphatidylcholine liposomes caused by a mixture of Triton X-100 and sodium dodecyl sulfate. *Biochim. Biophys. Acta (BBA)-Lipids Lipid Metab.* **1300**, 125–134 (1996).
270. Deo, N. & Somasundaran, P. Effects of sodium dodecyl sulfate on mixed liposome solubilization. *Langmuir* **19**, 7271–7275 (2003).
271. Maruyama, K., Unezaki, S., Takahashi, N. & Iwatsuru, M. Enhanced delivery of doxorubicin to tumor by long-circulating thermosensitive liposomes and local hyperthermia. *Biochim. Biophys. Acta (BBA)-Biomembranes* **1149**, 209–216 (1993).
272. Drummond, D. C., Meyer, O., Hong, K., Kirpotin, D. B. & Papahadjopoulos, D. Optimizing liposomes for delivery of chemotherapeutic agents to solid tumors. *Pharmacol. Rev.* **51**, 691–744 (1999).
273. Huang, S. K. *et al.* Liposomes and hyperthermia in mice: increased tumor uptake and therapeutic efficacy of doxorubicin in sterically stabilized liposomes. *Cancer Res.* **54**, 2186–2191 (1994).
274. Bielska, A. A., Schlesinger, P., Covey, D. F. & Ory, D. S. Oxysterols as non-genomic regulators of cholesterol homeostasis. *Trends Endocrinol. Metab.* **23**, 99–106 (2012).
275. Gregoriadis, G. & Davis, C. Stability of liposomes *in vivo* and *in vitro* is promoted by their cholesterol content and the presence of blood cells. *Biochem. Biophys. Res. Commun.* **89**, 1287–1293 (1979).
276. Ali, M. H., Kirby, D. J., Mohammed, A. R. & Perrie, Y. Solubilisation of drugs within liposomal bilayers: alternatives to cholesterol as a membrane stabilising agent. *J. Pharm. Pharmacol.* **62**, 1646–1655 (2010).
277. Socaciu, C., Bojarski, P., Aberle, L. & Diehl, H. A. Different ways to insert carotenoids into liposomes affect structure and dynamics of the bilayer differently. *Biophys. Chem.* **99**, 1–15 (2002).
278. Sospedra, P. *et al.* Physicochemical Behavior of Polylysine-[HAV-VP3 Peptide] Constructs at the Air-Water Interface. *Langmuir* **15**, 5111–5117 (1999).
279. HIFU Planet. <http://www.hifu-planet.co.uk/hifu-centres/>. (2016).
280. Braathen, L. R. *et al.* Guidelines on the use of photodynamic therapy for nonmelanoma skin cancer: An international consensus. *J. Am. Acad. Dermatol.* **56**, 125–143 (2007).
281. Tagami, T., Ernsting, M. J. & Li, S.-D. Efficient tumor regression by a single and low dose treatment with a novel and enhanced formulation of thermosensitive liposomal doxorubicin. *J. Control. release* **152**, 303–309 (2011).

282. Banno, B. *et al.* The functional roles of poly (ethylene glycol)-lipid and lysolipid in the drug retention and release from lysolipid-containing thermosensitive liposomes in vitro and in vivo. *J. Pharm. Sci.* **99**, 2295–2308 (2010).
283. Charcosset, C., Juban, A., Valour, J.-P., Urbaniak, S. & Fessi, H. Preparation of liposomes at large scale using the ethanol injection method: Effect of scale-up and injection devices. *Chem. Eng. Res. Des.* **94**, 508–515 (2015).
284. Lasic, D. D. Mechanisms of liposome formation. *J. Liposome Res.* **5**, 431–441 (1995).
285. Cancer.Gov. Cancer 5-Year survival by stage. Available at: <http://seer.cancer.gov/statfacts>.
286. Trédan, O., Galmarini, C. M., Patel, K. & Tannock, I. F. Drug resistance and the solid tumor microenvironment. *J. Natl. Cancer Inst.* **99**, 1441–1454 (2007).
287. Buehler, A., Herzog, E., Razansky, D. & Ntziachristos, V. Video rate optoacoustic tomography of mouse kidney perfusion. *Opt. Lett.* **35**, 2475–2477 (2010).
288. Jacques, S. L. Optical properties of biological tissues: a review. *Phys. Med. Biol.* **58**, R37 (2013).
289. Tokumasu, F., Jin, A. J., Feigenson, G. W. & Dvorak, J. A. Atomic force microscopy of nanometric liposome adsorption and nanoscopic membrane domain formation. *Ultramicroscopy* **97**, 217–227 (2003).